Role of Vascular Endothelial Growth Factor Signaling in Brown Adipocyte Survival, Proliferation and Function

Dissertation Advisor: Dr. Patricia A. D'Amore Mandrita Bagchi

Role of Vascular Endothelial Growth Factor Signaling in Brown Adipocyte Survival, Proliferation and Function

ABSTRACT

Both white and brown adipose tissues exhibit extensive vascularity. Increased angiogenesis in brown adipose tissue (BAT) is crucial for brown fat activation and thermogenesis in animals during cold acclimation. BAT can be similarly activated by food intake to generate heat through cellular respiration, in a process known as diet induced thermogenesis. Vascular endothelial growth factor (VEGF) is a potent angiogenic factor that regulates both pathological and physiological angiogenesis and can stimulate cell proliferation, migration, survival and vessel permeability. However, VEGF has also been shown to affect an increasing number of non-vascular cells such as skeletal muscle and kidney podocytes. The expression and function of VEGF in white and brown adipocytes are not fully understood. We have previously shown that the expression of VEGF is concomitantly regulated with skeletal muscle differentiation. Here we show that VEGF is expressed in BAT and all major white adipose depots in mice. VEGF expression was increased during white and brown adipocyte differentiation and was regulated in cultured brown adipocytes by the PPARγ agonist troglitazone and by PGC1α in BAT *in vivo*.

Systemic VEGF neutralization led to brown adipocyte apoptosis *in vivo*, loss of mitochondrial cristae and increased mitophagy and was associated with increased inflammation and fibrosis. VEGFR2 was expressed in both brown preadipocytes and adipocytes. Blockade of VEGF signaling using anti-VEGFR2 antibody DC101 increased brown adipocyte apoptosis *in vitro*. VEGF also functioned as a mitogen and survival factor for brown preadipocytes. VEGF 164 and VEGF 188, isoforms that can bind heparan sulfate proteoglycans, comprise >98% of total VEGF in BAT, subcutaneous and perigonadal fat depots. Embryos that lacked VEGF 164 and 188 displayed abnormal BAT development with fewer brown adipocytes, lower levels of mitochondrial uncoupling protein 1 and Cox IV.

These results indicate a direct role for VEGF signaling in brown adipocytes and preadipocytes and suggest the importance of heparan sulfate binding VEGF isoforms in BAT development. Elucidation of the role of VEGF signaling in adipocytes is vital to understanding adipose tissue expansion and activation and may reveal novel therapeutic targets for the activation of brown fat in humans.

TABLE OF CONTENTS

To my parents, Swapan and Nilanjana, my brother, Mainak & my husband, Sutirtha

Acknowledgements

I would like to wholeheartedly thank my mentors, all my colleagues, friends and family, many of whom I have named here. I would not have the privilege of writing this dissertation without your continuous encouragement and love.

I express my sincerest gratitude to my dissertation advisor, Dr. Patricia D'Amore. Pat has not only provided excellent guidance for my dissertation but has also trained me to be a good and meticulous scientist and has made sure that we learn how to effectively communicate science through good writing and presentation. Pat maintains a great lab, which reflects her own vivacity and enthusiasm and has been a wonderful place to work. I would like to thank all my colleagues for a fun-filled three years. In particular, I want to extend a very special thank you to Dr. Leo Kim for doing sFlt1 tail vein injections and perfusions for me and being very excited in my project all along and to Dhanesh Amarnani for helping me with the sFlt1 mouse work. I am also thankful to D'Amore lab alums, Dr. Tony Walshe, who so kindly took the leap of faith and did the first set of sFlt1 experiments for me and to Dr. Sunita Hett for being such a wonderful friend and guide in lab!

To all my DAC members – Drs Zoltan Arany, Ron Kahn and William Aird: thank you for your invaluable insights and continuous support in this project and my PhD. Starting a new thesis project in a new laboratory in my 5th year in graduate school, I would not be where I am now without your help! Thank you Zolt for stepping in as my defense chair at the last minute!

I would like to extend my deepest gratitude to my DAC chair, Dr. Ron Kahn, and his lab. Ron has been invaluable to my project and has supported me in every way possible in the last three years, be it from learning a new technique in his lab, to sharing reagents, collaborating on experiments and even practicing presentations in his lab. Thank you Ron for your unconditional support! I would also like to thank Dr. Jeremie Boucher from the Kahn lab. Thank you Jeremie for patiently going through my data several times, for your expert guidance, willingness to help out and, of course, for always answering my countless troubleshooting emails. Without your contribution my dissertation project would not be where it is and definitely would not be as much fun!

I am grateful to Dr. Saverio Cinti for his expert input on the electron microscopy data on brown fat and to Dr. Ana Maria Cuervo for her input on the autophagy observations and IHC staining. I would like to thank Laura Benjamin for supporting my research in Pat's lab and for good times in her lab at Research North from 2007 to 2009. I made many friends and great connections; in particular I would like to thank Dr. Rebekah O'Donnell and Rinku Pal for their continuous cheerleading on my behalf!

A heartfelt thank you goes out to Suzanne White at the BIDMC pathology core, for the great paraffin sections of fat, on orders that were mostly "rush". Thanks to Louise Trakimas for TEM sectioning. Thanks also to Jessica Lanzim, who took care of my mice and was always there to help me with any animal work.

I would also like to thank my mentors at Temple University, Drs. Tomasz Skorski, Malgorzata Skorska and Ruth Ost who got me interested in research in the first place.

I would love to thank my friends, both old and new, for their love and continuous encouragement. My friends in the BBS program and outside: it takes a “village to raise a PhD” and it would not have been possible without you, neither would it have been as much fun. In particular, I want to thank Raji Shankar, my former roommate, Anindita Deb and her family, who provided a home away from home for me in Boston, Jennifer Shay, Vinod Nambudiri, Sawona Biswas, Maryada Sharma, Sarah Jacobo and many others for always being there for me and believing in me. My life in Boston has been so much richer because of all of you!

A very special thank you to my wonderful family: my parents, my brother and my husband, Sutirtha. To my parents: I am where I am only because of your years of dedication and support. Had it not been for my Dad, I would not have developed the discipline and determination that I now have. Thank you Mom, for always being so compassionate and giving me the much needed pep talk whenever required. Thank you for always believing in me and for being my ultimate safety net. To my brother Mainak: we grew up together, and you perhaps have the best understanding of where I am coming from. Some of my best times in Boston were during the summers when you visited me here. Thank you for always being there for me. To Sutirtha, with feet firmly rooted to the ground and a heart that dares to dream, you are much of what I aspire to be. Your calm presence and steadfast support has been the rock in my life these last few months. I have enjoyed growing with you and I look forward to a lifetime of laughter and memories with you.

Finally, I am grateful to God for guiding and protecting me all my life, during my PhD and always and for the wonderful people and opportunities you brought my way.

List of Abbreviations

^{18}F-FDG	^{18}F-fluoro-2-deoxyglucose
BAT	Brown adipose tissue
DAPI	4', 6'-diamino-2-phenylindole
DIO	Diet induced obesity
DIT	Diet induced thermogenesis
DMEM	Dulbecco's modified Eagle's medium
ERRα	Estrogen-related receptor α
FBS	Fetal bovine serum
IF	Immunofluorescence
IHC	Immunohistochemistry
H&E	Hematoxylin and eosin
HFD	High fat diet
HIF1α	Hypoxia inducible factor 1α
HSPG	Heparan sulfate proteoglycans
MAPK	Mitogen-activated protein kinase
NE	Norepinephrine
Nrp1	Neuropilin-1
NST	Non-shivering thermogenesis
PAI-1	Plasminogen activator inhibitor 1

PBS	Phosphate buffered saline
PFA	Paraformaldehyde
PG	Perigonadal
PGC1α	Peroxisome proliferator-activated receptor gamma coactivator 1α
PI3K	Phosphatidylinositol 3-kinase
PlGF	Placental growth factor
PPARγ	Peroxisome proliferator-activated receptor-γ
SC	Subcutaneous
sFlt1	Soluble fms-like tyrosine kinase 1
SNS	Sympathetic nervous system
T3	Triiodothyronine
TEM	Transmission electron microscope
TGF-β	Transforming growth factor β
TNFα	Tumor necrosis factor α
TUNEL	Terminal Transferase dUTP Nick End Labeling
UCP1	Uncoupling protein 1
VEGF	Vascular endothelial growth factor
VEGFR1	Vascular endothelial growth factor receptor 1
VEGFR2	Vascular endothelial growth factor receptor 2
WAT	White adipose tissue

Index of Figures

Chapter 1 - Introduction

Chapter 2 - VEGF and VEGF receptor expression in white and brown adipose

Chapter 3 - Role of VEGF signaling in brown adipocytes

Chapter 4 - Isoform-specific role of VEGF in BAT development

Chapter 5 - Regulation of Vegf expression in brown adipocytes

Index of Tables

Chapter 1

INTRODUCTION

Adipose Tissue

Adipose tissue in mammals is categorized to two types, white and brown, according to their distinct physiological roles. White adipose tissue (WAT) serves as a storage depot for excess calories and functions as an endocrine organ to integrate various homeostatic processes. Brown adipose tissue (BAT) is a major thermogenic organ that generates heat under regulation of the sympathetic nervous system.

White Adipose Tissue

WAT was long thought to be a passive storage depot for excess calories, with few other functions. The steep rise in obesity and associated comorbidities, such as type 2 diabetes and cardiovascular disorders, over the past 30 years has fueled scientific research in this area.

Development and Distribution

Although most multicellular organisms have cells that store excess energy, adipocytes evolved to meet this need at the time of vertebrate radiation. Mammals, birds, reptiles, amphibians and many fish have cells that are readily identifiable as adipocytes, although their anatomical locations vary considerably across species. Most mammals have WAT dispersed throughout the body in two major types of depots – subcutaneous (SC) and intraabdominal (or visceral). In mouse, the inguinal fat is the major SC depot, whereas the visceral depots are in the retroperitoneal, periovarian (in females) and epididymal (in males) regions. In humans, the major intraabdominal depots of

A

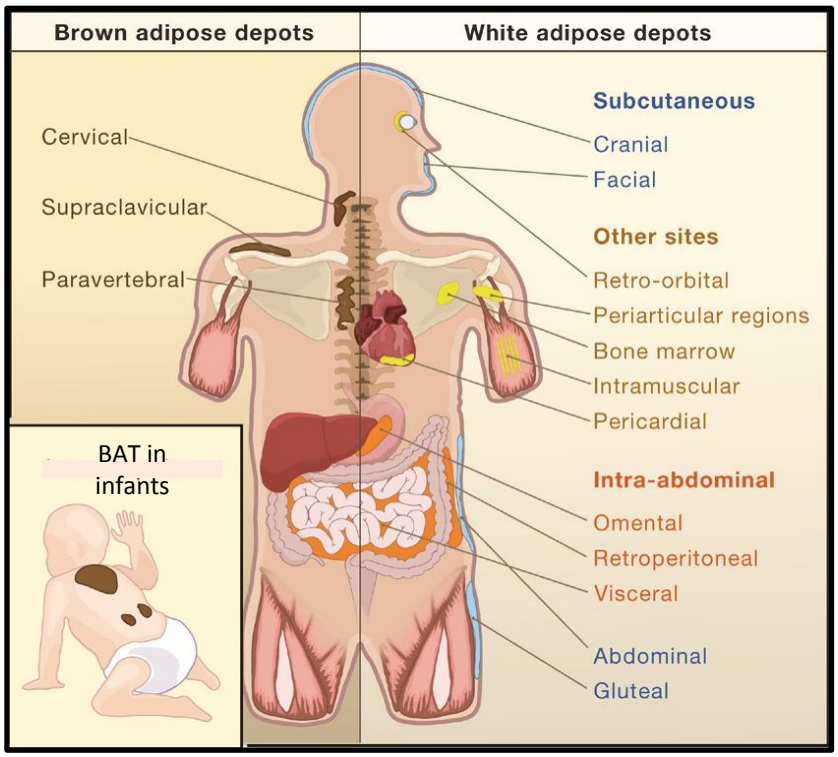

B

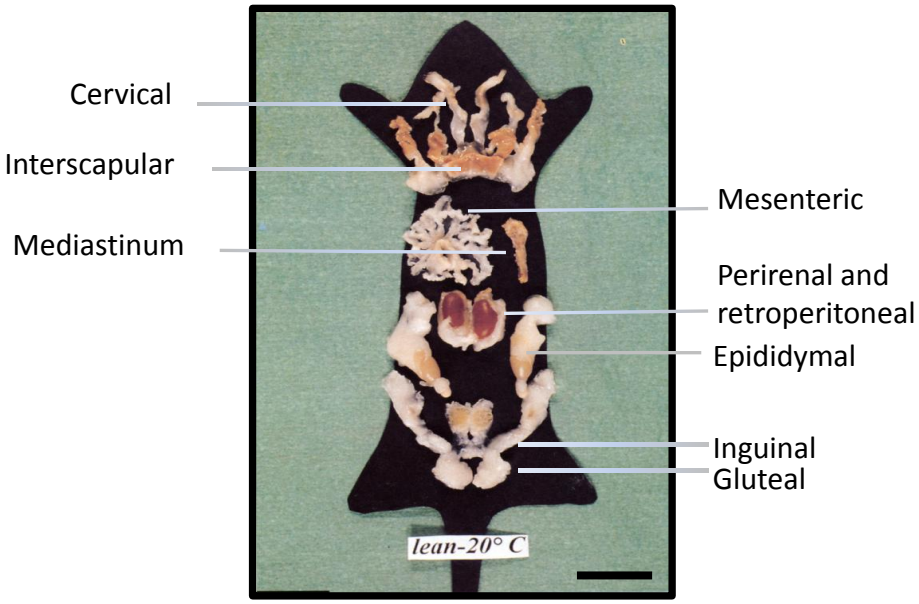

Figure 1.1. **Brown and white adipose depots.** (**A)** In humans, WAT is distributed throughout the body with subcutaneous and intra-abdominal depots representing the main compartments. BAT is abundant at birth (inset) and present in adulthood to a lesser extent. (**B)**Typical distribution of white and brown adipose in a lean mouse at 20C. WAT and BAT depots are present throughout life in rodents, but varies depending on weight and environmental temperature. Scale bar represents 2 cm. **(A)** adapted from Gestal et al. 2007, **(B)** adapted from *The Adipose Organ*, plate 1, Editrice Kurtis Ltd., 1999

WAT are around the omentum, intestines and perirenal areas, whereas SC depots are in the buttocks, thighs and abdomen. In addition, WAT can be found in many other areas, including in the retro-orbital space, on the face and extremities, and within the bone marrow (Gesta et al. 2007). The distribution of WAT varies considerably, not only across species but also between individuals of the same species. In humans, obesity in which fat deposition is localized in the SC depot (pear shaped obesity) is correlated with a lower risk of associated metabolic disorders while deposition in the intraabdominal depot (apple shaped obesity) correlates with a higher risk. How excess calories are directed to one depot versus the other is not understood. Gene expression profiling has revealed significant differences between different adipose depots in both rodents (Gesta et al. 2006) and humans (Vidal 2001; Vohl et al. 2004) (Figure 1.1).

WAT, similar to muscle and bone, is thought to have a mesodermal origin. Development of WAT begins at midgestation (in humans) or shortly after birth (in rodents) and gradually increases in size throughout life. Adipose tissue develops in close spatial and temporal association with the vasculature, and in a presumptive fat depot arteriolar differentiation precedes the appearance of preadipocytes. It was recognized very early on, that the development of adipocytes in close proximity to blood vessels indicated that an established vascular supply is necessary for adipose tissue development (Clark & Clark 1940); although, sometimes, adipose development is concurrent with arteriolar differentiation, depending on the depot (Hausman & Thomas 1986). In adults, fat depots consist of mature adipocytes and adipocyte precursors (as well as stromal and vascular

cells). Expansion of adipose tissue occurs through an increase in size of existing adipocytes as well as the recruitment of preadipocytes.

Structure

White adipocytes are 50 – 100 μm in diameter in humans and can be significantly larger in obese subjects. A single lipid droplet occupies more than 90% of the cell volume, the remaining consisting of a narrow rim of cytoplasm, a nucleus shunted to the side and few elongated mitochondria (Figure 1.2). Each lipid droplet is coated with perilipin, which protects the lipid from hydrolysis by lipases (lipolysis) under basal conditions but is necessary for stimulated lipolysis (Figure 1.3). WAT is extensively vascularized; virtually every adipocyte is in close proximity to at least one capillary (Gersh & Still 1945) (Figure 1.4). The microvasculature of adipose tissue, unlike muscle, retina and several other organs, does not have a particular orientation but is organized in a loose mesh within the connective tissue that surrounds adipocytes (Crandall et al. 1997). WAT depots vary in terms of cellular and tissue organization as well as vascular structure. For instance, in mouse the epididymal fat pad is more lobular compared to the SC depot, whereas the inguinal depot has brown preadipocytes interspersed amidst white adipocytes, which acquire brown-like characteristics upon sympathetic stimulation.

Function

WAT primarily functions as the storage site for excess calories, which are deposited as triglycerides within the droplet of each adipocyte. However, when glucose is limiting,

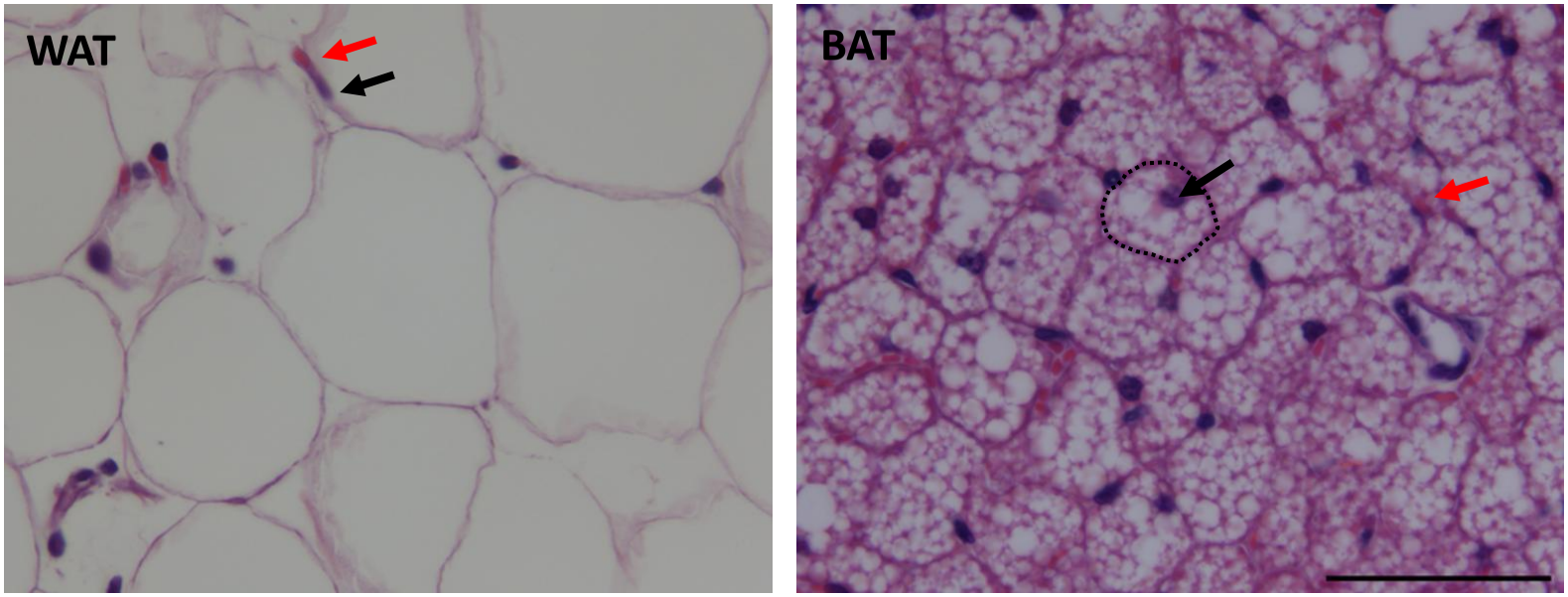

Figure 1.2. **Inguinal WAT and interscapular BAT H&E.** H&E of inguinal WAT (left) and interscapular BAT (right)of adult female mice demonstrating the larger size of white adipocytes compared to brown (the border of a single brown adipocyte is indicated by the dotted black line). The nucleus (black arrow) is roughly centrally located in brown adipocyte, whereas in a white adipocyte it is shunted to the side. Capillaries (red arrows) surround both white and brown adipocytes. Scale bar represents 50 µm.

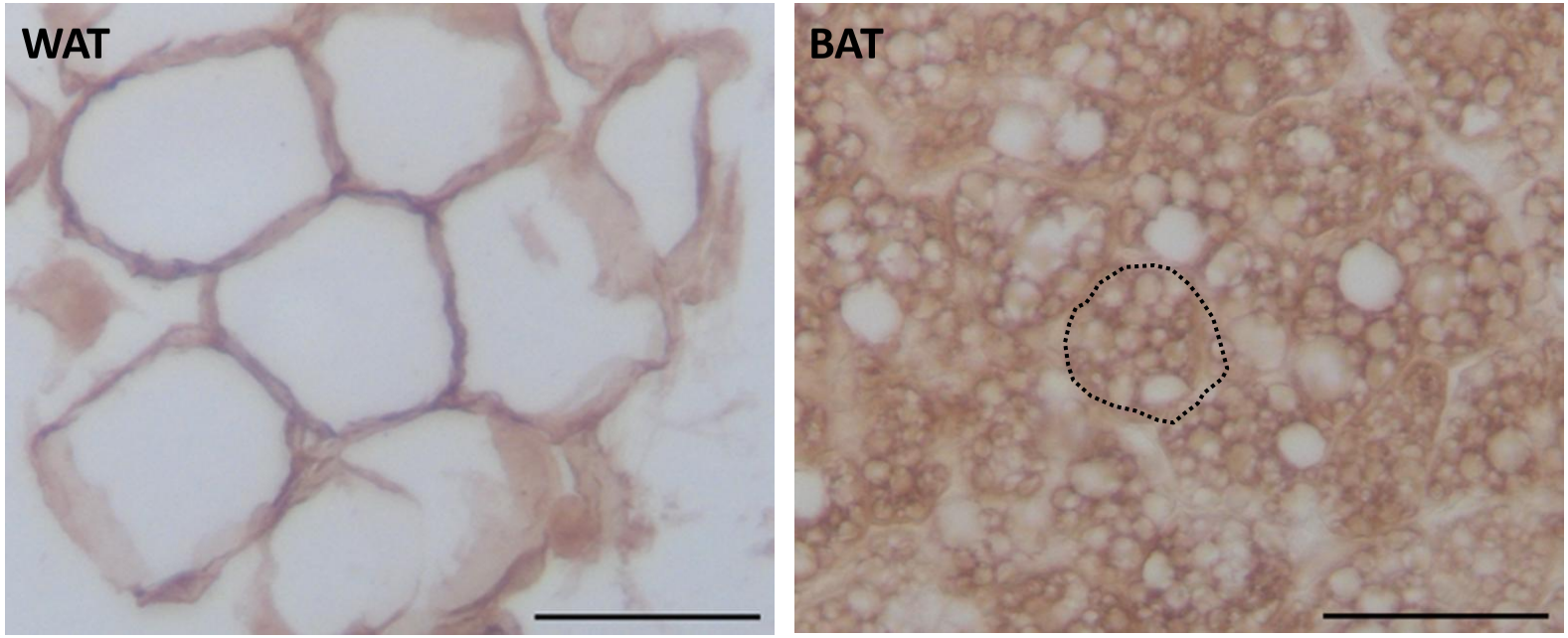

Figure 1.3. **Lipid droplets in white and brown adipocytes.** H&E of inguinal WAT (left) and interscapular BAT(right)of adult female mice demonstrating the unilocular (with a single large lipid droplet) structure of white adipocytes and the multilocular (many small lipid droplets) of brown adipocytes. Cell boundary marked with dotted black line. Perilipin forms a protective coating on lipid droplets preventing their hydrolysis by lipases under normal conditions. Scale bar represents 50 µm.

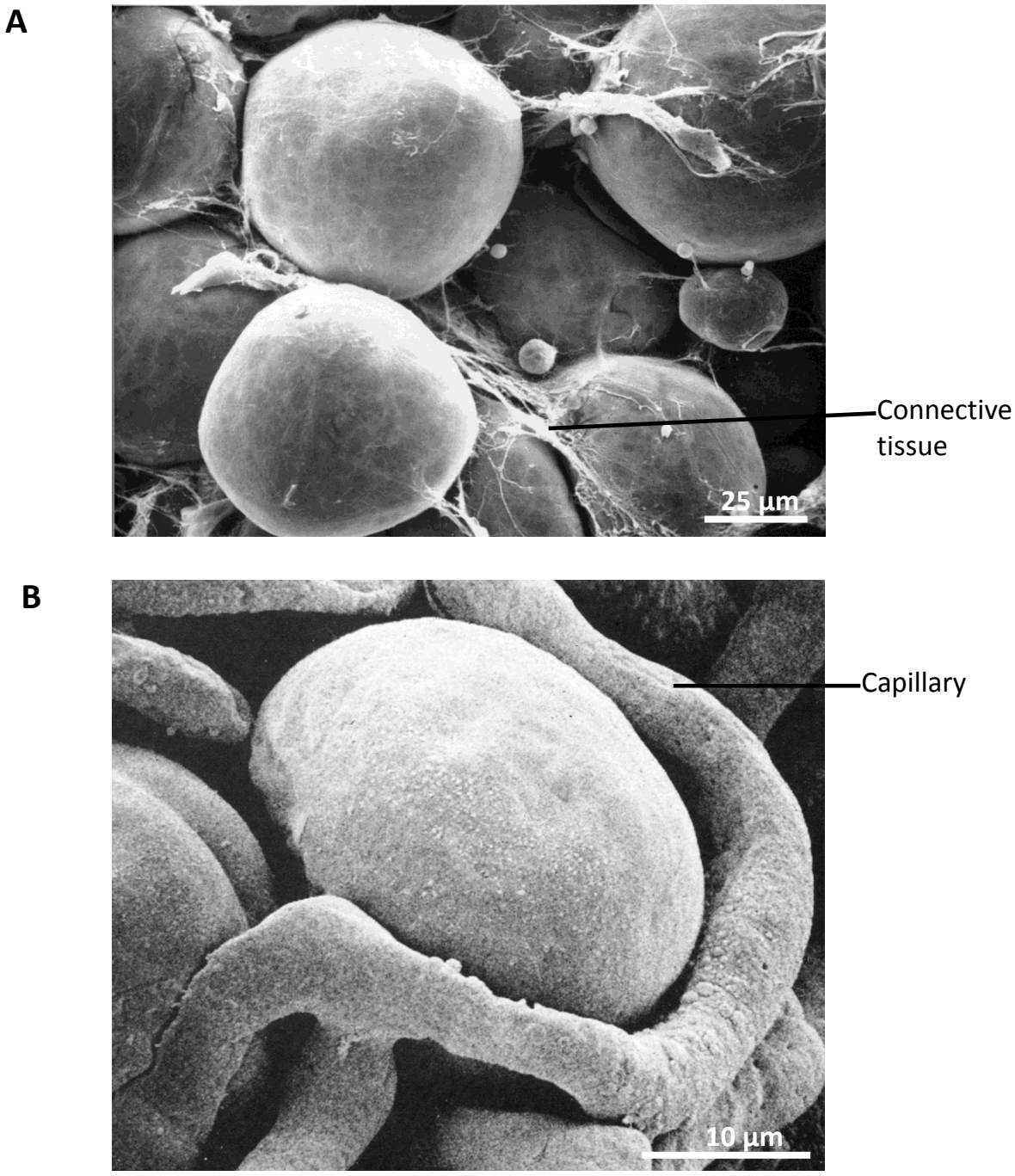

Figure 1.4. **Microvasculature and stromal cells of WAT.** Scanning electron micrograph (SEM) of white adipose tissue **(A)** Periovarian WAT depot of adult rat demonstrating large adipocytes associated with connective tissue. Scale bar represents 50 µm. **(B)** SEM of a capillary surrounding a white adipocyte demonstrates the association between adipocytes and the vasculature. Scale bar represents 10 µm. Reprinted with permission from *The Adipose Organ*, plates 25 (A) and 10 (B), Editrice Kurtis Ltd., 1999

neurohormonal stimulation induces lipases to release triglycerides from the lipid droplets into the circulation for use by other tissues as fuel.

WAT is the largest endocrine organ in mammals. Adipocytes synthesize and release peptide hormones, known as adipokines, that coordinate and integrate a wide array of homeostatic processes such as control of blood pressure, bone mass, thyroid and reproductive function and even the immune response (Trayhurn 2005). Notable among these adipokines are leptin, adiponectin, visfatin, resistin and omentin. Adipose tissue (but not necessarily adipocytes themselves) also secretes several cytokines, including tumor necrosis factor (TNF)-α, interleukins 1 and 6. Some of these secreted factors, such as adiponectin and visfatin, have a positive effect on overall insulin sensitivity, whereas others, like TNFα, reduce insulin sensitivity. Interestingly, even though obese subjects have more adipose tissue, their circulating adiponectin levels are lower compared to lean subjects (Yatagai et al. 2003).

Adipose tissue expansion and obesity

Fat depots grow by an increase in size of resident adipocytes through storage of more lipids as well as by recruitment of new adipocytes. This expansion is accompanied by remodeling of the vasculature and associated connective tissue. However, in most instances of diet-induced weight gain, WAT expansion occurs through hypertrophy of existing adipocytes, accompanied by insufficient vascular remodeling. As a result, adipocyte size is increased and capillary density is decreased, resulting in reduced perfusion and local

tissue hypoxia. In WAT, hypoxia is associated with an increased expression of inflammatory genes and decreased expression of adiponectin (Ye et al. 2007).

Adiponectin is a key insulin-sensitizing adipokine and one of the central mediators of insulin resistance. A modest increase in the level of adiponectin in *ob/ob* mice led to improvement across all metabolic parameters associated with obesity, from insulin resistance to β-cell dysfunction, although the mice remained obese (Kim et al. 2007). In addition, it was recently shown *in vivo and in vitro* that adiponectin transcription by PPARγ was dysregulated by cdk5, a cyclin dependent kinase that is activated by pro-inflammatory cytokines (Choi et al. 2010). In addition, increased expression of inflammatory cytokines such as monocyte chemotactic protein-1 by local hypoxia and endoplasmic reticular stress lead to recruitment of macrophages to adipose tissue, which secreted additional inflammatory cytokines such as TNFα and interleukin 1. Inflammatory cytokines contribute to insulin resistance by suppressing insulin action on peripheral tissue. Thus, these two processes, reduced circulating adiponectin and increased localized inflammation in the adipose tissue, contribute to development of obesity-associated insulin resistance and progression to type 2 diabetes.

However, not all who are obese develop type 2 diabetes or cardiovascular disorders. For some individuals, referred to as “metabolically healthy obese”, weight gain takes place through “healthy adipose tissue expansion” and is not accompanied by pathological consequences. Healthy adipose tissue expansion consists of enlargement of a fat pad through recruitment of new adipocytes, increased angiogenesis and appropriate vascular remodeling; there is no associated hypoxia, and minimal fibrosis and inflammation (Sun et

al. 2012). Thus, although there is increase in fat mass, it is not accompanied by insulin resistance and metabolic dysfunction. Recent studies, described later in this chapter, have aimed to facilitate healthy adipose tissue expansion in murine models of diet-induced obesity by promoting angiogenesis during the early phase of fat mass expansion (Sun et al. 2012).

Brown Adipose Tissue

Unlike WAT, BAT does not function as a storage depot for triglycerides, instead metabolizes them to generate heat when necessary. Thus, BAT is the major site for adaptive non-shivering thermogenesis (NST) in mammals. NST is the process of increased heat production, over basal metabolic levels, which is not a result of muscle activity and is mediated by the sympathetic nervous system ((SNS). BAT regulates thermogenesis during environmental stresses, such as reduced temperatures, to maintain body temperature and protect the organism from hypothermia (Smith 1964). BAT also secretes fatty acids (FA) and factors such as leptin (although at a much lower level than WAT), adiponectin, triiodothyronine (T3), that are thought to play endocrine roles (Cannon & Nedergaard 2004). Recent data suggest that BAT activity regulates vascular lipoprotein homeostasis by enhancing lipid clearance from plasma during short term cold exposure (Bartelt et al. 2011).

Distribution of brown adipose tissue

First described in 1551, BAT was long known to be present in small rodents, hibernating animals and newborn mammals, including human infants; essentially mammals that are not able to generate heat by shivering (muscular movement) and whose high

surface to volume ratio results in increased energy loss as heat (Smith & Horwitz 1969). In rodents, BAT is present in the interscapular, axillary and perinephric depots, of which the interscapular depot (often referred to as iBAT) is the largest and most commonly studied.

It was believed that BAT in humans atrophied with age and was completely absent in adults. However, in the last decade several landmark studies provided convincing evidence for the presence of metabolically active BAT depots in adult humans (for a review see Cypess & Kahn 2010). BAT in adult humans was originally identified in cancer patients being examined by positron emission tomography (PET) – computed tomography (CT) scanning to trace the uptake of ^{18}F-fluoro-2-deoxyglucose (^{18}F-FDG) by metabolically active tissue such as cancer metastases. In addition to sites of metastasis, this imaging revealed additional areas of strong ^{18}F-FDG uptake, particularly in the thoracic region, which were symmetrically distributed and hence unlikely to be tumors (Nedergaard et al. 2007); these sites were later identified as BAT depots. Currently, it is widely accepted that a significant fraction of adult humans possess BAT, although a consensus is yet to be reached regarding numbers. Because of the limitations of the ^{18}F-FDG above method in detecting BAT, estimates of the prevalence of BAT in the adult population have varied greatly across different reports from 7.5 to 25% and even 80% of patients examined (Cypess et al. 2009). The two most commonly detected BAT depots in adult humans are located in the supraclavicular and neck regions. In addition, a symmetrical pattern of BAT is seen along the spinal cord as a paravertebral depot, in the para-aortic area of the mediastinum and around the apex of the heart, as well as the perirenal depots, all generally demonstrating weaker ^{18}F-FDG uptake than those in the thoracic region (Figure 1.5). While this distribution

pattern is similar, but not identical, to BAT distribution in rodents, it closely corresponds with the distribution of BAT in human infants (Aherne & Hull 1966). Besides the above conventional BAT depots, brown adipocyte precursors are dispersed in certain WAT depots of both humans and rodents. These precursors can be induced to differentiate into mature brown adipocytes by catecholamines or by the expression of peroxisome proliferator-activated receptor coactivator 1α (PGC1α) (Tiraby et al. 2003). These induced brown adipocytes are referred to as "brite" (brown + white) adipocytes.

Development

BAT evolved significantly later than WAT, in parallel with endothermal vertebrates - birds and mammals - and their need to regulate body temperature through NST (Gesta et al. 2007). BAT forms much earlier during development than WAT and reaches its maximum mass shortly after birth. In mouse, BAT structures are first observed in the interscapular region around embryonic day 15 (E15); fat deposition in the form of single lipid droplets begins soon after. Prior to birth there is rapid expansion of fat mass, which continues postnatally accompanied by cell proliferation, a rise in triglyceride content in the form of multilocular droplets, an increase in mitochondria number as well as in activity of the mitochondrial respiratory enzymes, such as glycerol-3-phosphate dehydrogenase, succinate dehydrogenase and cytochrome C and differentiation of mitochondria ultrastructure. At birth, there is a temporary depletion of triglycerides, suggesting that BAT might be thermogenically active at birth. Postnatal expansion of BAT continues for several days until

the tissue is at its peak of differentiation and functional activity between postnatal day 6 and 15. In fact, norepinephrine (NE) injected into fetal rats perinatally increases enzyme activity significantly, indicating that brown adipose is responsive to NE even at a very early stage. Cortisone injections, on the other hand, reduced mitochondrial enzymatic activity, although BAT mass increased, possibly due to increased lipid accumulation (Skala & Hahn 1974). Around postnatal day 21, a second phase commences marked by involution of BAT and reduction of enzymatic activities, which likely coincides with decreasing demand for NST as this can be prevented by exposing the animals to cold or NE (Barnard 1969; Zhou et al. 2003; Skala & Hahn 1974; Hirning et al. 1989).

In humans, immature brown adipocytes can be detected as early as in the 29th week of gestation. The development of the tissue appears to follow that observed in mouse with rapid expansion of cell volume and mitochondrial biogenesis. Similarly, following birth, cells continue to grow, accompanied by a decrease in lipid content. Human infants have an estimated 30 g of BAT, about 1% their body weight (Aherne & Hull 1966; Hull 1976). In spite of the widespread decline in BAT through the first decade of life, most adults retain some functionally active BAT.

Along with muscle, cartilage, bone and white adipose, BAT has a mesodermal origin, but brown adipocytes at different anatomical locations have distinct lineages. In the interscapular and perirenal depots of mice, brown adipocytes are derived from a myf5-expressing progenitor that shares a common myoblastic lineage (Timmons et al. 2007), whereas brown adipocyte precursors interspersed within WAT depots and muscle are derived from myf5-negative cells that share a common non-myogenic lineage with white

adipocytes and have features different from brown adipocytes in the interscapular depot, including greater sensitivity to β3-adrenergic stimulation and cold exposure (Timmons et al. 2007; Seale et al. 2008). When induced by the latter, they differentiate to multilocular uncoupling protein (UCP)-1+ thermogenically active cells referred to as "brite" adipocytes described above.

Structure

There are significant differences between BAT and WAT structure at the tissue and cellular level. BAT consists of brown adipocytes interspersed with stromal cells and connective tissue in a rich vascular network (Figure 1.6). The blood vessels and individual brown adipocytes are directly innervated by the SNS, which regulates its key function, adaptive thermogenesis, through the release of NE (Figure 1.7).

Brown adipocytes are smaller than white adipocytes (38 – 45 μm vs. 50 – 100 μm) and are multilocular, containing several small lipid droplets (Figure 1.3). The cytosol is densely packed with numerous mitochondria (Figure 1.8), the site of thermogenesis, making them the most important organelles in the cell. The number and ultrastructure of the mitochondria vary depending on the level of thermogenic activity in BAT. Table 1 lists the major structural features of white and brown adipocytes.

Function

The major function of BAT is adaptive NST, which is regulated by the SNS through the release of catecholamines, primarily NE. BAT performs NST under two principal conditions: during cold acclimation to maintain body temperature and during diet-induced

thermogenesis (DIT). The notion that BAT participated in cold-induced NST was made several decades ago and was based on morphological changes observed in BAT when animals were exposed to cold (Smith & Horwitz 1969). Subsequent studies in rodents demonstrated the regulation of the process by the SNS, the role of mitochondria, and identified key molecular players in this process, including PGC1α, UCP1 and β-adrenergic receptors (Enerbäck et al. 1997; Puigserver et al. 1998). The recent identification of BAT in adult humans and measurements of glucose and FA- turnover in BAT using a tracer (Ouellet et al. 2012), also demonstrated that BAT functions as a cold-induced effector of NST in humans.

BAT produces heat following food intake, a response known as DIT. DIT, however, does not refer to the heat generated during food digestion. Instead, it refers to the induction of BAT thermogenic activity by catecholamines following increased food consumption over a prolonged period of time. The concept of metabolic efficiency is central to this discussion. Metabolic efficiency refers to the amount of energy stored per unit of energy ingested; high metabolic efficiency indicates that a larger fraction of energy is stored whereas low efficiency means that a larger fraction of the ingested energy is "lost" as ATP or heat. DIT by BAT results in lowered metabolic efficiency since a portion of the ingested calories is consumed in thermogenesis, instead of being stored as lipids and glycogen in WAT depots. Thus, by lowering metabolic efficiency, BAT can play a key role in protection from diet-induced obesity (DIO). Accordingly, ablation of BAT reduces energy expenditure and increases obesity in response to high-fat diets (Ghorbani et al. 1997; Guerra et al. 1998; Lowell et al. 1993).

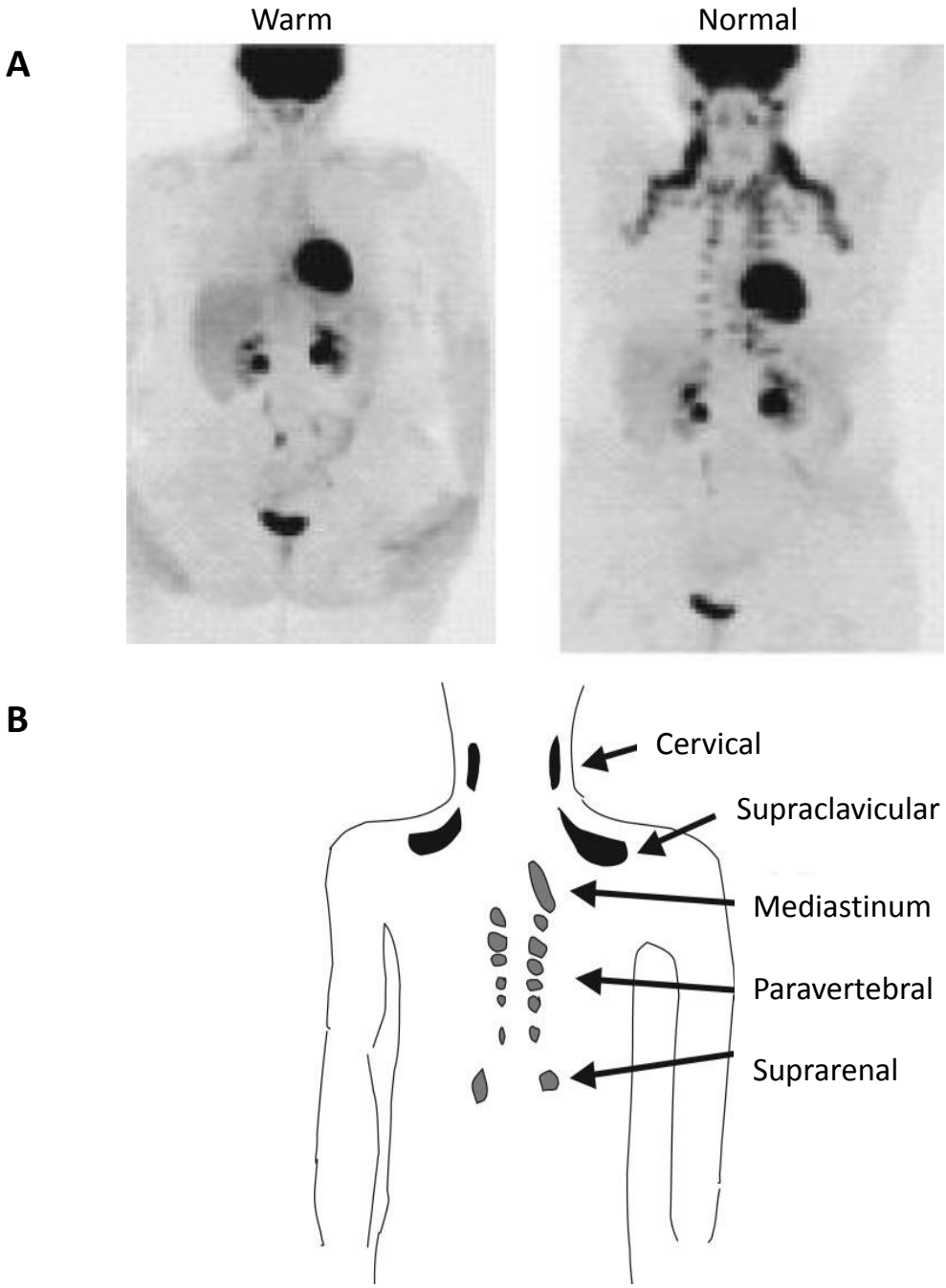

Figure 1.5. **Detection and distribution of BAT in adult humans (A)** Cold-induced brown adipose tissue activation in adult man. The same patient was investigated by FDG-PET twice a few days apart. *Left:* Patient was kept under warm conditions before injection and until imaging. The only uptake visible is that into the brain, heart, kidneys, and bladder. *Right:* the patient had been examined under routine conditions, i.e., in comparatively cold conditions. The characteristic symmetrical pattern of uptake into the supraclavicular, neck, paravertebral areas, etc., i.e., into brown adipose tissue, is now visible. **(B)** Sites of FDG uptake corresponding to brown adipose tissue in adult humans. The black areas are those that are most frequently described; the gray areas are not always found, even in humans positive in the black areas. Reprinted from *Am J Physiol Endocrinol Metab,* 293:444-452,2007.

Table 1 – Comparison of white and brown adipose tissue

Characteristic	White adipose tissue	Brown adipose tissue
Color	Cream or ivory	Brown
Adipocyte size (diameter)	50 – 100 µm	30-50 µm
Fat Storage	Unilocular lipid droplet	Multilocular lipid droplet
Mitochondria	Few	Numerous
Nucleus	Peripheral	Central
Unique marker	Leptin	UCP1
Primary function	Energy storage + endocrine	Energy expenditure by non-shivering thermogenesis
Prevalence in humans	Present in all adults	Abundant in infant, present in some adults
Development	Throughout life	Perinatal

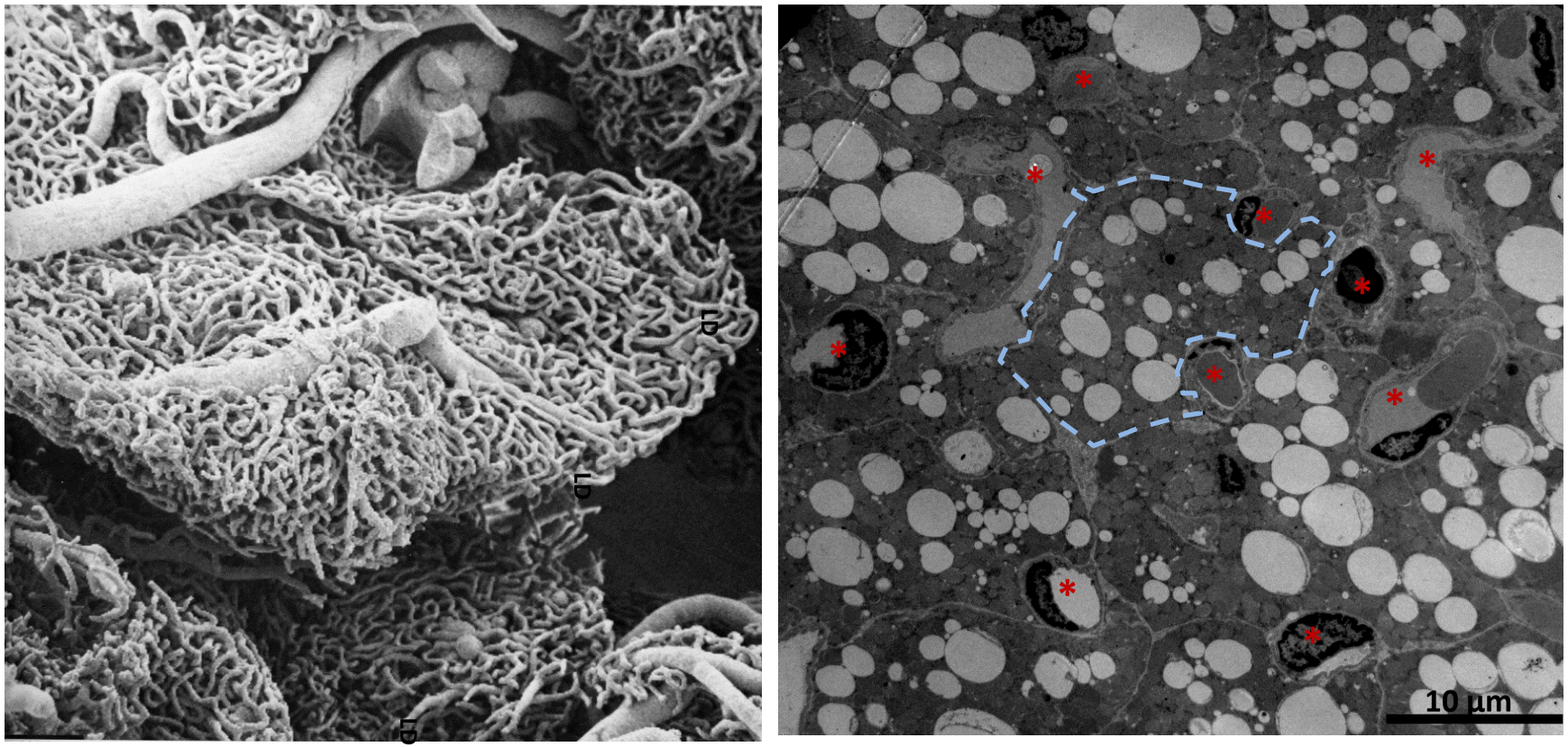

Figure 1.6. **Vasculature of brown adipose tissue.** (left) SEM showing the dense capillary network of a BAT lobule. It is a vascular cast made by perfusion with resin and subsequent dissolution of the tissue by sodium hypochloride digestion (right) Transmission electron micrograph (TEM) of BAT showing several brown adipocytes flanked by blood vessels (red asterisk) including capillaries and venules. The boundary of a brown adipocyte is indicated by dotted blue line and lipid droplets are indicated (LD). Scale bar represents 10 µm. **(A)** is reprinted with permission from *The Adipose Organ*, plate 10, Editrice Kurtis Ltd., 1999

A

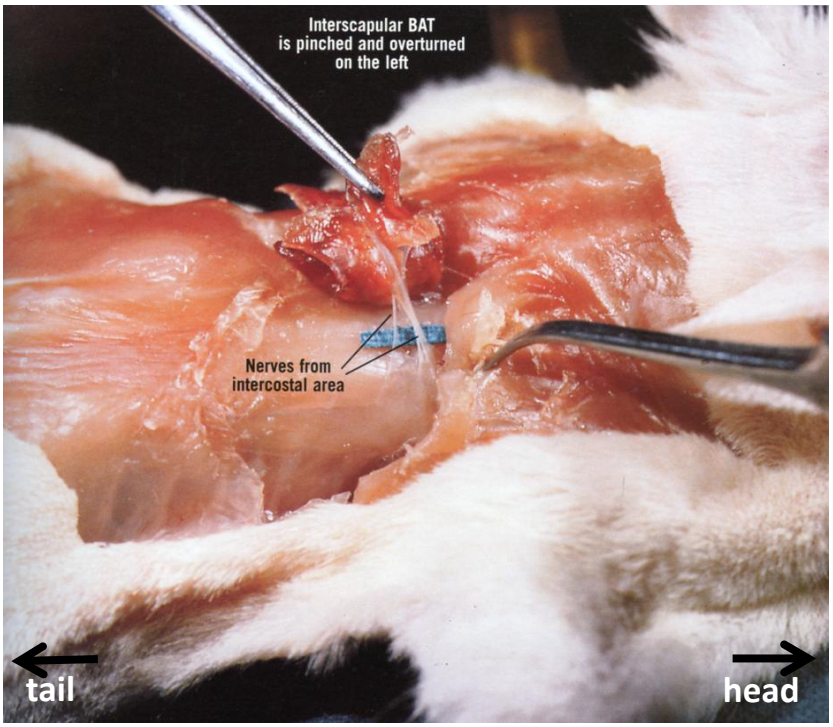

B

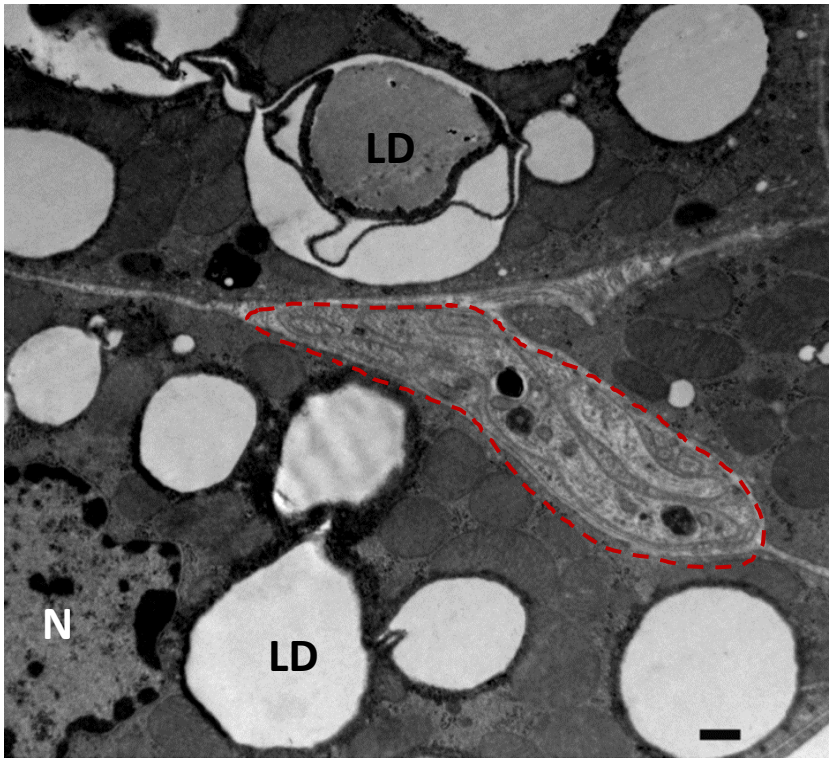

Figure 1.7. **Innervation of brown adipose tissue.** (**A)** Shown here are the nerves (5 total) from the right intercostal region reaching the ventral portion of adult rat interscapular BAT. The BAT has been pinched and folded back to reveal the nerves. (**B)** TEM of interscapular BAT showing cross section of a nerve ending (dotted red line) in between three brown aidpocytes. LD – lipid droplets; scale bar represents 500 nm. **(A)** was reprinted with permission from *The Adipose Organ*, plate 13, Editrice Kurtis Ltd., 1999

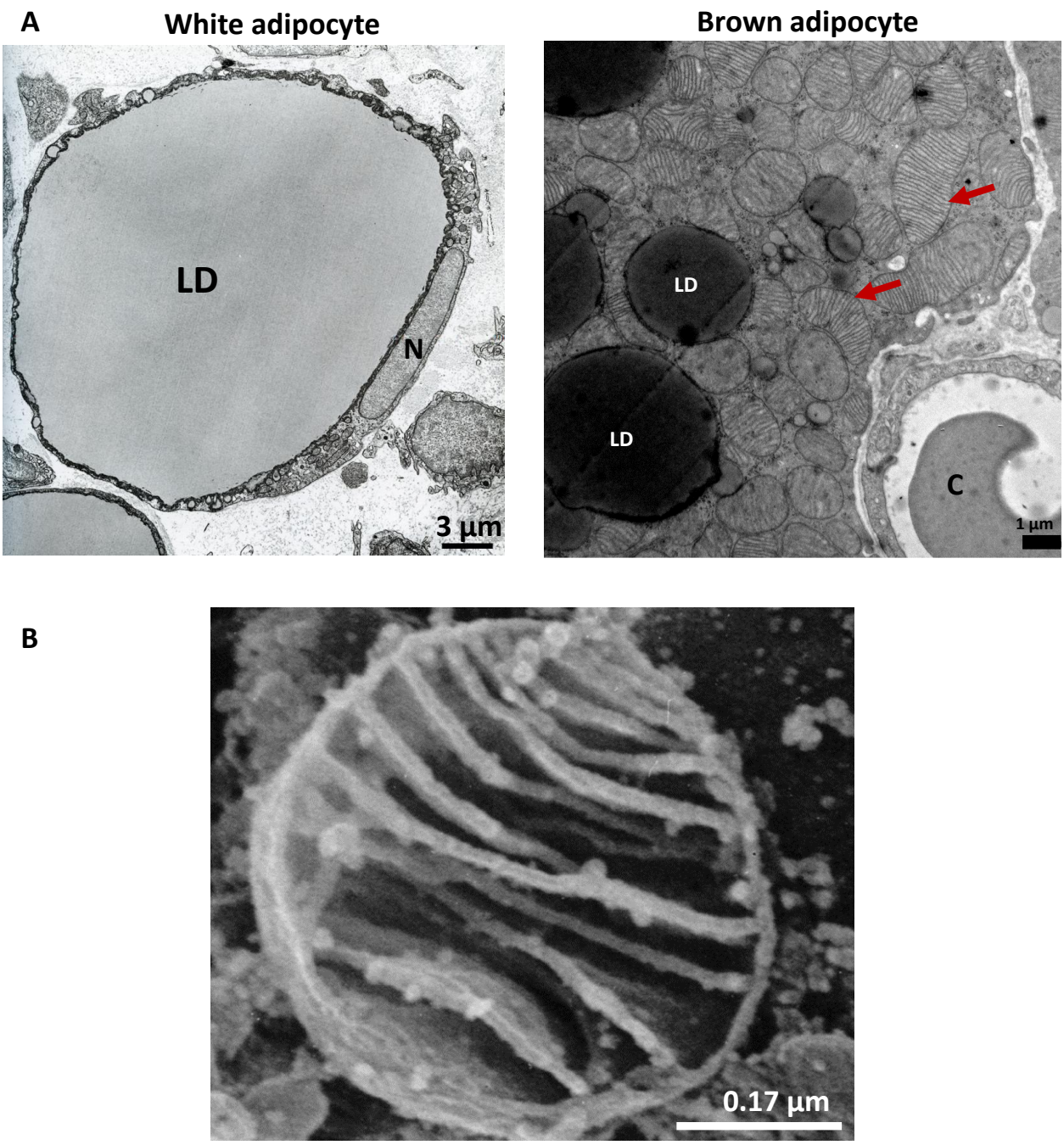

Figure 1.8. **Mitochondria in brown and white adipocytes** (**A)** TEM demonstrating the mitochondrial content of white (left) and brown adipocyte (right). Whereas a white adipocyte has a few mitochondria, the cytoplasm of a brown adipocyte is densely packed with mitochondria, which are critical for their function. White adipocyte mitochondria are elongated with a few, often incomplete cristae. Brown adipocyte mitochondria are larger, uniform and packed with numerous cristae (red arrows) (**B)** High magnification SEM of a typical brown adipocyte mitochondria demonstrating the transverse cristae. Scale bars are indicated. **(A)** adapted from Gestal et al. 2007, **(B)** adapted from *The Adipose Organ*, plate 5, Editrice Kurtis Ltd., 1999

DIT was first proposed more than thirty years ago based on experiments in which rats fed a "cafeteria diet" (composed of foods high in fats and sugars) gained less weight than expected from caloric intake and showed increased BAT activity (Rothwell & Stock 1979). With subsequent generation of transgenic mouse models, two lines of evidence pointed to a role for brown adipose-mediated DIT as a metabolic mechanism resulting in protection from obesity. One series of studies demonstrated that genetically obese animals had inefficient NST and atrophied BAT, implying that metabolic efficiency was increased as a result of inadequate BAT function. The other line of evidence made use of transgenic mouse models of key NST regulators demonstrating that the animals that were sensitive to cold were also quick to develop DIO, whereas those that exhibited increased thermogenesis were resistant to DIO (for a review see Lin & Li 2004). Notably, ablation of BAT (using a diphtheria toxin transgene targeted specifically to BAT) exhibited cold sensitivity and became obese (Lowell et al. 1993) Taken together, these results indicated the dual function of NST in temperature regulation and in the maintenance of body weight.

In adult humans, the contribution of BAT to metabolism is controversial, but it has been estimated that 50 g of maximally active BAT could account for up to 20% of the body's daily caloric expenditure (Rothwell & Stock 1983). Whether BAT is utilized for DIT in humans following "cafeteria diet" has not been investigated, in part due to the lack of appropriate non-invasive techniques to measure BAT activity under non-fasting conditions. However, a retrospective study that analyzed ^{18}F-FDG PET–CT images of 1972 adult patients found BAT activity to be inversely correlated with body mass index, age and blood glucose level, suggesting that reduced BAT activity likely contributes to a subset of age-related

obesity (Cypess et al. 2009). In addition to its capacity for NST, it was recently shown that activation of BAT via short-term cold exposure led to efficient channeling of FA into BAT through a metabolic program that increases uptake of TG-rich lipoproteins. As a result, lipid clearance from plasma became more efficient, implying that BAT might be an important regulator of blood lipid levels (Bartelt et al. 2011).

BAT structure is ideally adapted to its major function, NST, at both the tissue and cellular levels. At the tissue level, innervations by sympathetic nerve endings allows catecholamines released during SNS stimulation, by cold or food intake, to bind to β3 adrenergic receptors on the adipocytes and activate thermogenesis. During this process a dense capillary network enables rapid exchange of oxygen and carbon dioxide as well as efficient dissipation of the generated heat and its distribution throughout the body. Moreover, cold acclimation results in increased vascularity in BAT through angiogenic remodeling, increased blood flow and vaso-dilatation (Korac et al. 2008). For instance, cold induced a 12-fold increase in glucose uptake by BAT and was accompanied by doubling of perfusion (Orava et al. 2011). At the cellular level, the enormous capacity for thermogenesis derives from the large number of mitochondria in each adipocyte, each of which generates heat by the activity of the UCP1 protein, a key component of thermogenesis. Thus, the number and volume of mitochondria, and the number of cristae increase with thermogenic activity in mature brown adipocytes and are also indicative of the cell's thermogenic activity.

Regulation of thermogenic activity in BAT

The process of thermogenesis takes place in the mitochondria. PGC1α is a master regulator of mitochondrial biogenesis and oxidative metabolism in most cell types, including brown fat and skeletal muscle. Genetic ablation of PGC1α results in reduced capacity for cold-induced thermogenesis *in vivo* while ectopic expression of PGC1α in WAT induced expression of multiple target mitochondrial and thermogenic genes including UCP1. PGC1α thus is a crucial regulator of adaptive thermogenesis (Puigserver et al. 1998; Puigserver 2003).

In most eukaryotic cells, the mitochondria are the sites of aerobic respiration i.e., the Krebs cycle and the electron transport chain. Through the electron transport chain, which takes place in the inner mitochondrial membrane, a series of transmembrane enzyme complexes generate an electrochemical gradient by extrusion of protons (H+ ions) into the intermembrane space, and the gradient is converted to chemical energy in the form of ATP, by the membrane bound ATP-synthase. However, brown adipocytes express UCP1, a unique proton transporter localized to the inner mitochondrial membrane. When activated, UCP1 pumps protons from the intermembrane space into the mitochondrial matrix, bypassing the ATP-synthase and effectively uncoupling the electron transport chain, thereby allowing the electrochemical energy to dissipate as heat (Farmer 2008). UCP1 is activated by free FA and is inhibited by purine nucleotides.

Stimulation of the SNS leads to release of NE by nerve endings in BAT. NE then binds to the β3 adrenoreceptors on the plasma membrane of brown adipocytes and activates adenylyl cyclase, accelerating the conversion of ATP to the second messenger cAMP. cAMP

activates protein kinase A, which in turn, phosphorylates and activates hormone sensitive lipase as well as the transcription factor cAMP response element-binding protein (CREB). Phosphorylated hormone sensitive lipase translocates to lipid droplets, where it hydrolyzes the stored triglyceride into FA and glycerol. The release of FA has two purposes: fuel for thermogenesis and as activators of UCP1. In parallel, CREB leads to the activation of PGC1α, which increases UCP1 transcription.

BAT and the pandemic of obesity

Approximately 33% of the global population is obese and another 33% is overweight. Obesity results from caloric intake that exceeds energy expenditure over a prolonged period of time. Most of the excess calories are stored in WAT. Thus, approaches that decrease metabolic efficiency, such as aerobic exercise, are beneficial in avoiding weight gain. Accordingly, DIT in BAT can counteract the obese phenotype (Seale & Lazar 2009) (Figure 1.9). It is important to note that because basal metabolism in BAT, which does not require adrenergic stimulation, is not thermogenic, any pharmaceutical approach to increase the total amount of BAT must also include a method to ensure that the tissue is adequately stimulated, such as by providing adrenergic stimulation. The discovery of adipose-specific β3-adrenoceptors in both mice and humans raised hope that β3-selective agonists could stimulate energy expenditure without producing adverse side effects. Such compounds were effective for the treatment of obesity in rodents but performed poorly in limited clinical trials and suffered from lack of selectivity, low efficacy and poor bioavailability (Lin & Li 2004). On other fronts, polymorphisms in the UCP1 gene with

linkage to obesity are being investigated. In addition, a recent study reports the existence of a muscle-derived hormone, irisin, which is induced by exercise and causes 'browning' of WAT and thermogenesis, without cold or high fat died (HFD) in both mice and humans. Induction of such an agent could be a therapeutic approach to increase BAT thermogenesis

A greater understanding of the molecular regulators of BAT activity and the basis for its presence in some humans but not in others is required to manipulate the huge thermogenic capacity of this tissue. Important questions that remain include the following: Are there genes in addition to UCP1 that perform the uncoupling function? How can the thermogenic capacity of BAT be fully utilized? What is the function of the vasculature besides gas/nutrient exchange and heat dissipation? Would increasing vascular remodeling enhance efficiency of NST in BAT?

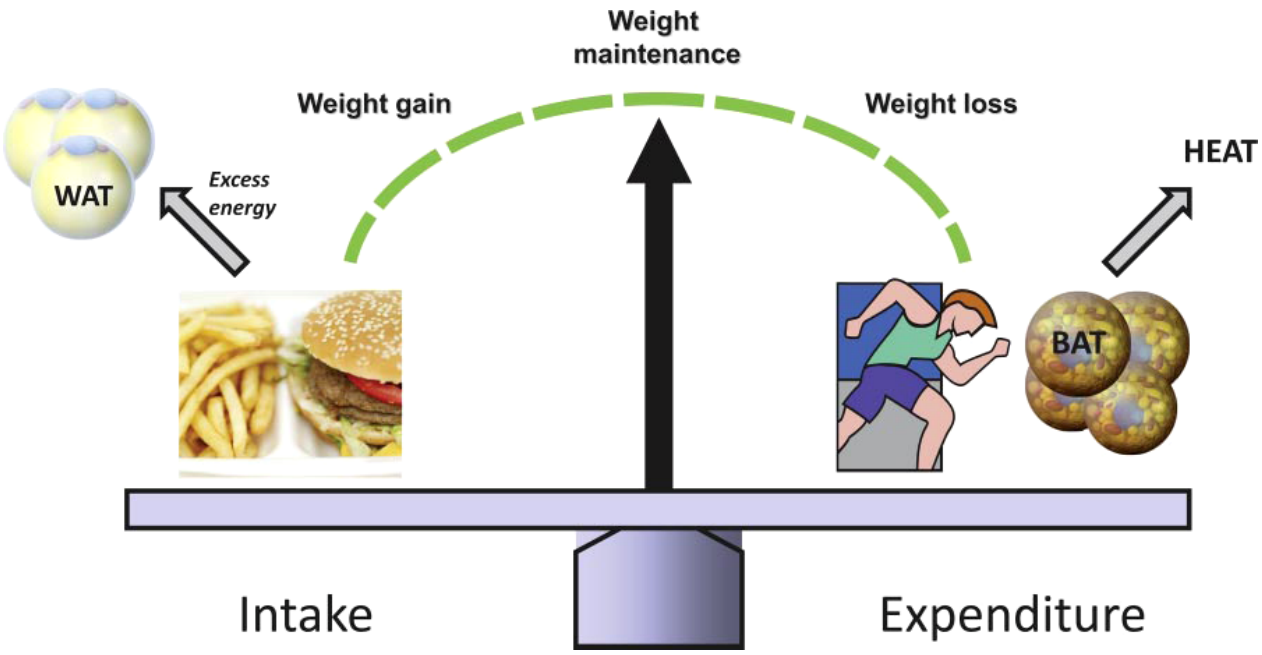

Figure 1.9. **Role of WAT and BAT in energy homeostasis**. Weight gain and obesity are caused by chronic periods of positive energy balance. Energy intake comes from food consumption, whereas is "burnt" through exercise and basic metabolic processes. Studies suggest that BAT activity could impact daily energy expenditure and can thus counteract weight gain if brown adipocytes can be activated by food intake-stimulated release of norepinephrine and "use up" energy to generate heat. Individual variability in the amount or function of this tissue may impact body weight. In addition, therapeutic expansion/activation of this tissue may prove to be an effective therapy for obesity. Reprinted with permission from *Diabetes,* 58:1482-1484,2009.

Angiogenesis

Angiogenesis is defined as the formation of blood vessels from pre-existing vessels and is responsible for the formation of a majority of capillaries both in the embryo and in the adult. During development, angiogenesis commences before the 20 somite stage (E9.5 in mouse) and mediates the dramatic expansion of the vascular plexus, initially formed by vasculogenesis, the *de novo* differentiation of endothelial cells. Most organs acquire their vasculature through a combination of angiogenesis and vasculogenesis. A majority of embryonic blood vessels as well as the vascularization of organs derived from the ectoderm-mesoderm, such as the brain and the kidney, take place via angiogenesis. Angiogenesis is responsible for vessel growth in the adult under normal physiological conditions such as in wound healing, phases of the female reproductive cycle and pregnancy, in skeletal muscle following bouts of exercise, in WAT during adipose tissue expansion, in BAT during adaptive thermogenesis, as well as in pathological conditions such as tumor growth and metastasis and ocular neovascularization.

Much of the research on the mechanisms of angiogenesis was spurred by Judah Folkman's observations in the early 1970's that a tumor did not grow beyond a critical mass (of 2-3 mm^3) without vascularization and the proposal that blocking tumor angiogenesis might be a valid approach to controlling tumor growth (Folkman et al. 1971; Folkman 1971). Fibroblast growth factors (FGF)-1 and 2 and vascular permeability factor/vascular endothelial growth factor (VPF/VEGF)-A were the first tumor derived angiogenic factors purified. Subsequently, many pro- and anti-angiogenic factors have been identified

including additional members of the VEGF family of growth factors, the fibroblast growth factors, semaphorins, the Notch signaling pathway, platelet derived growth factors and the angiopoietins. Ultimately, the balance between pro and anti-angiogenic factors in the tissue determines the growth or quiescence of the vasculature.

Angiogenesis occurs primarily through a process of sprouting from pre-existing vessels, usually venules. Vascular sprouts are led by specialized endothelial "tip cells" that respond to angiogenic stimuli and are connected to endothelial stalk cells that function in tube formation. The progression of angiogenesis is initiated by local destruction of the basement membrane and the dissociation of pericytes from the capillary, followed by migration of tip cells toward an angiogenic stimulus. Proliferation and alignment of endothelial cells follows and an endothelial cell tube forms, establishing a lumen. Pericyte and/or smooth muscle cell association and basement membrane deposition mediate vessel stabilization (for a review, see Patel-Hett & D'Amore 2011).

Adipose Tissue Angiogenesis

It has been long known that adipose tissue is extensively vascularized. In fact, as early as in 1945, a study comparing the vascularity (defined as the ratio of total surface of capillaries to the total volume of tissue supplied) of rat adipose tissue and skeletal muscle demonstrated that WAT exhibited a greater degree of vascularity than muscle (Gersh & Still 1945). BAT is even more richly vascularized that WAT. For optimal thermogenic activity, BAT requires a dense microvasculature to ensure a sufficient rate of perfusion, rapid exchange of oxygen and substrates and efficient distribution of the heat generated.

Link between angiogenesis and adipose function

The close spatial and temporal association between adipogenesis and vascularization requires an intimate cross talk between adipocytes, preadipocytes and endothelial cells. The macro- and micro-vasculature functions as gatekeeper for access of blood borne constituents such as gas, nutrients, hormones and growth factors to adipocytes (Sun et al. 2011; Hausman & Richardson 2004). The vasculature is critical for effective removal of FA released by adipocytes during fasting when the body shifts from using glucose to stored lipids as the primary energy source. Adipose tissue exhibits potent angiogenic capacity; adipose tissue implanted into the avascular rabbit cornea induced robust neovascularization, whereas implants of skeletal muscle and liver did not (Silverman et al. 1988). Moreover, tube-like capillaries sprout from explants of adipose tissue from human and mouse embedded in Matrigel (Gealekman et al. 2008). Conditioned media from differentiated 3T3 adipocytes induced angiogenesis in the chick chorioallantoic membrane angiogenesis assay (Castellot et al. 1982). In fact, long before its angiogenic properties were elucidated, adipose tissue was used by surgeons for wound healing and revascularization of the intestines, the myocardium (McAllister et al. 1951; Vineberg et al. 1965) and the bronchus in human lung transplantation (Silverman et al. 1988). Vascular expansion takes place in BAT during cold acclimation or DIT and angiogenesis is necessary to support the thermogenic activity during this phase. The vasculature of BAT differs from WAT in its response to NE, resulting in a doubling of blood flow in BAT (Orava et al. 2011).

WAT displays potent angiogenic activity *in vivo* and ex vivo, yet several studies have reported a decrease in blood flow and vascular density with obesity, resulting in local

hypoxia (for review, see Goossens 2008). Although HIF1α induction has been documented in WAT of obese patients (Cancello et al. 2005), it appears that hypoxic WAT is incapable of inducing angiogenesis to levels sufficient to compensate for the reduced blood flow observed during the WAT expansion associated with obesity.

Heterogeneity of the adipose vasculature

There is significant heterogeneity among the vasculatures of distinct adipose depots in terms of vessel morphology, capillary density and angiogenic potential. Capillary density varies among different parts of a depot as well as across different adipose depots (Gersh & Still 1945; Hausman & Richardson 2004). The pattern of vascularization of a depot is established very early during fat development and is predictive of the ultimate degree of vascularity in that depot (Crandall et al. 1997). Endothelial cells isolated from different adipose depots also differ in their proliferative capacity (Lau et al. 1996; Lau et al. 1990). The angiogenic activity of adipose varies by depot and possibly by species as well. For instance, there are reports of omental and SC fat implants inducing similar degrees of neovascularization (Silverman et al. 1988) whereas in another study a choloroform-methanol extract of omental, but not SC, depot induced neovascularization in the rabbit corneal pocket angiogenesis assay (Goldsmith et al. 1984). Humans SC fat had a greater angiogenic capacity compared to visceral fat in matrigel-embedded adipose tissue explants. In addition, the capillary density and angiogenic activity of SC, but not visceral, fat decreased with morbid obesity and was negatively correlated with insulin sensitivity (Gealekman et al. 2011).

Adipose lineage

While it is clear that adipose tissue expansion relies on blood vessel formation, the origin of these new vascular cells is unclear. In addition to adipocytes and vascular endothelial cells, adipose tissue contains other cell types such as adipose stromal cells and mesenchymal stem cells. The contribution of adipocyte stromal cells and mesenchymal stem cells to neovascularization is currently being investigated and some reports suggest that endothelial cells of the adipose may be derived from subpopulations of cells with distinct origins depending on the depot, contributing to their heterogeneity, differential gene expression profiles and different responses to treatment. Additionally, a recent study suggests an endothelial origin for murine and human adipocytes. In this study capillary sprouts from adipose tissue explants were shown to express preadipocyte markers and upon PPARγ activation lost their endothelial characteristics and displayed adipocyte features (Khanh-Van Tran et al. 2012).

Angiogenic factors and cross talk between the adipose and vascular cells

At least three cell types in adipose tissue produce angiogenic factors – adipocytes, adipose stromal cells and inflammatory cells. Together, these cells secrete a repertoire of pro- and anti-angiogenic factors, including VEGF-A, FGF-2, leptin, hepatocyte growth factor, insulin like growth factor, TNFα, transforming growth factor β (TGFβ), placental growth factor (PlGF), plasminogen activator inhibitor-1 (PAI-1), VEGF-C, visfatin, resistin, tissue factor, neuropeptide Y, heparin-binding epidermal growth factor, matrix metalloproteases 2 and 9, and granulocyte macrophage colony stimulating factor. While most of these

molecules have been shown to increase angiogenesis, some such as TGF-β and plasminogen activator inhibitor (PAI)-1, can have a pro- or an anti- angiogenic effect depending on their concentration and the tissue context. Additionally, inflammatory cells recruited to growing adipose tissue also secrete high levels of a number of factors such as TNF-α, VEGF, interleukins 1, 6 and 8. Adipose tissue also produces anti-angiogenic factors such as endostatin, thrombospondin-1 and soluble VEGFR2 and these are detected at high levels in overweight and obese patients (for a review, see Yihai Cao 2007).

VEGF, a potent angiogenic factor, is expressed at high levels by both BAT and WAT and accounts for most of the angiogenic activity in adipose tissue (Zhang et al. 1997; Fukumura et al. 2003). The role of VEGF in adipose tissue angiogenesis is covered in greater depth later in this chapter.

The adipokine visfatin is elevated in the serum of obese subjects and patients with type 2 diabetes. Visfatin induces endothelial cell proliferation and angiogenesis by increasing the expression of VEGF and VEGFR2 as well as MMP -2 and -9 via the PI3K/Akt and MAPK1/2 pathways (Adya et al. 2008). In addition, visfatin has a cardioprotective effect during myocardial infarction and plays a protective role in non-alcoholic fatty liver disease (Rosen & Spiegelman 2006).

The hormone leptin produced by adipocytes regulates food intake and energy homeostasis and it dysfunction leads to severe obesity, diabetes and infertility. Leptin also stimulates angiogenesis by binding to the leptin receptor in endothelial cells and induces tube formation *in vitro* and corneal neovascularization. In addition to its direct angiogenic activity, leptin stimulates angiogenesis synergistically with both FGF-2 and VEGF, and

endothelial fenestrations and vascular permeability with VEGF, although the exact mechanism of this synergistic interaction is not known (Cao et al. 2001).

PAI-1 has been shown to regulate endothelial cell migration *in vitro*. During embryonic adipose development, PAI-1 is secreted along with αvβ3 integrin by human preadipocytes and endothelial cells thus providing a mechanism for the formation of the organs as preadipocytes can migrate with the endothelial cells during angiogenesis (Crandall et al. 2000). PAI-1 can both positively and negatively regulate angiogenesis depending on dosage (Devy et al. 2002).

There are several additional examples of paracrine communication between endothelial cells and adipocytes. Media conditioned by endothelial cells promotes preadipocyte proliferation and extracellular matrix components secreted by endothelial cells stimulate preadipocyte differentiation *in vitro*. VEGF-B, which is highly expressed by BAT and skeletal muscle, signals through VEGFR1 and Nrp1 on the endothelium to regulate transcription of vascular FA transport proteins, which control FA uptake by the endothelium and thus its availability to the vascularized BAT or muscle (Hagberg et al. 2010). PPARγ agonist rosiglitazone increases formation of angiogenic sprouts from adipose tissue explants but not from aortic explants, and this is mediated via upregulation of angiopoietin-like factor 4 and VEGF in adipocytes (Gealekman et al. 2008). Similarly, results of a randomized clinical trial reported that adipose tissue from patient biopsies cultured on Matrigel had increased capillary density and enhanced angiogenic sprout formation following treatment with rosiglitazone (Gealekman et al. 2012) .

Tweaking the vasculature

In light of the demonstrated angiogenic capacity of adipose tissue, the close spatiotemporal coordination of adipogenesis and angiogenesis, and the multiple examples of paracrine interactions between adipocytes and endothelial cells, it is not surprising that a majority of obesity-associated disorders are coupled with vascular dysfunction. Pathological obesity is generally associated with a failure of vascular remodeling to keep pace with the expanding adipose tissue (Sun et al. 2011). This raises the prospect of regulating the expansion of adipose tissue by manipulating its vasculature as a novel therapeutic approach to obesity and associated metabolic comorbidities, especially type II diabetes. Numerous studies have investigated this possibility including: (i) application of broad spectrum anti-angiogenic peptides, such as endostatin and angiostatin (O'Reilly et al. 1994; O'Reilly et al. 1997); (ii) use of the small molecule TNP-470, which inhibits endothelial cell proliferation *in vitro* and angiogenesis *in vivo* (Morita et al. 1994; Wang et al. 2000); (iii) targeted induction of apoptosis in the vasculature of white adipose tissue using a pro-apoptotic homing peptide; and, (4) administration of anti-VEGF or anti-VEGF receptor antibodies to murine models of HFD-induced and genetic obesity using the LepR deficient *ob/ob* mice (Tam et al. 2009; Sun et al. 2012; Elias et al. 2012; Lu et al. 2012). In each case, administration of these anti-angiogenic agents resulted in a dose dependent and reversible reduction in weight and adipose tissue without significantly affecting food intake (Rupnick et al. 2002). Interestingly, administration of TNP-470 also demonstrated additional signs of improved metabolic health such as reduced serum low density lipoprotein levels and increased insulin sensitivity, signs of a treatment that would be important in preventing the development of type II diabetes in

obese subjects (Bråkenhielm et al. 2004). Induction of apoptosis in the vasculature of WAT in obese mice by targeting prohibitin, a specific marker of the adipose vasculature, resulted in ablation of the adipose and reduced body weight along with normalization of metabolism through increased insulin sensitivity and glucose tolerance (Kolonin et al. 2004). As prohibitin is also found in human WAT vasculature, this opens up the possibility of prohibitin as a therapeutic target that might lead to the destruction of WAT leaving the BAT and other organs unaffected.

Studies of anti-VEGF treatment in *ob/ob* mice, which are obese and have preexisting adipose tissue dysfunction, demonstrated that VEGF blockade led to improved metabolism through reduced weight gain, reduced adipocyte size, increased insulin sensitivity and decreased inflammatory factors. But anti-VEGF treatment during the early stages of HFD-induced adipose tissue expansion resulted in poor metabolic health, no weight change and reduced glucose tolerance (Sun et al. 2012; Tam et al. 2009). On the other hand, VEGF overexpression during early stages of HFD improved metabolic health by increasing insulin sensitivity, energy expenditure and lipid clearance while reducing hepatic steatosis (Elias et al. 2012). VEGF overexpression also resulted in "browning" of WAT and increased thermogenesis, which likely contributed to the increased energy expenditure observed in these mice. Notably, these studies demonstrate that the consequences of modulating angiogenesis on obesity and metabolic health are context-dependent: pro-angiogenic activity during early stages of adipose tissue expansion is beneficial, associated with protective effects on metabolism, whereas in the context of preexisting adipose tissue dysfunction anti-angiogenesic therapy was required to improve metabolic conditions.

Vascular Endothelial Growth Factor

VEGF-A (hereafter referred to as VEGF) was first purified in 1983 from the ascites fluid of guinea pig tumor on the basis of its potent ability to increase vascular permeability and known as vascular permeability factor (Senger et al. 1983) and soon after, from the conditioned media of folliculostellate cells as an endothelial cell specific mitogen (Ferrara & Henzel 1989). VEGF was subsequently determined to be a key regulator of angiogenesis.

Family

The VEGF family, of which VEGF-A is the founding member, is comprised of a number of secreted cysteine-knot glycoproteins including VEGF-A, VEGF-B, VEGF-C, VEGF-D, VEGF-E and PlGF. VEGF-B has been shown to play a central role in cardiac angiogenesis and was recently demonstrated to control endothelial FA uptake (Hagberg et al. 2010). VEGF-C and VEGF-D promote lymphatic vessel development whereas PlGF has been studied primarily in pathological conditions where it is thought to stimulate angiogenesis in coordination with VEGF-A. The VEGF family also consists of lesser known members such as VEGF-E, which was identified in certain viruses, the snake-venom derived VEGF-F and endocrine gland (EG)-VEGF, which acts only on endocrine gland endothelial cells. The VEGF family members are biologically active as homodimers although naturally occurring heterodimers of VEGF-A and PlGF have been reported.

Structure

Alternative splicing of the human VEGF gene produces eight isoforms, with the most abundant and well-studied isoforms being VEGF 121, 165 and 189 (120, 164 and 188 in mouse and rat). The isoforms differ in their ability to bind heparan sulfate and neuropilin-1 (for a review see Patel-Hett & D'Amore, 2011). Charged domains in VEGF164 and VEGF188 mediate their binding to heparan sulfate proteoglycans on the cell surface and in the extracellular matrix, where they may be sequestered and function locally. VEGF120 lacks these charged domains, so is freely diffusible and able to function at sites distant from the secreting cell. The distribution of VEGF isoforms varies among tissues, suggesting that different isoforms may play distinct roles in vascular development and in the adult (Ng et al. 2001) (Figure 1.10). This notion was substantiated by the distinct phenotypes of mice that were engineered to express single isoforms of VEGF (Carmeliet et al. 1999; Stalmans et al. 2002).

VEGF receptors

VEGF binds to the tyrosine kinase receptors VEGFR1 (also called Flt-1) and VEGFR2 (also known as Flk-1 or KDR in humans). VEGFR1 and VEGFR2 are 44% homologous at the amino acid level and each contains three functional domains – seven IgG like repeats in the extracellular domain, a single trans-membrane region and a cytoplasmic tyrosine kinase domain. Following VEGF binding, mediated by the second and third IgG repeats, the

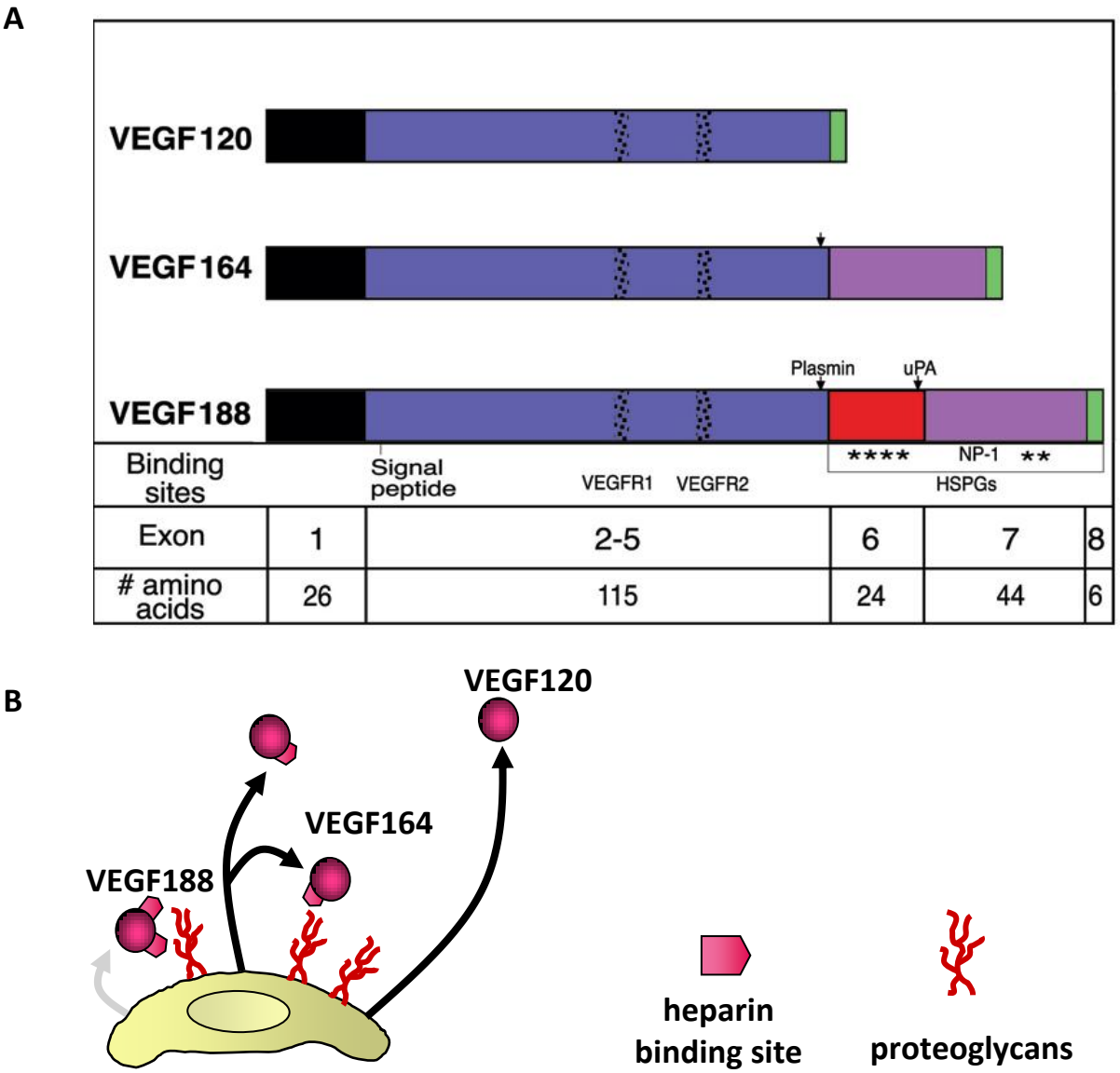

Figure 1.10. **VEGF isoforms and their localization. (A)** VEGF isoforms with their exons along with important properties of each exon. Binding to VEGFR2 and VEGFR1 is mediated by exons 1 through 5, Nrp1 binding by exon 7 and heparan sulfate binding by exons 6 and 7. As VEFG120 lacks both the above exons, it does not bind to heparan sulfate, while VEGF188, possessing both exons 6 and 7, tightly binds heparan sulfate, and VEFG164 binds heparan sulfate but to a lesser extent compared to VEGF188. **(B)** Differences in diffusibility of VEGF isoforms due to their differential ability to bind heparan sulfate proteoglycans. As VEGF120 does not bind heparan sulfate, it is readily diffusible and can function at a site distant from its site of production. VEGF188 strongly binds heparan sulfate, which is present in the cell membrane and extracellular matrix, and is thus contained within the juxtracrine vicinity of the secreting cell. VEGF164 binds heparan sulfate as well, but not as strongly as VEGF188 and thus can function locally as well as at a distance, and is the most abundant isoform. Image courtesy of P. D'Amore, unpublished.

receptors homo- or heterodimerize, which leads to activation of their kinase activity, autophosphorylation of multiple tyrosine residues and initiation of downstream signaling. While both receptors have high affinity for VEGF, VEGFR2 has ten-fold stronger tyrosine kinase activity compared to VEGFR1.

VEGFR2, thus, is the primary signaling receptor for VEGF, initiating several signaling cascades including phosphatidyl inositol 3-kinase, mitogen activated protein kinase, protein kinase C, AKT and phospholipase C pathways, leading to increases in endothelial proliferation, migration, MMP expression, survival and cell permeability. The critical role of this receptor is reflected in the fact that homozygous knockout of VEGFR2 leads to embryonic lethality at E8.5–9.5 due to defects in the development of hematopoietic and endothelial cells and the absence of yolk sac vasculature (Shalaby et al. 1995). Initially thought to be specific for endothelial cells, subsequent studies have reported expression of VEGFR2 in multiple non-endothelial cell types such as myocytes and kidney podocytes (Bryan et al. 2008; Guan et al. 2006).

With its high affinity for VEGF but weak tyrosine kinase activity, it is believed that VEFGR-1 functions as a “decoy” receptor, sequestering VEGF, thereby modulating signaling through VEGFR2 (Clauss 1998). In support of this, mice deficient for VEGFR-1 are embryonic lethal around E8.5 due to overgrowth of endothelial cells and impaired blood vessel formation (for a review see Nieves et al. 2009). In addition to the full-length membrane-bound form, VEGFR1 also exists as an alternatively spliced, soluble form (sVEFGR1 or sFlt1). sFlt1 binds VEGF with higher affinity than VEGFR2 and is implicated as a negative regulator of angiogenesis. The complexity of VEGFR-1 biology is underscored by the fact that even

though it is not thought to signal in endothelium, it has been shown to function in several non-endothelial cell types, including breast cancer cells and macrophages and monocytes. VEGF receptors also reportedly heterodimerize with neuropilin-1 and 2. While neuropilins enhance VEGFR-2 mediated signaling, it is unclear whether they are capable of independent signaling.

Expression

Using a mouse in which LacZ had been knocked into the VEGF locus, VEGF expression was shown to commence before gastrulation and was detectable at all stages of vascular development in the embryo (Miquerol et al. 1999). The cellular distribution and the extent of VEGF expression indicate its pleiotropic role in development. High levels of expression appeared to be associated with vasculogenesis and permeability, whereas lower levels were associated with angiogenesis and cell migration. In addition, VEGF was demonstrated to be expressed in a subtype of endothelial cells present in the endocardium (Miquerol et al. 1999). In the brain and the kidney, organs which are vascularized by angiogenesis, VEGF expression was detected by *in situ* hybridization around E16-17. Moreover, a tight spatial coordination was observed between the expression patterns of VEGF and VEGFR-2 and while VEGF was expressed by a wide variety of embryonic cells, VEFGR-2 expression was confined to the endothelium. In the adult, VEGF is expressed in a cell-specific manner in nearly all vascularized adult tissues including select endothelium, and VEGFR2 is constitutively phosphorylated across several tissues *in vivo*. The pattern of VEGF

expression is unique in each organ; in white and brown adipose tissue VEGF is produced by adipocytes, adipose stromal cells and inflammatory cells.

Function in endothelial cells

Tumor cells as well as epithelial and mesenchymal cells during development and in the adult secrete VEGF and it expression is further induced by hypoxia and other stimuli. Upon binding to VEGF receptors on the nearby endothelium, VEGF initiates angiogenesis and stimulates recruitment of newly formed blood vessels to the source tissue. VEGF promotes angiogenesis by inducing endothelial cell proliferation, migration, survival, extracellular matrix degradation, formation of fenestration and cell permeability. This process occurs extensively during embryonic angiogenesis and during physiological and pathological angiogenesis in the adult. During development, VEGF is essential for both vasculogenesis and angiogenesis. Vascular development is dependent on tight regulation of VEGF as deletion of a single VEGF allele in mice results in early embryonic lethality (by E9.5) due to severe vascular defects (Carmeliet et al. 1996; Ferrara et al. 1996), whereas slight overexpression of VEGF similarly results in embryonic lethality around E12.5 (Miquerol et al. 2000).

Early studies of VEGF neutralization in mouse tumor models (Kuo et al. 2001) revealed no obvious side effects, suggesting that VEGF is not required in the adult and making it an attractive target for the treatment of a variety of diseases. As a result, many agents have been designed to target either VEGF or its receptors. Though beneficial effects have been observed, particularly for use in the treatment of ocular angiogenesis, the

development of significant side effects suggest that VEGF is important in the maintenance of adult vasculature and non-vascular tissues. Indeed, several studies have demonstrated that one important role of VEGF in the adult is in the induction and maintenance of fenestrated capillaries, as blockage of VEGF signaling resulted in capillary regression in several organs including choroid plexus, thyroid, pancreatic islets and epididymal fat (Kamba et al. 2006), and loss of alveolar, tracheal, and peritubular capillary endothelium.

Function in non-endothelial cell types

Although VEGF was initially thought to target only endothelial cells, numerous studies have identified roles for VEGF on a wide range of non-endothelial cell types. VEGF is essential for the maintenance of choroid plexus structure and integrity, including ependymal cell function (Maharaj et al. 2008). VEGF also promotes Müller cell survival through autocrine signaling, has a paracrine neuroprotective effect on photoreceptors (Saint-Geniez et al. 2008), functions in an autocrine loop to promote the survival of kidney podocytes (Guan et al. 2006), as well as the maintenance of the retinal pigmented epithelium (Ford et al., 2011) skeletal muscle (Bryan et al. 2008), bone differentiation (Mayer et al, 2005) and in the structural and functional maintenance of arterial neuro-effector junctions.

VEGF in white and brown adipose

While adipocytes secrete a number of angiogenic factors, it has been demonstrated that VEGF mediates most of the angiogenesis in adipose tissue in both white and brown adipose tissue (Zhang et al. 1997; Fukumura et al. 2003). Conditioned media from

endothelial cells grown in the presence of VEGF promoted adipocyte differentiation *in vitro* more robustly compared to conditioned media without VEGF or with both VEGF and VEGF-neutralizing antibodies. This indicates that VEGF secreted by adipocytes functions in a paracrine manner by signaling through VEGFR2 on endothelial cells, which in turn secrete adipokines that promote adipogenesis *in vivo* and *in vitro* and its blockage prevented both adipose tissue neovascularization and adipogenesis (Fukumura et al. 2003) VEGF is also required for angiogenic plasticity of expanding WAT in murine models of HFD-induced obesity. From recent studies (described earlier in this chapter) it appears that the effect of VEGF in adipose tissue expansion and overall metabolic health may be context dependent: in the early stages of HFD increased VEGF expression facilitates healthy adipose tissue expansion and confers protection from metabolic insults, whereas in the context of pre-existing adipose tissue dysfunction blockage of VEGF signaling leads to improved insulin sensitivity and metabolic health (Sun et al., 2012).

Multiple reports have demonstrated that brown adipocytes express VEGF *in vivo* and *in vitro* and VEGF expression is lower in the BAT of genetically obese rats (Tonello et al. 1999; Asano et al. 1997). VEGF expression increases in primary rat preadipocytes differentiated to brown adipocytes, whereas there was a slight decrease in the expression of VEGF-B and C (Asano et al. 2001). VEGF expression in BAT increases upon adrenergic stimulation resulting from cold exposure or injection of β-adrenergic receptor agonists.

This VEGF expression is independent of the hypoxia that results from intense oxygen consumption during thermogenesis mediated by UCP1 as UCP1-null animals also displayed increased VEGF expression and angiogenesis following cold exposure. VEGF transcription in

brown adipocytes induced by NE is mediated by NE is mediated by cAMP and protein kinase A (PKA) (Fredriksson et al. 2000; Fredriksson et al. 2005; Xue et al. 2009). Further, a recent study has shown that exercise induced transcription of VEGF in skeletal muscle is mediated by PGC1α and is independent of HIF1α (Arany et al. 2008). Thus, it is possible that PGC1α also regulates hypoxia -independent VEGF expression in BAT.

Interest in its potential for weight control has led to significant work on the effect of VEGF neutralization in WAT, but very little is known on the role of VEGF in brown adipose. While there are several reports of VEGF expression in BAT and its role in promoting angiogenesis during cold acclimation, detailed analysis of the dynamics of this expression are not known. There are also no reports of expression of VEGF receptors in brown adipocytes, which forestalls investigation on the role of VEGF, if any, on brown adipocytes themselves, in addition to its role on the BAT endothelium. Adipose tissue is very plastic throughout adult life, yet adipose-derived tumors are rare, suggesting that both adipose tissue and its microvasculature are tightly regulated. Thus my aim was to study the dynamics of VEGF as well as VEGF receptor expression in white and brown adipocytes, hypothesizing that both are tightly coordinated during adipogenesis. I also hypothesized that VEGF must play a functional role in either white or brown adipocytes, depending on the VEGF receptor expression and activation in these cells, in addition to supporting adipose angiogenesis.

Chapter 2

EXPRESSION OF VEGF AND VEGF RECEPTORS IN WHITE AND BROWN ADIPOSE

Introduction

While there are multiple reports of VEGF production in white and brown adipocytes, detailed analysis of the dynamics of this expression during phases of adipocyte differentiation is lacking. VEGF expression has been shown to increase with differentiation of multiple cell types such as kidney podocytes, osteoblast differentiation and myocyte differentiation (Bryan et al. 2008; Guan et al. 2006; Mayer et al. 2005). In light of the fact that adipose tissue is a very plastic organ that undergoes adaptive tissue growth, like skeletal muscle, I hypothesized that VEGF expression increases during brown and white adipocyte differentiation. I also hypothesized that VEGF receptor expression on brown and/or white adipocytes would be indicative of a direct functional role of VEGF signaling in these cells. Therefore, in this chapter I have explored the expression of VEGF and VEGF receptors in white and brown adipocytes.

Results

VEGF and its receptors are expressed in BAT and all major WAT depots

The expression of VEGF and its receptors in brown adipose tissue (BAT) and white adipose tissue (WAT) were analyzed by RT-PCR in interscapular BAT as well as subcutaneous (SC) WAT from the inguinal region and visceral WAT from mesenteric, perigonadal (PG) and retroperitoneal depots of adult male mice (Figure 2.1). VEGF mRNA was detected in all BAT and WAT depots, with the highest expression in BAT, followed by SC and PG depots; all

expressed each of the three major VEGF isoforms. Mesenteric and retroperitoneal depots expressed lower levels of VEGF, mostly as the 164 isoform. VEGFR2 was expressed robustly in BAT, followed by PG and SC. Low expression was detected in the mesenteric depot whereas there was no detectable VEGFR2 in the retroperitoneal depot. VEGFR1 expression was similar to that of VEGFR2.

VEGF expression increases during 3T3L1 differentiation

To investigate the temporal relationship between VEGF expression and white adipocyte differentiation I examined the expression of VEGF in the 3T3L1 system, an established and well characterized model of *in vitro* white adipocyte differentiation (Green & Kehinde 1975). 3T3L1 preadipocytes were grown to confluence in Dulbecco's modified Eagle's medium (DMEM). Forty-eight hours after the cells reached confluence, adipocyte differentiation as induced by replacing the growth medium with DMEM containing insulin, dexamethasone, IBMX and fetal bovine serum (FBS) (Figure 2.2). Distinct morphological changes were observed as the 3T3L1 cells underwent differentiation; the cells changed in shape from a fibroblast-like appearance to spherical, lipid-containing cells. Intracellular lipid droplets were visible by light microscopy by the fifth or sixth day of differentiation, and increased in number and size. By day twelve of differentiation, more than 95% of cells had one or more large droplets (Figure 2.3A). The droplets were confirmed histochemically as lipid containing by staining with Oil Red O, which stains triglycerides and lipids (Figure 2.3B, left), and by the immunofluorescence (IF) with antibody to perilipin, an adipocyte marker that coats and protect lipid droplets from hydrolysis (Figure 2.3B, right).

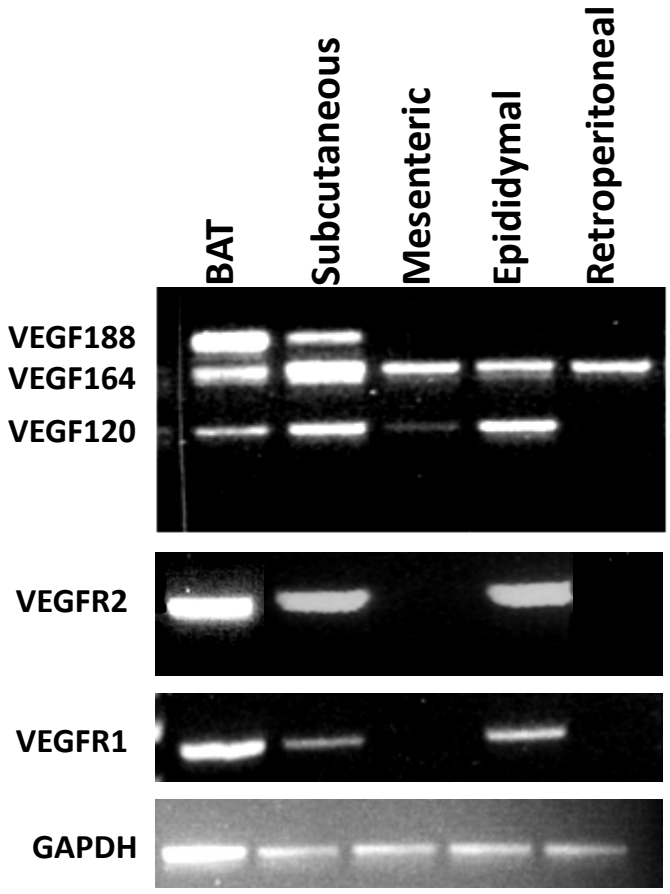

Figure 2.1. **VEGF and VEGF receptor levels in adipose depots.** mRNA expression of VEGF and receptors, VEGFR2 and VEGFR1, in BAT and subcutaneous, mesenteric, epididymal and retroperitoneal WAT depots of adult male mouse were measured by RT-PCR.

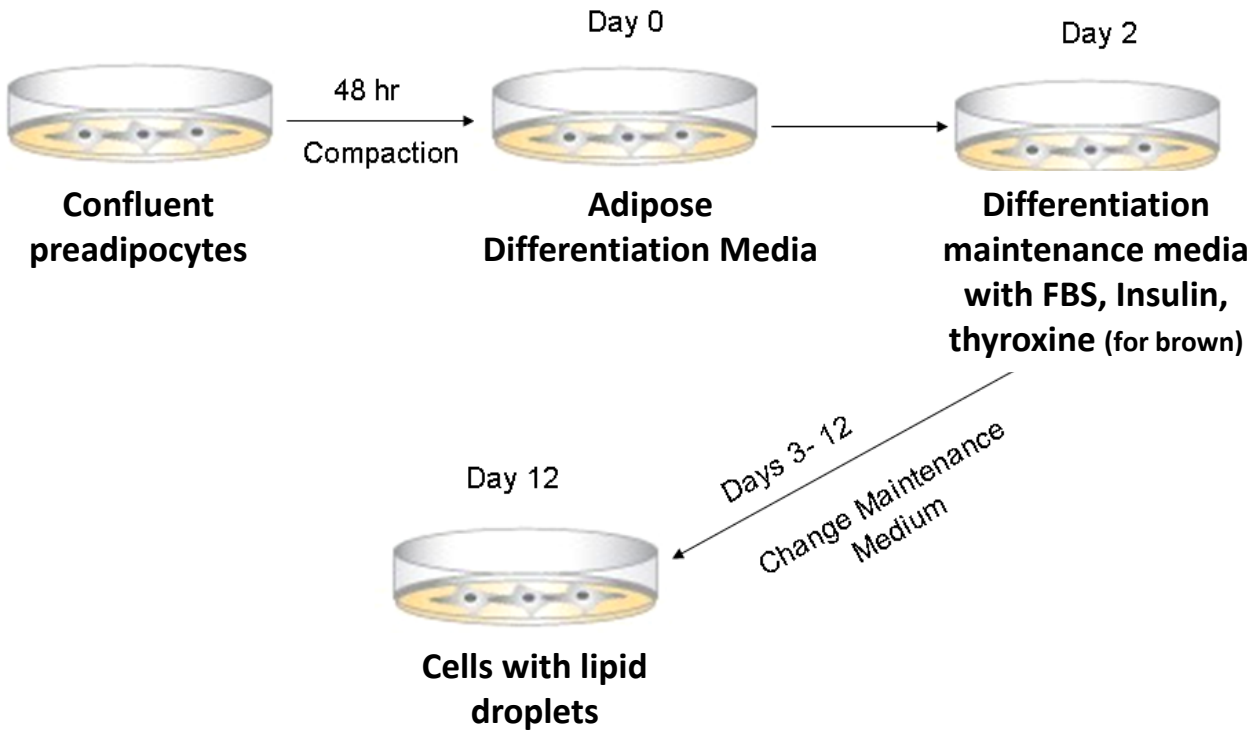

Figure 2.2. **Schematic representation of 3T3L1 and brown preadipocyte differentiation.** Undifferentiated preadipocytes were cultured for 48 hours beyond confluence in the growth media. On day 0, the media was replaced with adipose differentiation media, comprised of growth media supplemented with insulin, dexamethasone and isobutylmethylxanthine. After 48 hours, the differentiation media was replaced with differentiation maintenance media containing insulin. Cells were maintained in the maintenance media until fully differentiated judged by their morphology and accumulating lipid droplets (10-12 days for white adipocytes and 7-9 for brown adipocytes), replacing media every other day.

RNA was isolated from the cells at different time points during differentiation and analyzed by qRT-PCR for markers of adipocyte differentiation. Expression levels of the transcription factor PPARγ, which is essential for adipocyte differentiation, increased nearly eight-fold by day four compared to the beginning of differentiation (day zero) and rose steadily to a 15-fold increase by day twelve (Figure 2.4A, left). The expression of aP2, an adipocyte-specific fatty acid binding protein and well-characterized marker of adipocyte differentiation, increased 20-fold from day zero levels by day four and remained elevated through the 12 days examined (Figure. 2.4A, right). Analysis of VEGF mRNA levels in the differentiating 3T3L1 cells showed a five to seven - fold increase between days eight and 12 relative to levels at day zero (Figure 2.4B). Absolute quantification of VEGF isoforms using isoform-specific primers indicated that the level of each isoform increased with differentiation, with VEGF 164 the most abundant isoform at 50% of the total VEGF, VEGF 188 about 35% and VEGF 120 accounting for 15% of the total VEGF in mature differentiated 3T3L1 adipocytes (Figure 2.4C). This result demonstrates that VEGF expression increases concomitantly with adipose differentiation and is consistent with the notion that VEGF expression is coordinately regulated as part of the process of white adipocyte differentiation.

There was greater than 10-fold decrease in VEGFR2 levels by day four of differentiation and the levels remained low throughout differentiation (Figure 2.5A, left). There was no significant change in VEGFR1 expression during differentiation (Figure 2.5A, right). This was in contrast to mature primary adipocytes isolated from both inguinal and

epididymal fat pads of adult mice, and demonstrated to be mature adipocytes by expression of aP2, which showed robust expression of both VEFGR2 and VEGFR1 (Figure 2.5B). In an attempt to reconcile the difference, I examined isolated primary adipocytes for potential contamination by endothelial cells, which express VEGFR2 and should have separated with the stromal-vascular fraction during the isolation process. Immunofluorescence localization of the adipocyte marker perilipin and the endothelial cell marker endomucin (Kuhn et al. 2002), revealed unilocular white adipocytes with strong perilipin localization as single cells or in clumps of two-three cells. However, in a fraction of these clumps, several endomucin-positive endothelial cells were also observed (Figure 2.5C). Analysis of VEGFR2-LacZ mouse did not reveal VEGFR2 expression in white adipocytes, whereas endothelial VEGFR2 expression was observed in lungs. IHC localization of VEGFR2 did not detect any VEGFR2 on either SC or PG WAT depots (data not shown). These data indicated that VEGFR2, the primary VEGF signaling receptor, was not present in detectable levels in white adipocytes.

VEGF expression increases during brown adipocyte differentiation

To study VEGF expression during brown adipocyte differentiation I utilized an immortalized murine brown preadipocyte cell line, derived from neonatal brown adipocyte precursors, that has been shown to differentiate into brown adipocytes *in vitro* (Fasshauer et al, 2000). Brown preadipocytes were grown to confluence in DMEM and induced to differentiate as described for the 3T3L1 cells above (Figure 2.2). Intracellular lipid droplets

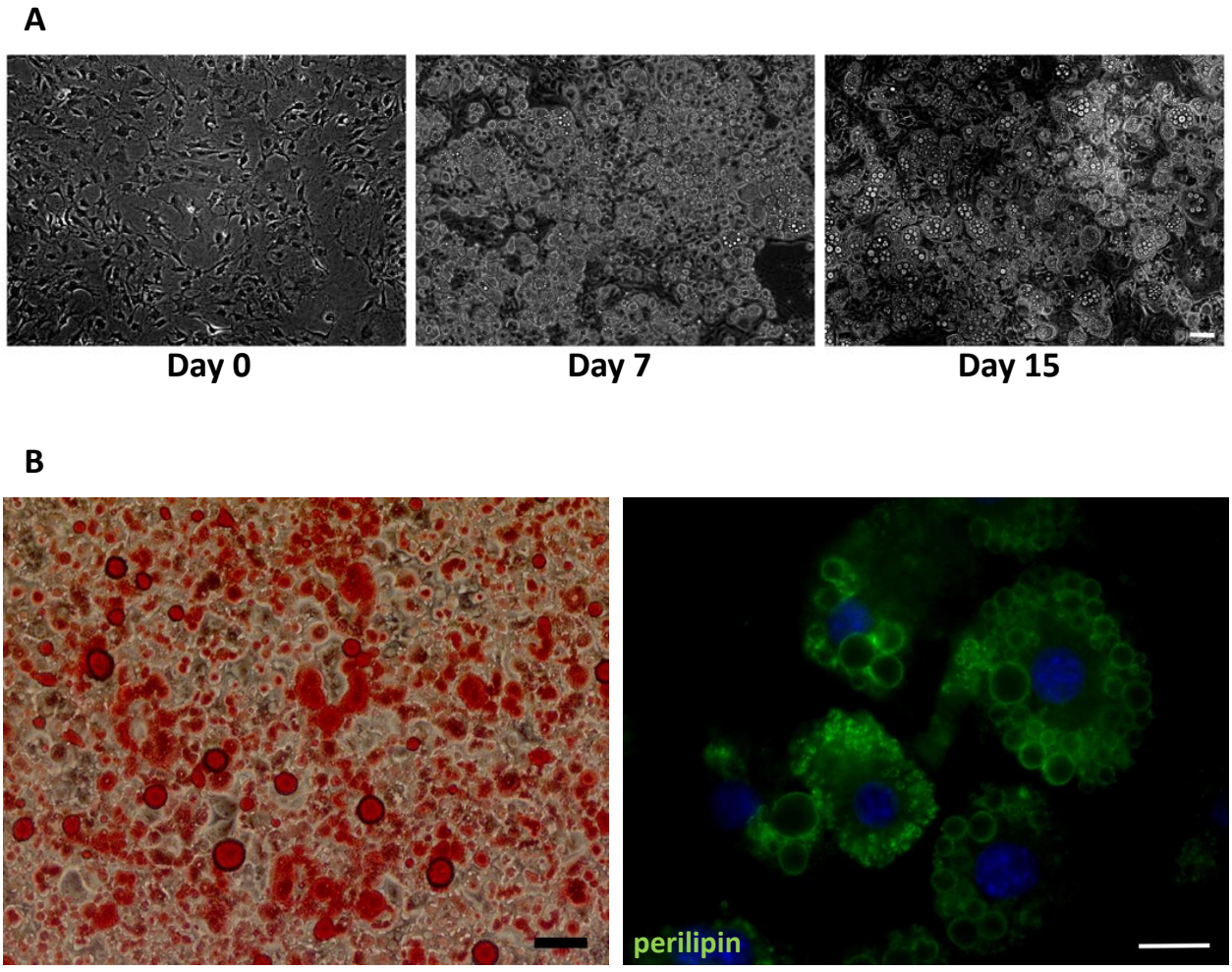

Figure 2.3. **Morphological and functional changes during 3T3L1 differentiation. (A)** Change in cell morphology from a fibroblast like appearance to cuboidal shape with accumulation of lipid during differentiation **(B)** Uptake of Oil Red O by triglycerides (bottom panel, left) and expression of perilipin (bottom panel, right) in differentiated adipocytes. Nuclei visualized by DAPI. Scale bar represents 50 µm.

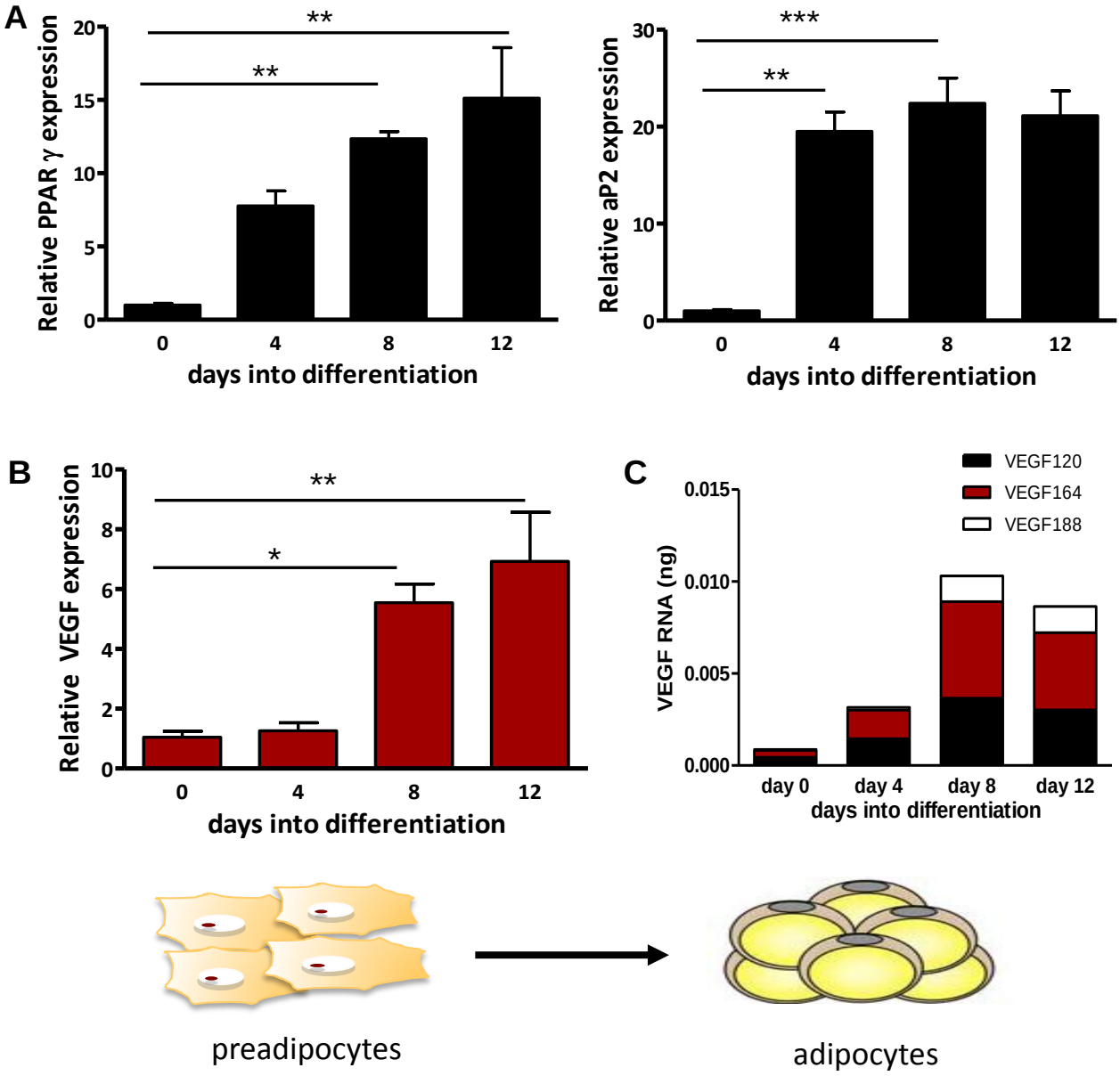

Figure 2.4. **Increase in VEGF expression during 3T3L1 differentiation (A)** Expression of adipocyte markers PPARγ (left) and aP2 (right). **(B)** VEGF expression increases during adipocyte differentiation along with adipocyte marker expression, quantified using quantitative PCR (qPCR) **(C)** Absolute quantification of VEGF isoforms during differentiation using qPCR with isoform specific primers. p*<0.05, p**<0.01, p***<0.001.

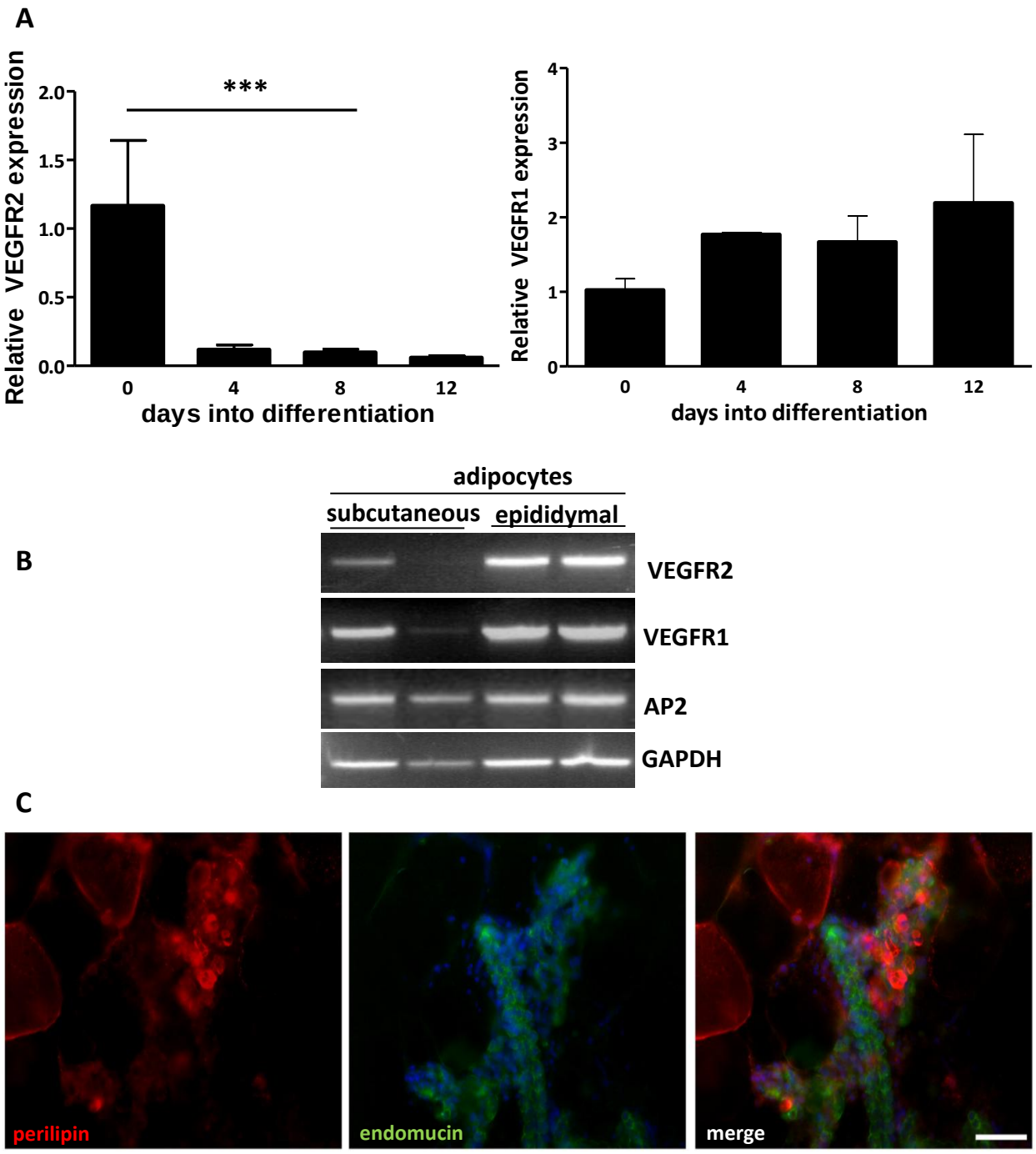

Figure 2.5. **VEGFR2 expression in white adipocytes *in vivo* and *in vitro* (A)** VEGFR2 expression decreases during 3T3L1 differentiation while VEGFR1 expression is not significantly changed, quantified using qPCR **(B)** VEGF receptor expression in white adipocytes isolated from subcutaneous and perigonadal WAT of two groups of wild type male mice **(C)** IF was performed on isolated adipocytes with the adipocyte marker, perilipin, and endothelial marker, endomucin, to determine whether there was contamination by stromal-vascular fraction. Representative images indicate that adipocytes isolated had some contamination with vascular endothelial cells. Nuclei visualized by DAPI . p***<0.001.

were visible as early as day three of differentiation and by day six, more than 95% of cells had multiple lipid droplets, morphologically resembling their *in vivo* counterparts (Figure 2.6A). The differentiation of brown adipocytes is accompanied by increased mitochondrial biogenesis. Accordingly, mitochondria in differentiated brown adipocytes were visualized using CMTM Rosamine MitoTracker, a mitochondria-specific vital dye, and lipid droplets were visualized by IF staining for perilipin (Figure 2.6B). RNA isolated from the cells at different time points during differentiation was analyzed by qRT-PCR for markers of adipocyte differentiation. Levels of PGC1α, a key regulator of brown adipocyte differentiation and of mitochondrial biogenesis, increased as early as day three of differentiation and the elevated levels were maintained throughout differentiation (Figure 2.7A, left). The expression of UCP1, a protein essential for brown adipocyte thermogenesis, was increased 50-fold by day six and 170-fold by day eight (Figure 2.7A, center). The expression of β3 adrenoreceptor, which is more abundant in brown adipocytes compared to the β1 and β2 isoforms and is important for activation of BAT by the sympathetic nervous system, was increased 30-fold by day three and 100-fold by day eight (Figure 2.7A, right). Analysis of VEGF mRNA expression by qPCR at various time points during differentiation demonstrated that brown preadipocytes expressed VEGF and that VEGF levels were increased by 2.5- to 3-fold over the course of differentiation (Figure 2.7B). Of the three VEGF isoforms, VEGF164 was the most abundant isoform whereas low levels of VEGF188 and 120 were also detected. VEGF164 constituted 90% of total VEGF at day zero and rose to 98% of total VEGF by day eight. While levels of VEGF120 also increased during the course of

differentiation, it decreased from approximately 10% of the total at day zero to about 1% at day eight. VEGFR2 was expressed by both brown preadipocytes as well as differentiated brown adipocytes, with the level of expression being slightly lower in the more differentiated cells. VEGFR1 was also expressed in brown preadipocytes and differentiated brown adipocytes. Additionally, Nrp1 was expressed by both undifferentiated cells and differentiated brown adipocytes (Figure 2.7D). As was observed for white adipocytes, these data suggest that VEGF expression may be coordinately regulated with the process of brown adipocyte differentiation. Moreover, the expression of VEGF receptors in both preadipocytes and differentiated brown adipocytes raises the possibility of an autocrine role for VEGF in these cell types.

VEGF expression increases in brown adipocytes following adrenergic stimulation

To test whether VEGF expression in BAT increases as a result of acute adrenergic stimulation adult mice were injected with the adrenergic receptor agonist CL 316243 (CL), which is specific for the β3 receptor isoform. BAT RNA was isolated from the mice at 2, 6 and 24 hours post injection. I first analyzed by qRT-PCR for known effectors of adrenergic stimulation in BAT. UCP1 mRNA levels doubled rapidly compared to control within two hours of injection and remained elevated at twenty four hours. PGC1α mRNA expression increased rapidly following CL injection, rising to 18-fold over control mice 2 hours after injection, and returned to baseline levels by twenty four hours post-injection (Figure 2.8A, left). The upregulation of VEGF expression by adrenergic stimulation followed a similar

pattern to that of PGC1α, peaking at 1.7-fold over control at 2 hours and showed a slight but consistent decrease by 24 hours post injection (Figure 2.8B). VEGF 164 and 188 were the most abundant isoforms, constituting 60% and 40% of total VEGF mRNA, respectively, while little or no VEGF 120 was detected. Following CL injection, proportion of VEGF 164 increased slightly from 60% to 75% of total VEGF whereas the level of VEGF 188 isoform decreased accordingly (Figure 2.8C).

To investigate whether the increase in VEGF expression measured in BAT following adrenergic stimulation was a direct effect on the brown adipocytes, brown adipocytes differentiated *in vitro* were treated with norepinephrine (NE) for 1 hour. As expected, the levels of PGC1α and UCP1 mRNA increased eight- and fourteen-fold, respectively, compared to untreated control cells (Figure 2.9A). Similar to the observations *in vivo*, there was a nearly 3-fold increase in the expression of VEGF mRNA within 1 hour of treatment compared to untreated cells (Figure 2.9B). These results indicate that quiescent (unstimulated) BAT expresses VEGF, which is elevated following adrenergic stimulation. The *in vitro* data shows that the increased VEGF expression in BAT following adrenergic stimulation is derived, at least in part, from brown adipocytes indicating that elevated VEGF expression was a direct effect of NE/β adrenergic agonists on brown adipocytes.

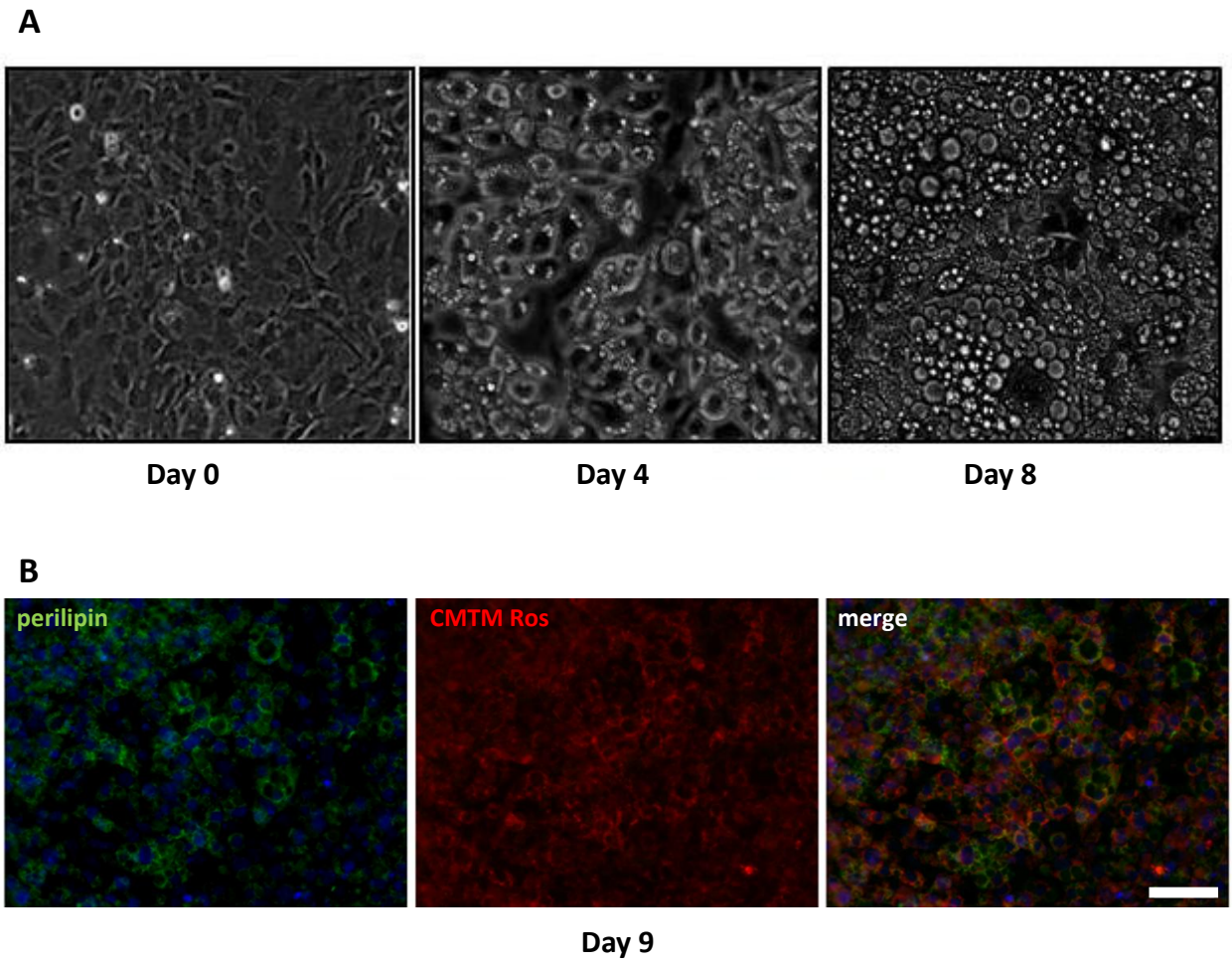

Figure 2.6. **Morphological and functional changes during brown adipocyte differentiation (A)** Change in cell morphology from a fibroblast to a multilocular appearance during differentiation **(B)** Lipid droplets are identified using perilipin (left), mitochondria is visualized using CMTM Rosamine MitoTracker on live cells, depicting large amount of mitochondria (middle), merge (right)**.** Nuclei visualized by DAPI . Scale bar represents 50 µm.

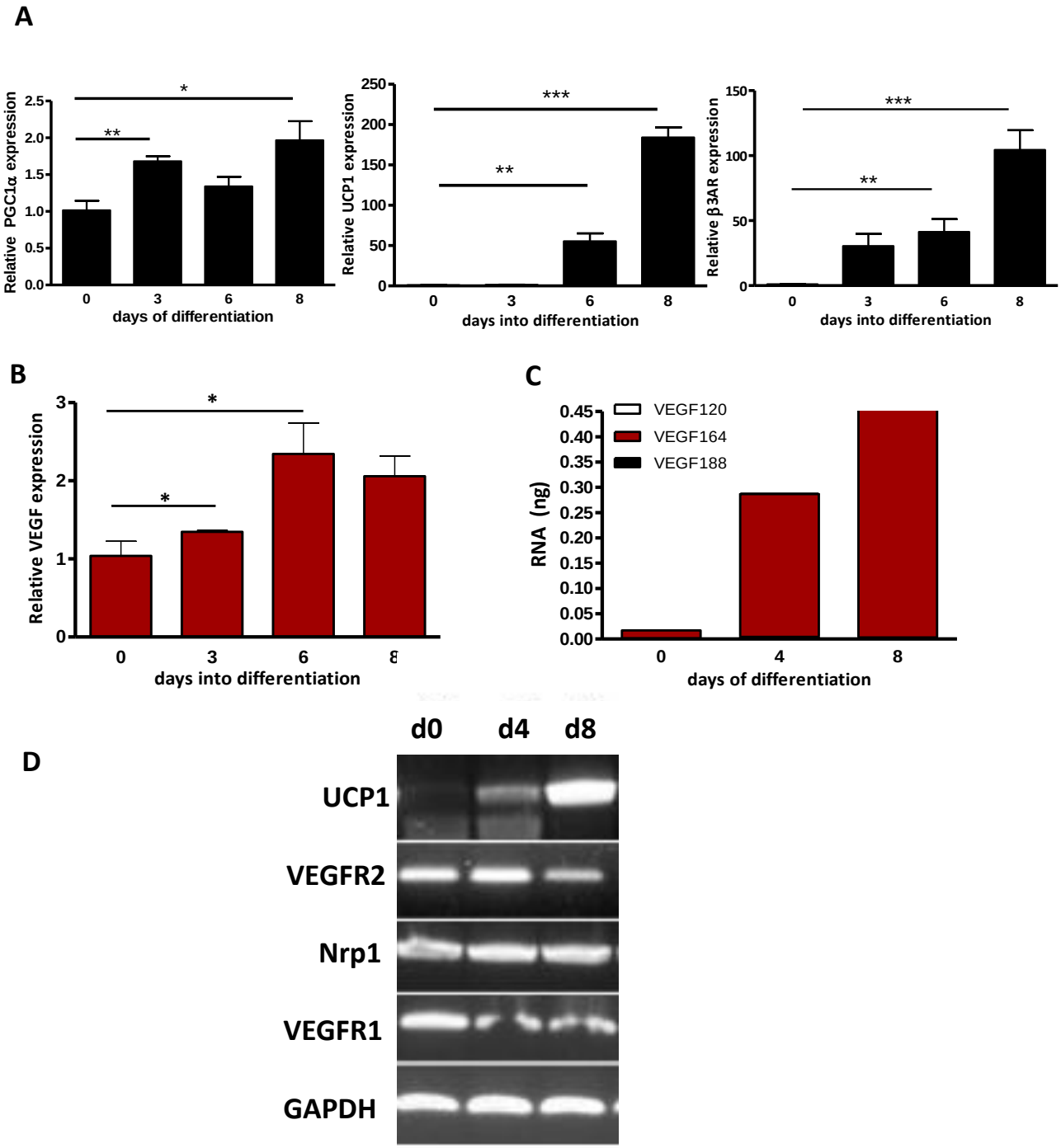

Figure 2.7. **Increase in VEGF expression during brown adipocyte differentiation. (A)** Expression of adipocyte markers PGC1α(left), UCP1(center) and β3 adrenergic receptors (right), quantified using qPCR. **(B)** Increase in VEGF expression during brown adipocyte differentiation in parallel to brown adipocyte markers shown in (A). **(C)** Absolute quantification of VEGF isoforms during differentiation using isoform specific primers and qPCR. **(D)** VEGF receptor expression during brown adipocyte determined by RT-PCR indicate strong VEGFR2 expression in both preadipocytes and differentiated adipocytes. p*<0.05, p**<0.01, p***<0.001.

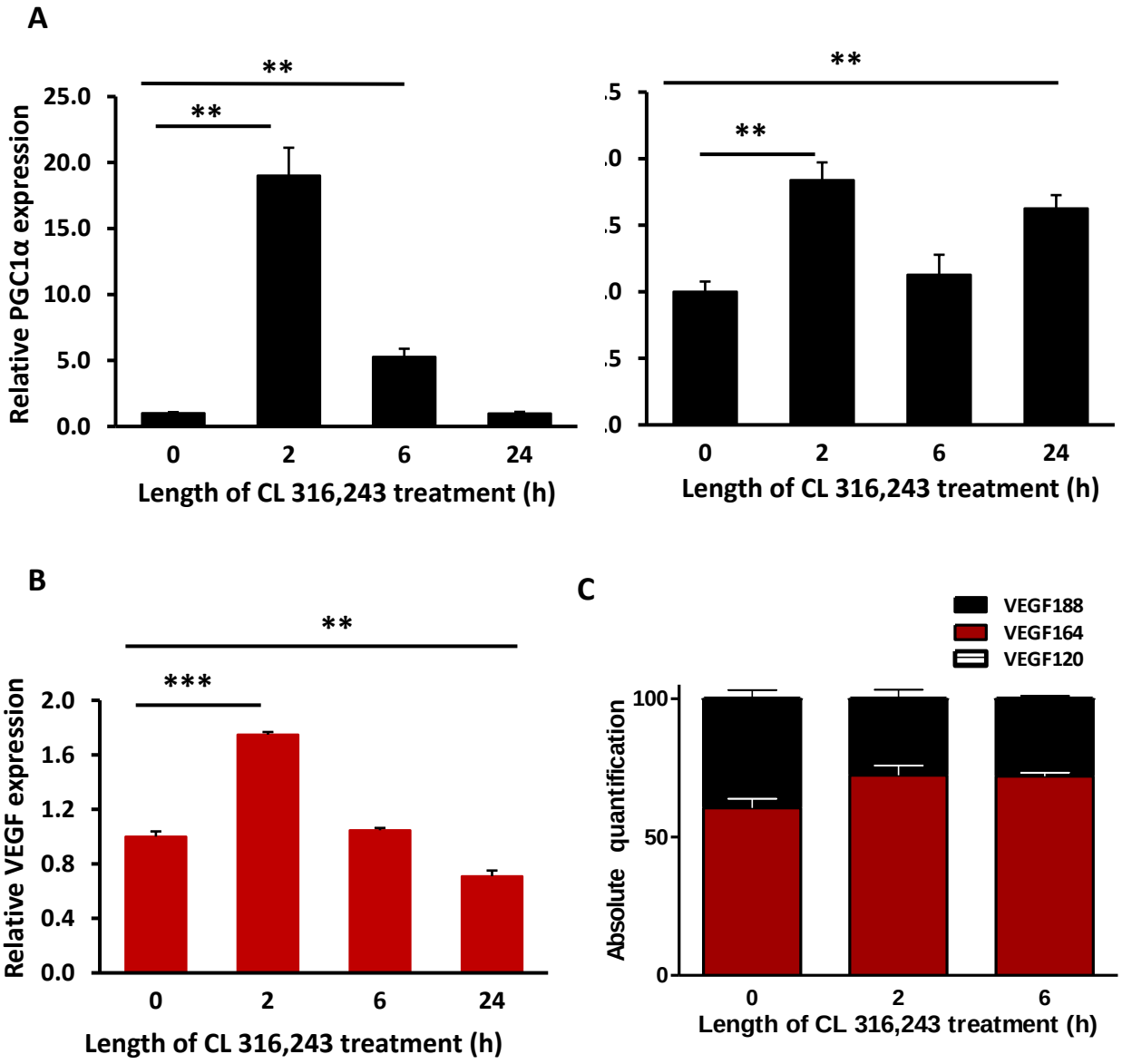

Figure 2.8. **VEGF expression increases in BAT *in vivo* following adrenergic stimulation by the β3 receptor agonist CL 316,243.** Mice were injected intraperitoneally with CL 316,243 and tissue was harvested at various time points from 2 hours to 24 hours post injection. **(A)** Increase in PGC1α (left) and UCP1 (right) expression, determined by qPCR, indicate activation of brown adipocytes. **(B)** VEGF expression is elevated during adrenergic stimulation and parallels PGC1α expression **(C)** Quantification of the percentage of VEGF isoforms contributing to total VEGF at various time points after adrenergic stimulation using absolute quantification with isoform specific primers. p**<0.01, p***<0.001.

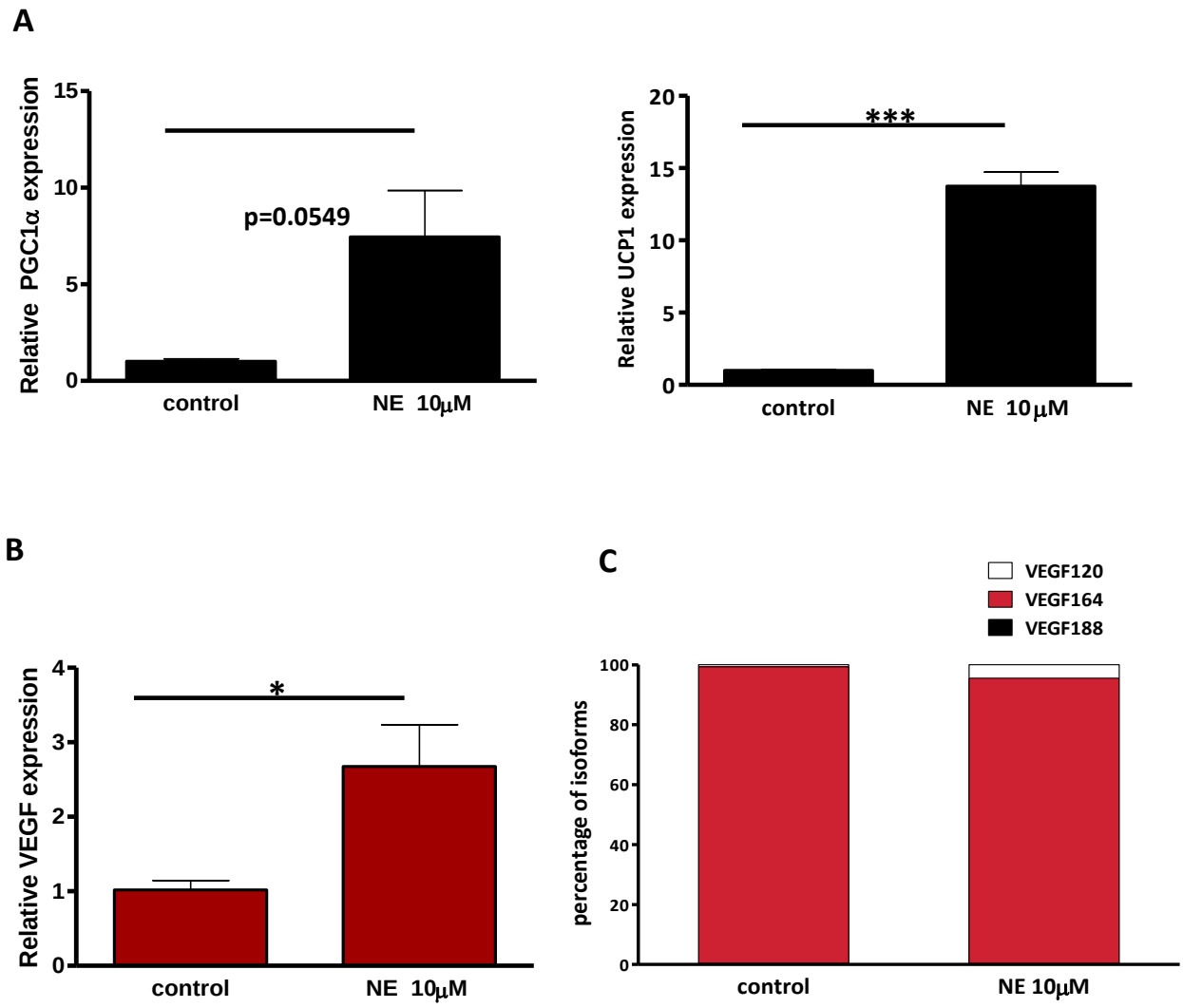

Figure 2.9. **VEGF expression increases in cultured brown adipocytes following treatment with norepinephrine.** Brown adipocytes on day eight of differentiation were serum starved for three hours and treated with 10 μM norepinephrine for 1 hour. **(A)** Robust increase in PGC1α (left) and UCP1 (right) expression indicate activation of brown adipocytes. **(B)** VEGF expression, determined by qPCR, is elevated during adrenergic stimulation and parallels PGC1α expression **(C)** Quantification of the percentage of VEGF isoforms contributing to total VEGF in unstimulated and stimulated brown adipocytes using absolute quantification with isoform specific primers. p*<0.05, p***<0.001.

Discussion

VEGF expression was detected in BAT and in all major WAT depots. The level of VEGF expression in BAT was higher than in any of the WAT depots, consistent with the densely vascularized nature of the tissue. Earlier reports of VEGF expression in BAT show a level of expression that was comparable to other highly vascularized tissue such as kidney, lungs and the heart (Asano et al. 1997; Tonello et al. 1999). In agreement with a prior report (Zhang et al. 1997), levels of VEGF among WAT depots, were higher in SC than PG. Numerous studies have reported that VEGF secretion by adipose tissue increases with the amount of adipose tissue and that plasma VEGF levels are positively correlated with body weight in both humans and mice (Gómez-Ambrosi et al. 2010; Miyazawa-Hoshimoto et al. 2005). One series of studies reported that VEGF secretion by primary adipocytes was only one-tenth that from adipose tissue explants maintained in media for 48 hours (Fain & Madan 2005; Fain et al. 2004). Though these observations may suggest that adipocyte-derived VEGF accounts about 10% of total adipose tissue VEGF in humans, these studies are also complicated by the fact that establishing cells in culture leads to significant changes in gene expression, which may impact these results. Further, the explants may be hypoxic which would result in a higher production of VEGF compared to the adipocytes in culture.

My results indicated that VEGF mRNA expression increases during 3T3L1 differentiation, a finding that is in agreement with earlier observations made in another adipogenic cell line, 3T3-F442A. In 3T3-F442A cells induced to differentiate into adipocytes increased VEGF was detected as early as day four of differentiation (Claffey et al. 1992),

whereas using 3T3L1 cells as a model, we observed increased VEGF expression around day eight of differentiation; results that are in concurrence with an earlier study that used these cells (Miyazawa-Hoshimoto et al. 2005). This difference in time course of expression could be attributed to the cell lines or to the sensitivity of techniques used to quantify VEGF. Our laboratory and others have demonstrated that VEGF expression increases in concert with differentiation in several systems including differentiating skeletal muscle (using C2C12 cells) (Bryan et al. 2008; Claffey et al. 1992), podocytes (Guan et al. 2006), osteoblasts (Liu et al. 2012; Mayer et al. 2005) and retinal pigmented epithelium (Ford et al. 2011), suggesting that VEGF expression is under the control of the same factors that regulate differentiation and therefore a part of the differentiation process itself.

I also demonstrate that all isoforms of VEGF are expressed during white adipocyte differentiation with VEGF164 and VEGF188, the heparan sulfate binding isoforms, comprising 90% of the total VEGF. Although the precise distribution of VEGF isoforms in white adipose had not been previously determined, one study did report that the mitogenic activity of adipocyte conditioned media on endothelial cells was maximal in the heparin sulfate binding fraction, supporting my observations that the heparan sulfate binding VEGF isoforms make up the majority of adipocyte VEGF (Zhang et al. 1997).

I did not detect VEGFR2 in white adipocytes *in vivo* or *in vitro*, an observation that is in agreement with previous findings using 3T3F442A preadipocytes which reported the absence of a direct effect of VEGF on adipocytes (Fukumura et al. 2003). On the other hand, VEGF secreted by adipocytes has been shown to be functionally active on endothelial cells; conditioned media from primary white adipocytes and differentiated 3T3L1 adipocytes

induced human umbilical vein endothelial cells proliferation (Zhang et al. 1997) and tube formation (Miyazawa-Hoshimoto et al. 2005) *in vitro,* which was blocked by anti-VEGF antibody. Additionally, in a model of SC fat pad created by transplantation of 3T3F442A cells into SCID mice, inhibition of VEGFR2 was shown to block not only angiogenesis and vessel remodeling in the implanted fat pad but also differentiation of the 3T3F442A cells into adipocytes. Whereas the addition of VEGF to preadipocytes in culture did not have any effect on their proliferation, survival or differentiation, conditioned media from endothelial cells cultured in the presence of VEGF increased preadipocyte proliferation and differentiation, effects that were largely abrogated by anti-VEGFR2 (Fukumura et al. 2003). Adipocyte-derived VEGF, therefore, plays a paracrine role to support both angiogenesis and adipogenesis. Serum VEGF levels are also elevated with increasing adiposity. Obese subjects have higher serum VEGF levels, which is lowered after bariatric surgery (García de la Torre et al. 2008). Thus it is possible that VEGF may play an endocrine role in vessel maintenance, and it remains to be determined whether the alteration of VEGF levels with obesity and related comorbidities like type 2 diabetes exacerbate angiogenesis in distant sites such as observed in proliferative diabetic retinopathy (Petrovic et al. 2008).

VEGF expression was also increased in concert with brown adipocyte differentiation. While it has been reported that VEGF is expressed in whole BAT tissue (Asano et al. 1997) as well as in brown preadipocytes and adipocytes (Tonello et al. 1999; Asano et al. 2001), there had been no quantitative measure of the change in VEGF or VEGF receptor expression during the course of brown adipose differentiation. My observation that VEGF levels increased in parallel with key modulators of brown adipocyte function such as PGC1α, UCP1

and β3 adrenoreceptors suggest that VEGF expression may be coordinately regulated as part of the process of differentiation. Elevated VEGF expression was similarly observed during myocyte and podocyte differentiation and was shown to be blocked when the process of skeletal muscle differentiation was prevented by use of a dominant negative MyoD (Bryan et al. 2008).

As VEGF has three major isoforms and we and others have demonstrated that the isoforms have differential expression in various tissues, I wanted to study the expression of VEGF isoforms during brown adipocyte differentiation. Preadipocytes expressed low levels of VEGF120, which further decreased to less than 1% in fully differentiated brown adipocytes. This observation is in agreement with my data on VEGF expression in adult BAT, where very low levels of VEGF120 were detected. As the VEGF isoforms differ in the presence or absence of charged domains that can mediate binding to heparan sulfate proteoglycans on the cell surface and extracellular matrix, they vary in their ability to diffuse. The relatively low levels of VEGF120 in BAT detected by us and others (Asano et al. 1997) suggest a dispensable role for the 120 isoform or functional redundancy with the other heparan sulfate binding isoforms. However, there was virtually no detectable VEGF 188 in cultured adipocytes, an observation that has been previously reported (Tonello et al. 1999) and appears to be a limitation of the *in vitro* culture system, which otherwise represents a good model of brown adipocyte differentiation as indicated by the robust expression of UCP1 and other brown adipocyte markers.

My results demonstrate the expression of the two major VEGF receptors, VEGFR2 and VEGFR1, as well as the co-receptor Nrp1, in preadipocytes as well as adipocytes. One of

the notable differences between white and brown adipocyte differentiation is in the level of VEGFR2 expression. VEGFR2 expression decreased significantly during white adipocyte differentiation and was not detectable in differentiated adipocytes. On the other hand, VEGFR2 was expressed at significant levels in both brown preadipocytes and in differentiated adipocytes. As VEGFR2 is the primary receptor for VEGF signaling, this observation is very interesting and suggests that VEGF may have a direct effect on brown adipocytes, which express VEGFR2, but not in white adipocytes.

Cold exposure stimulates release of NE by the sympathetic nervous system; its binding to adrenergic receptors in brown adipocytes results in adrenergic stimulation of BAT. In addition to exposure to cold temperatures, this phenomenon can be experimentally simulated by administration of NE or β3 adrenergic receptor agonists such as CL 316,243 *in vivo* or *in vitro*. As noted earlier, adrenergic stimulation is followed by cAMP mediated activation of PKA and an increase in PGC1α levels, which leads to mitochondrial biogenesis and increased expression of UCP1. As expected, treatment of cultured brown adipocytes with NE led to a robust increase in PGC1α and UCP1 and injection of mice with CL 316,243 produced a significant increase in PGC1α mRNA and a two-fold increase in UCP1 mRNA. The increase in UCP1 activity following adrenergic stimulation is regulated at both transcriptional as well as posttranslational levels; in the latter case fatty acids activate UCP1 by binding to its C terminal. Thus, the observed increase in UCP1 mRNA expression represents only a portion of the total increase in UCP1 activity. Cold exposure also results in BAT hyperplasia, an example of adaptive tissue growth, and is characterized by increased proliferation of brown adipocyte precursors and endothelial cells. Similar adaptive

responses are seen in muscle following endurance training and bouts of exercise where VEGF expression has been shown to increase.

VEGF expression similarly increases during adrenergic stimulation of BAT *in vivo* and *in vitro*. My findings agree with earlier reports of 2 to 3-fold increase in VEGF expression within a few hours of cold exposure or injection with β agonists (Asano et al. 2001; Fredriksson et al. 2005; Tonello et al. 1999). Absolute quantification of VEGF isoforms after CL injection *in vivo* revealed that VEGF isoforms 164 and 188 comprised 99.8% of total VEGF (Asano et al. 1997). An earlier report examining adrenergic stimulation in rats reported that VEGF120 levels increased from 11% to 30%. While the difference in levels of VEGF120 measured between my work and the earlier report are most likely attributed to sensitivity of measurement techniques (I used quantitative PCR and the prior report employed semi-quantitative PCR), both agree that the heparan sulfate binding isoform VEGF164 predominates. This is consistent with the fact that the increased VEGF during adrenergic stimulation would function both at a distance, on endothelial cells to promote angiogenesis, as well as locally, on adipocytes.

My investigation of the expression of VEGF and its receptors in white and brown adipose tissue demonstrate VEGF expression by white and brown adipocytes. VEGF expression increased during differentiation of white and brown adipocytes. My novel finding that VEGF receptors, VEGFR2, VEGFR1, as well as co-receptor Nrp1, are expressed in brown preadipocytes and adipocytes, raises the interesting possibility of an autocrine role of VEGF signaling in brown adipocytes and preadipocytes.

Chapter 3

ROLE OF VEGF SIGNALING IN BROWN ADIPOCYTES

Introduction

While it has been demonstrated that VEGF is expressed in BAT, preadipocytes and adipocytes, the sole function of VEGF was assumed to be as an angiogenic factor and potential actions outside of this have not been explored. Co-expression of VEGF and VEGFR2 has been observed in several cell types including podocytes (Guan et al. 2006), skeletal muscle (Bryan et al. 2008) and the retinal pigmented epithelium (Ford et al. 2011); in each of these cells VEGF signaling was also demonstrated to play a role. My observation that VEGF and VEGFR2 are present in brown adipocytes therefore, led me to hypothesize that VEGF signaling may play a functional role in brown adipocytes in addition to supporting angiogenic remodeling. In this chapter I have explored the role of VEGF signaling in brown preadipocytes and adipocytes *in vitro* and *in vivo*. I investigated if VEGF is important for brown preadipocyte survival and proliferation using *in vitro* assays and brown adipocyte survival and function *in vitro* and *in vivo.*

Results

VEGF is a mitogen for brown preadipocytes and acts asa survival factor through the PI3K-Akt pathway

The expression of VEGF, VEGFR2 and co-receptor Nrp1 in brown preadipocytes suggests that VEGF may function in an autocrine manner in these cells. To investigate a role for VEGF-VEGFR2 signaling in brown preadipocytes, VEGFR2 activation was assessed by

examining the phosphorylation of known tyrosine residues in unstimulated brown preadipocytes in regular culture conditions. Western blot analysis of lysates of preadipocytes revealed phosphorylation of VEGFR2 at tyrosine 951, indicating VEGF signaling through VEGFR2 (Figure 3.1).

Brown preadipocytes have been shown to be sensitive to serum starvation (growth factor withdrawal). To determine if VEGF signaling was playing a role in brown preadipocyte survival, cells were maintained in regular media but without serum, in the presence or absence of VEGF or the VEGFR2 neutralizing antibody DC101. After 12 hours of serum starvation, about a third of the cells were seen to be detached by light microscopy; this increased to greater than 80% by 24 hours. The levels of apoptosis marker protein from whole cell lysates of the above samples were analyzed by western Blotting. Cleavage of the inactive proenzyme caspase 3 to its smaller (17-19 kD and 12 kD), proteolytically active forms is considered a marker of apoptosis, as the cleaved fragments are critical executioner of apoptosis(Fernandes-Alnemri et al. 1994; Nicholson et al. 1995). As expected, nutrient-deprivation resulted in robust activation of caspase 3, demonstrated by the presence of the cleaved 17-19kD fragments. Culture of the cells with nutrient deprivation but in the presence of VEGF resulted in 70% reduction in caspase 3 cleavage and activation, indicative of reduced apoptosis. The addition of DC101 along with VEGF, thereby blocking VEGF signaling, resulted in 80% increase in caspase 3 cleavage levels and apoptosis compared to cells in VEGF alone. Additionally, the pattern of VEGFR2 phosphorylation was inversely correlated with caspase 3 activation, providing further evidence that VEGFR2 signaling was necessary for the observed protective effect.

The phosphatidylinositol 3-kinase (PI3K) -Akt pathway has been demonstrated to confer protection from apoptosis in multiple cells and is also reported to be downstream of the VEGF–VEGFR2 signaling cascade. To examine the signaling pathways involved in VEGF-conferred protection of brown preadipocytes from apoptosis, I examined Akt activation in the above samples. As expected, Akt was phosphorylated in control cells that were grown in normal growth media and did not show any apoptosis. In contrast, nutrient deprivation resulted in a nearly complete loss of Akt phosphorylation along with loss of VEGFR2 phosphorylation, indicating that Akt signaling was downstream of VEGF-VEGFR2 signaling in brown preadipocytes. The presence of VEGF resulted in robust Akt phosphorylation compared to levels in control samples, and the addition of DC101 reduced this phosphorylation by 80% (Figure 3.1).

To determine the role of VEGF signaling in preadipocytes, we assessed the effect of VEGF on preadipocyte proliferation. Preadipocytes were cultured in low serum in the presence or absence of 10ng/ml VEGF and counted daily. The growth of brown preadipocytes with VEGF led to a stimulation of cell proliferation when compared to untreated cells, with an increase in cell number of 70% at 48 hours (Figure 3.2).

Blockage of VEGF signaling sensitizes brown adipocytes to apoptosis

The association between VEGF expression and adipocyte differentiation as well as the expression of VEGF receptors in differentiated brown adipocytes demonstrated earlier, suggest that VEGF may play a role in mature brown adipocytes. In light of my observation

that VEGF acted as a survival factor for brown preadipocytes, I hypothesized that VEGF might serve a similar function for brown adipocytes.

While nutrient deprivation does not lead to death of mature brown adipocytes, TNFα in combination with low (10 μg/ml) dose of cycloheximide (CHX) has been shown to induce apoptosis in brown adipocytes, with a maximal effect between 4 to 6 hours, without cytotoxicity due to CHX alone (Boucher et al. 2010; Miranda et al. 2010; Nisoli et al. 1997). To study the effect of VEGF signaling on brown adipocyte survival, brown adipocytes differentiated *in vitro* were treated with 10 nM TNFα and 10 μg/ml CHX for 6 hours in the presence or absence of VEGFR2 neutralizing antibody, DC101. Quantification of cells revealed that whereas TNFα/CHX alone resulted in a 7% reduction in the number of cells compared to untreated brown adipocytes, treatment with DC101 in addition to TNFα/CHX resulted in a 15% reduction in the number of brown adipocytes compared to those treated only with TNFα/CHX (Figure 3.3A). This level of cell death is significant as adipocytes are known to be relatively resistant to apoptosis. For an additional measure of survival, the percentage of cells with caspase 3 activation was measured. FACS analysis revealed a 5-fold increase in the number of adipocytes with cleaved caspase 3 in TNFα/CHX –treated cells grown with DC101 compared to cells grown with TNF/CHX (Figure 3.3B), indicating that blockade of VEGF signaling sensitizes brown adipocytes to apoptosis.

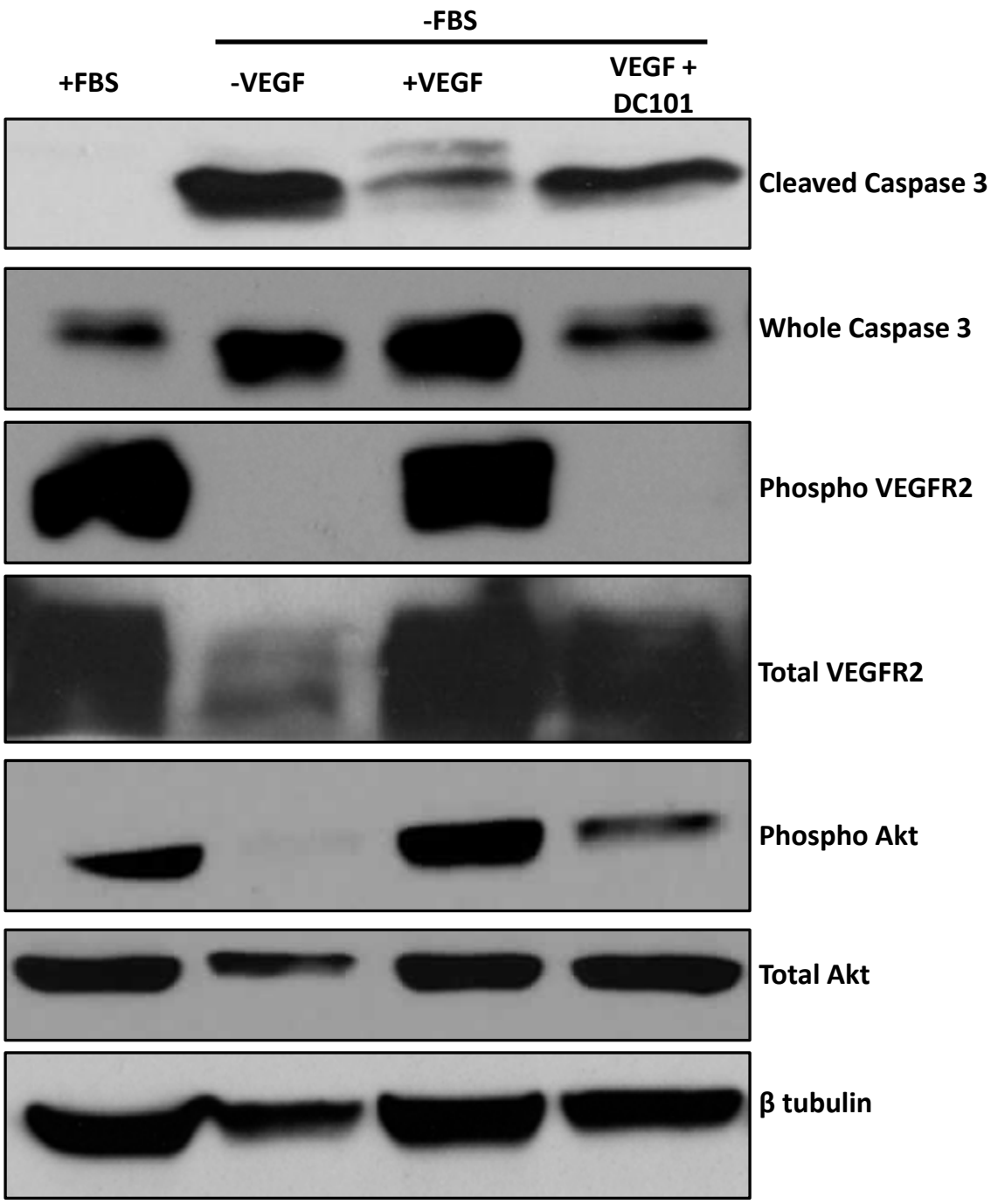

Figure 3.1. **VEGF activates PI3K/Akt pathway and mediates brown preadipocyte survival.** Serum-starved brown preadipocytes cultured in 25ng/ml VEGF for 12h were protected from apoptosis, judged by the reduced expression of cleaved (activated) caspase 3, which was lost upon the addition of VEGFR2 blocking antibody 15µg/ml DC101. Phosphorylation of VEGFR2 at Y951 was detected to check for active VEGF signaling and phosphorylation of Akt at S453 was done to check for PI3K/Akt activation.

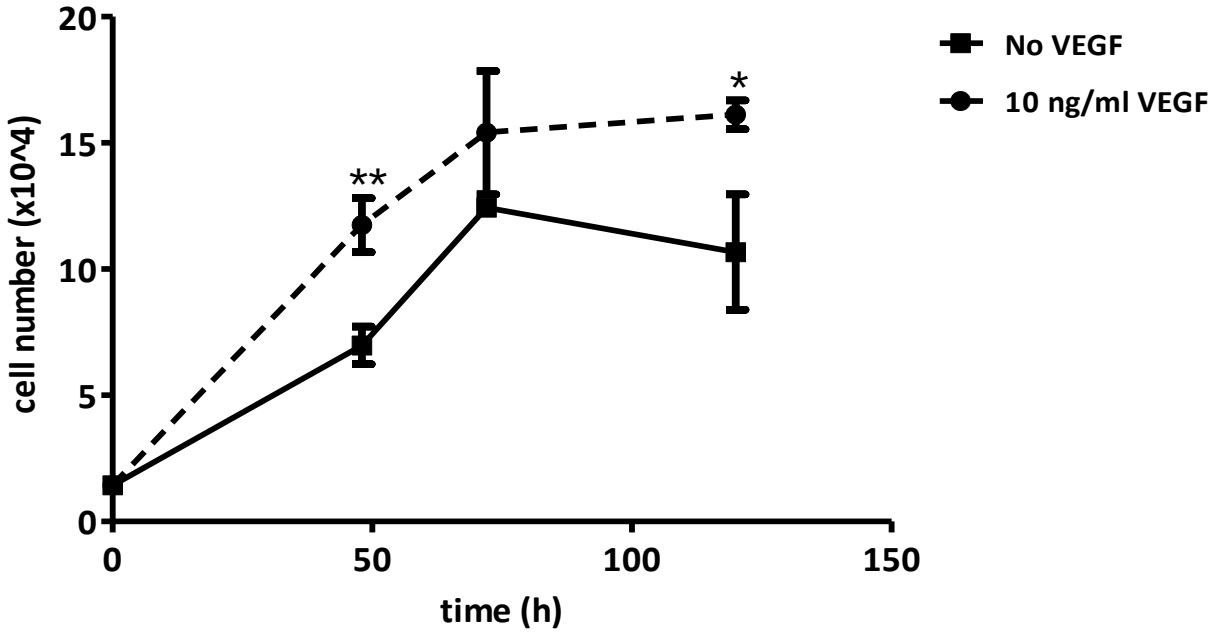

Figure 3.2. **VEGF increases brown preadipocyte proliferation.** Increase in number of brown preadipocytes grown in 1% FBS in the presence of 10 ng/ml VEGF compared to 1% FBS alone. p**<0.01, p*<0.05.

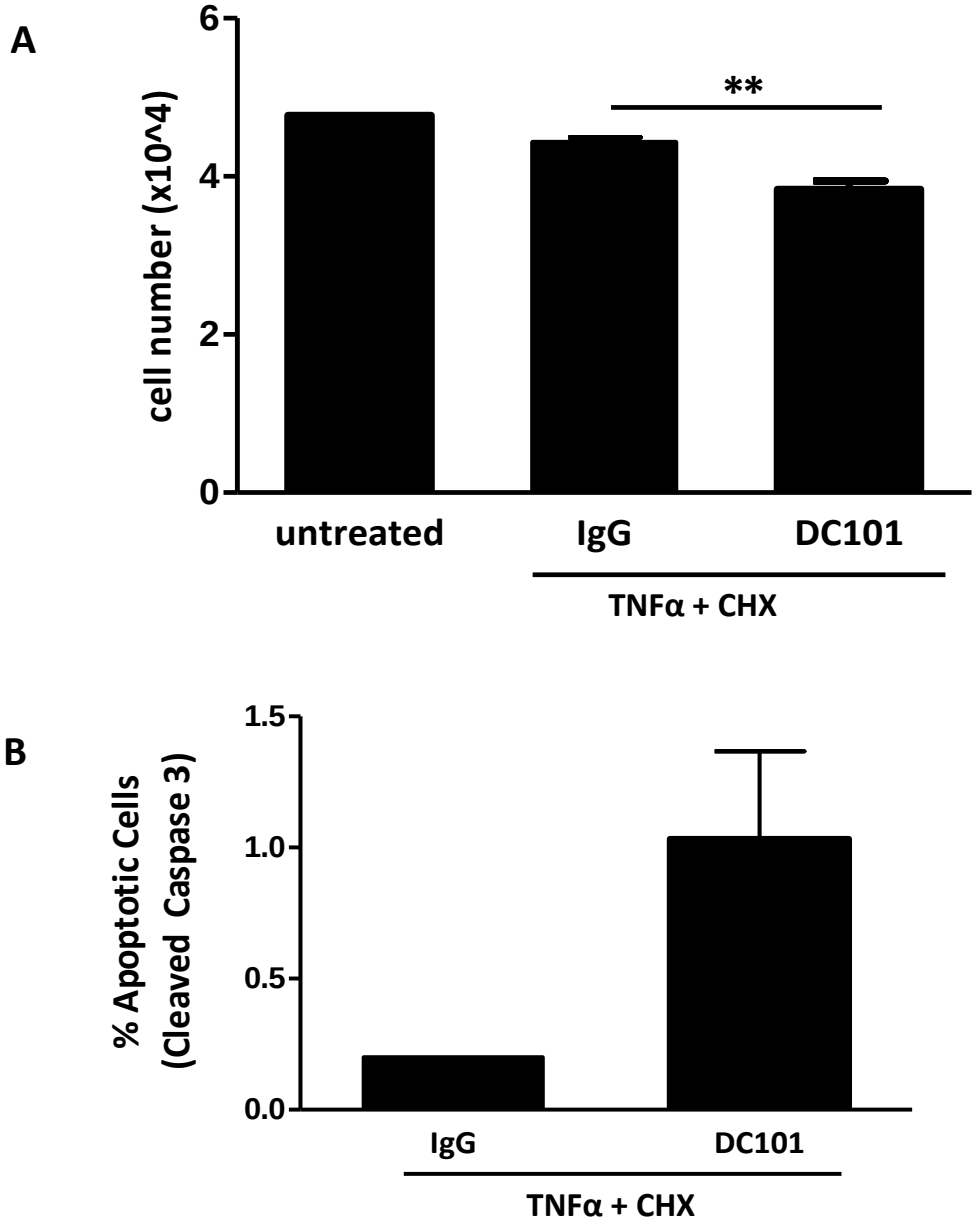

Figure 3.3. **Blockage of VEGF signaling sensitizes brown adipocytes to apoptosis.** Differentiated brown adipocytes at day 7 were treated with 10nM TNFα and 10μg/ml CHX for 6 hours to induce apoptosis, in the presence or absence of VEGF-blocking antibody DC101 (15 μg/ml). **(A)** Cell numbers revealed treatment with DC101 in addition to TNFα/CHX led to reduced survival and fewer brown adipocytes compared to TNFα/CHX alone; p**<0.01 **(B)** Apoptotic adipocytes detected using FACS analysis for cleaved (activated) caspase 3 also revealed an increased apoptosis in the presence of DC101; p = 0.067.

VEGF neutralization reduces BAT vascular density

Given my observation indicating a role of VEGF in brown adipocytes and preadipocytes *in vitro*, I next investigated a possible function for VEGF in the adult BAT. To block VEGF signaling *in vivo* mice were injected intravenously with an adenovirus expressing sFlt1 (Ad-sFlt1) or an empty adenovirus (Ad-null). Previous work from our group has shown that this is an effective model for systemic VEGF neutralization, and that a circulating sFlt1 level of at least 200 ng/ml is required for effective VEGF neutralization and that these levels can be maintained for up to 28 days (Maharaj et al. 2008; Ford et al. 2011 and unpublished data). Thus, mice were injected with adenovirus via the tail vein, serum was collected five days after injection to measure circulating sFlt1 levels and tissue was harvested from the mice seven days post injection (Figure 3.4).

To examine BAT capillary density of mice with systemic VEGF neutralization, BAT sections were probed with antisera against the endothelial-specific glycoprotein, endomucin, which is expressed by the endothelium of capillaries and veins but not arteries (Kuhn et al. 2002; dela Paz & Patricia a D'Amore 2009). Seven days following injection of the adenovirus, there was a marked reduction in microvessel density in the Ad-sFlt1 injected mice compared to Ad-null injected mice (Figure 3.5A). Whole tissue lysates from BAT of both groups were examined for the levels of endomucin (as a surrogate for vascular density) by Western blotting and revealed a 50% decline in endomucin levels in the BAT of Ad-sFlt 1 injected mice (Figure 3.5B), indicating that VEGF neutralization led to a reduction in the microvascular density of brown adipose tissue.

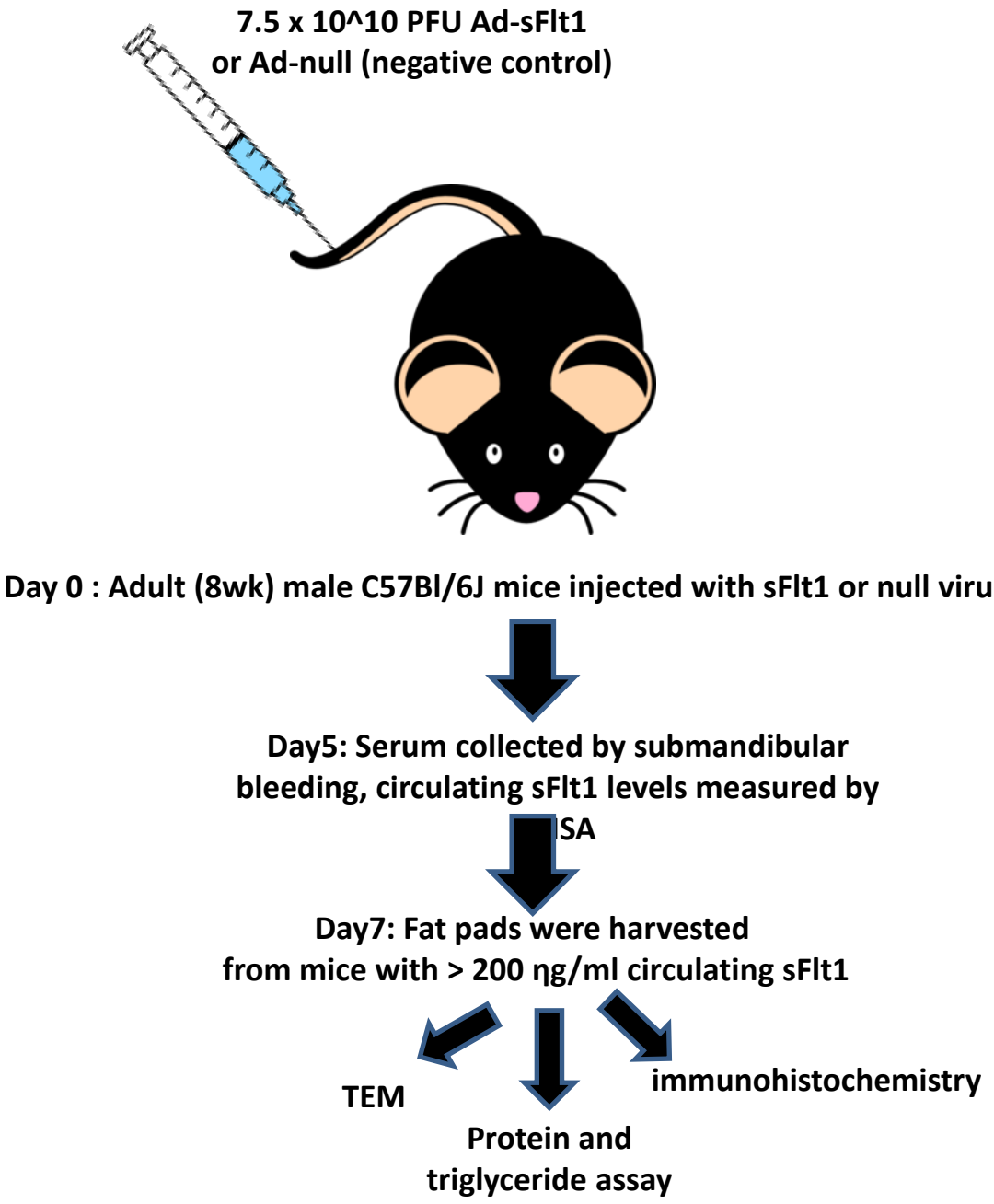

Figure 3.4. **Schematic representation of Ad-sFlt1 tail-vein injections for systemic VEGF neutralization.** 8 week old male C57Bl/6J mice were injected with sFlt1 or null adenovirus via the tail vein. Serum levels of sFlt1 were measured by ELISA 5 days post injection. Mice expressing at least 200 ng/ml of circulating sFlt1 were included in the study. Circulating sFlt1 levels can be maintained up to 28 days post injection. 7 days post injection mice were sacrificed and fat pads harvested for protein, histology and ultrastructure analysis using TEM. For TEM mice were first perfused with appropriate fixative.

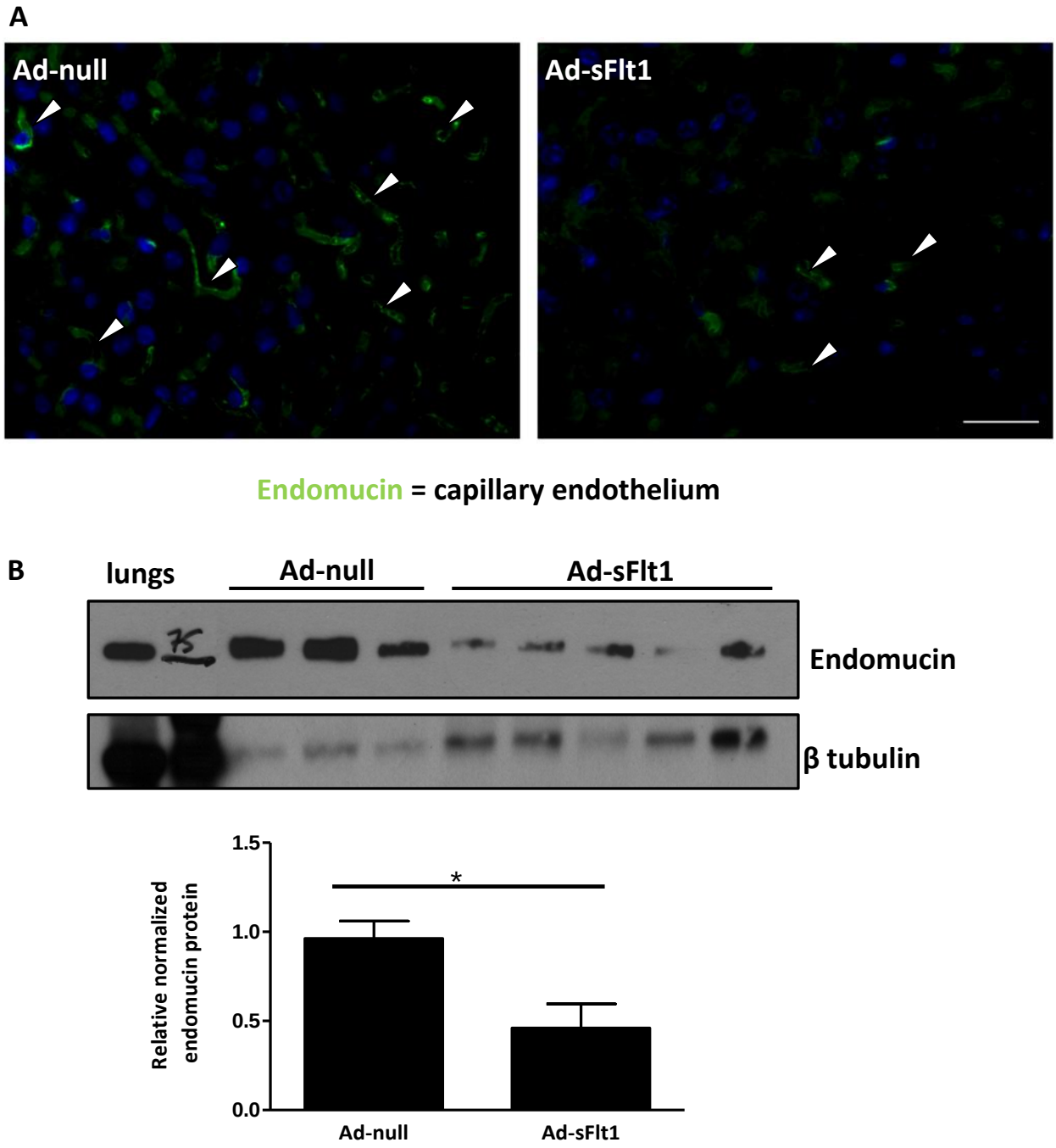

Figure 3.5. **VEGF neutralization reduces BAT vascular density. (A)** Capillary density of sFlt1 and control BAT sections were examined by IF with endomucin, which marks the microvasculature. Nuclei were labeled with DAPI. There were fewer capillaries (white arrowheads) in the sFlt1-injected BAT compared to null. Scale bar represents 50 µm **(B)** Total endomucin protein levels in whole tissue lysates from BAT detected by Western Blotting (top) and quantification of endomucin levels normalized to β tubulin was done as a surrogate for vascular density; p*<0.05

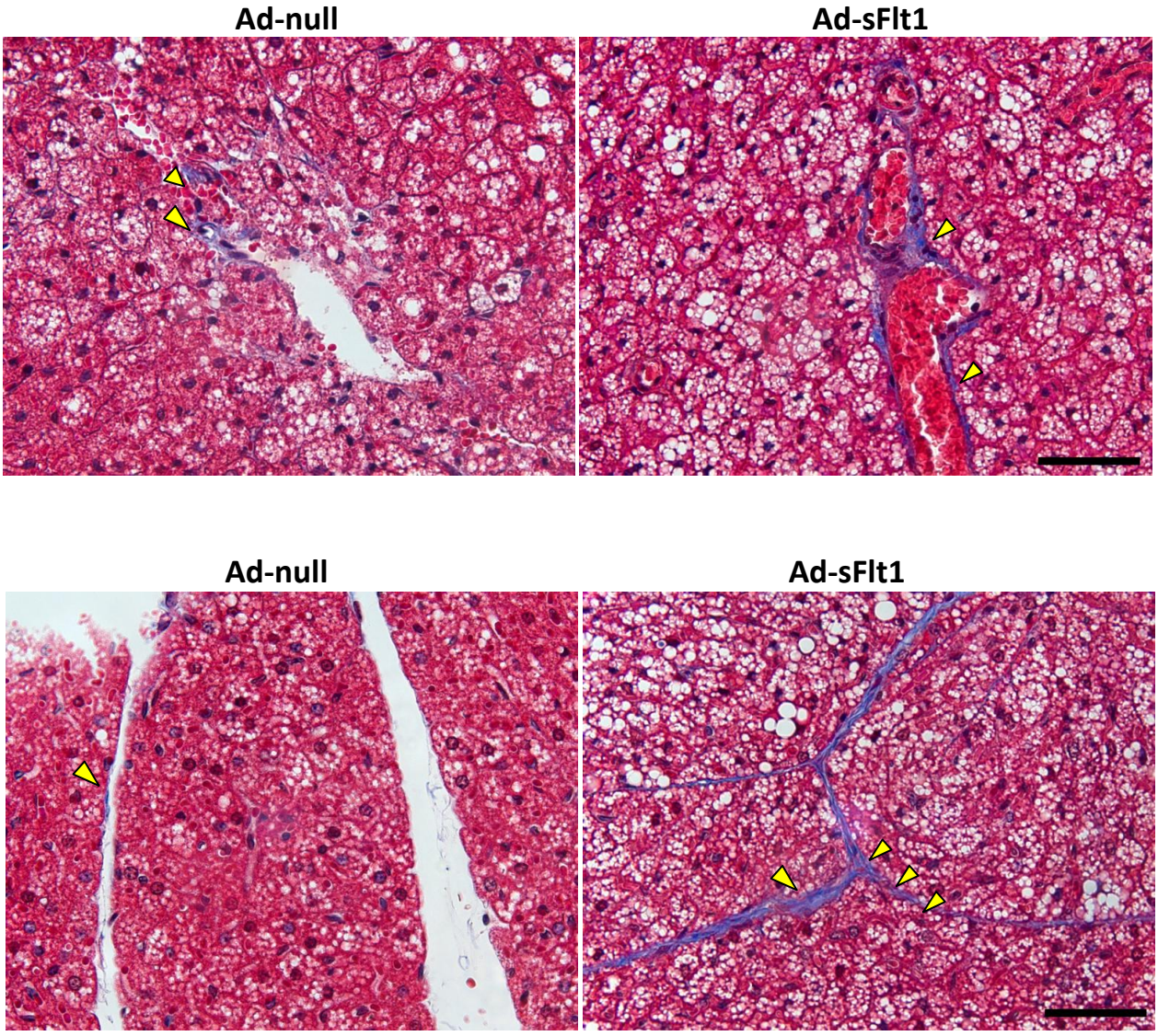

Figure 3.6. **VEGF neutralization is associated with fibrosis of BAT.** Collagen deposition in BAT of sFlt1 and control mice detected by Masson's trichrome staining. Increased collagen (yellow arrowheads), indicative of fibrosis, was observed around veins and arteries as well as between brown adipocytes in the sFlt1-expressing mice. Collagen was detected as thin sheets in the control mice as well, but not at levels that are outside of normal. Scale bar represents 50 µm.

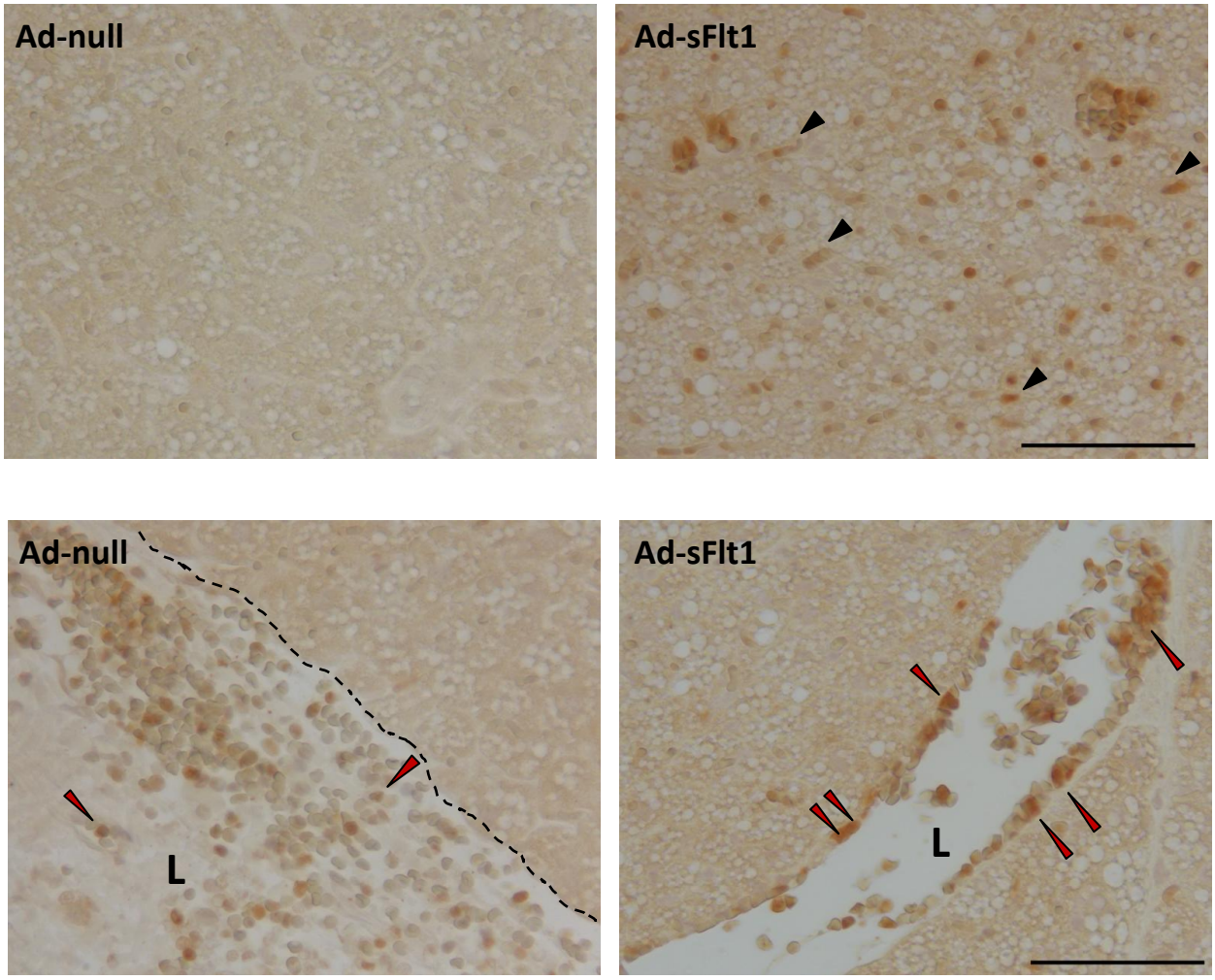

Figure 3.7. **VEGF neutralization is associated with inflammation of BAT.** IHC localization of F4/80 revealed infiltrating macrophages (black arrowheads) in the BAT of ad-sFlt1 injected mice but none in ad-null mice. F4/80 positive cells were detected attaching to the vessel walls of sFlt1 mice (red arrowheads), suggesting local inflammation, while no attachment was detected in null mice. Dotted black line – endothelial lining, L – lumen, scale bar represents 50 µm.

VEGF neutralization is associated with fibrosis and inflammation of BAT in vivo

Reduced microvessels often result in tissue hypoxia, which can, in turn, lead to fibrosis and local inflammation (Halberg et al. 2009). Collagen I, the predominant collagen in adipose tissue (Napolitano 1963), was detected by Masson's trichrome staining (TRI), which stains muscle red, nuclei dark purple and collagen bright blue. Collagen appeared as thick blue depositions around adipocytes and blood vessels in the sFlt1-expressing mice compared to the thin collagen sheets in the wild type mice, which is normal (Figure 3.6).

IHC localization of F4/80 revealed the presence of a large number of macrophages in the BAT of sFlt1-expressing mice, whereas no macrophages were observed in the BAT of control mice (Figure 3.7). The features of immune cell infiltration, including adhesion and extravasation of the F4/80 positive cells, were observed in the sFlt1-injected BAT and suggest that VEGF neutralization resulted in local inflammation in BAT.

VEGF neutralization leads to brown adipocyte apoptosis in vivo

Since blockage of VEGF signaling resulted in increased apoptosis *in vitro*, I wanted to investigate the effect of VEGF neutralization on brown adipocyte survival *in vivo*. Apoptosis was first assessed by IHC localization of activated (cleaved) caspase 3 in BAT. Many cells stained positively for cleaved caspase 3 in the BAT of sFlt1-expressing mice compared to only a few positive cells in null mice (Figure 3.8). High magnification revealed that these cells, occurring in clusters or singly, were adipocytes with activated caspase 3 accumulation

in the cytosol surrounding lipid droplets (Figure 3.8, bottom panel); a few endothelial cells with activated caspase 3 were also observed.

To confirm apoptosis by another approach and to quantify apoptotic cells, Terminal Transferase dUTP Nick End Labeling (TUNEL) assay was performed (Figure 3.9A). TUNEL staining similarly revealed a large number of apoptotic (TUNEL +) cells in the BAT of sFlt1-expressing mice compared to null. To distinguish the adipocytes from the vascular cells, BAT sections were co-stained with endomucin to identify the endothelium (Figure 3.9B). There was a six to seven-fold increase in the number of apoptotic adipocytes in the BAT of sFlt1-expressing mice compared to control BAT. The BAT of mice that had been injected with Ad-null had ten or fewer apoptotic cells per section (Figure 3.9C). These data indicate that VEGF acts as a survival factor for brown adipocytes *in vivo*.

Effect of VEGF neutralization on brown adipocyte morphology and mitochondrioma in vivo

Lipid droplets

Whereas brown adipocytes from the control mice had numerous small lipid droplets that is typical of BAT histology, brown adipocyte of sFlt1-expressing mice exhibited much larger lipid droplets (Figure 3.10), a phenotype that is indicative of increased lipid content and unusual in normal brown adipocytes of lean mice . This morphological difference was readily observed during histological analysis by H&E and Masson's trichrome staining as well as during ultrastructural analysis with TEM. This was surprising as the BAT mass was

reduced after VEGF neutralization and thus was not a direct outcome of adipocyte hypertrophy (data not shown).

Mitochondria

As mitochondria are central to the function of brown adipose, I wanted to assess the effect of VEGF neutralization on mitochondrial ultrastructure. Ultrastructural analysis of BAT taken from control mice seven days post injection revealed that each adipocyte contained numerous mitochondria. However, the number of mitochondria was reduced by about 30% in brown adipocytes of ad-sFlt1 injected mice compared to control (Figure 3.11A). Control mice contained mitochondria that were uniform in shape and size, displayed dense, tightly packed cristae that spanned the width of each mitochondrion. In contrast, mitochondria in brown adipocytes from sFlt1-expressing mice often lacked cristae or had cristae that were incomplete, irregular in arrangement and/or did not span the mitochondrion (Figure 3.11B). Incomplete or absent cristae are associated with mitochondrial degeneration and inactivity. The mitochondrial anomalies, along with the presence of large lipid droplets in brown adipocytes of sFlt1-expressing mice, suggest that VEGF neutralization may lead to reduced brown adipocyte function.

Electron microscopic examination of the brown adipocytes of sFlt1-expressing mice also revealed autophagosome engulfing double-membraned organelles reminiscent of mitochondria, structures that were not observed in null mice (Figure 3.12A). The individual mitophagic vesicles appeared either electron dense or light, likely reflecting the stage of autophagic degradation. The light chain (LC)-3 proteins, LC3-I and II, are widely used as markers of autophagy (Kabeya et al. 2000). During autophagy, LC3-I is converted to LC3-II,

Figure 3.8. **VEGF neutralization leads to brown adipocyte apoptosis in vivo.** Apoptosis detected by IHC localization of activated (cleaved) caspase 3. *Top panel*: Adipoyctes with activated caspase 3 (black arrowhead) are rare in the BAT of control mice; low magnification (left), high magnification (right). *Middle and lower panels*: Apoptotic cells, with cleaved caspase 3 in the cytosol surrounding lipid droplets, occur frequently in clumps or singly near vessels in the BAT of sFlt1 expressing mice. L-lumen, LD-lipid driplet, scale bar represents 50 μm.

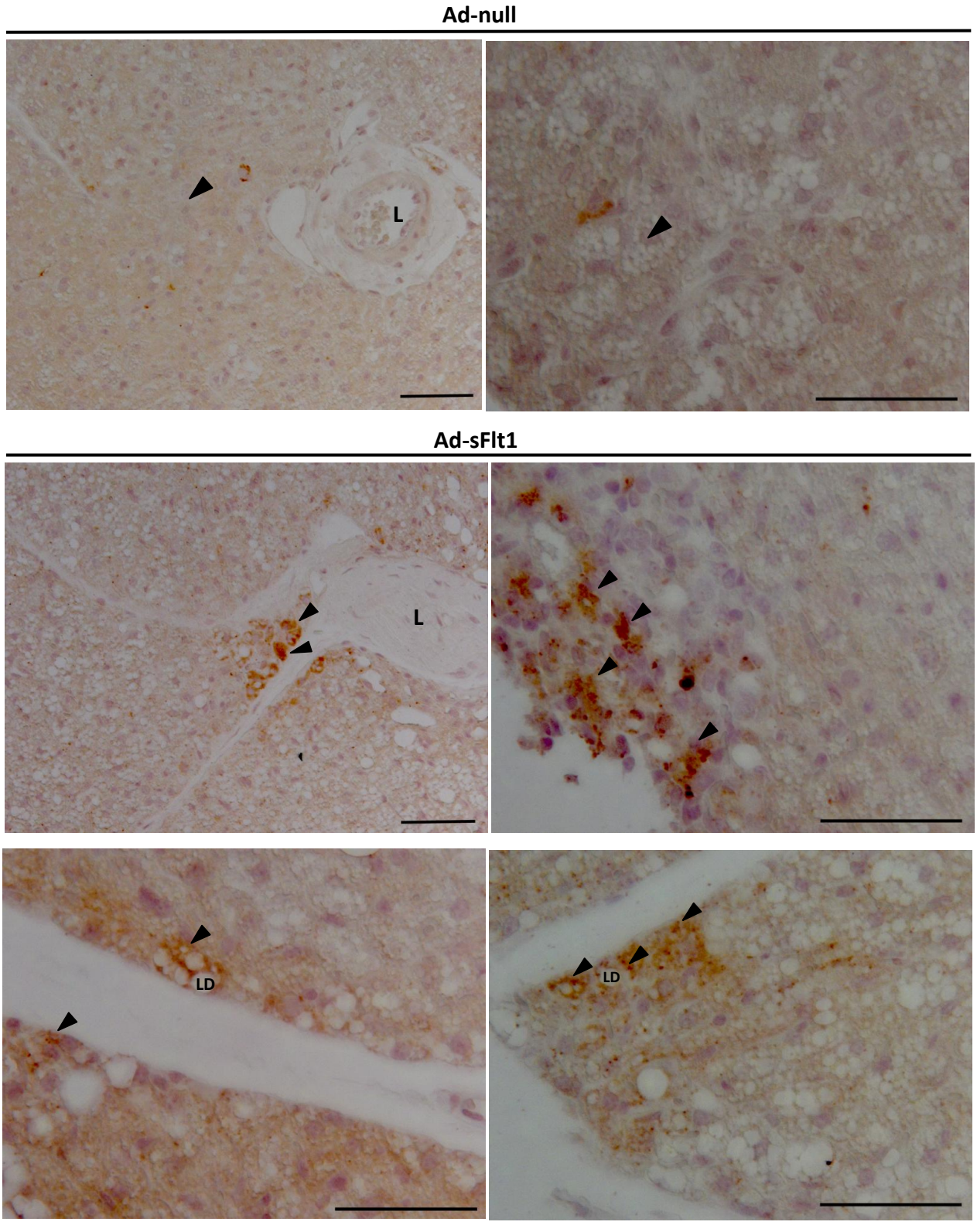

Figure 3.8 (continued)

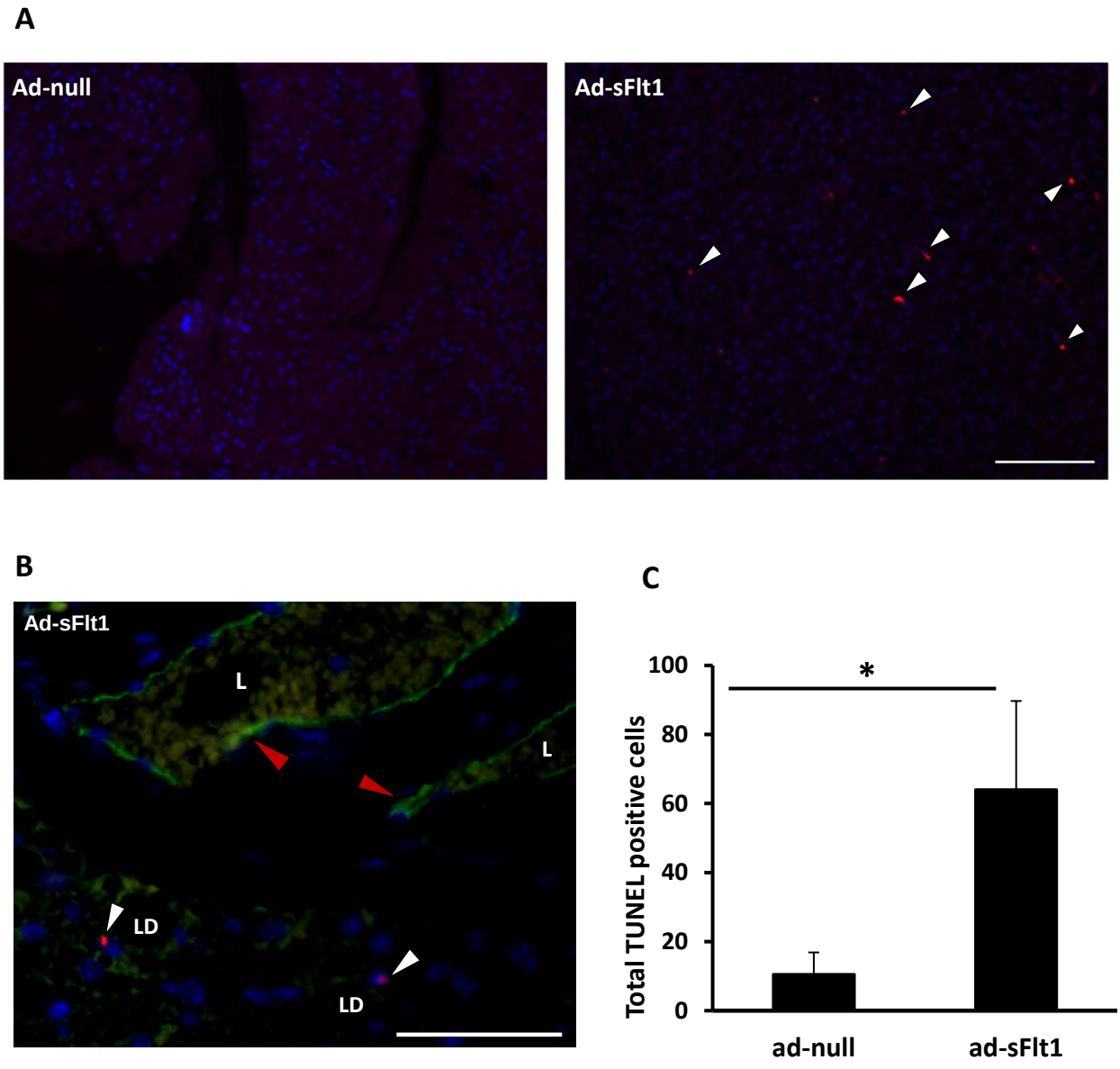

Figure 3.9. **Quantification of apoptosis in BAT after VEGF neutralization. (A)** TUNEL staining of BAT sections demonstrating that BAT of mice injected with ad-sFlt1 have more TUNEL+ cells (white arrowheads) compared to null. Scale bar represents 100µm. **(B)**TUNEL+ adipocytes (white arrowheads) versus endothelial cells (red arrowheads) were identified by co-staining with endomucin and only TUNEL+ adipocytes were counted for quantification. **(C)** Quantification of TUNEL+ cells in each section reveals more than a six fold increase in apoptosis in sFlt1 BAT. L-lumen, LD-lipid driplet, scale bar represents 50 µm; p*<0.05

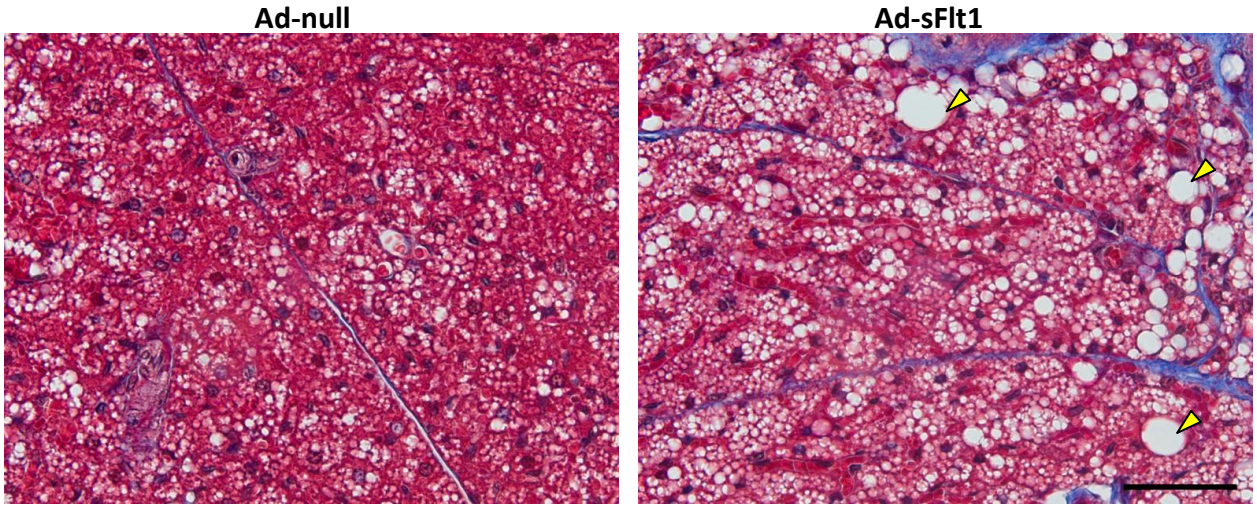

Figure 3.10. **VEGF neutralization results in alteration in brown adipocyte lipid droplets.** Brown adipocyte histology analyzed by Masson's trichrome stain demonstrating multiple small lipid droplets in each cell typical of brown adipocyte morphology (left), whereas ad-sFlt1 injected mice had significantly larger lipid droplets (yellow arrowhead) not usually observed in lean mice. Scale bar represents 50 µm

which become associated with autophagic vesicles (Tanida et al. 2004) and therefore indicates autophagy. Thus, to further characterize the observed mitochondrial autophagy, I assessed LC3B levels in BAT using IHC. A light brown pattern of puncta was distributed diffusely throughout the cytosol of individual cells in both null and sFlt1-expressing mice, reflecting a basal level of autophagy. However, in the sFlt 1-expressing mice many adipocytes exhibited denser dark brown puncta within the cytoplasm, suggestive of a higher abundance of autophagosomes (Figure 3.12B). This staining pattern was rarely observed in null mice, an observation that is consistent with our TEM analysis that did not reveal mitophagy in any BAT from control mice. Increased mitophagy is associated with reduced lipolysis in WAT (Singh et al. 2009) and reduced thermogenesis in BAT (Milosevic & Ukropina 2008). These observations of altered mitochondrial structure in BAT associated with VEGF neutralization supports a role for VEGF in the maintenance of brown adipocyte survival/integrity.

The effects of VEGF on brown adipocytes and preadipocytes observed *in vivo* and *in vitro* are summarized in Table 2.

Figure 3.11. **VEGF neutralization results in reduced mitochondria and disrupted ultrastructure. (A)** Average number of mitochondria per field indicates a significant decrease in the total number of mitochondria in ad-sFlt1 injected mice. **(B)** (*Left)* Electron micrograph of brown adipocyte showing abundant mitochondria, lipid droplets (LD) and a nearby vessel (L) in control mice. Mitochondria were typical of functional brown adipocytes, numerous and densely packed with complete double membrane cristae (white arrowhead). (*Right)* Fewer mitochondria present in sFlt1 brown adipocytes; a majority of mitochondria showed obvious signs of degeneration such as incomplete cristae, involuting cristae etc (red arrowhead) and several lacked cristae entirely (yellow asterisks); high magnification depicted in bottom panel. L – lumen, LD - lipid droplet, scale bar represents 500 nm ; p=0.00007

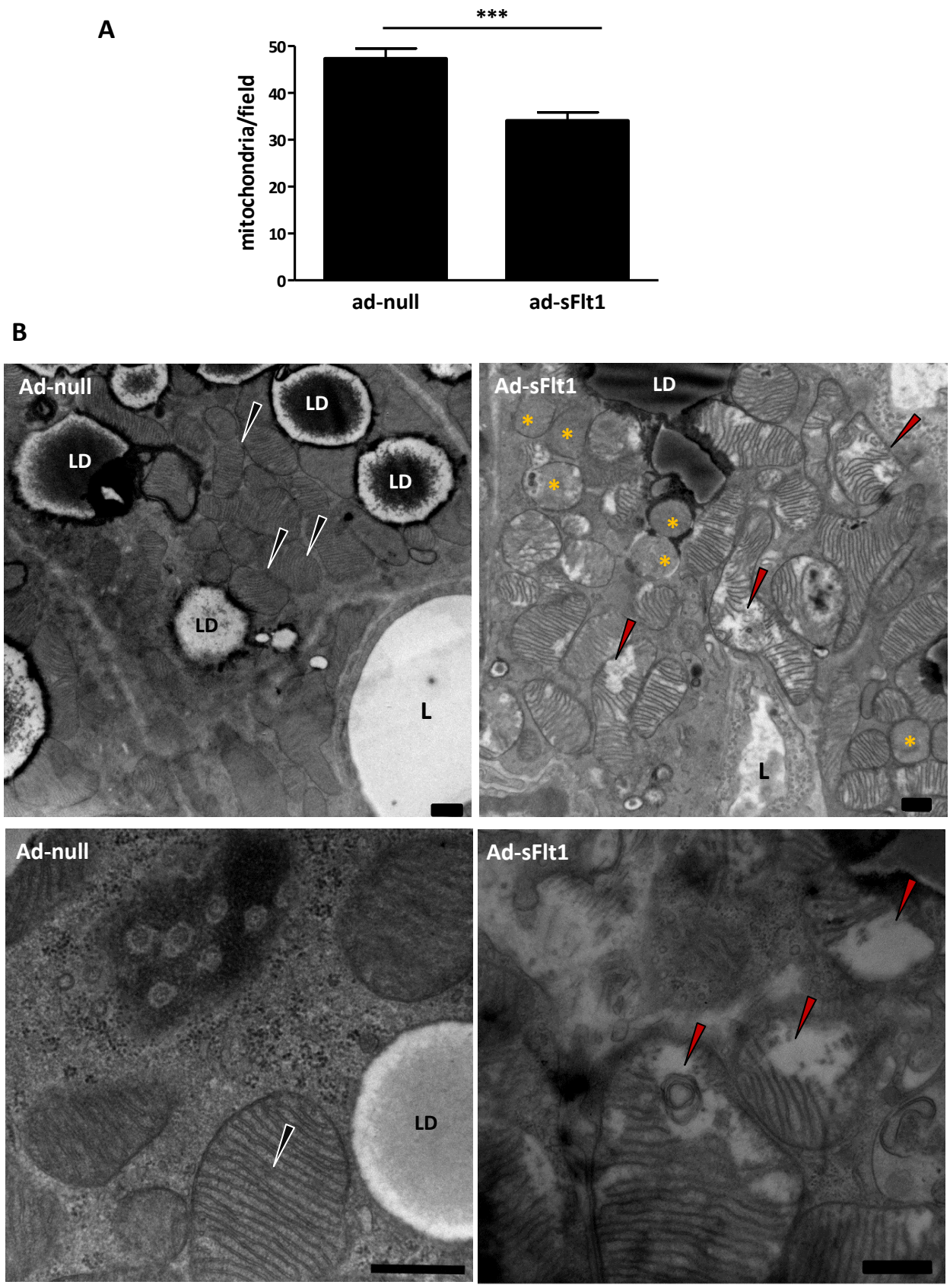

Figure 3.11 (continued)

Figure 3.12. **VEGF neutralization results in brown adipocyte mitophagy. (A)** Electron micrograph of brown adipocyte from ad-sFlt1 injected mice showing autophagy of mitochondria (red arrowhead). *Left:* Advanced stage of autophagy in which the autophagosome has already fused with a lysosome and material has degraded resulting in a lower density compared to the surrounding tissue. The double membranous structure present in the autophagolysosome is indicative of a mitochondria. Right: An early stage of mitophagy in which the intact mitochondria is being engulfed by an autophagosome. Note that the engulfed mitochondria appears healthy with complete cristae indicating that mitophagy in sFlt1-expressing mice is not a clearance pathway for abnormal mitochondria but a separate mechanism for reduction in overall mitochondria. Scale bar represents 500nm. **(B)** IHC localization of the autophagic marker LC3B. Puncta indicate autophagosomes with which the LC3B form II is associated. There are increased puncta in sFlt1 BAT compared to null mice. N – nucleus, LD - lipid droplet, scale bar represents 50 μm.

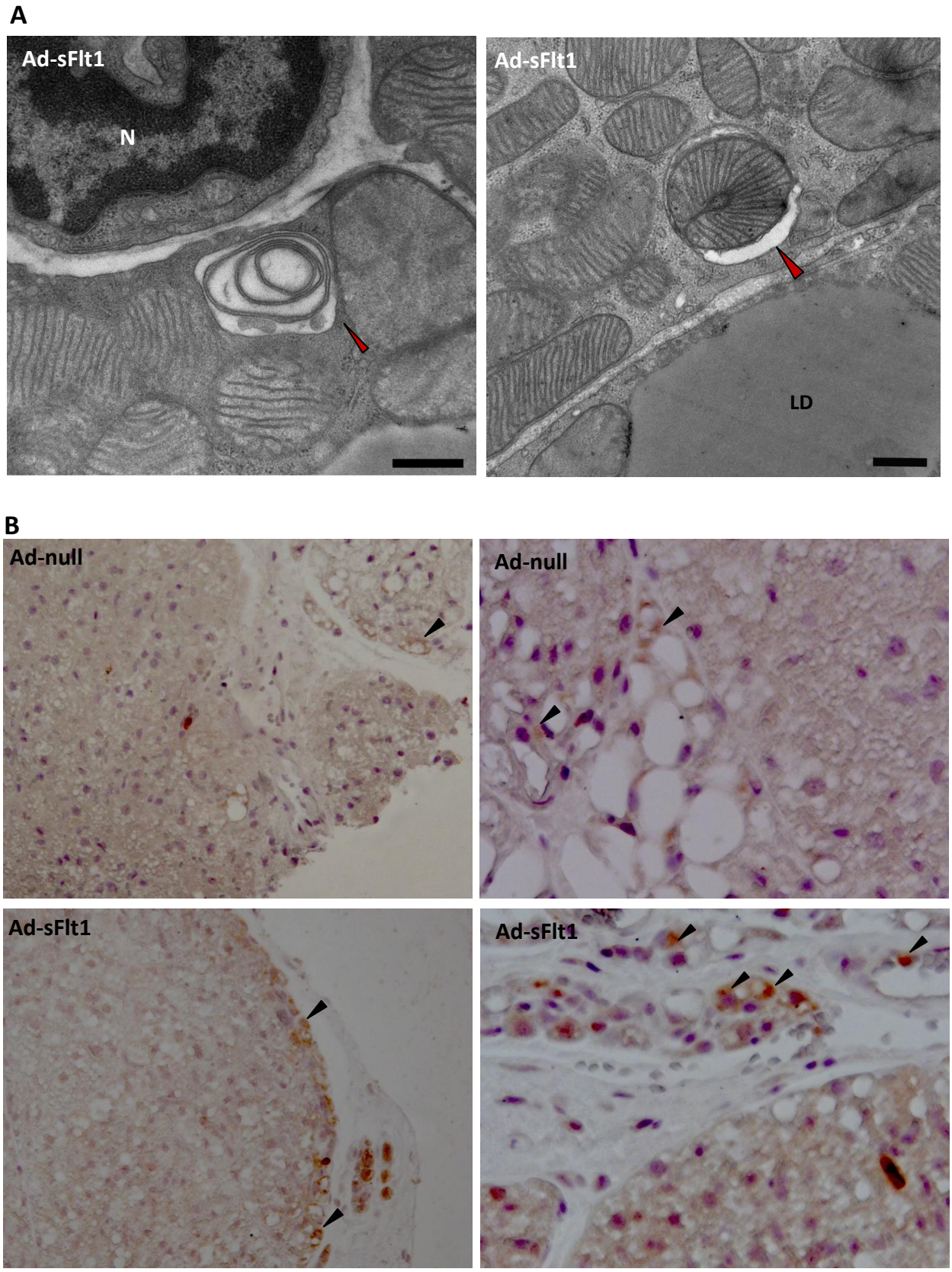

Figure 3.12 (continued)

Table 2 – Summary of effects of VEGF on brown adipocytes *in vitro* and *in vivo*

Function	*In vitro*	*In vivo*
Preadipocyte proliferation	VEGF increases	Not studied
Preadipocyte apoptosis	VEGF decreases	Not studied
Adipocyte apoptosis	DC101 increases apoptosis	sFlt1 increases apoptosis
Adipocyte differentiation	No significant effect	Not studied
Lipid droplet morphology	Not studied	sFlt1 increases lipid droplet size
Number of mitochondria	Not studied	sFlt1 decreases
Mitochondria morphology	Not studied	Abnormal with sFlt1
Mitochondria autophagy	Not studied	sFlt1 increases
BAT fibrosis	-	sFlt1 increases
BAT inflammation	-	sFlt1 increases

Section in pink indicates features associated with brown to white transdifferentiation. Section in green indicates probable effect of hypoxia resulting from capillary dropout.

Discussion

There are now numerous reports that the action of VEGF is not confined to the vasculature. A variety of non-endothelial cells express VEGFR2, the primary VEGF signaling receptor, and VEGF has been shown to act on these cells to mediate proliferation, differentiation and/or survival. Multiple lines of evidence, such as the presence of both VEGF and VEGF receptors in brown adipocytes, the dynamics of VEGF expression during brown adipocyte differentiation and cold acclimation of BAT, led me to hypothesize that VEGF signaling plays a role in brown adipocytes.

The increased metabolic capacity of cold acclimated-BAT results not only from elevated thermogenic activity in individual adipocytes but also a greater number of adipocytes. Hyperphagia or cold adaptation in BAT is accompanied by robust hyperplasia as a result of proliferation of both preadipocytes and endothelial cells. In fact, ^{3}H -thymidine labeling revealed a 70-fold increase in the number of proliferating cells in rats exposed to cold for two days compared to those at normal temperature (Bukowiecki et al. 1982). Whereas vascular remodeling takes a few days to a few weeks, we and others have observed that VEGF levels increase rapidly after cold exposure or adrenergic stimulation and return to initial (pretreated) levels 24 hours after treatment. This disconnection between time frame of increases in VEGF levels and that of vascular remodeling suggests that VEGF may regulate proliferation in brown preadipocytes. Furthermore, it was recently demonstrated that approximately ten percent of adipocytes are renewed annually throughout adult life, irrespective of body mass index (Spalding et al. 2008). While the

latter study was focused on white adipocytes, this observation nevertheless underscores the tight regulation of preadipocyte proliferation, differentiation and apoptosis.

Apoptosis in brown preadipocytes is regulated by insulin through PI3K/Akt signaling (Boucher et al. 2010; Miranda et al. 2010). I have demonstrated that VEGF also signals in these cells through VEGFR2 and the PI3K/Akt pathway to confer protection from apoptosis. While a role for VEGF in brown preadipocyte apoptosis has not been reported until now, it is a survival factor for a number of other cell types such as photoreceptors, podocytes and the retinal pigmented epithelium (Saint-Geniez et al. 2008; Ford et al. 2011; Guan et al. 2006). The data here demonstrate that VEGF acts as a mitogen on brown preadipocytes. As preadipocytes express VEGF and also VEGFR2, which we have shown is phosphorylated; it is likely that VEGF signals through an autocrine loop in these cells.

The effect of systemic VEGF neutralization on BAT has been investigated during cold acclimation (Xue et al. 2009) where it was shown to block angiogenesis. As there have been no reports on the effect of VEGF neutralization on unstimulated BAT or brown adipocytes I assessed the role of VEGF through systemic VEGF neutralization achieved by adenovirus mediated sFlt1 overexpression. VEGF neutralization reduced microvascular density of BAT, measured using the endothelial cell marker endomucin, by 50% in seven days of VEGF neutralization. A recent study reported that overweight/obese subjects had 44% lower capillary density compared to lean individuals (Pasarica et al. 2009). Thus, the level of capillary dropout in BAT (or BAT rarefaction) resulting from sFlt1 overexpression in my experiments is within the physiologically relevant range observed in obesity.

As adipose tissue is the most plastic organ in the adult; both hyperphagia or cold acclimation resulting in hyperplasia of BAT as well as WAT expansion during weight gain are accompanied by angiogenesis and remodeling of the adipose tissue vasculature. To adapt to the function and characteristics of adipose tissue, therefore, it is imperative that the microvasculature of adipose tissue be particularly plastic. In a study reporting the plasticity and VEGF dependency of adult vascular beds, thyroid and pancreatic islet vasculature were found to be the most plastic with about 70% reduced capillary density after 14 days of VEGF neutralization using ad-sFlt1 (Kamba et al. 2006), whereas microvasculature of the brain and retina are not affected in that time (Saint-Geniez et al. 2008). In comparison, our observation of a 45% reduction in microvascular density (judged by endomucin protein levels) after only seven days of VEGF neutralization, therefore, underscores the plasticity of adipose tissue vasculature and how it is primed for remodeling during adaptive tissue growth. Fenestrated capillaries with high levels of VEGFR2 have been found to be more plastic, whereas microvascular beds such as the retina and brain that have been shown to be more "stable" are characterized by a high pericyte to endothelial cell ratio. Therefore it would be interesting to examine the pericyte distribution and fenestrations in the BAT vasculature. High levels of VEGF expressed by BAT and the significant capillary dropout in BAT noted after seven days of VEGF neutralization is also consistent with the concept that high local levels of VEGF in a tissue reflect a strong dependence on VEGF compared to the vasculature in regions with lower VEGF levels (Saint-Geniez et al. 2008; Kamba et al. 2006).

As oxygen diffuses from the capillary bed, its partial pressure falls from approximately 100 mm Hg as it leaves the vessel to almost zero within as little as 100 µm

(Folkman et al. 2000). Reduced capillary density therefore results in local hypoxia. Hypoxia has been documented in the adipose tissue of obese humans and mice. Recent studies have demonstrated that fibrosis and inflammation are part of the response of adipose tissue to hypoxia (Pasarica et al. 2009; Halberg et al. 2009; Sun et al. 2012). The molecular response to hypoxia was modeled in a transgenic mouse that overexpressed HIF1α in adipose at levels found in the WAT of genetically obese *ob/ob* mice (Halberg et al. 2009). These transgenic mice had significantly increased collagen deposition in SC WAT compared to control mice. The levels of other extracellular matrix components such as collagens I, III and VI were also increased. Moreover, the adipose of the HIF1α-overexpressing mice was significantly more inflamed than that of the controls as evidenced by the presence of infiltrating macrophages. A recent study also reported that partial pressure of oxygen was lower in the adipose of overweight/obese humans compared to lean subjects and low partial pressure of oxygen was correlated with increased expression of inflammatory cytokines such as CD68 and macrophage inflammatory protein 1α (Pasarica et al. 2009).

In my experiments, systemic VEGF neutralization was associated with both the above hypoxia-mediated pathological outcomes, fibrosis and inflammation. Ad-sFlt1 injected mice had increased fibrosis, detected by Masson's trichrome staining of collagen fibers. This observation complements recent reports that adipose-specific overexpression of VEGF led to a reduction of fibrosis in adipose tissue of mice fed high fat diets (Sun et al. 2012) and is consistent with *in vitro* studies that demonstrated hypoxia induced expression of collagen I, fibronectin and TIMP1, in various mesenchymal cell lines. Similarly, there was increased local inflammation, judged by the presence of F4/80 positive cells present in BAT

and attaching to the endothelium wall of ad-sFlt1 injected mice. This finding is in agreement with an earlier report from our group demonstrating that VEGF (or TGFβ) neutralization resulted in a significant increase in the number of leukocytes rolling along the mesenteric endothelium. That study also showed elevated expression of surface adhesion molecules that mediated increased leukocyte adhesion, indicating an essential role for VEGF (and TGFβ) in maintaining the endothelium in a non-activated state (Walshe et al. 2009). The data here complement a recent report which showed that increased adipose expression of VEGF lessened inflammation associated with high fat died, measured by reduced expression of inflammatory cytokines such as TNFα and IL6 compared to control mice (Sun et al. 2012). Whether the inflammatory infiltrate is induced by adipocyte death or in response to chemokines secreted by BAT is unclear.

Local hypoxia is one of the earliest characteristics of adipose tissue expansion and leads to a cascade of obesity-associated adipose tissue dysfunctions, such as fibrosis and inflammation. Inflammation is a key link between obesity and pathogenesis of type 2 diabetes. In my experiments VEGF neutralization leads to fibrosis and inflammation in BAT, which resemble those observed in dysfunctional adipose tissue associated with obesity. These findings raise the possibility that reduced local VEGF expression and inadequate vascular remodeling may lie upstream of fibrosis and inflammation in adipose tissue.

Systemic VEGF neutralization resulted in brown adipocyte apoptosis, indicating that VEGF is important for mature brown adipocyte survival *in vivo*. As brown adipocytes express both VEGF as well as its receptors, VEGFR1 and VEGFR2, this finding also suggests an autocrine role for VEGF in brown adipocytes *in vivo*. This notion is supported by

observations *in vitro*. Cultured brown adipocytes, in which apoptosis was induced by treatment with TNFα and CHX, showed a higher level of cell death when VEGF signaling was blocked with DC101. This is physiologically relevant because circulating TNFα is significantly higher in obese animals, is known to induce apoptosis in brown adipocytes and my data suggest that the cytotoxic effects of TNFα may be aggravated in the absence of VEGF. Significantly more apoptosis was noted with systemic VEGF neutralization than in brown adipocytes treated with DC101 *in vitro*. These differences may be due to variation in duration of VEGF withdrawal, which was a few days *in vivo* compared to six hours *in vitro*. Additionally, as sFlt1 neutralizes the VEGF ligand, signaling through VEGFR2 and VEGFR1 are both blocked. Since both VEGFR2 and VEGFR1 are expressed in brown adipocytes, it is possible that there is compensatory VEGF signaling through VEGFR1. However, further experiments are needed to test this hypothesis. Further, sFlt1 also binds placental-derived growth factor and while there are no reports of placental growth factor expression in brown adipocytes, this possibility cannot be completely ruled out. Yet another explanation is that increased apoptosis is a secondary effect of VEGF neutralization on brown adipocytes, in response to the capillary regression resulting from VEFG neutralization. However, given my results on cultured brown adipocyte it seems unlikely that the increased brown adipocyte apoptosis *in vivo* is entirely a secondary effect, but may explain the difference between the degrees of apoptosis observed *in vitro* compared to *in vivo*. VEGF has been demonstrated to be protective for other highly specialized cell types such as photoreceptors, the retinal pigmented epithelium, Müller cells and podocytes .

Mitochondria are critical to brown adipocyte function, and a high density of mitochondria is a hallmark of functional brown adipocytes. The mitochondrial phenotype (or mitochondrioma), which is a measure of both mitochondria number and morphology, is a reliable indicator of the state of brown adipocyte activity. In active functional brown adipocytes, mitochondria are densely packed in the cytoplasm with transverse cristae spanning the entire length of the mitochondria (for a review see Cinti 2007). Active brown adipocytes are converted to an inactive state through degeneration of mitochondria, which are marked by partial or complete loss of cristae, and decrease in the number of mitochondria (Cigolini et al. 1986). Transdifferentiation of brown to white adipocytes is also accompanied by changes in the mitochondrioma. Systemic VEGF neutralization resulted in significant changes in the brown adipocyte mitochondrioma; there were fewer mitochondria in each cell compared to controls as well as histological evidence of massive mitochondrial degeneration, in the form of complete or partial loss of cristae and mitochondrial autophagy.

Autophagy, a lysosomal degradative pathway that mediates the removal and breakdown of cellular components, is critical to the maintenance of cellular homeostasis and for supplying the cell with metabolic substrates in times of nutrient deprivation (Czaja 2010). There are at least three distinct autophagic pathways: macroautophagy, microautophagy and chaperone-mediated autophagy. Macroautophagy is a multistep process through which portions of cytoplasm and/or organelles are sequestered in double or multi-membrane structures, known as an autophagosomes, and delivered to the lysosome for degradation. Fusion of the autophagosome with the lysosome, leads to the

formation of an autophagolysosome or autophagic vacuole. Although macroautophagy is generally considered a nonselective lysosomal process, there are instances in which organelles, such as mitochondria, appear to be preferentially sequestered, a process termed mitophagy (for a review see Kundu & Thompson 2005). Autophagy-related 7 (Atg7), which is critical for macroautophagy, is an ubiquitin E1-like enzyme that is involved in the formation of the autophagosome (Ichimura et al. 2000; Kabeya et al. 2004; Wu et al. 2006) and in the conversion of LC3 form I to the autophagy specific form II (Kabeya et al. 2000).

The profound changes in mitochondria along with the large lipid droplets seen in BAT from mice with systemic VEGF neutralization have at least two probable explanations. First, VEGF neutralization may result in transdifferentiation of brown adipocytes to white adipocytes, as seen in obesity. Two recent reports have demonstrated the effects of increased VEGF expression on WAT in mice engineered to overexpress VEGF specifically in adipose. Adipose specific VEGF expression resulted in WAT depots acquiring brown adipocyte-like properties, also known as "browning", including elevated levels of UCP1 and PGC1α compared to control mice (Sun et al. 2012). In addition, VEGF overexpression led to increased BAT mass and elevated UCP1 and PGC1α protein levels in BAT. An increase in body temperature in these mice compared to control mice was indicative of increased BAT activity (Elias et al. 2012). My results are consistent with these observations and suggest that the absence of VEGF leads to the opposite i.e. loss of brown adipocyte characteristics.

Recent work has demonstrated that autophagy may play a role in adipocyte differentiation (Singh et al. 2009a). Mice lacking the key macroautophagy regulator, Atg7, exhibited reduced white adipose and increased brown adipose. The reduced WAT depots

had morphologic and molecular features of brown adipocytes, including elevated levels of UCP1 and PGC1α. These findings indicated that the lack of autophagy favored the transdifferentiation of brown adipocytes from white adipocytes. While the mechanism of transdifferentiation remains to be determined, it has been hypothesized that autophagy, via the removal of the large numbers of mitochondria in brown adipocytes, may drive a critical remodeling function that mediates conversion of brown adipocytes to white adipocytes (Dong & Czaja 2011). My findings support this hypothesis as significant mitophagy is observed in brown adipocytes of ad-sFlt1 injected mice, along with fewer mitochondria and large lipid droplets, features atypical of brown adipocytes and suggestive of an early phase of brown to white transdifferentiation.

A second explanation for the changes in mitochondria seen in BAT with VEGF neutralization may be that reduction in capillary density presumably results in a nutrient poor environment for brown adipocytes which can trigger mitophagy. Mitophagy enables energy conservation by reducing overall number of mitochondria, the major fuel consumers of the cell, and by recycling their components. Mitochondrial degeneration also reduces the number of functional mitochondria and lowers the overall fuel requirements of the cell. Without active mitochondria to utilize triglycerides as fuel, they are stored in large lipid droplets in the brown adipocyte as it transitions from an active to an inactive state. To test this hypothesis, metabolic activity, such as rate of triglyceride oxidation and mitochondrial function of brown adipocytes from sFlt1 and control mice must be compared. In addition, to determine if VEGF neutralization is associated with transdifferentiation of brown adipocytes to white adipocytes or whether the brown adipocytes simply become inactive, levels of

leptin, expression of which is much higher in white adipocytes than brown adipocytes, should be compared in the BAT of sFlt1–expressing and control mice.

The role of brown adipose-derived VEGF is manifold and complex. VEGF promotes survival and proliferation signaling in brown adipocytes and acts on endothelial cells to stimulate angiogenesis as well as vascular cell survival. VEGF may have yet unidentified roles in brown adipocyte function that are key to normal BAT activity and the blockage of VEGF signaling could contribute to the pathogenesis of metabolic disorders. Given that many therapies for diseases employ VEGF neutralization; these agents should be used with caution as long term use may lead to unexpected and undesired side effects.

Chapter 4

ISOFORM-SPECIFIC ROLE OF VEGF IN BAT DEVELOPMENT

Introduction

The VEGF gene is alternatively spliced and polycationic regions encoded by exons 6 and 7 mediate binding to heparan sulfate proteoglycan, which determines their extracellular localization. The VEGF120 isoform, which does not include exons 6 and 7, does not bind heparan sulfate proteoglycans and is freely diffusible; VEGF188, which contains both exons 6 and 7, binds strongly to heparan sulfate and remains largely cell- and matrix-associated; and, VEGF164, which includes only exon 7, displays intermediate properties. The pattern of VEGF isoform expression varies among tissues both during development and in the adult (Ng et al., 2001). Mice expressing single VEGF isoforms, generated by deletion of splice sites or by replacement of genomic DNA (Carmeliet et al. 1999; Stalmans et al. 2002), demonstrated that the VEGF isoforms played distinct roles during development and in the adult both in vascular and non-vascular cells. Thus, I sought to investigate the distribution and role of the VEGF isoforms in adipose tissue.

Results

VEGF isoform expression in fat depots

To characterize the profile of VEGF isoform expression in BAT and WAT, qPCR was performed using isoform-specific VEGF primers. Absolute quantification of VEGF isoforms in white and brown fat depots revealed that together VEGF164 and 188 comprised >99% of total VEGF whereas VEGF120 accounted for <0.5% of total VEGF in both BAT and SC. In

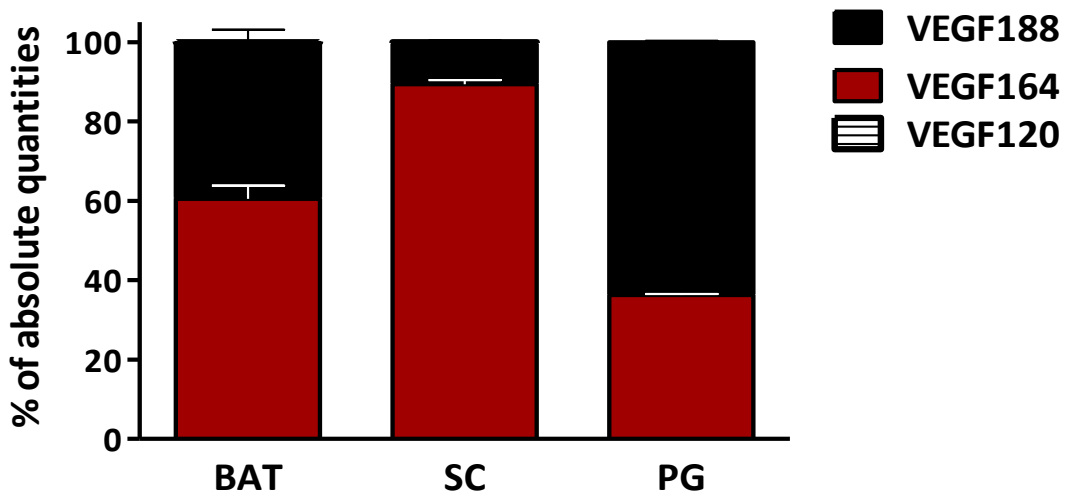

Figure 4.1. **VEGF164 and 188 are the predominant isoforms in adipose tissue, which expresses very little VEGF120.** The absolute amount of each isoform of VEGF was determined by quantitative PCR using isoform specific primers and serial dilutions of a known amount of standard. The total VEGF mRNA was the sum of the three isoforms. The percentage of each isoform was calculated based on the total VEGF thus obtained.

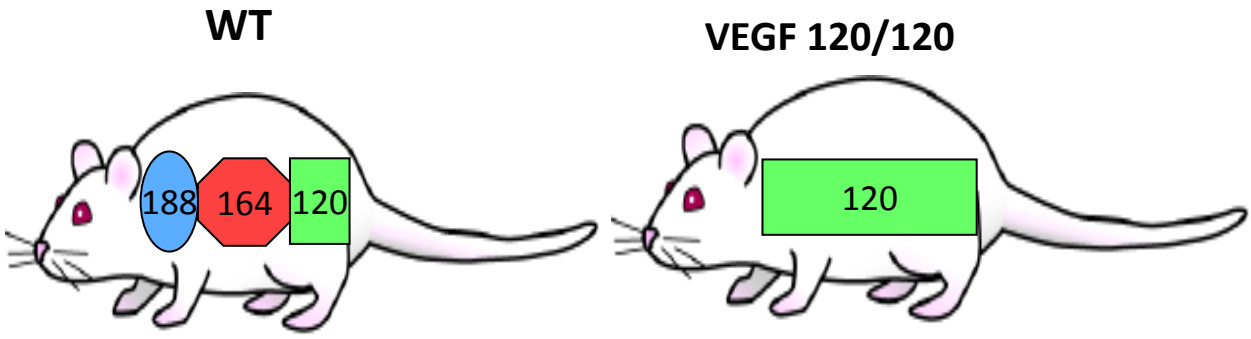

Figure 4.2. **VEGF120 isoform specific mouse.** This mouse was engineered by targeted deletion of exons 6 and 7 of the VEGF gene by homologous recombination in all cells, so that transcription of only VEGF120 is possible. These mice express the same total amount of VEGF, but only in the 120 isoform and present multiple vascular and organ specific abnormalities. (Carmeliet et al., 1999)

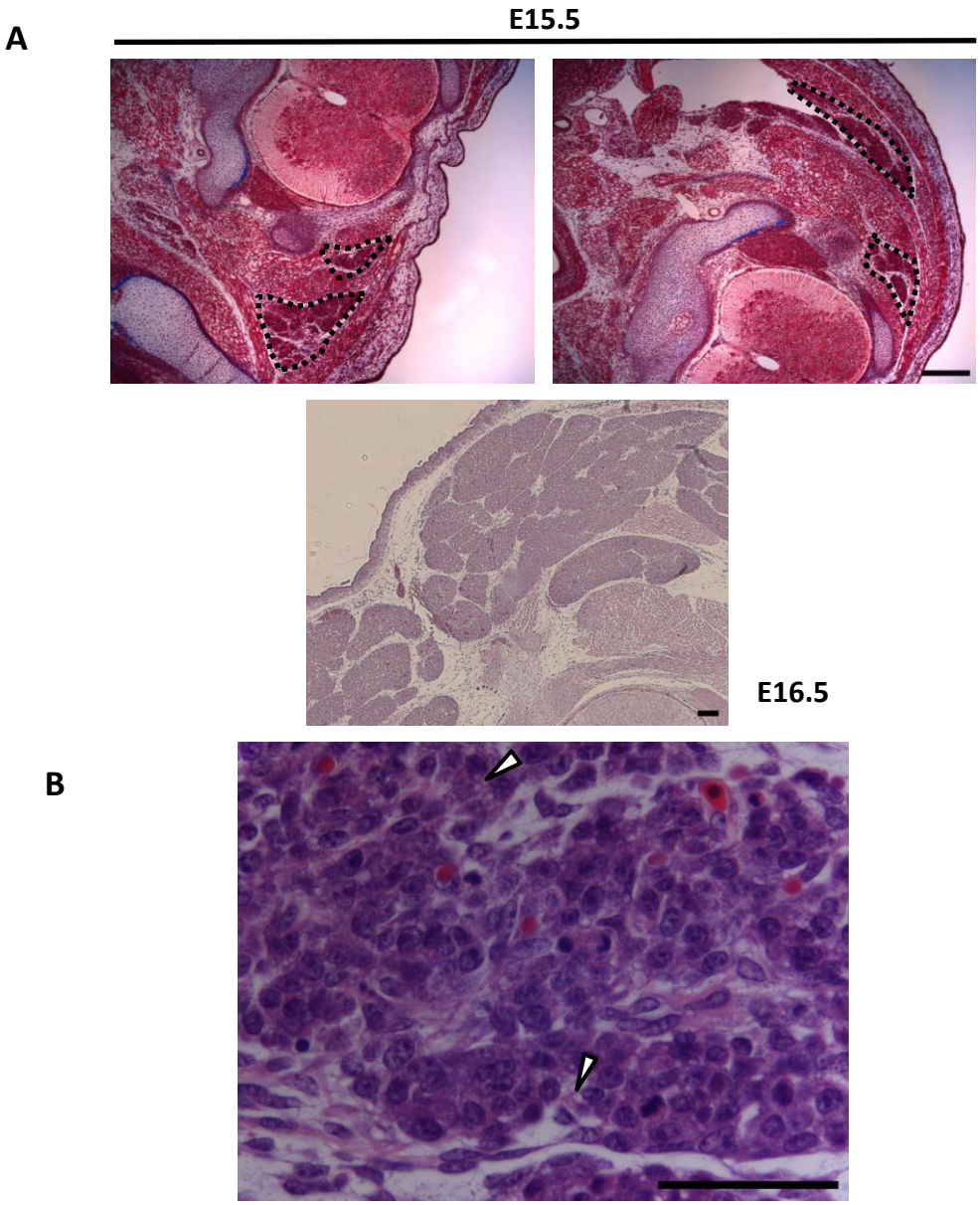

Figure 4.3. **Brown adipose tissue in the wild type mouse embryo.** BAT develops around E15 in the mouse. (A) Embryonic interscapular BAT depots at E15.5, visualized by Masson's trichrome staining, are depicted (*top panel*). The right and left depots are visible (dotted black line) on either side of the notochord on the dorsal part of the embryo. *Bottom panel*: embryonic BAT at E16.5, visualized by H&E. The right and left sides are now closer, indicating rapid expansion of BAT mass. The appearance at this stage is very similar to interscapular BAT of neonatal mice**.** Scale bar represents 100 µm. **(B)** Higher magnification of interscapular BAT, visualized by H&E, at E15.5. They have densely packed cells with cuboidal morphology and tiny lipid droplets (arrowheads). Scale bar represents 50 µm.

BAT, 45% of the VEGF was VEGF164 and 55% was VEGF188, whereas VEGF in SC was 84% VEGF164 and 16% VEGF188 (Figure 4.1).

Abnormal BAT Morphology in VEGF 120/120 Embryo

To investigate the role of more locally acting VEGF isoforms, 164 and 188, in adipose development, I examined adipose tissue in mice, which were genetically engineered to express only the 120 isoform (VEGF120/120), but at a level comparable to total VEGF in wild type mice (Figure 4.2). Since VEGF 120/120 mice die during late gestation and WAT forms only after birth, my analyses were confined to BAT, which develops in the interscapular region around E15.5. The notochord and dorsal dermal layer separate the left and right interscapular BAT depots and there is rapid expansion of BAT mass such that by E16 there is significant amount of interscapular BAT (Figure 4.3). As E15.5 was the latest time point at which VEGF 120/120 mouse could be obtained, the structure of BAT from VEGF 120/120 and wild type E15.5 littermates was examined using hematoxylin & eosin and Masson's trichrome staining. There was a significant reduction in the volume of brown adipose tissue (dotted white line) in 120/120 embryos compared to their wild type littermates (Figure 4.4A). Whereas brown adipocytes in wild type mice were arranged in compact clusters, brown adipocytes in VEGF 120/120 mice were disorganized and scattered in the interscapular region, with large gaps containing some collagen deposition separating much smaller clusters of adipocytes (Figure 4.4B). Typical of this stage in development, brown adipocytes in wild type mice were cuboidal in shaped and had tiny lipid droplets. In contrast, there was no apparent lipid accumulation in the adipocytes of VEGF 120/120 mice

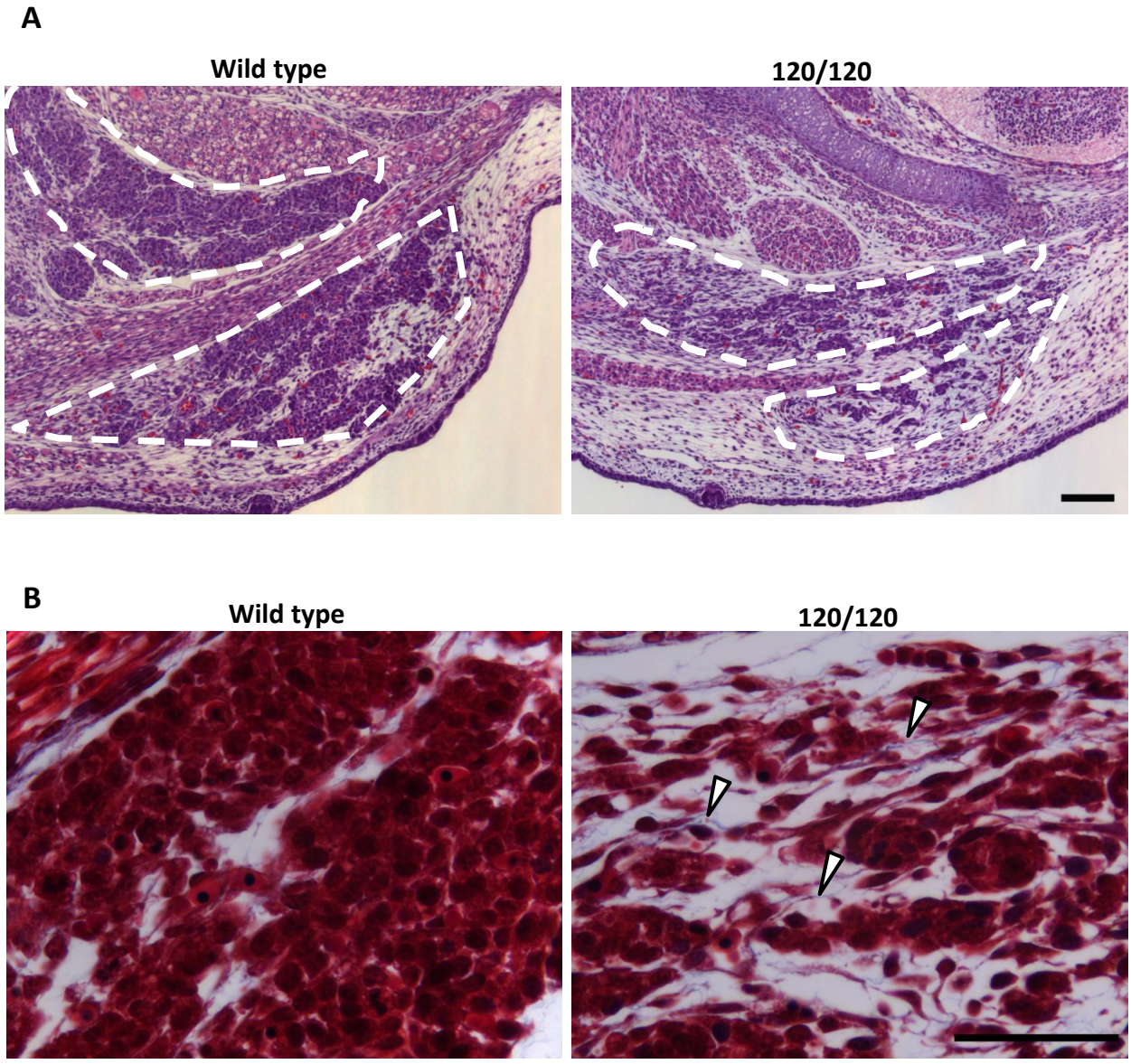

Figure 4.4. **Reduced BAT and abnormal BAT organization in embryo with only VEGF120 (A)** Morphology of brown fat in wild type (left) and VEGF 120/120 (right) embryos at E15.5 revealed by H&E staining shows reduced embryonic brown adipocytes in the interscapular depot of 120/120 embryo compared to wild type **(B)** Masson's Trichrome (higher magnification) reveals disorganized tissue structure. Small clusters of embryonic brown adipocytes are surrounded by abundant extracellular matrix, with some collagen deposition (arrowhead). Scale bar represents 50 µm.

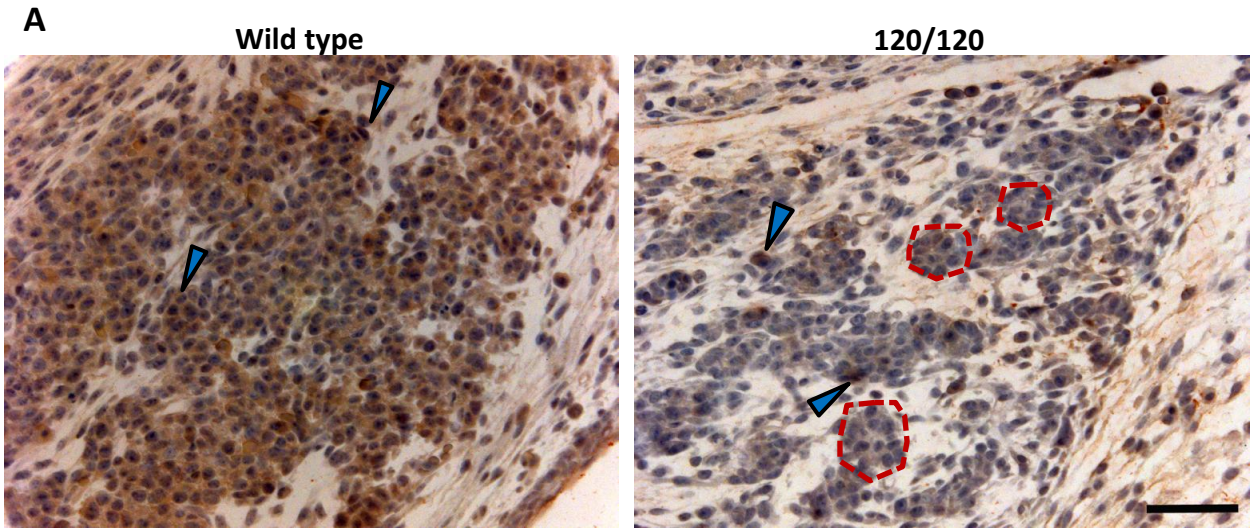

Figure 4.5. **Abnormal brown adipocyte differentiation and mitochondrial content of embryonic BAT with only VEGF120 (A)** IHC localization of UCP1, a brown adipocyte marker, showing robust expression in wild type but reduced and mosaic expression in 120/120 brown adipocytes. Dotted red lines indicate clusters of brown adipocyte cells in 120/120, in which most cells have a low expression compared to wild type, with a few cells depicting strong expression (blue arrowheads). **(B)** IHC localization of the mitochondrial marker Cox IV depicting strong expression in almost all wild type cells and low expression (white arrowheads) in most 120/120 cells, with very few depicting strong expression (red arrowheads) . Scale bar represents 50 µm.

Abnormal mitochondrial protein expression in VEGF 120/120 Embryo

To gauge the functional integrity of the brown adipose, I examined the distribution of UCP1, which is essential for brown adipocyte thermogenesis, and Cox IV protein, a member of the electron transport chain and a well established mitochondrial marker. Brown adipocytes in wild type embryos stained strongly for both UCP1 and Cox IV whereas in VEGF 120/120 embryo there was a significant decrease in number of cells expressing UCP1 (Figure 4.5A). Cox IV expression was also reduced in the VEGF120/120 brown adipocytes relative to that of wild type; in the VEGF120/120 mice there was a high level of Cox IV expression (Figure 4.5B red arrowheads) in a few cells and low-to-undetectable levels in other cells (white arrowheads). The relative absence of mitochondrial markers indicates that the putative brown adipocytes were not properly differentiated. There was no difference in apoptosis between the VEGF 120/120 and wild type brown adipocytes at E15.5 (data not shown) nor was there any measurable difference in cell proliferation, which was visualized by IHC with Ki67 and phosphorylated histone H3 antibodies (data not shown). These observations suggest that the reduction in brown adipocytes at E15.5 is likely due to decreased cell survival or proliferation at an earlier point in development, possibly at the stage of adipocyte precursors or adipoblast.

Discussion

Nearly all of the VEGF in BAT and WAT depots are isoforms that bind heparan sulfate proteoglycans (VEGF164 and VEGF188). The pattern of VEGF isoform distribution varies

widely among vascularized tissues. For example, VEGF188 is the predominant VEGF isoform in the lungs whereas the retinal pigmented epithelium (RPE) expresses virtually no VEGF188 (Saint-geniez et al. 2009). Based on the distribution of VEGF among a variety of tissues our laboratory has observed that the pattern of VEGF isoform expression in a tissue appears to be 'consistent' with the proximity between the VEGF source and its target(s). For instance, in the lung VEGF188 is produced by type II pneumocytes, which are separated from their target, the alveolar capillaries, by a very thin basement membrane (Galambos et al., 2003) and the lungs of mice lacking the heparan sulfate-binding forms of VEGF (i.e. expressing only VEGF 120) reveal extensive microvascular and pulmonary defects. In the eye, on the other hand, the RPE produces VEGF120 and VEGF164, but virtually no VEGF188, presumably reflecting the fact that VEGF produced by the RPE must diffuse across, Bruch's membrane, an elastic lamina, to reach the choriocapillaris. Accordingly, mice that express only VEGF188 display age-dependent degenerative changes in the RPE-choroid complex (Saint-Geniez et al. 2009). Similarly, in the brain the choroid plexus epithelium produces predominantly VEGF120, which supports not only the underlying fenestrated microvasculature but diffuses into the cerebrospinal fluid to act on the VEGFR2-expressing ependymal cells of the ventricular lining (Maharaj et al. 2008). Thus, the predominance of VEGF188 and VEGF164 in BAT suggests that VEGF plays both an autocrine role to support the integrity and survival of brown adipocytes and a paracrine function to promote angiogenesis during development and then vascular maintenance in the adult.

VEGF 120/120 mice express VEGF at the same level as total VEGF in wild type mice (Carmeliet et al. 1999) and die in late gestation due to defects in pulmonary and cardiac

angiogenesis. Mice expressing only VEGF120 exhibited defective ocular development including microphthalmia, abnormal lens differentiation and hyperplastic hyaloid vessels (Saint-Geniez et al. 2009). The diminished volume of BAT and the abnormal organization of the brown adipocytes that do develop in 120/120 embryos could be due to a direct effect on brown adipocytes or be secondary to defective angiogenesis. Observations that VEGF 120/120 mice exhibit abnormal vascularization and angiogenesis in multiple organs such as lungs, heart and cartilage (Zelzer et al. 2002) favor the latter hypothesis, particularly because angiogenesis precedes adipogenesis in the development of adipose depots (Hausman & Richardson 2004). On the other hand, the mitochondrial abnormality detected in the 120/120 adipocytes, coupled with my observations of mitochondrial degeneration in mature brown adipocytes of mice with systemic VEGF neutralization, suggest that there may also be a direct effect of VEGF on embryonic brown adipocytes. The resulting phenotype may well be an outcome of a possible direct effect of VEGF on adipocytes as well as an indirect effect through abnormal angiogenesis and further analyses of BAT development at different time points in 120/120 embryos is needed to better analyze the phenomenon.

Based on my observations that VEGF promotes adipocyte survival it was surprising that no apoptosis was detected in the 120/120 embryos at the stage examined. However, my finding that VEGF is a mitogen for preadipocytes points to the possibility of reduced proliferation and/or survival of brown adipocyte precursors which led to a diminished population of adipocyte precursors available to differentiate to. A recent report investigating forebrain development reported reduced proliferation of neural precursors in

VEGF 120/120 mice and suggested a role for the heparan sulfate binding VEGF isoforms in maintenance of the neural precursor population (Darland et al. 2011). In order to test this hypothesis, a reliable marker unique to brown adipocyte precursors would be required to examine embryos at earlier stages of development. While the existence of such markers is not widely reported, there is some evidence to suggest that engrailed1 and c-myc are expressed in precursor cells in the interscapular BAT depot.

My results, along with other reports on phenotypes of mice expressing single VEGF isoforms, emphasize the fact that the various VEGF isoforms serve different yet overlapping roles. Whereas mice lacking only one allele of VEGF die at E8.5, mice expressing only VEGF120 survive until late gestation, indicating that VEGF120 can at least partially compensate for the functions of the other isoforms. On the other hand, the specific abnormalities exhibited by mice expressing only one VEGF isoform underscore the distinct functions of each isoform in individual tissue and cellular contexts.

Chapter 5

REGULATION OF VEGF EXPRESSION IN BROWN ADIPOCYTES

Introduction

In light of my observations that VEGF expression increases concomitantly with adipocyte differentiation and VEGF plays a significant role in brown adipocytes, it appears likely that VEGF expression and brown adipocyte differentiation are coordinately controlled by the same molecular regulators. The transcription factor PPARγ, the master regulator of adipogenesis, and its transcriptional cofactor PGC1α are crucial in brown adipocyte differentiation and function. I therefore hypothesized that VEGF expression is regulated by PPARγ and PGC1α in brown adipocytes.

Results

PPARγ agonists increase VEGF expression in brown adipocytes in vitro

PPARγ expression during brown adipocyte differentiation was examined by qRT-PCR (Figure 5.1). By day three of differentiation PPARγ expression was increased nearly 10-fold compared to undifferentiated cells, and remained high during the eight day course of differentiation. The increased VEGF expression (Figure 2.7) followed the pattern of PPARγ expression. The levels of hypoxia inducible factor (HIF)1α, a known regulator of VEGF, were observed to decrease over the course of differentiation (Figure 5.1) as did the expression estrogen related receptor (ERR)α, another recently described regulator of VEGF in skeletal muscle (data not shown). To test my hypothesis, differentiated brown adipocytes were treated with the PPARγ agonist troglitazone and RNA was collected from samples at various

time points following treatment. Analysis of VEGF mRNA expression revealed a 1.5-fold increase in the expression of VEGF within six hours of treatment and a nearly two-fold increase after twelve hours of treatment compared to untreated cells; the increase was sustained through 24 hours post TZD treatment (Figure 5.2). Expression of aP2, which is a known target of PPARγ and was used as a positive control, also increased compared to untreated cells, reaching a nearly six-fold increase following 24 hours of TZD treatment.

VEGF expression in BAT is reduced in the absence of PGC1α

PGC1α is crucial for BAT thermogenesis and has been shown to induce VEGF expression in skeletal muscle following exercise through the ERRα transcription factor (Chinsomboon et al. 2009). Moreover, the pattern of VEGF expression in BAT with CL 316,243 stimulation temporally mirrored that of PGC1α (Figure 2.8). Thus, to investigate whether PGC1α can alter VEGF expression in BAT I examined VEGF mRNA levels in the BAT of PGC1α knockout mice. VEGF RNA was significantly reduced in the BAT of adult male PGC1α null mouse, with an average VEGF expression of 40% of that in wild type (Figure 5.3). Preliminary observations of heterozygous mice showed that VEGF expression was 70% that of wild type mice, suggesting a dose dependent regulation of VEGF by PGC1α.

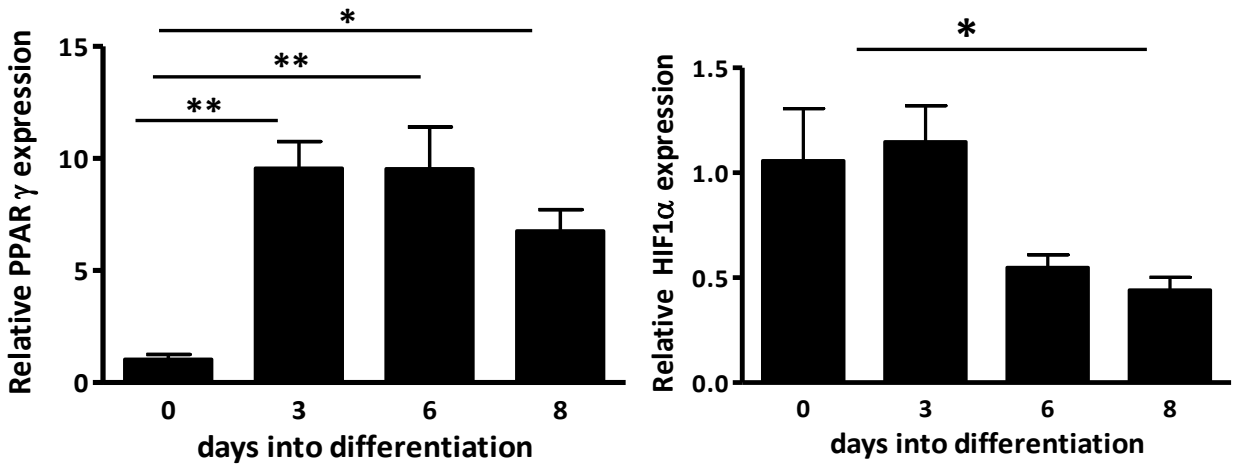

Figure 5.1. **Transcription factor expression during brown adipocyte differentiation.** PPARγ expression increases during brown adipocyte differentiation while HIF1α expression decreases, determined by qPCR. p*<0.05, p**<0.01.

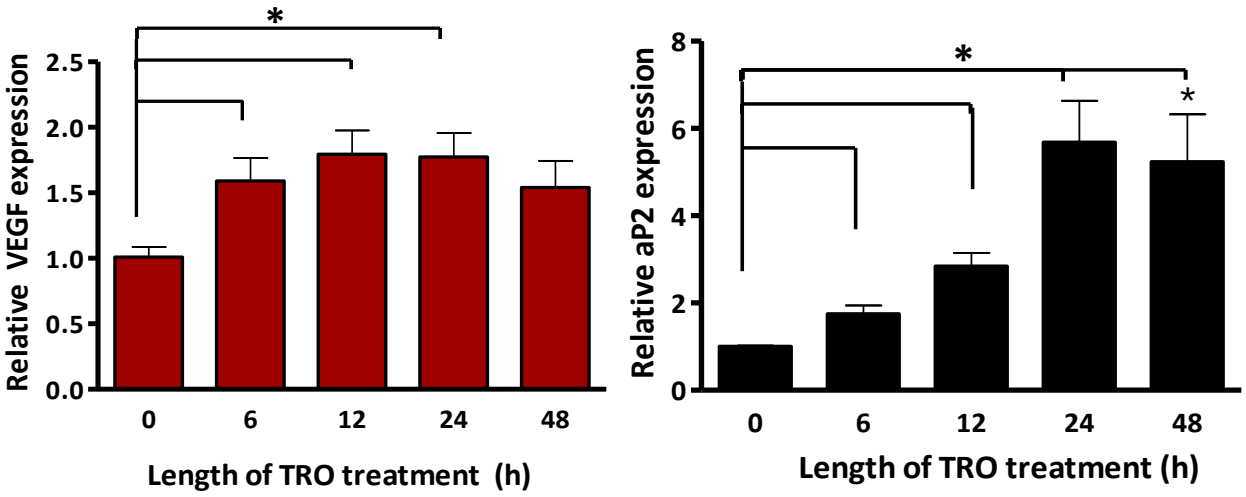

Figure 5.2. **Induction of VEGF in brown adipocytes following treatment of PPARγ agonist troglitazone.** Brown adipocytes on day eight of differentiation were treated with 1μM troglitazone (TRO) and expression of VEGF measured at various time points using qPCR. VEGF expression is induced within six hours of treatment and sustained upto 24 hours. aP2 expression is used as a control for PPARγ transcription activity as a known transcriptional target of PPARγ. p*<0.05

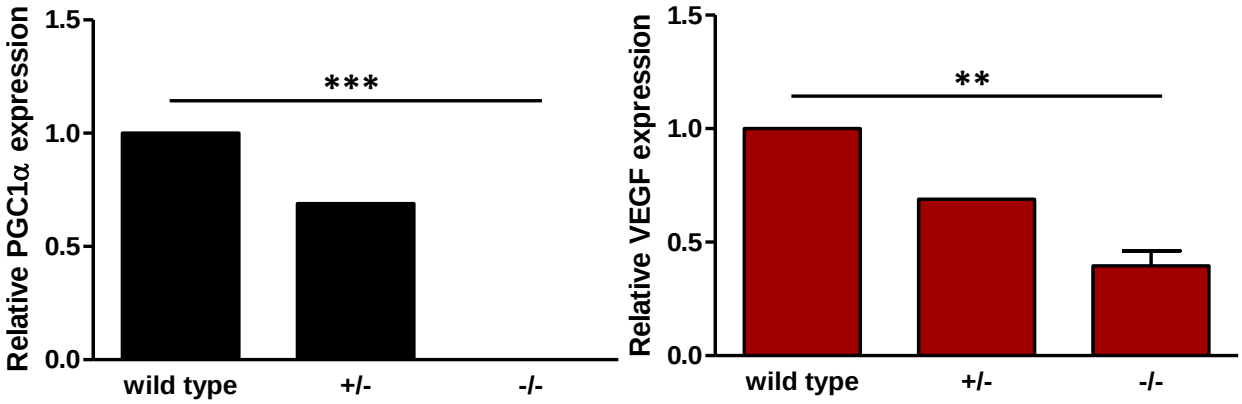

Figure 5.3. **Reduced VEGF expression in BAT of PGC1α knockout mice.** VEGF expression (right) in the BAT of adult male mice lacking one or both alleles of PGC1α examined by qPCR, indicated dose dependant decrease in levels of VEGF in the absence of PGC1α (left). p**<0.01, p***<0.001.

Discussion

Diverse VEGF expression is regulated by hormonal and developmental signals. The transcription factor HIF1α is a major mediator of hypoxia-induced gene expression changes and has been shown to regulate VEGF expression. In fact, hypoxic regulation of VEGF expression via HIF1α is the best characterized mechanism of VEGF control, including during vascularization of some tissues such as retina (Ferrara et al. 2003). However, this mechanism was not likely to play a role in the observed VEGF expression that accompanied *in vitro* brown adipocyte differentiation as the cells in culture are not hypoxic. Interestingly, in spite of the intense focus on the role of HIF1α in the regulation of VEGF, deletion of the hypoxia-response element in the VEGF promoter resulted in a viable mice with only minor phenotypes whereas VEGF -/- and +/- mice are embryonic lethal. The dispensable nature of HIF1α-mediated VEGF transcription suggests that HIF1 is much less important in the regulation of VEGF than previously suspected. My data suggest PPARγ/PGC1α-mediated regulation of VEGF transcription in adipocytes. VEGF expression was increased after treatment of differentiated brown adipocytes with TZD and was significantly reduced in the BAT of mice lacking PGC1α.

Several studies have reported the PPARγ-activation mediated regulation of VEGF. In vascular smooth muscle cells and murine macrophages both endogenous and synthetic PPARγ agonists increase VEGF expression by 1.5- to 2-fold and 2.5- to 3-fold, respectively, through transcriptional activation of the VEGF promoter (Jozkowicz et al. 2000). Furthermore, oxidized low density lipoproteins increase VEGF expression through PPARγ

activation in a number of human monocyte/macrophage cell lines and in human coronary artery endothelial cells (Inoue et al. 2001). On the other hand, both endogenous and synthetic PPARγ agonists have been demonstrated to repress VEGF expression in human endometrial cells also through its activity on the VEGF promoter (Peeters et al. 2005). Rosiglitazone has been shown to repress VEGF expression by 40 – 55% in tumor cell lines derived from lung carcinoma and glioblastoma (Panigrahy et al. 2002). Thus, it appears that the effect of PPARγ activation on VEGF expression is dependent on the cell type and tissue context.

Work by our group has previously demonstrated that VEGF expression increases during myocyte differentiation *in vitro* and that this increase is regulated by the transcription factor MyoD, a key myogenic differentiation factor, which associates with the VEGF promoter (Bryan et al. 2008). It has also been shown that VEGF expression in skeletal muscle induced by intense exercise does not involve the canonical hypoxia response pathway and HIF1α. Rather, it is mediated by PGC1α through the transcription factor ERRα binding to conserved binding sites in the promoter and first intron of the VEGF gene to activate VEGF transcription (Chinsomboon et al. 2009). PGC1α increases during brown adipocyte differentiation as well as following adrenergic stimulation, and is a key effector of the thermogenic response in brown adipocytes (Puigserver 2003; Kajimura et al. 2010). VEGF expression in brown adipocytes has also been demonstrated to be independent of hypoxia during cold acclimation, and regulated via a β3 adrenoreceptor/cAMP/PKA pathway (Fredriksson et al. 2000; Fredriksson et al. 2005; Xue et al. 2009).

Thus, we hypothesized that PGC1α would also regulate VEGF expression in normal brown adipocytes and during cold acclimation. Our preliminary results indicating a dose-dependent association between VEGF expression and PGC1α levels *in vivo* are consistent with this hypothesis. A recent report showing that PGC1α and -β mediate VEGF expression in brown adipocytes during hypoxic conditions provides further evidence in support of PGC1 mediated regulation of VEGF (Pino et al. 2012). While PGC1α is required for VEGF expression in BAT, as a cofactor it requires a transcription partner to alter gene expression. Based on my preliminary data, I propose a model in which PGC1α and PPARγ regulate VEGF expression in brown adipocytes.

Future studies will examine whether the absence of PPARγ activation affects VEGF expression in brown adipocytes and if VEGF expression is altered by endogenous PPARγ activators. Moreover, it would also be of interest to determine whether VEGF increase observed during adrenergic stimulation, while independent of hypoxia and HIF1α, is regulated by PPARγ. Since PPARγ agonists are used in the treatment of type 2 diabetes, their effects on the expression of VEGF is clinically relevant.

Chapter 6

GENERAL DISCUSSION

Discussion

While several studies have reported the production of VEGF in BAT and brown adipocytes and have demonstrated the role of VEGF in adipose tissue angiogenesis, the function of VEGF on brown adipocytes themselves has not been explored. A few recent studies have provided interesting hints, such as the increased BAT function and "browning " of WAT observed in mice expressing adipose specific transgenic VEGF, to suggest that VEGF may play a direct role in brown adipocytes (Sun et al. 2012; Elias et al. 2012).

My examination of white and brown fat depots revealed high levels of VEGF isoforms and their receptors VEGFR1 and VEGFR2 in most depots with BAT having a higher expression of both VEGF and receptors when compared to WAT. In addition, VEGF expression was coordinately regulated with brown adipocyte differentiation as evidenced by the concomitant increase in the expression of PPARγ, PGC1α, UCP1 and the adrenergic receptor type β3 with VEGF. Differentiated, but not precursor, brown preadipocytes expressed PGC1α and UCP1, the hallmark genes of brown adipocytes, and responded to norepinephrine stimulation by increased mitochondrial biogenesis and UCP1 expression. The expression of VEGFR2 in undifferentiated preadipocytes and differentiated brown adipocytes was a surprising and novel finding. VEGFR2 was phosphorylated in unstimulated cultured brown preadipocytes and adipocytes indicating active VEGF signaling in these cell types. VEGF expression also appeared to be coordinately regulated with WAT differentiation where the increase in VEGF during 3T3L1 differentiation was temporally correlated with the expression of PPARγ and with the expression of aP2, a known adipocyte

marker. In contrast to differentiated brown adipocytes, VEGFR2 was not expressed in white adipocytes, a finding that is consistent with a previous report (Fukumura et al., 2003).

My finding of VEGFR2 phosphorylation in cultured brown preadipocytes and differentiated adipocytes supports the hypothesis of autocrine or juxtacrine VEGF signaling. In support of this notion, the addition of VEGF induced preadipocyte proliferation *in vitro* and VEGF was a survival factor for both preadipocytes and mature adipocytes *in vitro*. These results were corroborated *in vivo*; systemic neutralization of VEGF resulted in apoptosis of brown adipocytes as early as seven days post injection and was associated with inflammation and fibrosis, presumably the result of the significant cell death and hypoxia.

Examination of the ultrastructure of BAT from sFlt1-expressing mice revealed abnormal mitochondria with partial or complete loss of cristae, a phenotype that is commonly associated with reduced mitochondrial activity and degeneration (Cinti 2007; Cigolini et al. 1986). Adipocytes in mice with systemic VEGF neutralization also displayed macroautophagy of mitochondria (mitophagy), a phenomenon completely absent in control BAT, along with an increase in autophagosomes, judged by the presence of LC3B form II puncta. The mitochondrial autophagy in brown adipocytes seen with VEGF neutralization was intriguing as it has been proposed that mitophagy regulates brown-white transdifferentiation of adipocytes and negatively correlates with brown adipocyte fate (Singh et al. 2009b). Inhibition of mitophagy by deletion of the critical autophagy regulator Atg7 decreased WAT mass, increased “browning” of white adipocytes, including brown specific gene expression, reduced lipid storage, and increased BAT mass (Singh et al. 2009b). The BAT from mice expressing sFlt1 exhibited large fusing lipid droplets, a characteristic

more typical of white adipocytes, and a trend towards higher triglyceride content was also observed even though the BAT mass itself was reduced in sFlt1-expressing mice compared to controls. Our findings complement this report as increased mitophagy is associated with loss of brown adipocyte characteristics and features indicative of early stage of brown to white transdifferentiation. Another likely explanation is that systemic VEGF neutralization results in dysfunctional or inactive brown adipocytes in which the mitochondria are not employed in fatty acid oxidation, and thus targeted for autophagy to maintain cellular homeostasis and conserve cellular resources. Consistent with our observation of decreased brown adipose features, it has recently been demonstrated that adipose tissue-specific VEGF expression results in "browning" of white adipose tissue, increased BAT mass and function, and protection against high fat diet and insulin resistance (Elias et al. 2012; Sun et al. 2012).

The pattern of VEGF isoform expression varies among tissues both during development and in the adult (Ng et al., 2001). Examination of VEGF isoform expression in BAT revealed that VEGF188 and VEGF164 each comprised approximately 50% of total VEGF with VEGF120 accounting for less than 1%. The splice variants of VEGF have different binding affinities to heparan sulfate: VEGF120 lacks heparan sulfate binding sites and is freely diffusible, whereas VEGF188 binds strongly to heparan sulfate. VEGF188 largely remains matrix- and cell- associated and is thought to act locally whereas VEGF164 has intermediate properties. Our laboratory has found that the pattern of VEGF isoform expression in various tissues reflects the proximity between the VEGF source and its target(s). The predominance of heparan sulfate-binding VEGF isoforms in BAT is consistent

with my findings that VEGF functions in brown adipocytes in an autocrine or juxtacrine manner. To investigate the role of VEGF188 and VEGF164 in development of BAT, I used mice that were engineered to express only VEGF120 (Carmeliet et al. 1999). The absence of VEGF188 and 164 led to significant morphological abnormalities in the embryonic brown adipocytes, including disorganization and a marked reduction in number relative to embryonic wild type brown adipocytes. There was no detectable difference in adipocyte proliferation or apoptosis at the time point examined. Based on my *in vitro* observations that VEGF is a mitogen for preadipocytes, I speculate that the BAT anomalies seen in VEGF 120/120 mice may be the result of decreased survival or proliferation of brown preadipocytes.

UCP1 expression was markedly reduced in the brown adipocytes of VEGF 120/120 mice, with most cells displaying little or no expression, a phenotype indicative of incomplete differentiation. Mitochondrial content was also significantly reduced, indicating impaired mitochondrial biogenesis. This finding in VEGF 120/120 mice was consistent with my observation that systemic VEGF neutralization resulted in massive mitochondrial degeneration and reduced mitochondrial number and may point to a novel role for VEGF in the regulation of adipocyte metabolism. VEGF has been shown to regulate a variety of functions in other cell types. For instance, in murine podocytes VEGF is involved in homeostasis of slit diaphragm proteins such as podocin and CD2AP that are required for the function of the glomerular filtration barrier (Guan et al. 2006). VEGF promotes myotube hypertrophy *in vitro* and neutralization of VEFG leads to myotube hypotrophy (Bryan et al. 2008) and increases bone mineralization during osteogenic differentiation (Mayer et al.

2005). Culture of RPE cells with VEGF neutralization results in blunted and reduced microvilli, structures which facilitate the critical interaction between RPE and photoreceptor outer segments (Ford et al. 2011). Alternatively or additionally, the observed mitochondrial degeneration may be an indirect effect resulting from an overall nutrient poor environment due to capillary dropout after systemic VEGF neutralization.

We previously demonstrated that the expression of VEGF is coordinately regulated as part of the myogenic differentiation program where it serves not only to induce angiogenesis but in an autocrine function in differentiating myocytes. MyoD, the transcription factor critical for myogenic differentiation regulated VEGF transcription in C2C12 myocytes *in vitro* (Bryan et al. 2008). Here we show that VEGF expression is coordinately increased during normal brown adipocyte differentiation and that its expression in brown adipocytes is positively regulated by PPARγ agonists *in vitro* and PGC1α *in vivo*, both critical for brown adipocyte differentiation and function. Based on my preliminary data I propose a model in which PGC1α mediates VEGF expression in brown adipocytes with the transcription factor PPARγ in tandem with the process of brown adipocyte differentiation and during cold acclimation.

The formation of a vasculature is essential for proper organ development and function and is tightly regulated by various pro- and anti-angiogenic factors. The resulting vascular network is specialized with features, such as fenestrations or tight junctions, to meet the needs of the organ it supplies. As for virtually all other tissues, adipogenesis and angiogenesis are spatially and temporally coupled (Crandall et al. 1997). In the adult, adipose tissue is one of the most plastic organs. Cold acclimation is marked by profound

hyperplasia in BAT of preadipocytes and endothelial cells (Bukowiecki et al. 1982). The mass of WAT varies greatly with body weight and expanding adult WAT is characterized by endothelial cell proliferation (Crandall et al. 1997). It is well known that VEGF is critical for adipose tissue angiogenesis. Administration of neutralizing antisera against VEGFR2 to obese mice led to significantly lower body weights and improved metabolic function (Sun et al. 2012). On the other hand, increased expression of VEGF in adipose tissue improved insulin sensitivity and metabolic profile during the early stages of high fat diet-induced weight gain, as well as inducing browning of WAT depots and increased BAT mass (Sun et al. 2012; Elias et al. 2012). This underscores the pivotal role of VEGF in adipose angiogenesis. Our work has identified an additional function of VEGF in BAT, its direct beneficial effects on brown adipocytes to promote their survival, proliferation and maintenance of brown adipocyte mitochondrioma.

Our work and that of others have demonstrated that VEGF acts in an autocrine manner on non-endothelial cell types of multiple adult tissues. In addition to those described earlier in this chapter, VEGF promotes survival of Muller cells of the adult retina (Saint-Geniez et al. 2008), induces neuronal differentiation of astroglial cells of the adult brain (Li et al. 2012), functions in the maintenance of the ependymal cells of the of the choroid plexus overlying fenestrated vessels (Maharaj et al. 2008), promotes the survival and maintenance of RPE (Ford et al. 2011), increases survival and slit diaphragm protein homeostasis in podocytes (Guan et al 2006) and promotes osteoblast differentiation over adipocyte differentiation in mesenchymal stem cells through an intracrine signaling

pathway involving VEGF receptors (Liu et al. 2012). Our findings add to the growing list of pleiotropic effects of VEGF.

Future studies on the role and regulation of VEGF in brown adipose are likely to reveal valuable insights on the scope of its role in brown adipocytes. For instance, it would be interesting to study the effect of blockage of VEGF signaling *in vivo* in brown adipocytes only, which can be achieved by adipocyte specific VEGFR2 knockout as it would not affect the action of adipocyte-secreted VEGF on the neighboring endothelium. The role of VEGF on brown adipocytes during BAT acclimation to cold or hyperphagia would also be relevant, in particular because activating BAT is a major goal in combating obesity.

Closing Thoughts

I have demonstrated that VEGF and its primary receptor VEGFR2 are expressed in brown adipocytes. VEGF signaling plays a significant role in brown adipose function and maintenance through its effects on both brown preadipocytes and mature brown adipocytes. VEGF functions as a mitogen and a survival factor on preadipocytes rescuing them from apoptosis induced by growth factor withdrawal. Further, VEGF has anti-apoptotic effects on mature brown adipocytes *in vivo* and *in vitro* and plays a role in maintenance of brown adipocyte mitochondrioma *in vivo*, in addition to its paracrine role to promote angiogenesis in BAT. VEGF has an isoform specific role in BAT development and brown adipocyte mitochondrial biogenesis. VEGF is regulated by both the critical adipose transcription factor PPARγ and the transcriptional cofactor, PGC1α. Taken together my

findings identify novel functions of the endothelial growth factor VEGF in the context of brown adipocytes that are significant from a translational standpoint because brown fat activation and angiogenic intervention are each promising therapeutic targets for obesity and associated metabolic dysfunction.

Chapter 7

MATERIALS AND METHODS

Materials

Antibodies

Antibodies used for Western blotting included: anti-phospho-Y951-VEGFR2 (1:300; #4991), VEGFR2 (1:1000, #2479), cleaved caspase 3 (1:1000, #9661), whole caspase 3 (1:1000, #9662), phospho-S473-Akt (1:250, #9271), pan-Akt (1:1000, #9272) purchased from Cell Signaling Technologies (Danvers, MA, USA). Antiserum against β-tubulin (1:500, ab6046) was purchased from Abcam (Cambridge, MA, USA). Anti-endomucin (1:1000, sc-65495) was purchased from Santa Cruz Biotechnology (Santa Cruz, CA, USA). Secondary antibodies used included horseradish peroxidase (HRP)-conjugated anti-rabbit immunoglobulin G (IgG) from donkey (1:7500; GE Healthcare, Buckinghamshire, UK). Antibodies used for immunohistochemistry to UCP1 (1:500; ab10983), cox IV (1:1000; ab16056), F4/80 (1:100; ab6640) were purchased from Abcam, LC3B (1:200, # 2775) and cleaved caspase 3 (1:100) from Cell Signaling Technology and perilipin (1:200; P1873) from Sigma-Aldrich (St. Louis, MO, USA). Secondary antibodies for immunohistochemistry were biotinylated anti-rat IgG (1:400) and anti-rabbit IgG (1:500), both raised in goat (Vector Laboratories, Burlingame, CA, USA) and for immunofluorescence were Alexa Fluor-488 conjugated anti-rat and Dylight 549-conjugated anti-rabbit IgG (1:300, Invitrogen).

Methods

Animal models

C57Bl/6J wild type and VEGF 120/120 mice were used. For ad-sFlt1 and CL 316,243 studies, eight-week old male C57Bl/6J mice were purchased from Jackson Laboratories (Bar

Harbor, ME, USA). VEGF 120/120 mice were generated by targeted deletion of exon 6 and 7 of the VEGF gene, which encode the 164 and 188 isoforms, as previously described (Carmeliet et al., 1999). VEGF 120/120 embryos were generated by breeding C57Bl/6J VEGF 120/+. The ages of the embryos were calculated based on plug date, which was defined as E0. Timed-pregnant females were euthanized at E15.5. PGC1α -/- mice were generated by breeding PGC1α +/- mice on a C57Bl/6J background. All mice were maintained on a regular chow diet and kept on a 12-hour light-dark cycle. Adult mice were euthanized by carbon dioxide inhalation; embryos older than E13.5 were euthanized by decapitation. All protocols for animal use were reviewed and approved by the Schepens Eye Research Institutional Animal Care and Use Committee in accordance with the National Institutes of Health guidelines.

3T3L1 culture and differentiation

3T3L1 cells were maintained as subconfluent cultures in Dulbecco's modified Eagle's medium (DMEM containing 4.5g/L of glucose, L-glutamine and sodium pyruvate (Cellgro; Manassas, VA, USA) supplemented with 10% FBS (Atlanta Biologicals; Lawrenceville, GA, USA), 100U/ml penicillin and 100µg/ml streptomycin (Lonza; Basel, Switzerland) (hereafter referred to as growth medium). To induce differentiation, cells were cultured for 48 hours beyond confluence in the growth medium described above. On day 0, the medium was then replaced with adipose differentiation medium, which comprised growth media supplemented with 10µg/ml insulin, 1µM dexamethasone and 0.5mM isobutylmethylxanthine (IBMX), all from Sigma-Aldrich. After 48 hours, the differentiation

medium was replaced with adipose maintenance medium, which is growth medium supplemented with 5µg/ml insulin. Cells were maintained in the maintenance medium until fully differentiated (10-12 days) and medium was replaced every other day (Figure 2.2).

Brown preadipocyte culture and differentiation

Brown preadipocytes were generously provided by Dr. C. R. Kahn (Joslin Diabetes Center) and were maintained as subconfluent cultures in the growth media described above. To induce differentiation, cells were cultured to confluence and allowed to grow in the above growth media for an additional forty-eight hours. Growth medium was then replaced with fresh brown adipose differentiation medium (day 0) consisting of growth media with 20nM insulin, 1µM dexamethasone, 0.5 mM IBMX, 1nM triiodothyronine (T3; Sigma) and 0.125mM indomethacin (Sigma). After forty-eight hours, the differentiation medium was replaced with adipose maintenance medium made by supplementing DMEM growth media with 1nM T3 and 20nM insulin. Cells were maintained in the maintenance medium until fully differentiated (usually eight days) and medium was replaced every other day (Figure 14). In the studies using norepinephrine, fully differentiated brown adipocytes (day eight) were incubated in serum-free medium for three hours, followed by treatment with 10µM norepinephrine for 1 hour. For treatment with PPARγ agonists, fully differentiated cells (day eight) were treated with 1µM troglitazone (Sigma) in regular growth medium for 6, 12, 24 and 48 hours.

RNA isolation, cDNA synthesis

Total RNA was isolated from adipocytes using RNA Aqueous 4PCR Kit (Life Technologies, formerly Ambion; Grand Islands, NY, USA), following the manufacturer's instructions. RNA concentration and integrity were determined using the Nanodrop 2000 (Thermo Fisher Scientific, Waltham, MA, USA). RNA was treated with DNase to remove contaminating DNA as follows: 8-10µg of RNA was treated with 50U of DNase (Life Technologies) in a total volume of 50µl of 1x DNase Digestion Buffer for 30 min at 37°C. DNase Inactivation Agent was added, followed by incubation at room temperature for 2-3 min and centrifugation at 10,000 x g for 1.5 min. The resulting DNA-free RNA supernatant was used subsequently for reverse transcription (RT) and cDNA synthesis. RT was performed on 1µg RNA using SuperScript III (Life Technologies, formerly Invitrogen) as per the manufacturer's instructions. Briefly, RNA was incubated with random hexamers, oligo$(dT)_{12-18}$ and deoxyribonucleotide triphosphates (DNTP) in an aqueous base for 5 min at 65°C , and 1 min on ice followed by addition of the first-strand buffer and remaining reagents. Then final reaction mixture (20µl) contained 1µg RNA, 50ng of random hexamers, 200ng of oligo$(dT)_{12-18}$ and 10nmoles of deoxyribonucleotide triphosphates (DNTP), 200U SuperScript III, 40U RNaseOUT and 5µM DTT (all from Life Technologies) in 1x first-strand buffer. The cDNA synthesis reaction was as follows: 5 min at 25°C, 45 min at 50°C followed by enzyme inactivation at 70°C for 15 min. cDNA generated from this reaction was diluted 1:25 with nuclease-free water.

Real time PCR

For gene expression analysis, 5µl of the cDNA (10ng of equivalent RNA) was amplified in each PCR amplification reaction using 500nM forward and reverse primers and SYBR Green Master mix (Roche Diagnostics, Indianapolis, IN, USA), according to the manufacturer's instructions. Primer sequences used are listed in Table 3. Reactions were performed on the Roche LightCycler® 480 II. PCR cycles consisted of an initial denaturation step at 95°C for 10 min, followed by 40 cycles of 95°C for 15 sec, 60°C for 30 sec and 72°C for 1 min. Each sample was subjected to melting curve analysis to confirm amplification specificity. Samples were run in triplicate and included three water controls for each gene analyzed. Samples were normalized to TATA box binding protein (TBP) and expressed as relative fold change using the ΔΔCt method of relative quantification.

For absolute quantification of VEGF isoforms a standard curve was constructed for each of the three isoforms by amplifying serial dilutions (10^3 - 10^9ng DNA/reaction) of a plasmid coding for a single isoform using primers specific for each isoform. The level of individual isoforms in each experimental sample was calculated relative to the standard curve. Each sample and dilution was run in triplicate, as described above. Results were expressed as the mean ± SEM.

Semi-quantitative PCR analysis

Total mRNA and cDNA were prepared as described above. One microliter of cDNA was used as a template in a 25µl amplification mixture containing 200mM dNTPs, 1U *Taq* DNA polymerase (Roche Diagnostics) and 0.2µM of the primer pairs indicated in Table 4.

Samples were amplified for 35 cycles, and amplification products were separated by agarose gel electrophoresis, stained with ethidium bromide, and visualized by UV light.

Administration of β3 agonist CL 316,243

Adult male C57Bl/6J mice were injected intraperitoneally with ~100 – 120µL CL 316,243 or saline (control) at a final dose of 1 mg/kg body weight, which is the most commonly used dose for CL 316,243-mediated adrenergic stimulation in mice *in vivo*, from a 0.25mg/ml stock solution. Five mice were used for each time point. Mice were euthanized and tissue was harvested two, six and 24-hours post injection. Tissue for RNA isolation was directly placed in TRIzol® (Life Technologies) and stored in -80˚C.

Proliferation assay

Cells were plated at a density of 10,000 cells per well of a 24-well plate in regular growth media and allowed to attach overnight. Growth medium was removed and cells were washed once with serum free DMEM and re-fed with DMEM containing 1% FBS with or without 10ng/ml VEGF. Cells were counted at 24 hour intervals for five consecutive days using a Coulter Counter (Beckman Coulter, Brea, CA, USA). Each time point was set up in triplicate.

Table 3 – Primers for qPCR mouse genes

Target gene	Forward Primer	Reverse Primer
aP2 (FABP4)	ATGAAATCACCGCAGACGACAGGA	TGTGGTCGACTTTCCATCCCACTT
PGC1α	AGCCGTGACCACTGACAACGAG	GCTGCATGGTTCTGAGTGCTAAG
PPARγ	GACATCCAAGACAACCTGCTG	GCAATCAATAGAAGGAACACG
VEGF	GCACATAGAGAGAATGAGCTTCC	CTCCGCTCTGAACAAGGCT
VEGF 188	GCCAGCACATAGAGAGAATGAGC	AACAAGGCTCACAGTGAACGCT
VEGF 164	GCCAGCACATAGAGAGAATGAGC	CAAGGCTCACAGTGATTTTCTGG
VEGF 120	GCCAGCACATAGAGAGAATGAGC	CGGCTTGTCACATTTTTCTGG
TBP	ACCCTTCACCAATGACTCCTATG	TGACTGCAGCAAATCGCTTGG
UCP1	GGCATTCAGAGGCAAATCAGCT	CAATGAACACTGCCACACCTC

Table 4 – Primers for RT-PCR for mouse genes

Target gene	Forward Primer	Reverse Primer	Amplicon Size
aP2	CTGGAAGACAGCTCCTCCTCGAAG	TAATCAACATAACCATATCCAAT	585
GAPDH	GTGGCAAAGTGGAGATTGTTGCC	GATGATGACCCGTTTGGCTCC	291
Nrp1	TCAGGACCATACAGGAGATGG	TGACATCCCATTGTGCCAAC	619
UCP1	TATCATCACCTTCCCGCTG	GTCATATGTTACCAGCTCTG	505
VEGF	CCTCCGAAACCATGAACTTTCTGCTC	CAGCCTGGCTCACCGCCTTGGCTT	665, 593, 461
VEGFR1	GAGAGCATCTATAAGGCAGCGGATT	CACGTTTACAATGAGAGTGGCAGTG	456
VEGFR2	TACACAATTCAGAGCGATGTGTGGT	CTGGTTCCTCCAATGGGATATCTTC	499

Apoptosis assay

Apoptosis was induced in brown preadipocytes through nutrient deprivation. Preadipocytes were plated and grown to confluence in regular growth medium. Cells were rinsed twice for five min in serum free DMEM. Cells were then placed in serum free medium. VEGF (25ng/ml) and/or DC101, a neutralizing antisera against mouse VEGFR2 (15µg/ml) for 12 hours. Cells were rinsed twice in PBS (which was collected), trypsinized, pooled with medium and PBS and centrifuged. Whole cell lysates were prepared and analyzed for presence of the pro-apoptotic protein marker cleaved caspase 3 and other proteins by Western blotting as described.

Apoptosis was induced in fully differentiated brown adipocytes by treatment with 10nM TNFα (Genway Biotech, San Diego, CA, USA) and 10µg/ml CHX for 6 hours in the presence or absence of DC101 as above. Cell survival was analyzed after the treatment. Cell number was counted using a Coulter Counter as described above. For detection of cleaved caspase positive cells, cells were incubated with Alexa Fluor®488-conjugated cleaved caspase 3 antibody (Cell Signaling Technologies, cat # 9669) and FACS analysis was conducted using Cytofix/Cytoperm Fixation Permeabilization kit (BD Biosciences, San Jose, California, USA; cat # 554714), following the manufacturer's instructions. Briefly, cells were rinsed in PBS, trypsinized and collected as above. The cells were then washed once in staining buffer (Opti-MEM (Life Technologies) with 1% BSA) fixed in 4% paraformaldehyde (PFA) for 15 min at 4˚C, permeabilized in BD Perm/Wash buffer (BD Biosciences, Cat # 554714) for 15 min , incubated in 50µl of the primary antibody (1:100) for 30 min in the dark, washed once in BD Perm/Wash buffer and resuspended in 350µl staining buffer for

FACS analysis. The cells were protected from light at all times following antibody incubation. Percentage of cleaved caspase 3-positive cells was analyzed using a Fluorescence Activated Cell Sorter (FACS) (BD LSR II, BD Biosciences).

TUNEL assay

Apoptotic cells in BAT were detected in paraffin sections by the TUNEL assay using the In Situ Cell Death Detection TMR Red kit (Roche Diagnostics), following the manufacturer's instructions, with some modifications. Briefly, paraffin sections were rehydrated, deparaffinized, boiled in citrate buffer, pH 6.0 for 20 min and permeabilized for 5 min in cold PBS containing 0.2% Tween-20. Sections were then incubated at 37 °C covered from light in TUNEL reaction mix containing biotinylated nucleotides and terminal deoxynucleotidyl transferase (TdT) enzyme for 1 hour, washed three times in PBS and mounted. DNase treatment was performed as a positive control, and incubation without TdT enzyme was conducted as a negative control. 4',6'-diamino-2-phenylindole (DAPI) labeling was used to identify cell nuclei. When immunofluorescence was combined with TUNEL assay to identify cell type, immunostaining was conducted first; the cells were then fixed for 10 min in 4% PFA, followed by TUNEL assay as described. For quantification, three sections from each BAT sample were scanned entirely and images were taken of all TUNEL positive cells with an Axioscope microscope (Carl Zeiss Microscopy LLC, Thornwood, NY, USA). The number of TUNEL positive cells was represented as the average number of apoptotic cells per section, for five mice expressing sFlt1and three control mice.

Adenovirus mediated sFlt1 expression

Mice were anesthetized using ketamine/xylazine and injected with ~7.5 x 10^10 pfu of sFlt virus in 100µl volume via the tail vein. Adenoviruses administered intravenously are delivered primarily to the liver, targeting the hepatocytes and non-parenchymal (Kupffer and endothelial) cells. Production of the gene of interest is mediated by infection of these cells, which secrete the protein into systemic circulation (Reviewed in Sakurai et al., 2008). Five days post injection, serum was collected by submandibular bleeding and circulating sFlt1 levels were determined by ELISA (R&D Biosystems, Minneapolis, MN,USA; Cat # MVR100). Animals with circulating levels of sFlt1 of 200ng/ml or higher were included in the study. Ad-null-infected mice showed no detectable sFlt1. Eight mice were used in each group. Mice were euthanized seven days post injection and tissues dissected. Three mice from each group were perfused for electron microscopy as described. For the remaining animals, total body weight as well as the weights of BAT and major WAT depots were noted. For histology, the tissues were placed directly in 4% PFA and fixed for 48 hours. Tissue for protein/triglyceride analyses was flash frozen immediately in liquid nitrogen and stored in -80˚C.

One possible issue concern regarding the use of adenoviral vectors is the innate immune response that can be triggered by systemic administration (reviewed in Sakurai et al. 2008). However, we have used this model of adenoviral-mediated expression extensively (Maharaj et al. 2008; Ford et al. 2011; Saint-Geniez et al. 2008). Measurement of circulating levels of TNF-α in Ad-null and Ad-sFlt1 animals revealed no increase in TNF-α, whereas

positive controls such as culture media from LPS-stimulated macrophages contained more than 1500pg/ml of TNF-α (Walshe et al. 2009).

Western blot analysis

To prepare whole cell lysates, cells were homogenized in RIPA lysis buffer containing 0.1% SDS (Sigma-Aldrich) over three freeze-thaw cycles, sonicated for ~ 5 sec, centrifuged at 12,000xg for 10 min at 4˚C and supernatant collected and stored at -80˚C. Protein concentration was measured using a BCA assay (Bio-Rad Laboratories, Hercules, CA, USA). Equivalent amounts of proteins from 30 to 60µg, depending on the sensitivity of the antibody to be used, were separated by SDS-PAGE under reducing conditions, and transferred to an Immobilon-P membrane (Millipore, Billerica, MA, USA). The membrane was incubated in blocking buffer (5% non-fat milk in PBS with 0.1% Tween) for 30-60 min and immunoblotted with the appropriate primary and secondary antibodies diluted in 0.5 – 3% non-fat milk in PBS with 0.1% Tween. Membranes were washed in PBS with 0.1% Tween. Proteins were visualized with SuperSignal West Pico, Dura or Femto extended duration substrates (Pierce Biotechnologies, Rockford, IL, USA). For reprobing, membranes were stripped by incubation for 30 min in 6.25 mM Tris-HCl, pH 6.8, 2% SDS and 100 mM β-mercaptoethanol at 50 °C, blocked and reprobed.

Immunohistochemistry and immunofluorescence

Embryos (E15.5) and BAT were fixed overnight in 4% PFA in PBS and embedded in paraffin, sectioned (5µM) and stained with hematoxylin & eosin for routine histology and Masson's Trichrome to stain connective tissue. For immunohistochemistry, sections were

deparaffinized, rehydrated, boiled in citrate buffer (pH 6.0) for antigen retrieval, incubated with 1% hydrogen peroxide in methanol for 10 min to block endogenous peroxidase activity, and permeabilized with PBS containing 0.2% Tween for 5 min. For immunohistochemistry with the anti-LC3B antibody, sections were permeabilized in 100% methanol for 20 min at -20°C. Blocking of non-specific binding was accomplished by incubation in buffer made of serum from the host species of the secondary antibody (3%) in PBS with 0.2% Tween for 1 hour at room temperature before incubation with appropriate primary antibodies in blocking buffer overnight at 4°C in a humidified chamber. After washing three times in PBS, sections were incubated with biotinylated anti-rat or anti-rabbit antibodies in blocking buffer for 1 hour at room temperature, followed by three additional washes. The primary antibody was visualized using avidin-biotin-horseradish peroxidase and DAB substrate (Vector ABC kit; Vector Laboratories); tissues were counterstained with hematoxylin for labeling cell nuclei. Isotope-matched IgGs served as negative controls for each experiment. For immunofluorescence on paraffin sections, a procedure similar to that for immunohistochemistry was followed except antigen retrieval in citrate buffer was followed by incubation of sections in PBS with 0.2% sodium borohydride for 10 min to quench autofluorescence and incubation with hydrogen peroxide was not performed.

For immunofluorescence of differentiated adipocytes, cells were grown on sterilized coverslips in 12-well plates until fully differentiated. Cells were fixed in 4% PFA for 10 min, washed, incubated in blocking buffer, followed by overnight incubation with appropriate primary antibodies. Samples were washed three times in PBS, followed by incubation with fluorophore conjugated anti-rat or anti-rabbit secondary antibodies for 1 hour at room

temperature, washed in PBS and counterstained with DAPI for identification of cell nuclei. Cells on coverslips were mounted on slides using mounting media (1:1 PBS and glycerol).

To visualize mitochondria in differentiated brown adipocytes, live unfixed cells were incubated in 100nM CMTM-Rosamine (MitoTracker Orange, Invitrogen) for 30 min at 37˚C, fixed in 4% formalin for 15 min, washed three times in PBS. If immunofluorescence was to be performed on the same samples, the cells were also permeabilized in ice cold acetone for 5 minutes followed by blocking and incubation with primary antibody.

Electron microscopy

Seven days following adenovirus injections, mice express ad-sFlt1 and the control ad-null mice were deeply anesthetized with ketamine (73 mg/kg) and xylazine (1.8 mg/kg) and perfused via the aorta with 10ml sodium cacodylate buffer 0.1 M, pH 7.4, for 2 min followed by 10ml fixative of PFA/ glutaraldehyde, 2.5% each in 0.1M sodium cacodylate buffer, pH 7.4 (Electron Microscopy Sciences; Hatfield, PA, USA). Perfusion was accomplished with a 21-gauge cannula inserted into the aorta via the left ventricle. Fluid drained through the right atrium, and animals' death from exsanguination was immediate upon perfusion. The BAT was dissected and fixed in the same fixative for 72 hours at 4˚C. A secondary fixation was performed overnight at 4˚C in 1% osmium tetroxide and 1.5% potassium ferrocyanide. Osmium is the main fixative for lipids, which are not extracted during processing, allowing the adipocytes to maintain their morphology. This was followed by dehydration and embedding in propyleneoxide resin. Ultrathin sections were treated with 1% uranyl acetate followed by 0.2% lead citrate for visualization of cell ultrastructure

and examined by transmission electron microscopy using a Tecnai TM G2 Spirit BioTWIN transmission electron microscope (Oregon, USA).

Statistical analysis

Values are expressed as mean ± SEM unless specified. Statistical analysis was performed using an unpaired Student t-test for comparison between two groups and one way Anova for comparison between multiple groups (***, $P < 0.001$; **, $P < 0.01$; *, $P < 0.05$; ns, $P < 0.05$, ns: $P > 0.05$).

Appendix

RhoB Controls Adult Angiogenesis and Lymphangiogenesis through VEZF1

Damien Gerald[1], Irit Adini[2], Sharon Shechter[1], Carole Perruzzi[1], Joseph Varnau[1], Benjamin Hopkins[1], Shiva Kazerounian[1], Peter Kurschat[2], Stephanie Blachon[3], Mandrita Datta[1], David Sherris[4], Michael Klagsbrun[2], Heidi Stuhlmann[5], Alan C. Rigby[6], Janice A. Nagy[1,#] and Laura E. Benjamin[1,#]

This represents work done in Mandrita's former thesis laboratory. She performed groundwork of demonstrating that RhoB regulates the transcription of Prox1, master regulator of lymphatic differentiation, and that VEZF1 does not mediate Prox1 expression directly, through techniques such as cloning of the Prox1 promoter fragments, luciferase assay etc. She also optimized short hairpin RNA mediated silencing of RhoB and VEZF1 in primary lymphatic and blood vascular endothelial cells.

RhoB controls adult angiogenesis and lymphangiogenesis through VEZF1

Damien Gerald[1], Irit Adini[2], Sharon Shechter[1], Carole Perruzzi[1], Joseph Varnau[1], Benjamin Hopkins[1], Shiva Kazerounian[1], Peter Kurschat[2], Stephanie Blachon[3], Mandrita Datta[1], David Sherris[4], Michael Klagsbrun[2], Heidi Stuhlmann[5], Alan C. Rigby[6], Janice A. Nagy[1,#] and Laura E. Benjamin[1,#]

1- Center for Vascular Biology Research and Department of Pathology, Beth Israel Deaconess Medical Center, Harvard Medical School, Boston, MA ; 2- Department of Surgery, Children's Hospital, Harvard Medical School, Boston, MA ; 3- Laboratoire de Neurobiologie et Développement, Institut de Neurobiologie Alfred Fessard, CNRS UPR 3294, Gif-sur-Yvette, France ; 4- VaculoMedics Inc., Jamaica Plain, MA ; 5- Department of Cell and Developmental Biology, Weill Cornell Medical College, New York, NY ; 6- Center for Vascular Biology Research and Department of Medicine, Beth Israel Deaconess Medical Center, Harvard Medical School, Boston, MA

Corresponding Authors:
Janice A. Nagy
Center for Vascular Biology Research and Department of Pathology
Beth Israel Deaconess Medical Center
Harvard Medical School
Research North Building
99 Brookline Avenue
Boston MA, 02215
Email: jnagy@bidmc.harvard.edu

Laura. E. Benjamin
Current Address:
ImClone Systems, a wholly owned subsidiary of Eli Lilly
450 East 29th Street
New York, NY 10016
Email: laura.benjamin@imclone.com

Key Words: Angiogenesis, Lymphangiogenesis, Wound Healing, DTH, Retinopathy, RhoB, VEZF1

RhoB, a stress-induced small GTPase, modulates cellular responses to growth factors, genotoxic stress and neoplastic transformation. Here, we show that RhoB loss converts retinopathy-associated, pathological angiogenesis to a more physiological phenotype. RhoB loss also reduces angiogenesis, while enhancing lymphangiogenesis, during skin wound healing in adult mice, which reveals unique and opposing roles of RhoB in blood versus lymphatic vasculatures. By comparing primary human blood and lymphatic endothelial cells, we link these biological responses to the differential regulation of sprouting and proliferation by RhoB. Mechanistically we demonstrate that nuclear RhoB-GTP controls expression of different gene sets in both endothelial lineages through VEZF1-mediated transcription, thus establishing the first intra-endothelial molecular mechanism responsible for the characteristic phased response of early angiogenesis and delayed lymphangiogenesis following injury. Finally, we identify a small molecule inhibitor of VEZF1-DNA interaction that recapitulates RhoB loss in ischemic retinopathy, providing proof-of-concept for the therapeutic value of targeting transcription factors.

Page intentionally left blank

Large organisms exhibit two different vascular networks essential for life. The circulatory blood vascular network, arising during embryonic development by both vasculogenesis and angiogenesis, provides oxygen, nutrients, hormones and cells to tissues, and collects carbon dioxide and other metabolic waste products[1]. The blind-ended lymphatic vascular network that subsequently originates from the embryonic cardinal vein by budding and differentiation of a subpopulation of blood endothelial cells, regulates tissue fluid homeostasis, immune cell trafficking and absorption of dietary fats [2]. Similarly in adults, numerous studies have shown that angiogenesis precedes lymphangiogenesis in damaged tissues[3-9]. However, the underlying mechanisms that timely coordinate these processes are still elusive. Considering the close identity between blood and lymphatic endothelial cells, a central question still unresolved is how blood vessels quickly engage in the revascularization of damaged tissues, while the growth of lymphatics is delayed in response to the same pathological stimulus? RhoB is an immediate early response gene rapidly inducible by many stimuli including genotoxic stress, cytokines and growth factors[10-13]. In contrast to its related members of the Rho/Rac/Cdc42 family of small GTPases, RhoB is primarily localized on endosomes and in the nucleus, and has been shown to regulate vesicle and growth factor receptor trafficking [14-17]. *RhoB* null mice are viable, indicating that RhoB is dispensable for normal development [18], however, RhoB deletion in mice can increase tumor formation[19]. Furthermore, studies in RhoB knockout mice indicate that RhoB is a critical modifier of apoptosis triggered by genotoxic stress. In transformed fibroblasts, RhoB promotes apoptosis in response to DNA damage[18]. In contrast, RhoB protects transformed keratinocytes from UVB-induced apoptosis, suggesting that RhoB's functions are dependent upon the nature of stress and the cell context[13]. Our previous studies revealed for the first time the contribution of this small GTPase to the blood vasculature in the developing retina, which is associated with defective endothelial tip cell sprouting in RhoB null mice[20]. We found that RhoB is an important determinant of Akt stability and trafficking to the nucleus, and that this function plays a stage-specific role in the survival of sprouting blood vessel endothelial cells (BVECs) that contribute to new blood vessel assembly during post-natal retinal development. Given its critical role in the stress response, we hypothesized that RhoB might be relevant in adult pathological scenarios involving endothelial cell challenge, such as wound healing, inflammation, or reperfusion injury. Here, we show that *RhoB* null

mice exhibit decreased angiogenesis leading to normalization of pathological angiogenesis associated with ischemic retinopathy, but earlier, increased and abnormal lymphangiogenesis following dermal injury or inflammation. Using human primary BVECS versus LVECs, we demonstrate that RhoB serves opposing roles in regulating proliferation and sprouting capability of these two endothelial populations. To further understand these exclusive functions of RhoB, we focused on a recently identified zinc finger transcription factor VEZF1, involved in embryonic angiogenesis and lymphangiogenesis[21]. For the first time, we confirmed the interaction of RhoB and VEZF1 in cells. And we explored the function of the RhoB-VEZF1 complex in both adult endothelia *in vivo*. Our transcriptome analysis of BVECS and LVECs uncovers relevant and new genes targeted by VEZF1 and co-regulated by RhoB-GTP. Lastly, we identified a small molecule specifically selected to interfere with VEZF1 binding to DNA, which recapitulates the ability of RhoB loss to normalize the pathological angiogenesis in the ischemic retina.

RESULTS

RhoB loss normalizes blood vasculature in oxygen-induced retinopathy and reduces angiogenesis accompanying wound healing

To analyze the impact of RhoB on postnatal angiogenesis, we first employed the mouse model of oxygen-induced retinopathy (OIR)[22] to create a pathological angiogenic environment in neo-natal *RhoB*$^{-/-}$ mice. After 5 days at 70% oxygen (P7-P12), analysis of the retinal vasculature indicates profound vessel regression, particularly in the central portion of the retina near the optic disc (OD), and confirms that the initial vascular response to high oxygen is not altered in the absence of *RhoB* (Fig. 1a). Subsequently, after 5 days of room air (P12-P17), *wt* pups mounted a robust pathological neovascularization in the retina typified by abnormalities in vascular structure (formation of glomeruloid bodies or "vascular tufts" (arrowheads), large avascular areas (star), and endothelial cell invasion through the inner limiting membrane (ILM) into the vitreous (arrows). High invasion rate into the *wt* vitreous was quantified by counting EC nuclei anterior to the ILM in H&E histological sections. In contrast, *RhoB*$^{-/-}$ mice showed a dramatic reduction of glomeruloid bodies, and 100-fold reduced intra-vitreous invasion rate. Thus, *RhoB* loss during ischemic retinal neovascularization was accompanied by reduced blood vessel growth and the conversion of the resultant neovascular network from a pathological to a more physiological phenotype.

To evaluate the impact of *RhoB* deletion in another tissue, we subjected the mouse ear skin to a full thickness wound using a 2 mm biopsy punch. New blood vessels were induced in the granulation tissue of *wt* mice by 7 days after wounding (Fig. 1b). In contrast, *RhoB*$^{-/-}$ mice exhibited poor neovascularization within the granulation tissue with a 2-fold decreased vascular density compared to *wt*. Interestingly in *RhoB*$^{-/-}$ mice, immunostaining for CD31 revealed not only the presence of positively stained blood vessels, but additional structures with a different morphology and weak staining intensity (arrowheads). CD31 is a protein also known to be expressed by lymphatic endothelial cells[23]. To validate the lymphatic identity of these additional vascular structures, we used an antibody against podoplanin, a protein that is specifically expressed in the lymphatic endothelium (Fig. 1c). Co-localization of CD31 and podoplanin confirmed the identity of these structures as lymphatic vessels infiltrating and surrounding the

granulation tissue in *RhoB*$^{-/-}$ mice (arrowheads). Taken together, these results indicate that RhoB plays a positive role in the formation of new blood vessels in different vascular beds responding to stress, and prompted us to further explore the lymphatic vasculature of *RhoB*$^{-/-}$ mice.

RhoB enhances lymphangionenesis associated with wound healing and inflammation

To directly determine the participation of RhoB in the response of the mature lymphatic network to a pathological challenge, we assessed the effect of *RhoB* loss on lymphangiogenesis associated with cutaneous wound healing using the mouse ear model. By day 7 post-wounding, *in vivo* injection of high-molecular-weight FITC-dextran tracer directly into the dermal lymphatic vessels in *wt* mice did not reveal any obvious formation of new lymphatics associated with the granulation tissue, in agreement with previous studies[6,9,24] (Fig. 2a and Movie S1). On the other hand, *RhoB*$^{-/-}$ mice exhibited a profound lymphangiogenic response as judged by the rapid increase in the filling of a distinct lymphatic network with the FITC-dextran tracer beginning between 2-10 seconds after tracer injection and progressively increasing by 30 seconds (2-fold increase) (Movie S2). These results indicate more numerous lymphatic vessels as well as an elevated interconnectivity in the lymphatic vessel network adjacent to the *RhoB*$^{-/-}$ wound. Thereafter, between 30 and 60 seconds, the appearance and accumulation of FITC-dextran in the tissue immediately surrounding the filled lymphatics (arrowheads), far from the tracer injection site, suggests an abnormal structure of these new lymphatics leading to the enhanced leakage of fluid and macromolecules. Confocal analysis following whole mount staining of lymphatics with anti-podoplanin on tracer-injected ears confirmed the abnormal structure of the lymphatic vessels in the *RhoB*$^{-/-}$ granulation tissue, i.e., lymphatic lumen enlargement and impaired barrier integrity leading to accumulation of FITC-dextran in the surrounding tissue (respectively, arrowhead and star, Fig. 2b).

To demonstrate that the abnormal lymphatic structure in *RhoB*$^{-/-}$ stressed skin leads to defective draining function, we induced a delayed-type hypersensitivity (DTH) reaction using oxalozone as a

sensitizing agent[25]. The level of edema accompanying chronic inflammation in the ears was assessed by measurement of ear thickness (Fig. 2c). The maximum extent of edema, reached by 2 days after oxalozone application, was significantly higher in *RhoB*$^{-/-}$ ears as compared to *wt*. Thereafter, ear swelling declined more slowly and remained significantly higher in *RhoB*$^{-/-}$ compared to *wt* mice even after 11 days, indicating that resolution of fluids that accumulated during the inflammatory phase is impaired in the *RhoB*$^{-/-}$ mice. Visualization of the lymphatic network at 7 days post-challenge by intralymphatic injection of high-molecular-weight FITC-dextran tracer revealed a massive lymphangiogenic response in *RhoB*$^{-/-}$ mice characterized by more numerous lymphatic vessels, enhanced lymphatic interconnectivity, and dramatic FITC-dextran leakage into the surrounding tissue (Fig. 2d and Movie S4) as compared to *wt* (Movie S3). These data indicate that the absence of *RhoB* permits the formation of an early, excessive and dysfunctional lymphangiogenic response, which disrupts the normal pattern of edema resolution.

RhoB differentially affects BVEC and LVEC proliferation and sprouting

To comparatively assess the function of RhoB in blood versus lymphatic endothelia, we used pure populations of human primary blood (BVECs) and lymphatic (LVECs) endothelial cells isolated from foreskin (Fig. S2). First, we determined the relative amounts of RhoB protein found in BVECs versus LVECs during resting conditions (cells at 100% confluence for 48h without media renewal), or during proliferative conditions (cells collected 24h and 48h after challenge initiated by trypsinization of confluent cultures followed by re-plating at 50% density) (Fig. 3a). RhoB was constitutively expressed in both resting and proliferating BVECs. In contrast, RhoB protein was barely detectable in LVECs at rest and at 48h after challenge. Interestingly, the level of RhoB protein increased in both BVECs and LVECs 24h after proliferative challenge, suggesting that RhoB plays a critical role in both BVECs and LVECs in their immediate response to stress. To further analyze the function of RhoB in BVECs and LVECs, we either silenced or overexpressed *RhoB,* by siRNA nucleofection or adenovirus infection, respectively, and then subjected confluent cultures of the modified cells to proliferative stress (Fig. 3b). Immunostaining of pre-confluent cells 24h following proliferative stress, with an antibody against the proliferation marker

Ki67, showed that *RhoB* silencing decreased the percent of proliferating BVECs two-fold, but nearly doubled the percent of proliferating of LVECs (Fig. 3c). In direct contrast, *RhoB* overexpression significantly promoted the proliferaton of BVECs, but repressed LVECs proliferation. Using a 3D sprouting assay, we also observed a differential response of BVECs and LVECs to alterations in *RhoB* expression (Fig. 3d). Indeed, *RhoB* silencing reduced the sprouting of BVECs induced by VEGF-A and led to increase sprouting of LVECs stimulated by VEGF-C. In contrast, *RhoB* overexpression had the reverse effect, i.e., higher number of BVECs sprouting in response to VEGF-A, and repressed LVECs sprouting in response to VEGF-C. These results demonstrate that RhoB serves cell autonomous, yet opposing, roles in two essential features of blood and lymphatic endothelial cell biology, i.e., proliferation and sprouting, thus corroborating our *in vivo* observations.

RhoB collaborates with VEZF1 during stress-induced angiogenesis and lymphangiogenesis

To decipher the molecular mechanisms responsible for the differential effect of RhoB in blood and lymphatic vascular beds, we investigated the possibility that *RhoB* is functionally linked to the zinc finger transcription factor *VEZF1,* previously shown to regulate embryonic angiogenesis and lymphangiogenesis and a RhoB-interacting protein *in vitro*[14,21]. We crossed mice from the *RhoB* and *VEZF1* knockout strains and generated an allelic series of mice, i.e., $RhoB^{+/-}$, $VEZF1^{+/-}$ and $RhoB^{+/-}VEZF1^{+/-}$. Using the OIR assay as our read-out of pathological angiogenesis, we observed that loss of only one *RhoB* allele did not alter the pathological angiogenic response in the retina of $RhoB^{+/-}$ mice as compared to *wt* (Fig. 4a compared to Fig. 1a). However, $VEZF1^{+/-}$ mice exhibited a reduced pathological angiogenic response (2-fold decrease in the number of nuclei interior to inner limiting membrane) (Fig. 4a), which is further reprogrammed to more physiological angiogenesis in $RhoB^{+/-}VEZF1^{+/-}$ mice, similarly to $RhoB^{-/-}$ mice (Fig. 4a compared to Fig. 1a). In parallel, we assessed the lymphangiogenic response to challenge using the ear wound model. By day 7 post-wounding, in dramatic contrast to what we observed in the $RhoB^{-/-}$ mice (Fig. 2a), injection of high-molecular-weight FITC-dextran tracer did not reveal new lymphatics in the region immediately

surrounding the site of the wound in *RhoB*$^{+/-}$ mice (Fig. 4b and Movie S5). In contrast, in *RhoB*$^{+/-}$ *VEZF1*$^{+/-}$ mice, the lymphangiogenic response was comparable to that observed in the *RhoB*$^{-/-}$ mice (Fig. 4b and Movie S7 compared to Fig. 2a). Interestingly, *VEZF1*$^{+/-}$ mice exhibit an intermediate lymphatic phenotype with the emergence of several leaky lymphatics around the granulation tissue (arrowhead, Fig. 4b and Movie S6).

To address the interaction of RhoB with VEZF1 at the molecular level in BVECs and LVECs, we investigated the subcellular localization of these two proteins. Importantly, although RhoB was detected predominantly in the cytoplasm of both BECs and LECs, we also observed this small GTPase in the nucleus of both cell types, where VEZF1 proteins were exclusively detected (Fig. 4c). Moreover, RhoB and VEZF1 could be co-immunoprecipitated indicating the presence of a protein complex containing this small GTPase and this zinc-finger transcription factor (Fig. 4d). Taken together, these studies strongly argue that *RhoB* genetically interacts with *VEZF1* in the regulation of the altered blood vascular response to ischemia as well as in the temporal repression of lymphangiogenesis during wound healing, and indicate that RhoB belongs to a nuclear transcriptional complex containing VEZF1.

RhoB and VEZF1 share relevant target genes for BVEC and LVEC proliferation and sprouting

To uncover how the collaboration between RhoB and VEZF1 affects BVEC and LVEC biology, we set about to identify the cohort of target genes whose expression is influenced by these two proteins. To accomplish this aim, we performed Affymetrix microarray analysis after silencing either *RhoB* or *VEZF1* in both endothelial cell types (Fig. S3). Interestingly, a significant number of the deregulated probe sets in *RhoB* silenced BVECs matched the deregulated probe sets in *VEZF1* silenced BVECs (214 down-regulated and 243 up-regulated probe sets). Similarly, 1413 down-regulated probe and 1280 up-regulated probe sets in *RhoB* silenced LVECs compared favorably to the deregulated probe sets in *VEZF1*-silenced LVECs, suggesting that these deregulated probe sets could correspond to the specific genes targeted by

VEZF1 and co-regulated by RhoB. Using Gene Ontology (GO) classification to query the function of the target genes shared by RhoB and VEZF1, we identified ontology categories important for different aspects of endothelial cell biology including their proliferation and sprouting (Table S1). Among the subsets of shared target genes (Table S2), we confirmed the role of RhoB and VEZF1 in the regulation of expression of a finite number of particularly relevant genes by QRT-PCR (Fig. 5a). For example, the VEGF-A receptor, VEGF-R2, and its co-receptor, Neuropilin1 (NRP1), were both down-regulated in BVECs after silencing of either RhoB or VEZF1 (2-fold decrease in silenced cells compared to control). Although these two genes were also detected in the LVECs microarrays, QRT-PCRs revealed a lower basal level of expression and an insignificant decrease after silencing of either RhoB or VEZF1 in these cells, suggesting a predominant effect of RhoB-VEZF1 on VEGF-R2 and NRP1 expression in BVECs compared to LVECs. By contrast, the metallopeptidase inhibitor, TIMP3, was more highly expressed in LVECs, suggesting that down-regulation of this protein, triggered by both *RhoB* and *VEZF1* knockdown, has a particularly potent impact in LVECs compared to BVECs. We also validated relevant genes deregulated by RhoB-VEZF1 that have previously been shown to be involved in BVEC proliferation and sprouting (e.g., PHD2, Endothelin1) or LVEC proliferation and sprouting (e.g., MMP2, CyclinE2). Moreover we identified new genes not previously recognized as being involved in lymphatic vessel biology (TIMP3, Vasohibin1). Interestingly, these genes exhibit different relative patterns of mRNA expression that most likely highlight specific promoter configurations.

To further identify the direct target genes of VEZF1, and more importantly, those that are also co-regulated by RhoB, we analyzed the binding of these two proteins to a number of selected promoters by chromatin immunoprecipitation (Fig. 5b). Interestingly we discovered sequences containing potential VEZF1 DNA binding sites in the promoter regions of VEGF-R2 and NRP1. These regions exhibit 3-fold and 2-fold enrichment, respectively, after VEZF1 or RhoB-Flag chromatin immunoprecipitation, specifically in BVECs. In contrast, the chromatin of the TIMP3 and Vasohibin1 promoter regions, which also contains putative VEZF1 DNA binding sites, is enriched 4-fold after VEZF1 or RhoB-Flag immunoprecipitation, specifically in LVECs. Analysis of the Endothelin1 promoter, known to be a direct target of VEZF1, confirms chromatin enrichment after VEZF1 or RhoB-Flag immunoprecipitation in

BVECs. Taken together, these data suggest that RhoB works in conjunction with VEZF1 on specific promoters to regulate the expression of essential direct target genes involved in the proliferation and sprouting of endothelial cells (BVECS and LVECs). Of critical importance, these sets of direct targets appear to be different in BVECs versus LVECs.

RhoB-GTP specifically controls BVEC and LVEC proliferation

A crucial feature of any small GTPase is the ability to toggle its intrinsic GTPase activity between "on" and "off" states, as determined by the ratio of the GTP-bound to the GDP-bound forms of the enzyme [26]. To assess the importance of these two states in the regulatory function of RhoB in endothelial cells, we prepared adenoviral vectors encoding mutants of RhoB and used them to elicit overexpression of three different forms of the RhoB GTPase (wild type (adRhoB); the RhoB dominant negative form corresponding to the GDP-bound state (adRhoB-DN); and the RhoB constitutively active form corresponding to the GTP-bound state (adRhoB-CA). Overexpression of wild type (wt) or mutant RhoB was performed in BVECs and LVECs undergoing proliferative challenge and the corresponding GTP levels were measured by GTP pulldown assay (Fig. 6a). As expected, neither BVECs nor LVECs infected with adRhoB-DN exhibited any detectable amount of GTP-bound RhoB, while both cell types infected with adRhoB-CA showed high levels of expression of the GTP-bound form of RhoB. Interestingly, following wt RhoB overexpression, a substantial amount of RhoB in the GTP-bound state could be detected in both BVECs and LVECs, indicating that both cell types maintain RhoB in a predominantly active form under proliferating conditions. To evaluate the possibility that the state of RhoB determines its localization within the cell, we analyzed the subcellular pattern of our mutants RhoB (Fig. 6b). Wt RhoB and all mutants of RhoB, including the dominant negative RhoB, were detected in the cytoplasm as well as in the nucleus of BVECs and LVECs, indicating that both the GTP- and the GDP-bound states of RhoB can be found within the nucleus.

To determine the biological effect of the GTP-bound versus the GDP-bound form of RhoB on endothelial cell proliferation, we measured the proliferative index of BVECs and LVECs overexpressing either wt or mutant RhoB (Fig. 6c). As previously observed, wt RhoB promotes and represses the proliferation of BVECs versus LVECs, respectively. Interestingly, whereas RhoB-DN did not affect the proliferation rate of either type of endothelial cell, RhoB-CA influenced the proliferation of BVECs and LVECs similarly to wt RhoB. This lack of effect on proliferation by the RhoB-DN correlates with its inability to regulate genes previously identified as RhoB-VEZF1 targets such as VEGF-R2, NRP1 and TIMP3 (Fig. 6d). Altogether, these results suggest that both forms of RhoB may exist as part of the nuclear RhoB-VEZF1 transcriptional complex. However, only RhoB-GTP has the ability to regulate the expression of genes that are specific targets of VEZF1 and modulate the proliferation rate of blood and lymphatic vessel endothelial cells.

A small molecule targeting VEZF1-DNA interaction normalizes angiogenesis accompanying OIR.

Data already presented suggest that RhoB promotes pathological angiogenesis accompanying OIR (Fig.1a), in collaboration with VEZF1 (Fig. 4a). Therefore, we hypothesized that by interfering with the RhoB-VEZF1 pathway we might restore physiological revascularization in this setting. To target the RhoB-VEZF1 complex we focused on the DNA binding domain of VEZF1 that is composed of a zinc finger domain designed to recognize a specific DNA promoter sequence[27]. C_2H_2 zinc fingers occur in tandem arrays with many transcription factors composed of three or more fingers working in concert to target the transcription factor to its appropriate promoter[28,29]. An *in silico* approach was adopted to identify a small molecule that could inhibit the interaction of VEZF1 with DNA (VasculoMedics, private communication). This work discovered the small molecule VEZF1-compound 6 (VEC6) that significantly repressed NRP1 promoter-dependent luciferase activity in the presence of RhoB and VEZF1 overexpression (Fig. 7a). To further validate the efficacy of this compound, the expression pattern of several target genes downstream of RhoB and VEZF1 was evaluated in BVECs and LVECs undergoing

proliferative stress in the absence or presence of VEC6 (Fig. 7b). VEC6 repressed the expression of VEGF-R2, NRP1 and TIMP3 as determined by RTPCR. Interestingly, VEC6 phenocopies the opposing effects of RhoB-VEZF1; i.e., this small molecule is able to repress the proliferation of BVECs, and promote the proliferation of LVECs (Fig. 7c). Importantly, these data provide additional support that VEC6 is working "on target" to effectively modulate the RhoB-VEZF1 complex. To evaluate the efficacy of this compound *in vivo*, $RhoB^{+/-}$ mice were subjected to the OIR assay in the presence of VEC6 or DMSO (vehicle), which were administered daily by intraperitoneal injection during the pathological phase (P12 to P17) (Fig. 7d). The mice treated with DMSO did not exhibit any modification in the pathological angiogenic response as compared to previous studies (Compare Fig. 7d to Fig. 1a and Fig. 4a). However, VEC6 treatment increased the emergence of blood vessels with a normal morphology (arrowheads), and reduced both the avascular areas and pathological glomeruloid bodies (>2-fold decrease in the number of nuclei interior to inner limiting membrane). In conclusion, these data indicate that VEC6, identified by *in silico* approach, modulates the activity of the RhoB-VEZF1 complex by disrupting the VEZF1-DNA interaction interface, and they validate its efficacy *in vivo*.

DISCUSSION

Typically, the response of the blood vasculature to inflammation, ischemia, and wounding precedes that of the lymphatic network[3,4,24]. However, the mechanisms governing the coordinated response of these two major vascular networks to pathological challenge are still poorly understood. By studying RhoB null mice, we observed that loss of RhoB decreased the extent of pathological angiogenesis in the ischemic retina. We confirmed this regulatory role of RhoB in the dermal vasculature, i.e., loss of RhoB led to a reduction in angiogenesis in response to wounding. In addition, we noted that lymphangiogenesis, following both dermal wounding and inflammatory challenge, was enhanced in RhoB null mice. Upon further investigation, we learned that, although RhoB is induced in both blood and lymphatic endothelial cells subjected to proliferative stress, RhoB promotes proliferation and sprouting in BVECs, but represses these functions in LVECs. To our knowledge, this is the first demonstration of a single protein (i.e., RhoB), which serves intra-cellular and opposing regulatory roles in two closely related endothelial cell types (Fig. 8a).

To understand the underlying molecular mechanism(s) responsible for these intriguing and differential functions of RhoB, we investigated the interaction of RhoB with the transcription factor VEZF1. For the first time, we uncover the importance of a direct interaction between RhoB and VEZF1 in both blood and lymphatic endothelial cells, and document that it is the GTP-bound form of RhoB that exclusively regulates VEZF1-mediated transcription in both endothelial cell types. Notably, there have been very few reports that directly involve GTPases in regulating gene transcription. RhoA and Rac1 have been observed in the nucleus and are reported to directly contribute to transcriptional complexes involving the transcription factors Glucocorticoid Receptors and TCF4, respectively[30,31]. Our results provide further evidence for a requirement of an associated GTPase activity to bring about efficient gene transcription by certain transcription factors. Recently, it has been shown that the p68RacGAP interacts with VEZF1 and facilitates the hydrolysis of the GTP form of Rac1 in endothelial cells[32]. This finding suggests that future studies will be needed to identify the different regulatory partners, e.g., the GAPs and GEFs, participating in the RhoB regulation of VEZF1 mediated transcription.

Next, we identified direct and indirect downstream target genes that are co-regulated by RhoB and VEZF1. Importantly, we determined that the sets of direct target genes of the RhoB-VEZF1 complex differ in BVECs versus LVECs. We propose that this differential regulation is responsible, at least in part, for the well-documented phenomenon of delayed lymphangiogenesis observed in pathological settings reported *in vivo* [3,4,24]. Among the direct target genes that we identified in BVECS, VEGF-R2, NRP1 and Endothelin1 are known to support angiogenesis. Downregulation of another gene, i.e., PHD2, is involved in normalization of tumor vascular network[33]. Of the set of target genes that we identified in LVECs, MMP2 has already been linked with lymphatic sprouting[34], but two other genes, i.e., TIMP3 and Vasohibin1, have not previously been implicated in LVEC biology. Thus, our study contributes important new information to the growing list of genes specific to the blood versus lymphatic vasculature.

Finally, using an in silico approach we were able to successfully design a small molecule inhibitor, i.e., VEC6, targeting the VEZF1/DNA binding interface, that was able to recapitulate the effects of the loss of RhoB in the ischemic retina. This finding suggests that the RhoB-VEZF1 complex represents an interesting new target for developing novel therapies against numerous pathologies with a vascular component, e.g., diabetic retinopathy. However, VEC6 is also able to induce LVEC proliferation *in vitro* similar to silencing of *RhoB*, suggesting the possibility of a pro-lymphangiogenic effect *in vivo*. Further work using a second generation of inhibitory molecules more suited for *in vivo* studies in adult mice will be needed to address the question of lymphatic sensitivity and responsiveness. Notably, this question emphasizes the broader worth of considering more generally the lymphatic vascular network as a potential side target of any pro- or anti-angiogenic therapy.

Overall our work highlights the importance of the RhoB-VEZF1 pathway in the temporal regulation of angiogenesis and lymphangiogenesis during wound healing. Tissue damage (e.g. skin wounds) triggers a healing response precisely coordinated through different phases, i.e., hemostasis/Inflammation, proliferation, and remodeling/repair (Fig. 8b). The early angiogenic response participates in the initial inflammatory phase by facilitating recruitment of inflammatory cells into the wound bed (Movie S8). Thereafter, the formation of local edema enhances the migration of inflammatory

cells, endothelial cells, and myofibroblasts through the loose fibrin-rich provisional matrix of the granulation tissue to begin wound repair. Subsequently, the formation of new lymphatics aids in the drainage of excess fluid, cells and debris, to allow the remodeling phase to proceed, ultimately resulting in wound closure. Thus, RhoB actively participates in ensuring the delay in lymphangiogenesis that appears to be crucial to the success of the overall wound-healing program.

Although we were unable to evaluate the impact of the RhoB-VEZF1 pathway on wound closure in the ear model, our parallel study of dorsal skin excisional wound healing revealed that healthy *RhoB*$^{-/-}$ mice did not exhibit any significant difference in the time required for complete wound closure as compared to *wt* mice[35]. This result correlates with previous work on the effects of VEGF-A overexpression on wound healing. Indeed, earlier and increased lymphangiogenesis elicited by VEGF-A did not affect the time required for wound closure in healthy animals[6]. In contrast, VEGF-C over-expression accelerated wound closure by inducing angiogenesis, lymphangiogenesis and recruitment of inflammatory cells in diabetic animals[9]. We recently observed a similar phenomenon in RhoB$^{-/-}$ diabetic mice suggesting that the impact of deregulation of angiogenesis and/or lymphangiogenesis could be exacerbated in pathological conditions such as those occurring in diabetic animals. Future studies will address the effects of RhoB loss on pathological angiogenesis and lymphangiogenesis associated with tumour growth and metastasis.

In conclusion, we propose that the immediate early response gene *RhoB*, in its GTP-form, interacts with the transcription factor VEZF1, to regulate, at least in part, the distinct blood and lymphatic endothelial responses to different pathological stimuli. Additional analysis of this small GTPase will further our understanding of its differential angiogenic and lymphangiogenic regulatory mechanisms and identify new therapeutic strategies for appropriate intervention.

METHODS

Mice. *RhoB*$^{-/-}$ mice, a gift from George Prendergast [18], were maintained in both SV129 and FVB backgrounds. *VEZF1*$^{+/-}$ mice, a gift from Heidi Stuhlmann [21] were maintained in the SV129 background. In order to study the functional cooperation between *RhoB* and *VEZF1 in vivo*, *RhoB*$^{-/-}$ mice in the SV129 background were crossed with *VEZF1*$^{+/-}$ mice in the SV129 background. Resulting double heterozygotes were crossed to obtain all required genotypes in one litter (*RhoB*$^{+/-}$, *VEZF1*$^{+/-}$, *RhoB*$^{+/-}$*VEZF1*$^{+/-}$). All studies were conducted in compliance with the Beth Israel Deaconess Medical Center IACUC guidelines. **Retinopathy of Prematurity**. Mice were exposed to 75% oxygen beginning on postnatal day P7. A minimum of 8 groups were used; depending on the litter, each group contained from 5-8 pups. Mice were then returned to room air on day P12. Retinas were harvested on day P17, fixed in formalin (10% formaldehyde) for 1 hour, and incubated with FITC-Lectin BS-1 (Sigma) in PBS containing 0.2% Triton-X100 and 10% Goat serum O/N at 4^{O}C. The retinas were washed (4-5 times for 1 hr) in PBS. Approximately 4 incisions at the edges were made to flatten the retinal cup onto a glass slide for fluorescent microscopy and digital photography using a Leica MZFIII microscope and a Leica DC200 digital camera. Pups used for studies involving treatment with VEZF1 inhibitors were injected into I.P. with 30mg/kg/day of test compound from P12 to P17 and then retinas were processed and imaged as above.

Ear Acute Injury and Chronic Inflammation. Full-thickness wounds were created in the center of the ears of adult (6-8 weeks) mice using a 2 mm biopsy punch. At 7 days post injury ears were examined by whole mount staining and/or by intravital microscopy to assess both angiogenesis and lymphangiogenesis. Chronic inflammation was induced by delayed-type hypersensitivity (DTH) in the ear skin of RhoB null and WT mice as described previously in[25]. Briefly, adult mice (6-8 weeks) were sensitized by topical application of a 2% oxazolone (4-ethoxymethylene-2 phenyl-2-oxazoline-5-one; Sigma, St Louis, MO) solution in acetone/olive oil (4:1 vol/vol) to the shaved abdomen (50 µl) and to each paw (5 µl). Five days later, ears were challenged by topical application of 1% oxalozone solution (20 µl). Ear swelling was assessed by ear thickness measurement using a Mitutoyo caliper each day for 11

days following challenge. Lymphangiogenesis was assessed by intravital microscopy.

Ear Whole Mount Staining. Whole mounts of ears were prepared for confocal microscopy using the protocol of [8]. Mouse ears were dissected and placed in 4% PFA. Dorsal and ventral aspects of each ear were separated by first cutting along the entire edge of the ear and then peeling the two halves apart. After 3 hr fixation, tissues were blocked overnight in PBS containing 5% goat serum and 0.3% Triton-X100. Tissues were then incubated successively overnight in primary antibodies (CD31 [MEC13.3, 553370, BD Pharmigen], and Podoplanin [ab11936, Abcam]) and secondary antibodies (Jackson) each diluted 1/200 in blocking solution. Samples were mounted on glass slides and observed with a confocal microscope (Zeiss LSM 510 Meta). Confocal 3D projections were processed by Zeiss LSM Image software. Each 3D projection image corresponds to a tissue thickness of 100 µm. CD31 signal of 3D projections was quantified by using the measure function (% Area) from NIH ImageJ software, after selection of the wound angiogenic area (white lines).

Ear Intravital Microlymphangiography. These experiments were performed as described[36]. Briefly, mice were anesthetized with Avertin and placed in a transparent acrylic resin mold. Ears were mounted flat on the resin support and held in place by silicone vacuum grease and viewed in a Leica MZFLIII fluorescent microscope. High molecular weight FITC-dextran (2000 kDa lysine-fixable, Invitrogen at 20 µg/µl in saline) was injected into the lymphatics through a 10 µm pre-pulled borosilicate glass micropipette (World Precision Instruments, Sarasota, FL) attached to a 500 µl Hamilton syringe fitted with a threaded plunger. Using a micromanipulator (WPI), the micropipette was injected into the dorsal surface of the periphery of the ear in order to engage a lymphatic lumen. Additional tracer (5-20 µl) was then slowly injected under the control of a threaded plunger. The progress of the fluorescent tracer through the lymphatic network was followed in real time by digital image capture (60 frames/minute) using a Leica DC350 FX digital camera in conjunction with Image-Pro Plus 6.2 Software. The resultant image stack was then combined to produce a movie of tracer transport. Isolated frames, corresponding to specific times following tracer injection, were used to quantify the FITC-dextran tracer signal in each image using the measure function (% Area) from NIH ImageJ software.

Human Dermal Microvascular Endohelial Cell Isolation and Culture. Primary dermal human microvascular endothelial cells (HMVECs) from human foreskins (from at least four separated individuals) were isolated as previously described by using immunomagnetic beads[37]. Both BVECs and LVECs were isolated with magnetic Dynabeads pre-associated with CD31 (Invitrogen). Subsequently, LVECs were separated from BVECs by using goat anti-mouse Dynabeads associated with Podoplanin antibody (Angiobio). A total of six different cell isolation lots were used at passage 4-5 for all *in vitro* experiments. Each experiment was performed on at least two different cell isolation lots. HMVECs were grown in pre-coated plates with collagen I in MCDB131 medium (CellGro) supplemented with L-Alanyl-L-Glutamine (CellGro, 2mM) and MVGS supplement (Cascade Biologics).

Transfection. siRNA transfection in HMVECs was performed using HMVEC-L Nucleofector kit (Lonza). Briefly, cells at 100% confluence were harvested with trypsin-EDTA and washed in PBS. 100 µl of nucleofection solution was used for $1x10^6$ cells. Program S-005 was used for transfection. The cells were then removed from the cuvette and plated into a pre-coated 6 well cell culture plate. Final siRNA concentration was 50 µM in plate. RhoB and VEZF1 were silenced by using pre-designed siRNAs from Ambion (RhoB: siRNA ID# 42060, 41981, 41889, and VEZF1: siRNA ID# S15222, S15223, S15224). Silencer Select Negative Control #1 siRNA was used as control. Transfection of Hela cells was performed using TransIT-HelaMONSTER transfection kit (Mirus). VEZF1 overexpression was obtained by transfection of human VEZF1 expression vector from Origene. Luciferase assays were performed using the Dual-Luciferase Reporter Assay System (Promega).

Adenovirus and Mutagenesis. RhoB-Flag adenoviruses were generated using AdEasy Adenoviral system (Promega). Briefly, human *RhoB* coding sequence was amplified from human primary endothelial cell cDNA and inserted in pShuttle-IRES-hrGFP-1. Site-directed mutagenesis of *RhoB* was induced by PCR using Phusion High-Fidelity DNA polymerase (Fynnzymes) and *Dpn* I digestion. Mutagenic primers were used to prepare mutants for Constitutive Active (G14V) and Dominant Negative (T19N) forms of RhoB. All wild type and mutant sequences were checked by DNA sequencing. AdEasy recombinants were generated by electroporation of BJ5183 cells containing pAdEasy-1 vector, with *Pme* I linearized

shuttle vector. Adenoviruses were expanded in 293FT cells. All viruses were purified with the two-step CsCl centrifugation procedure. Purified adenoviruses were stored in Viral Preservation Media (Tris HCl 20 mM pH8, MgCl2 2mM, sucrose 5%) at -80°C. Cells were infected at a MOI of 50 pfu/cell.

Cell Immunostaining. Human dermal endothelial cells were grown in complete medium on coverslips pre-coated with collagen. Cells were collected after 24 h in order to assess the proliferation rate with Ki67 antibody (18-0191Z, ZYMED) or at confluence for Prox-1 (20R-PR039, Fitzgerald) and CD31 (555444, BD Pharmingen) immunostaining to confirm BVECs versus LVECs population identity. Cells were fixed with 4% paraformaldehyde for 5 min, followed by permeabilization and blocking with PBS containing, 5% goat serum, 0.1% Triton X-100 for 1h at room temperature. Primary antibodies were diluted 1/200 in blocking solution without Triton X-100 and then incubated with cells at 4^{o}C for O/N. Cells were then incubated with appropriate secondary antibody (Jackson). Coverslips were washed and mounted in Dako Fluorescent Mounting Medium containing DAPI (3µg/ml). Quantification of the proliferation rate with Ki67 antibody was determined by the analysis of three independent experiments and the consideration of ten random fields for each experiment.

Sprouting assay. Spheroid production was performed as described in[38]. Briefly, in 96 well plates, 400 endothelial cells per well were seeded in 100 µl/well of MVGS media containing 20% Methylcellulose (Sigma). After 24h, cell aggregates, named spheroids, were collected and centrifuged. Then, three-dimensional cultures of spheroids were prepared by using the overlay method as previously described[39]. In brief, spheroids were resuspended in media containing 2% Growth factor-reduced Matrigel (BD Biosciences), and seeded on top of the underlay containing a 50:50 mixture Matrigel and Bovine collagen I (PureCol, 3mg/ml, Inamed Biomaterials). Before mixing, collagen I was neutralized as described (citation of Seton-Rogers et al, 2005, PNAS, #5, p1257). Stimulatory cytokine, (human VEGF-A (25 ng/ml) or human VEGF-C (100 ng/ml) (RD Systems), respectively for BVECs and LVECs) was added to the Matrigel/collagen I underlay mixture. After 24h of stimulation, phase-contrast pictures were taken using a microscope (Nikon eclipse TE300) equipped with a camera (Leica, DFC 350 FX). Fluorescent images of GFP positive cells were obtained by confocal microscopy (Zeiss LSM 510 Meta). For

quantification, the cumulative sprout length of 15 randomly selected spheroids from three independent experiments was reported per data point.

Cell Extracts and Immunoblot analysis. Cytoplasm extracts were obtained by using a cytoplasmic lysis buffer (Triton X-100 0.25%, Tris-HCl 10 mM pH8, EDTA 5mM, EGTA 0.5 mM and proteases inhibitors (SIGMA-P8340)). After centrifugation, the nuclei pellet was resuspended in Urea lysis buffer (Urea 8M, Tris HCl 50 mM pH8, EDTA 5mM and proteases inhibitors). Total extracts were performed by direct cell digestion in Urea lysis buffer. Western blot analysis was performed as in[40], using antibodies recognizing human RhoB (CellSignaling-2098), RhoA (Bethyl-lab-929), VEZF1 (Abcam-ab50970), Tubulin (Calbiochem-CP06), DNA polymerase β (Abcam-26343), LYVE-1 (UpState-07-538), Prox1 (Fitzgerald20R-PR039), CD31 (BDPharmingen-555444), Podoplanin (Angiobio-11-003), VEGFR3 (SantaCruz-sc-321), and Flag tag (Abcam-ab1162).

Co-Immunoprecipitation (Co-IP) and Chromatin-Immunoprecipitation (ChIP). Co-IPs and ChIPs were performed using 0.5 x 10^6 cells per IP. Prior to Co-IPs, proteins were cross-linked with 1.5mM EGS agent [41]. For ChIPs, proteins were first cross-linked with 1.5 mM EGS, and proteins were then cross-linked to DNA with 1% Formaldehyde. After cytoplasmic fractionation, nuclei were digested in Complete Digestion Buffer from Nuclear complex Co-IP kit (Active motif). DNA was sheared by sonication. IP protocol was followed as described by supplier. Each IP was performed using 6 µg of antibodies against human VEZF1 (Abcam-ab85414), Flag tag (Sigma-F1804) and human Polymerase II (Covance-MMS-126R) and compared to IgG controls. Cross-linked proteins from Co-IPs were separated by treatment with 1M Hydroxylamine-HCl solution pH 8.5 (1:1 vol/vol), and analyzed by Western blotting. For ChIPs, DNA was purified as described in[42]. DNA enrichment was analyzed by Real Time PCR.

GTP pulldown assay. RhoB activity was assessed by measuring the amount of GTP-bound form of RhoB using the small GTPase activation assay (STA-403) from Cell Biolabs. 5 x 10^6 cells were used for each pulldown reaction performed with Rhoketin RBD Agarose beads, as described by manufacturer. The proteins were revealed by immunoblot analysis using antibodies recognizing human RhoB and Flag tag.

Analysis of Gene Expression. Total RNAs from two independent cell isolation lots, each from at least four separate individuals, were isolated using RNeasy Kit and treated by DNase I during extraction steps (Qiagen). cDNAs were prepared from 0.5 µg total RNA using random hexaprimers as templates and SuperScript III (Invitrogen). Quantitative real-time RT-PCR was carried out on an AbiPrism 7500 system using SYBR Green. The primer sequences are available upon request. For Affymetrix GeneChip probe array, 1 µg total RNA of one cell isolation lot from at least four separate individuals was synthetize as cRNA, which was hybridized to Affymetrix HT Human U133A GeneChips. Fold change of gene expression and Gene Ontology (GO) analysis were established using the dChip software[43] . Present probe sets with a differential expression ≥ 1.5 fold and $p < 0.05$ were taken into account.

Statistical Analysis. Results were presented as mean±SEM. Statistical significance of all data were analyzed using the unpaired two-tail Student's t test in the Microsoft Office Excel 2003 software. p values < 0.05 were considered to be statistically significant.

FIGURE LEGENDS

Figure 1 RhoB deletion blocks oxygen-induced pathological angiogenesis in the retina and decreases vessel density in skin wound-induced granulation tissue. (**a**) Whole mount staining of blood vessels (BS-I lectin) in the retina of *wt* and *RhoB*$^{-/-}$ pups subjected to hyperoxia from P7 to P12, and then returned back to normoxia from P12 to P17 (OD = Optic Disc). Histological (H&E) analysis of *wt* and *RhoB*$^{-/-}$ retinas at P17. Quantification of nuclei number interior to Inner Limiting Membrane (ILM) (n = 10 mice per genotype, mean±SEM). (**b**) Confocal analysis following whole mount staining of CD31 expression in the granulation tissue present 7 days after ear wounding (with 2 mm biopsy punch) in adult *wt* and *RhoB*$^{-/-}$ mice (6-8 weeks old). Quantification of CD31 positive staining in the neovasculature of the granulation tissue (delineate with white lines) (n = 6 mice per genotype, mean±SEM). (**c**) Confocal analysis following whole mount staining of CD31 and podoplanin expression in the granulation tissue present 7 days after wounding. Arrowheads highlight lymphatic vessels and denote areas of co-localization of CD31 and podoplanin in the merged image thus confirming the identity of the lymphatic vessels. Scale bars: Whole mount staining = 100 µm, H&E sections = 50 µm (a), 200 µm (d-c).

Figure 2 RhoB loss leads to enhanced and abnormal lymphangiogenesis in response to stress. (**a**) Intravital microlymphangiography by *in vivo* injection of FITC-Dextran (MW 2000 kDa) into lymphatics of ear skin 7 days after ear wounding (2 mm biopsy punch) in adult *wt* and *RhoB*$^{-/-}$ mice. Dextran positive areas in isolated frames taken from the movies at early (2-10 seconds (s), middle (30s) and late (60s) times following tracer injection were quantified in (g) (n = 7 mice per genotype, mean±SEM). (**b**) Confocal analysis following *in vivo* FITC-dextran injection in lymphatics and whole mount staining of podoplanin expression in the granulation tissue present 7 days after ear wounding in adult *wt* and *RhoB*$^{-/-}$ mice. Arrowhead and star respectively highlight dextran leakage from an abnormal lymphatic vessel and tracer accumulation in the adjacent tissue of *RhoB*$^{-/-}$ mice in the merged image. (**c**) Induction of DTH reactions in the ear skin of adult *wt* and *RhoB*$^{-/-}$ mice using oxalozone. Ear swelling is expressed as the increase (Δ) over the original ear thickness in µm. Ear thickness was measured daily for 11 days following challenge using a Mitotoyu caliper (n = 12 mice per genotype, mean±SEM). (**d**) Intravital microlymphangiography by *in vivo* injection of FITC-Dextran (MW 2000 kDa) into lymphatics of ear skin 7 days after inflammation induced by oxalozone in adult *wt* and *RhoB*$^{-/-}$ mice. FITCdextran positive areas in isolated frames taken from movies at early (2-10 seconds (s)), middle (30s) and late (60s) times following tracer injection were quantified (n = 6 mice per genotype, mean±SEM). Scale bars: 1mm (a-d) and 100 µm (b).

Figure 3 Differential regulation of BVECs and LVECs proliferation and sprouting by RhoB. (**a**) Representative Western blot showing the endogenous level of RhoB protein in BVECs and LVECs in the resting state (100% confluence for 48 h without media renewal) versus the proliferative state (24h and 48h after challenge initiated by cell plating at low, i.e., 50%, density). Western blotting for a related GTPase, RhoA, did not indicate any variation in RhoA expression levels in BVECs or LVECs under resting or proliferative conditions and thus confirmed the specificity of the RhoB antibody and the unique regulation of *RhoB* in these cells. Tubulin was used as loading control. (**b**) Representative Western blot showing the efficiency of *RhoB* silencing by siRNA nucleofection, and the level of *RhoB* overexpression following adenovirus infection, in BVECs and LVECs 24h after proliferative challenge. The RhoB-Flag protein was detected using antibodies directed against the RhoB protein and by antibodies against the Flag tag. (**c**) Proliferation index of BVECs and LVECs after *RhoB* silencing and *RhoB* overexpression at 24h after proliferative challenge, determined as the ratio of the number of Ki67 positive cells to the total number of cells (expressed as %, mean±SEM). (**d**) Sprouting from BVECs and LVECs spheroids in 3D Matrigel-collagen I matrix, induced for 24h by VEGF-A or VEGF-C, respectively, after *RhoB* silencing (phase-contrast pictures) or *RhoB* overexpression (fluorescent confocal projections). GFP expression, resulting from infection with the RhoB adenoviral vector containing an IRES-GFP, was used as an internal control for the overexpression experiments. Individual sprouts in *RhoB*-silenced cells are noted by red (BVECs) or green (LVECs) arrowheads, and in *RhoB*-overexpressing cells by white arrowheads. Quantitative analysis of endothelial cell sprouting was performed by measuring the cumulative length of all of the sprouts originating from one spheroid (described in [38]), using NIH ImageJ software (mean±SEM). Scale bars: 50 µm (d).

Figure 4 Functional interaction between RhoB and VEZF1 during oxygen-induced pathological angiogenesis and lymphangiogenesis associated with wound healing. (**a**) Whole mount staining of blood vessels (BS-I lectin) in the retina of *RhoB*$^{+/-}$, *VEZF1*$^{+/-}$ and *RhoB*$^{+/-}$*VEZF1*$^{+/-}$ pups (P17) subjected to OIR assay (OD = Optic Disc). Histological H&E analysis of *RhoB*$^{+/-}$, *VEZF1*$^{+/-}$ and *RhoB*$^{+/-}$*VEZF1*$^{+/-}$ retinas at P17. Quantification of nuclei number interior to Inner Limiting Membrane (ILM) (n = 6 per genotype, mean±SEM). (**b**) Intravital microlymphangiography by *in vivo* injection of FITC-Dextran (MW 2000 kDa) into lymphatics of ear skin 7 days after ear wounding (2 mm biopsy punch) in adult *RhoB*$^{+/-}$, *VEZF1*$^{+/-}$ and *RhoB*$^{+/-}$*VEZF1*$^{+/-}$ mice, shown at 60 seconds post tracer injection. Dextran positive areas in isolated frames taken from the movies at early (2-10 seconds (s), middle (30s) and late (60s) times following tracer injection were quantified (n = 6 mice per genotype, mean±SEM). (**c**) Representative Western blot of nuclear and cytoplasmic extracts showing the dual localization of RhoB in both nuclei and cytoplasm of BVECs and LVECs, whereas another RhoGTPase, RhoA, was detected only in the cytoplasm. In contrast, VEZF1 was exclusively detected in nuclei. DNA Polβ and Tubulin proteins were used as internal controls for nuclear and cytoplasmic extracts, respectively. (**d**) Representative Western blot following immunoprecipitation of overexpressed Myc-RhoB in Hela cells using an antibody against Myc tag. Overexpressed VEZF1 proteins were only co-immunoprecipitated in presence of Myc-RhoB. Scale bars: Whole mount staining = 100 µm, H&E sections = 50 µm (a), 1mm (b).

Figure 5 Target Genes shared by RhoB and VEZF1 in BVECs and LVECs. (**a**) Relative mRNA levels of VEGF-R2, NRP1, PHD2, Endothelin1, TIMP3, MMP2, CyclinE2 Vasohibin1 in BVECs and LVECs following silencing of either RhoB or VEZF1 as determined by QRT-PCR (performed in triplicate on two different cell isolation lots, mean±SEM). (**b**) *In vivo* binding of VEZF1 and RhoB-Flag to the promoter region of target genes, i.e., VEGF-R2, NRP1, Endothelin1, TIMP3, Vashohibin1, MMP2 containing predicted *in silico* VEZF1 DNA binding sites (red triangle in schematic drawing of promoters) assessed by ChIP experiments. The start site of transcription is referred as +1. Position of primers used for QPCR experiments is represented by blue arrows. The enrichment for each DNA fragment upon immunoprecipitation of VEZF1 and RhoB-Flag is illustrated as histograms based on % of input (QPCR performed in triplicate on two different cell isolation lots, mean±SEM).

Figure 6 BVEC and LVEC proliferation is specifically regulated by GTP-bound state of RhoB.

(**a**) Representative Western blot for detection of RhoB protein activation by GTP pulldown assay after adenoviral-mediated overexpression of wt RhoB-Flag (adRhoB) and RhoB mutants, i.e., adRhoB-DN for Dominant Negative (GDP-bound state), adRhoB-CA for Constitutive Active (GTP-bound state). adGFP was used as the control. Anti-RhoB and anti-Flag antibodies successfully detected all RhoB-Flag proteins in input samples. Anti-RhoB antibody exhibits a non-specific cross-reactivity with rhotekin proteins used for GTP-bound Rho GTPase trapping (star). (**b**) Proliferation index of BVECs and LVECs after overexpression of wt RhoB-Flag and its mutants at 24h after proliferation challenge, determined as the ratio of the number of Ki67 positive cells to the total number of cells (expressed as %, mean±SEM). adGFP was used as the control. (**c**) Relative levels of VEGF-R2 and NRP1 in BVECs, and TIMP3 in LVECs after overexpression of wt RhoB-Flag and its dominant negative mutant adRhoB-DN at 24h after proliferation challenge as determined by QRT-PCR (mean±SEM).

Figure 7 Normalization of pathological angiogenesis during OIR by small molecules targeting VEZF1 binding to DNA. (**a**) Schematic drawings of the human NRP1 promoter containing predicted *in silico* VEZF1 DNA binding sites (red triangles) depicting VEZF1 (red oval) binding to DNA, and RhoB (green circle) binding to VEZF1. The start site of transcription is referred as +1. The small molecule NSC 11435 named compound VEC6 docking to this VEZF1 zinc finger pocket (indicated by blue crosses) was screened for its ability to interfere with the interaction between VEZF1 and its DNA binding site leading to decreased promoter transactivation by the RhoB-VEZF1 complex. Activity of the human NRP1 promoter in Hela cells (control) and Hela cells overexpressing RhoB and VEZF1 (RhoB/VEZF1) in presence of solvent (DMSO) or VEC6 (20nM for 24h) (3 independent experiments, each containing duplicates, mean±SEM). (**b**) Relative levels of VEGF-R2, NRP1, TIMP3 in BVECs and LVECs following treatment with compound VEC6 (20 nM for 24h) as determined by QRT-PCR (mean±SEM). (**c**) Proliferation index of BVECs and LVECs treated with compound VEC6 at 24h after proliferative challenge, determined as the ratio of the number of Ki67 positive cells to the total number of cells (expressed as %, mean±SEM). (**d**) Whole mount staining of blood vessels (BS-I lectin) in the retina of *RhoB*$^{+/-}$ pups subjected to OIR and treated with vehicle (DMSO) or compound VEC6 by daily intraperitoneal injection between P12 and P17 (OD = Optic Disc). Histological analysis (H&E staining) of *RhoB*$^{+/-}$ retinas at P17 following treatment with DMSO or VEC6. Quantification of the number of nuclei interior to Inner Limiting Membrane (ILM) (8 animals per group, mean±SEM). Scale bars: Whole mount staining = 100 µm, H&E sections = 50 µm.

Figure 8 Model for RhoB-mediated coordination of the angiogenic and lymphangiogenic responses to pathological challenge initiated by dermal wounding. (**a**) After tissue challenge initiated by dermal wounding and in response to numerous extracellular signals that remain to be explored *in vivo*, the immediate early response gene *RhoB* is induced and its protein accumulates in both blood and lymphatic vascular endothelial cells. The GTP-bound form of RhoB (red star) partially localizes in the nucleus of these cells, where its physical interaction with the transcription factor VEZF1 regulates the differential expression of specific direct target genes in BVECs and LVECs leading to an increase in BVEC proliferation and sprouting and a simultaneous decrease in LVEC proliferation and sprouting. Accordingly, RhoB null mice exhibit reduced angiogenesis versus earlier, augmented and abnormal lymphangiogenesis in this and other pathological scenarios. (**b**) We propose that the opposing roles served by RhoB in these two endothelial cell types contribute to the coordination of an early angiogenic response versus a delayed lymphangiogenic response previously observed in wound healing. In this setting, the early angiogenic response participates in the initial inflammatory phase by facilitating recruitment of inflammatory cells into the wound bed (day 5-7). The delayed lymphangiogenesis allows these cells time to initiate tissue repair. Thereafter, the new lymphatics support the resolution of the local edema (small black arrows) by draining fluid excess, cells and debris (big black arrow) (day 9-14).

ACKNOWLEDGEMENTS

This work was supported by US Public Health Service NIH grant HL071049 (L.E.B.), Deutsche Forschungsgemeinschaft DFG, KU1497/1-1 (P.K.) and Lymphatic Research Foundation Posdoctoral Fellowship (D.G.). A.C. Rigby was a consultant for Vasculomedics involved in the identification of VEC6. L.E. Benjamin has moved to a full-time position at ImClone Systems, a wholly owned subsidiary of Eli Lilly.

1. Carmeliet, P. Angiogenesis in life, disease and medicine. *Nature* **438**, 932-936 (2005).
2. Tammela, T. & Alitalo, K. Lymphangiogenesis: Molecular mechanisms and future promise. *Cell* **140**, 460-476 (2010).
3. Clark, E.R. Reaction of experimentally isolated lymphatic capillaries in the tails of amphibian larvae. *Anat. Rec.* **24**, 181-191 (1922).
4. Clark, E.R. & Clark, E.L. Observations on the new growth of lymphatic vessels as seen in transparent chambers introduced into the rabbit's ear. *Am. J. Anat.* **51**, 49-87 (1932).
5. Witmer, A.N.*, et al.* VEGFR-3 in adult angiogenesis. *J Pathol* **195**, 490-497 (2001).
6. Hong, Y.K.*, et al.* VEGF-A promotes tissue repair-associated lymphatic vessel formation via VEGFR-2 and the alpha1beta1 and alpha2beta1 integrins. *FASEB J* **18**, 1111-1113 (2004).
7. Scavelli, C.*, et al.* Lymphatics at the crossroads of angiogenesis and lymphangiogenesis. *J Anat* **204**, 433-449 (2004).
8. Eichten, A., Shen, H.C. & Coussens, L.M. Three-dimensional visualization of blood and lymphatic vasculature in tissue whole mounts using confocal microscopy. *Curr Protoc Cytom* **Chapter 12**, Unit 12 15 (2005).
9. Saaristo, A.*, et al.* Vascular endothelial growth factor-C accelerates diabetic wound healing. *Am J Pathol* **169**, 1080-1087 (2006).
10. Jahner, D. & Hunter, T. The ras-related gene rhoB is an immediate-early gene inducible by v-Fps, epidermal growth factor, and platelet-derived growth factor in rat fibroblasts. *Mol Cell Biol* **11**, 3682-3690 (1991).
11. Fritz, G., Kaina, B. & Aktories, K. The ras-related small GTP-binding protein RhoB is immediate-early inducible by DNA damaging treatments. *J Biol Chem* **270**, 25172-25177 (1995).
12. Fritz, G. & Kaina, B. rhoB encoding a UV-inducible Ras-related small GTP-binding protein is regulated by GTPases of the Rho family and independent of JNK, ERK, and p38 MAP kinase. *J Biol Chem* **272**, 30637-30644 (1997).
13. Canguilhem, B.*, et al.* RhoB protects human keratinocytes from UVB-induced apoptosis through epidermal growth factor receptor signaling. *J Biol Chem* **280**, 43257-43263 (2005).
14. Lebowitz, P.F. & Prendergast, G.C. Functional interaction between RhoB and the transcription factor DB1. *Cell Adhes Commun* **6**, 277-287 (1998).

15. Gampel, A., Parker, P.J. & Mellor, H. Regulation of epidermal growth factor receptor traffic by the small GTPase rhoB. *Curr Biol* **9**, 955-958 (1999).
16. Fernandez-Borja, M., Janssen, L., Verwoerd, D., Hordijk, P. & Neefjes, J. RhoB regulates endosome transport by promoting actin assembly on endosomal membranes through Dia1. *J Cell Sci* **118**, 2661-2670 (2005).
17. Huang, M., Duhadaway, J.B., Prendergast, G.C. & Laury-Kleintop, L.D. RhoB regulates PDGFR-beta trafficking and signaling in vascular smooth muscle cells. *Arterioscler Thromb Vasc Biol* **27**, 2597-2605 (2007).
18. Liu, A.X., Rane, N., Liu, J.P. & Prendergast, G.C. RhoB is dispensable for mouse development, but it modifies susceptibility to tumor formation as well as cell adhesion and growth factor signaling in transformed cells. *Mol Cell Biol* **21**, 6906-6912 (2001).
19. Huang, M. & Prendergast, G.C. RhoB in cancer suppression. *Histol Histopathol* **21**, 213-218 (2006).
20. Adini, I., Rabinovitz, I., Sun, J.F., Prendergast, G.C. & Benjamin, L.E. RhoB controls Akt trafficking and stage-specific survival of endothelial cells during vascular development. *Genes Dev* **17**, 2721-2732 (2003).
21. Kuhnert, F.*, et al.* Dosage-dependent requirement for mouse Vezf1 in vascular system development. *Dev Biol* **283**, 140-156 (2005).
22. Smith, L.E.*, et al.* Oxygen-induced retinopathy in the mouse. *Invest Ophthalmol Vis Sci* **35**, 101-111 (1994).
23. Baluk, P. & McDonald, D.M. Markers for microscopic imaging of lymphangiogenesis and angiogenesis. *Ann N Y Acad Sci* **1131**, 1-12 (2008).
24. Shimamura, K., Nakatani, T., Ueda, A., Sugama, J. & Okuwa, M. Relationship between lymphangiogenesis and exudates during the wound-healing process of mouse skin fullthickness wound. *Wound Repair Regen* **17**, 598-605 (2009).
25. Kunstfeld, R.*, et al.* Induction of cutaneous delayed-type hypersensitivity reactions in VEGF-A transgenic mice results in chronic skin inflammation associated with persistent lymphatic hyperplasia. *Blood* **104**, 1048-1057 (2004).
26. Fritz, G. & Kaina, B. Rho GTPases: promising cellular targets for novel anticancer drugs. *Curr Cancer Drug Targets* **6**, 1-14 (2006).
27. Koyano-Nakagawa, N., Nishida, J., Baldwin, D., Arai, K. & Yokota, T. Molecular cloning of a novel human cDNA encoding a zinc finger protein that binds to the interleukin-3 promoter. *Mol Cell Biol* **14**, 5099-5107 (1994).
28. Blancafort, P. & Beltran, A.S. Rational design, selection and specificity of artificial transcription factors (ATFs): the influence of chromatin in target gene regulation. *Comb Chem High Throughput Screen* **11**, 146-158 (2008).
29. Jamieson, A.C., Miller, J.C. & Pabo, C.O. Drug discovery with engineered zinc-finger proteins. *Nat Rev Drug Discov* **2**, 361-368 (2003).
30. Buongiorno, P., Pethe, V.V., Charames, G.S., Esufali, S. & Bapat, B. Rac1 GTPase and the Rac1 exchange factor Tiam1 associate with Wnt-responsive promoters to enhance beta-catenin/TCF-dependent transcription in colorectal cancer cells. *Mol Cancer* **7**, 73 (2008).
31. Kino, T.*, et al.* Rho family Guanine nucleotide exchange factor Brx couples extracellular signals to the glucocorticoid signaling system. *J Biol Chem* **281**, 9118-9126 (2006).

32. Aitsebaomo, J.*, et al.* p68RacGAP is a novel GTPase-activating protein that interacts with vascular endothelial zinc finger-1 and modulates endothelial cell capillary formation. *J Biol Chem* **279**, 17963-17972 (2004).
33. Mazzone, M.*, et al.* Heterozygous deficiency of PHD2 restores tumor oxygenation and inhibits metastasis via endothelial normalization. *Cell* **136**, 839-851 (2009).
34. Bruyere, F.*, et al.* Modeling lymphangiogenesis in a three-dimensional culture system. *Nat Methods* **5**, 431-437 (2008).
35. Bravo-Nuevo, A.*, et al.* RhoB loss prevents streptozotocin-induced diabetes and ameliorates diabetic complications in mice. *Am J Pathol* **178**, 245-252 (2011).
36. Nagy, J.A.*, et al.* Vascular permeability factor/vascular endothelial growth factor induces lymphangiogenesis as well as angiogenesis. *J Exp Med* **196**, 1497-1506 (2002).
37. Richard, L., Velasco, P. & Detmar, M. A simple immunomagnetic protocol for the selective isolation and long-term culture of human dermal microvascular endothelial cells. *Exp Cell Res* **240**, 1-6 (1998).
38. Augustin, H.G., (Ed.). *Methods in Endothelial Cell Biology*, (Springer *Lab Manuals*, 2004).
39. Debnath, J., Muthuswamy, S.K. & Brugge, J.S. Morphogenesis and oncogenesis of MCF-10A mammary epithelial acini grown in three-dimensional basement membrane cultures. *Methods* **30**, 256-268 (2003).
40. Gerald, D.*, et al.* JunD reduces tumor angiogenesis by protecting cells from oxidative stress. *Cell* **118**, 781-794 (2004).
41. Zeng, P.Y., Vakoc, C.R., Chen, Z.C., Blobel, G.A. & Berger, S.L. In vivo dual cross-linking for identification of indirect DNA-associated proteins by chromatin immunoprecipitation. *Biotechniques* **41**, 694, 696, 698 (2006).
42. Rinn, J.L.*, et al.* Functional demarcation of active and silent chromatin domains in human HOX loci by noncoding RNAs. *Cell* **129**, 1311-1323 (2007).
43. Li, C. & Wong, W.H. Model-based analysis of oligonucleotide arrays: expression index computation and outlier detection. *Proc Natl Acad Sci U S A* **98**, 31-36 (2001).

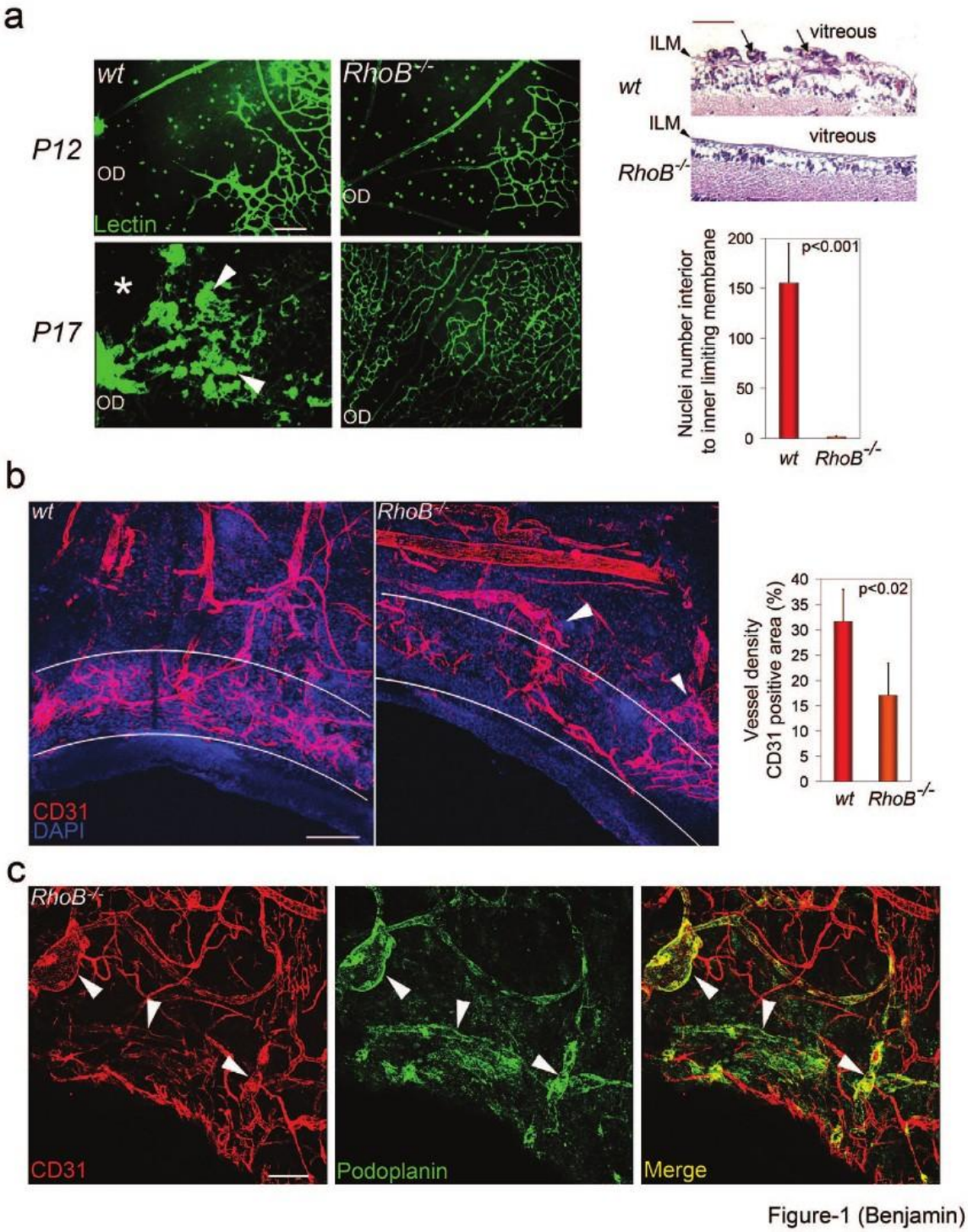

Figure-1 (Benjamin)

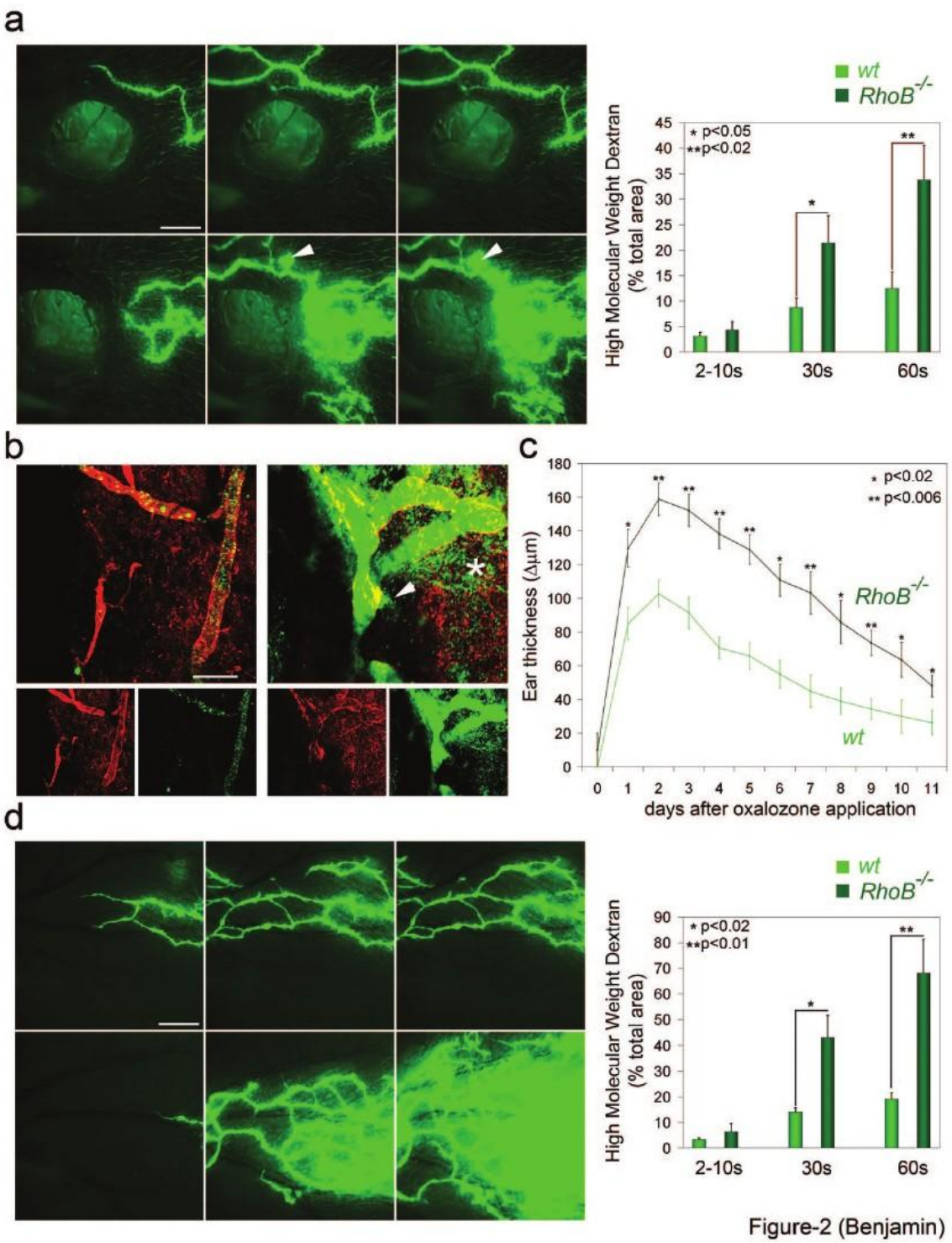

Figure-2 (Benjamin)

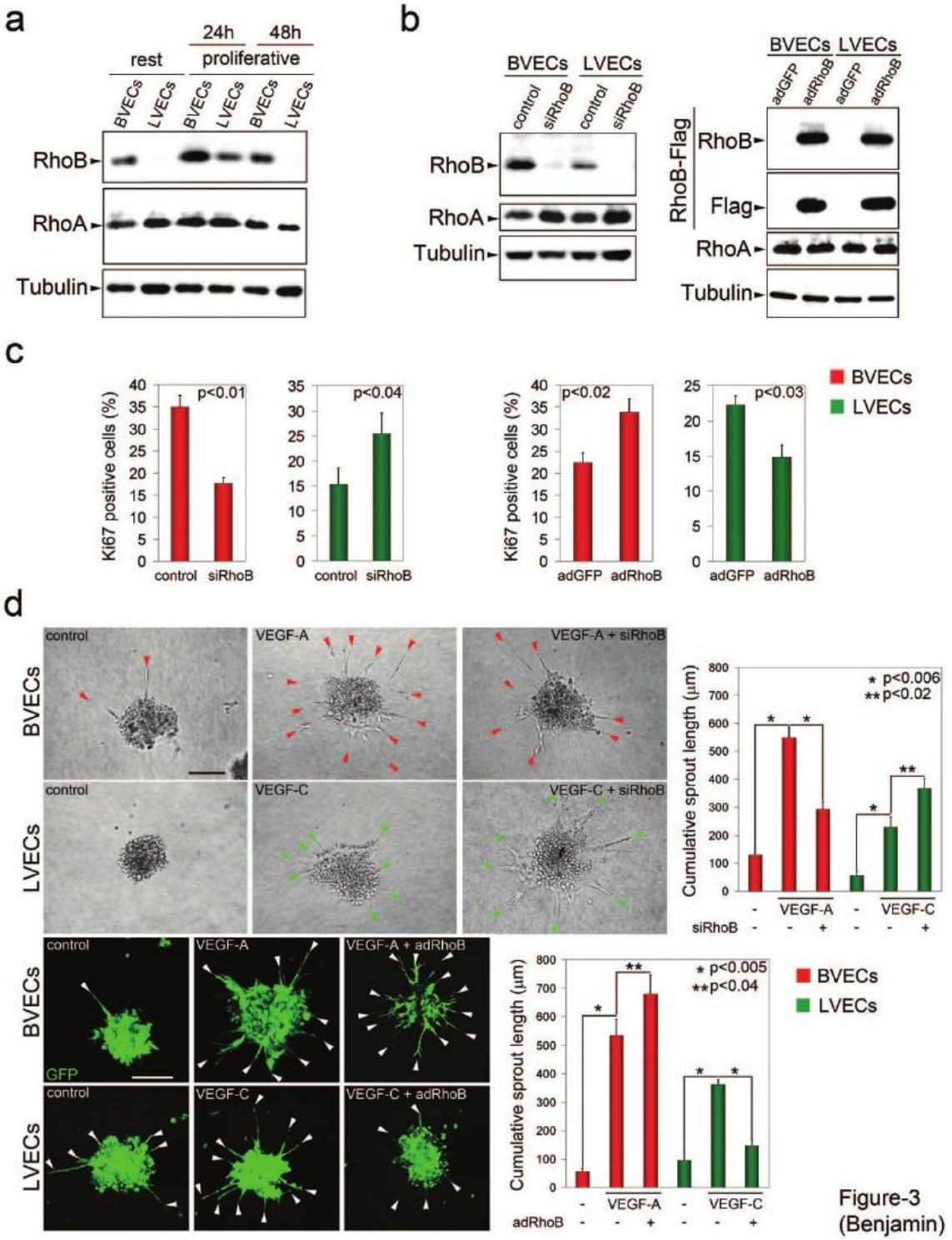

Figure-3
(Benjamin)

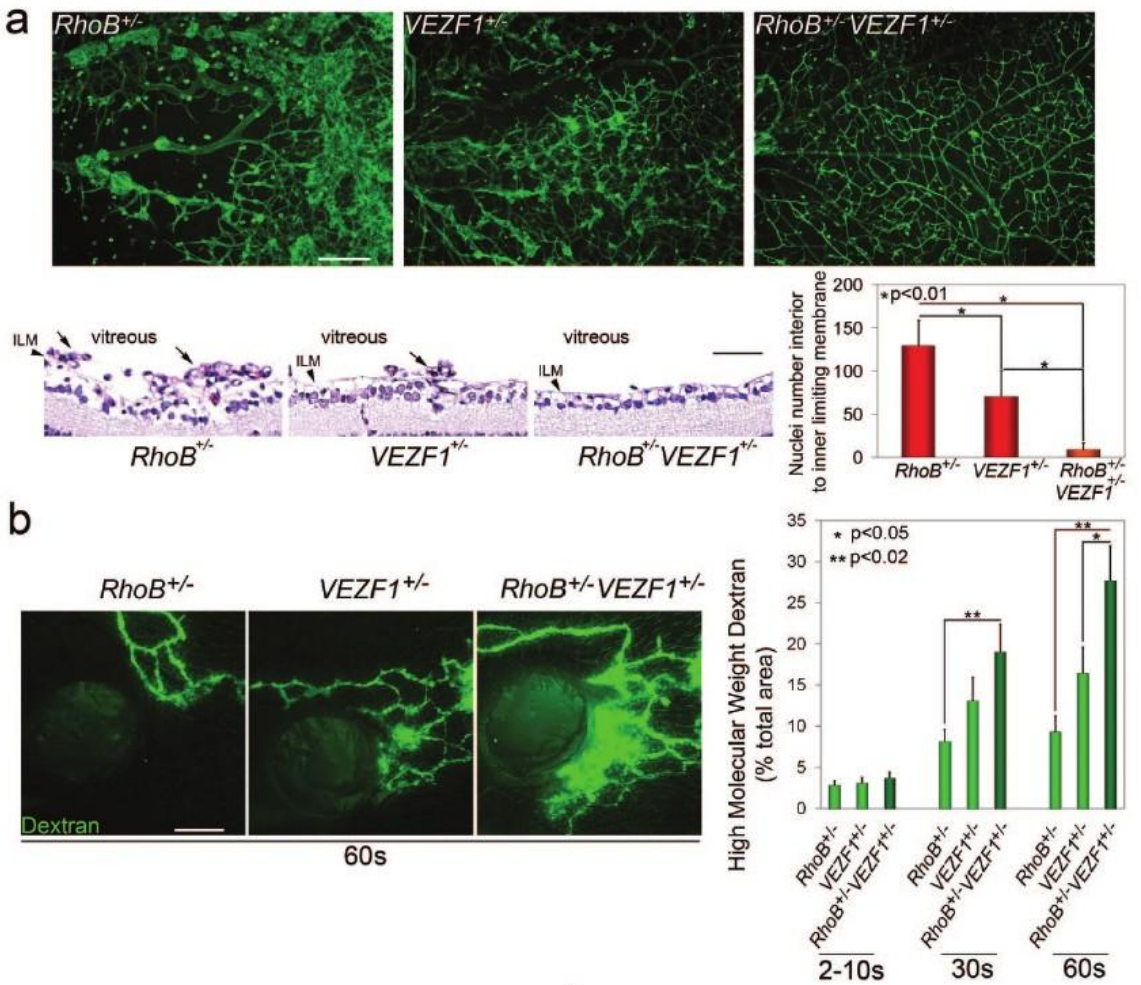

Figure-4 (Benjamin)

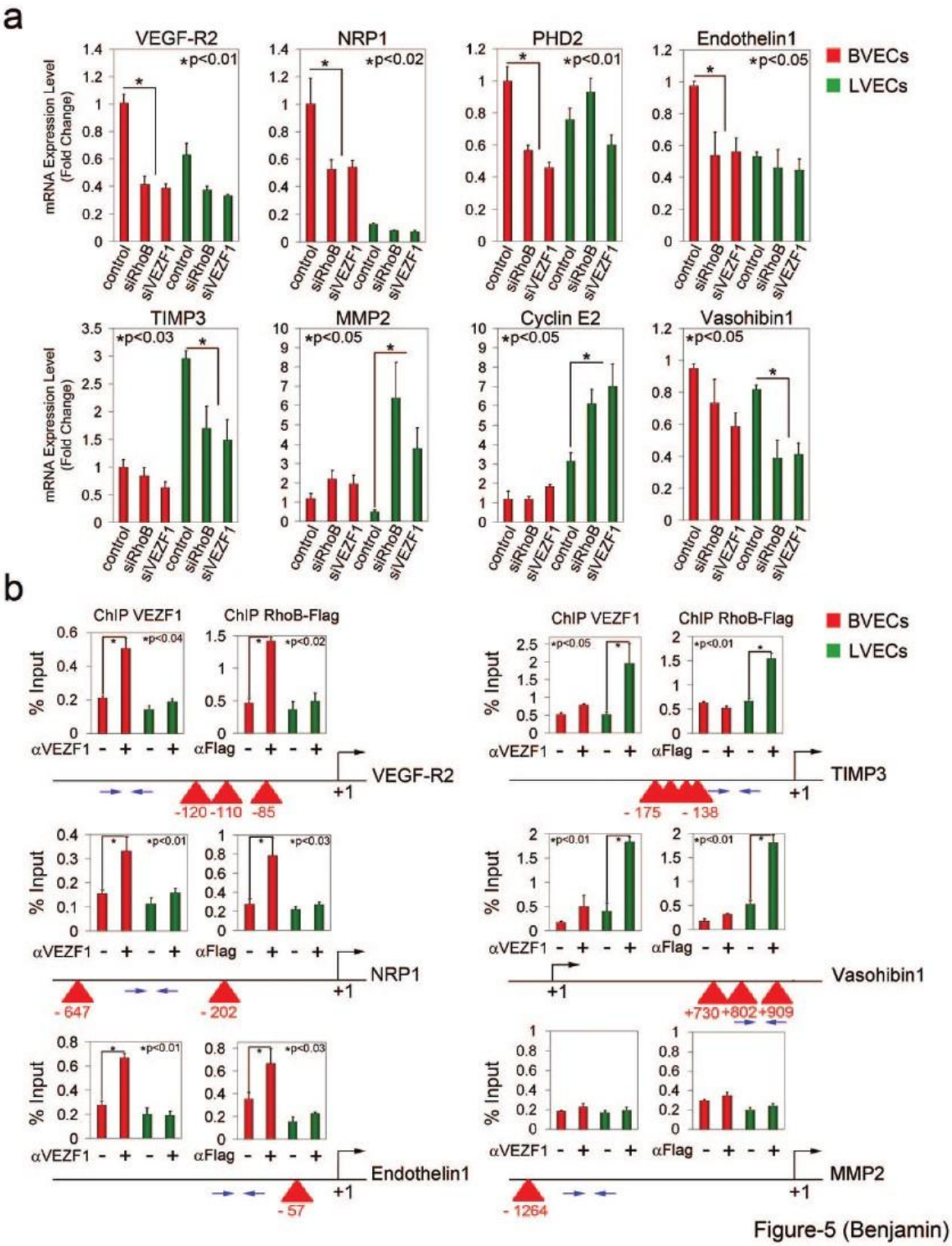

Figure-5 (Benjamin)

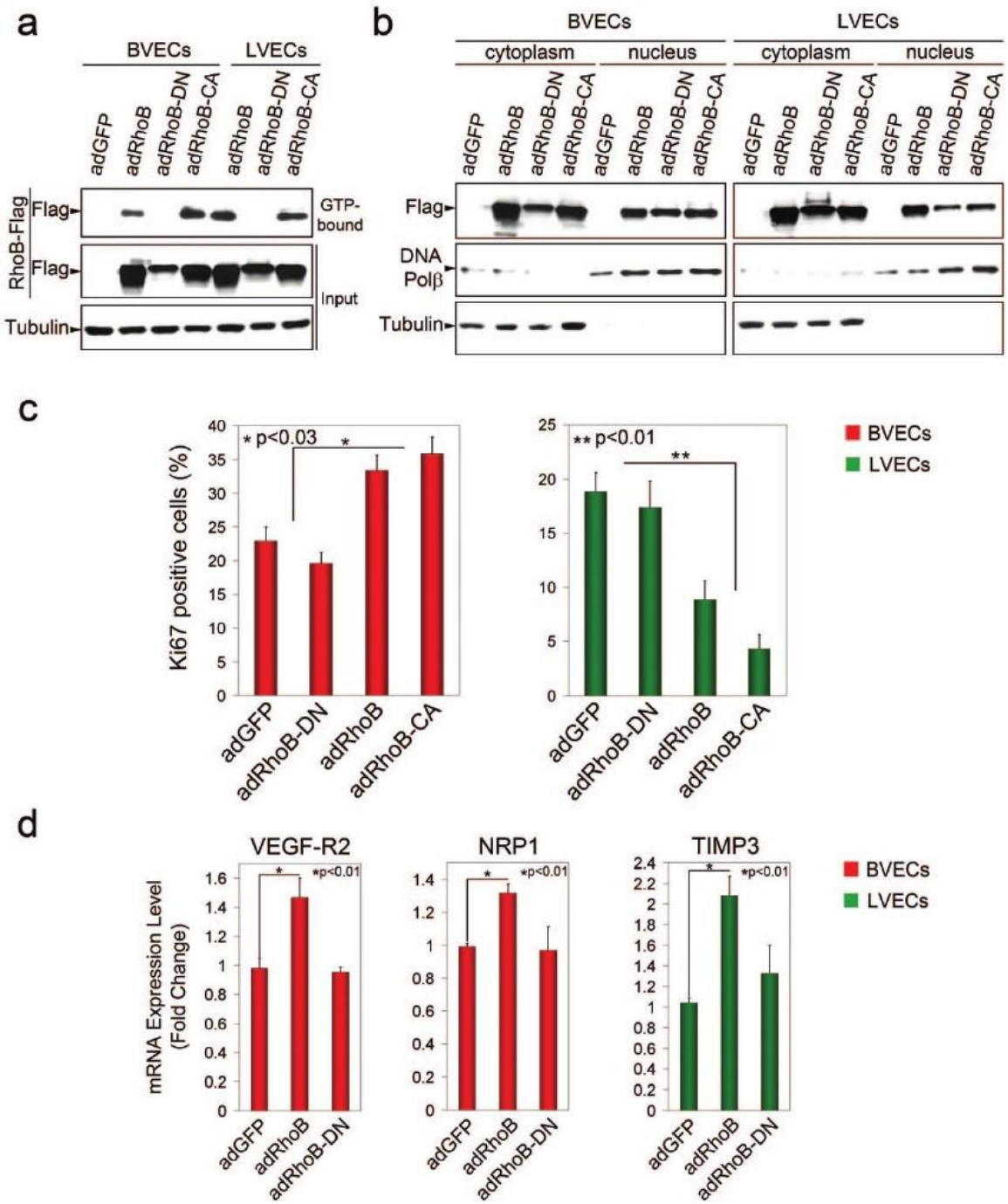

Figure-6 (Benjamin)

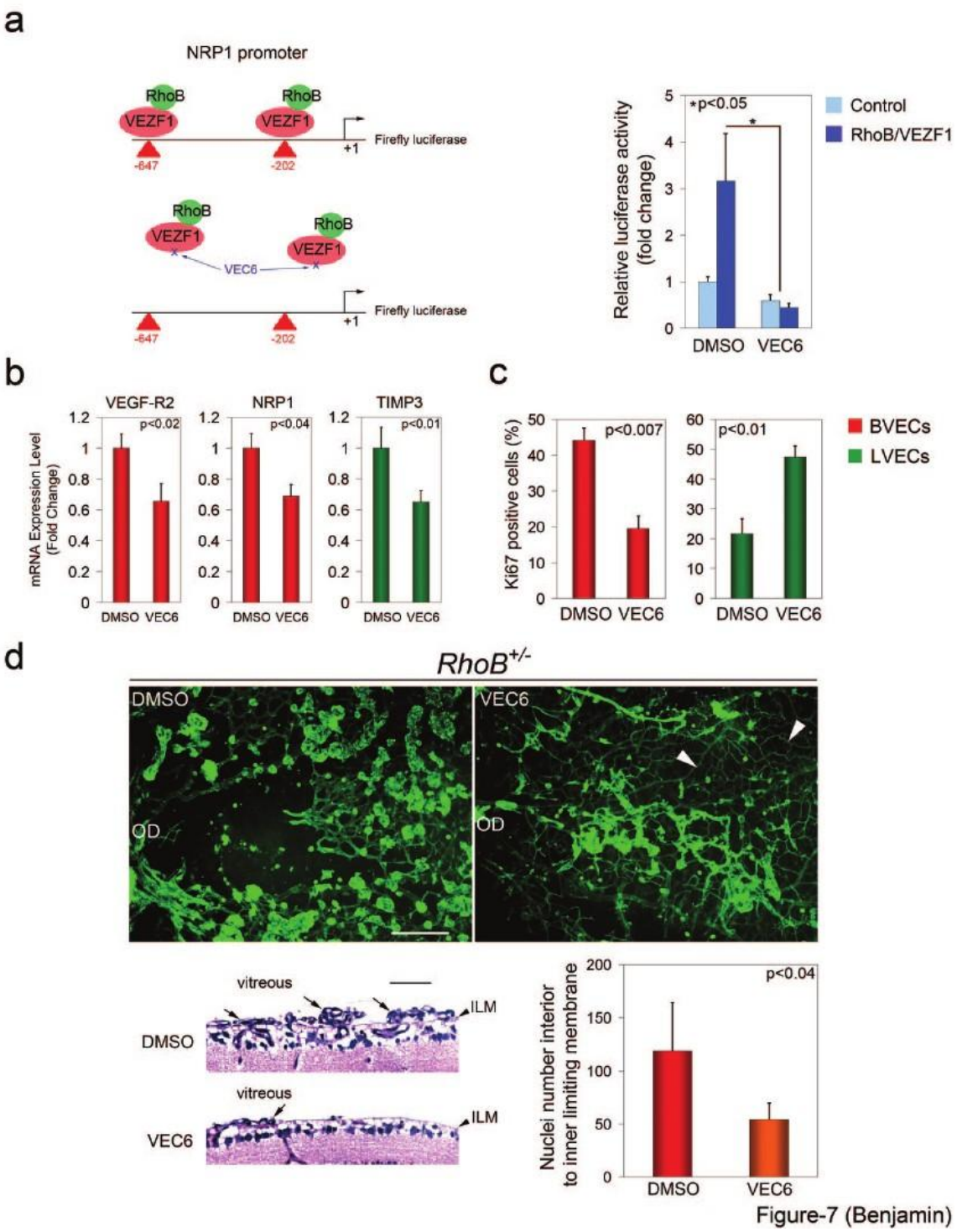

Figure-7 (Benjamin)

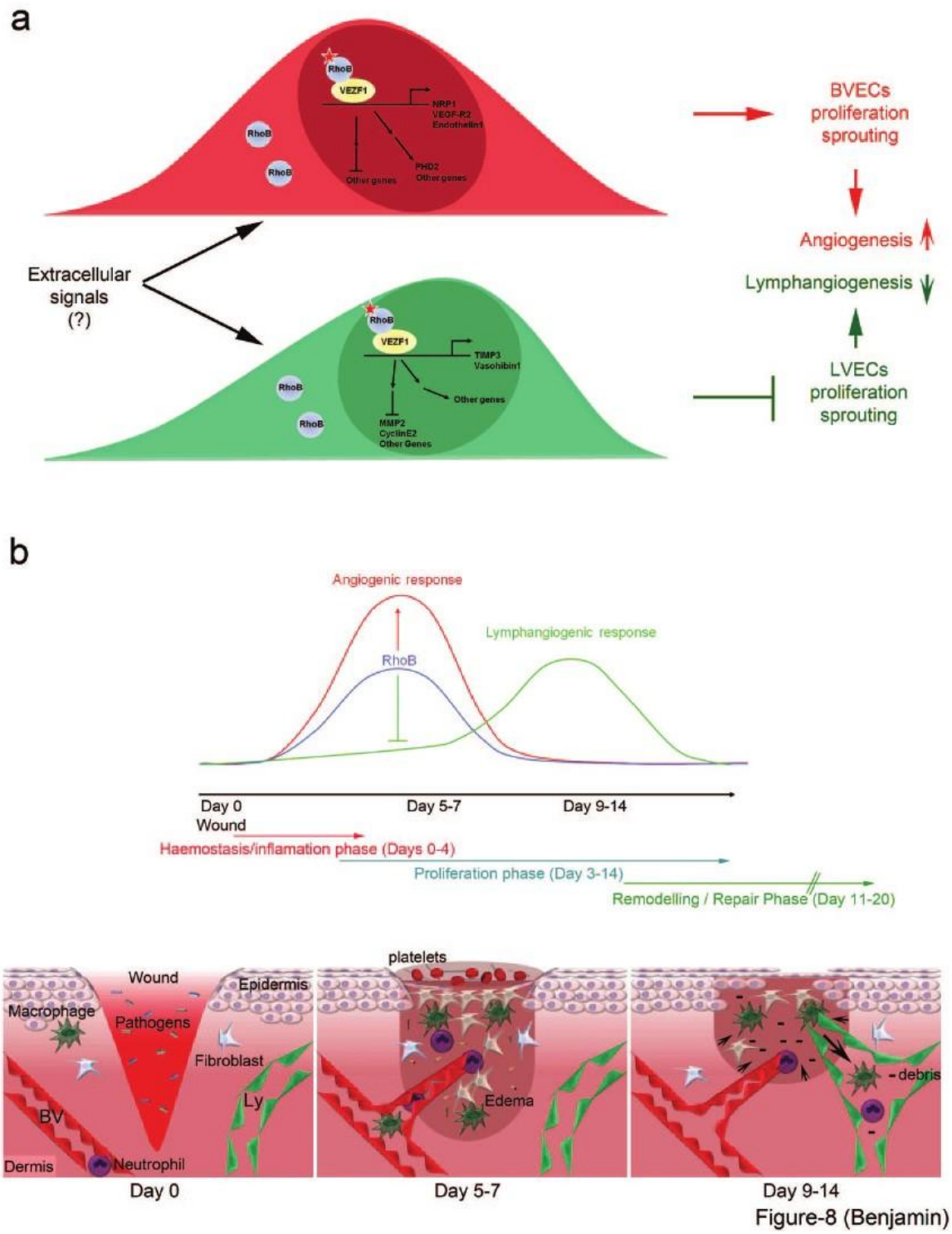

Figure-8 (Benjamin)

BIBLIOGRAPHY

BIBLIOGRAPHY

Aherne, W. & Hull, D., 1966. Brown adipose tissue and heat production in the newborn infant. *The Journal of Pathology and Bacteriology*, 91(1), pp.223–34.

Arany, Z. et al., 2008. HIF-independent regulation of VEGF and angiogenesis by the transcriptional coactivator PGC-1alpha. *Nature*, 451(7181), pp.1008–12.

Asano, a et al., 1997. Adrenergic activation of vascular endothelial growth factor mRNA expression in rat brown adipose tissue: implication in cold-induced angiogenesis. *The Biochemical Journal*, 328 (Pt 1, pp.179–83).

Asano, a, Irie, Y. & Saito, M., 2001. Isoform-specific regulation of vascular endothelial growth factor (VEGF) family mRNA expression in cultured mouse brown adipocytes. *Molecular and Cellular Endocrinology*, 174(1-2), pp.71–6

Barnard, T., 1969. The Ultrastructural Differentiation of Brown Adipose Tissue in the Rat. *Journal of Ultrastructure Research*, 29, pp.311- 332.

Bartelt, A. et al., 2011. Brown adipose tissue activity controls triglyceride clearance. *Nature Medicine*, 17(2), pp.200–5.

Boucher, J. et al., 2010. A kinase-independent role for unoccupied insulin and IGF-1 receptors in the control of apoptosis. *Science Signaling*, 3(151), p.ra87.

Bryan, B.A. et al., 2008. Coordinated Vascular Endothelial Growth Factor Expression and Signaling During Skeletal Myogenic Differentiation. *Molecular Biology of the Cell*, 19(March), pp.994–1006.

Bråkenhielm, E. et al., 2004. Angiogenesis inhibitor, TNP-470, prevents diet-induced and genetic obesity in mice. *Circulation Research*, 94(12), pp.1579–88.

Bukowiecki, L. et al., 1982. Brown adipose tissue hyperplasia: a fundamental mechanism of adaptation to cold and hyperphagia. *The American Journal of Physiology*, 242(6), pp.E353–9.

Cancello, R. et al., 2005. Reduction of macrophage infiltration and chemoattractant gene expression changes in white adipose tissue of morbidly obese subjects after surgery-induced weight loss. *Diabetes*, 54(8), pp.2277–86.

Cannon, B. & Nedergaard, J., 2004. Brown Adipose Tissue : Function and Physiological Significance. *Physiological Reviews*, 84(1), pp.277–359.

Cao, R et al., 2001. Leptin induces vascular permeability and synergistically stimulates angiogenesis with FGF-2 and VEGF. *Proceedings of the National Academy of Sciences of the United States of America*, 98(11), pp.6390–5.

Cao, Yihai, 2007. Science in medicine Angiogenesis modulates adipogenesis and obesity. *Journal of Clinical Investigation*, 117(9).

Carmeliet, P et al., 1996. Abnormal blood vessel development and lethality in embryos lacking a single VEGF allele. *Nature*, 380(6573), pp.435–9.

Carmeliet, P. Ng, Y-S. Nuyens, D. D'Amore, P. and Shima, D., 1999. Impaired myocardial angiogenesis and ischemic cardiomyopathy in mice lacking the vascular endothelial growth factor isoforms VEGF 164 and VEGF 188. *Nature Medicine*, 5(5), pp.495–502.

Castellot, J.J., Karnovsky, M.J. & Spiegelman, B M, 1982. Differentiation-dependent stimulation of neovascularization and endothelial cell chemotaxis by 3T3 adipocytes. *Proceedings of the National Academy of Sciences of the United States of America*, 79(18), pp.5597–5601.

Chinsomboon, J. et al., 2009. The transcriptional coactivator PGC-1alpha mediates exercise-induced angiogenesis in skeletal muscle. *Proceedings of the National Academy of Sciences of the United States of America*, 106(50), pp.21401–6.

Cigolini, M. et al., 1986. Isolation and ultrastructural features of brown adipocytes in culture. *Journal of Anatomy*, 145, pp.207–16.

Cinti, Saverio, 2007. The Adipose Organ. In J. Fantuzzi & T. Mazzone, eds. *Nutrition and Health: Adipose Tissue and Adipokines in Health and Disease*. Humana Press Inc., Totowa, NJ, pp. 3–19.

Claffey, K.P., Wilkison, W.O. & Spiegelman, B M, 1992. Vascular endothelial growth factor. Regulation by cell differentiation and activated second messenger pathways. *The Journal of Biological Chemistry*, 267(23), pp.16317–22.

Clark, E.R. & Clark, E.L., 1940. Microscopic studies of the new formation of fat in living adult rabbits. *American Journal of Anatomy*, 67, pp.255–285.

Clauss, M., 1998. Functions of the VEGF receptor-1 (FLT-1) in the vasculature. *Trends in Cardiovascular Medicine*, 8(6), pp.241–5.

Crandall, D.L. et al., 2000. Autocrine regulation of human preadipocyte migration by plasminogen activator inhibitor-1. *The Journal of Clinical Endocrinology & Metabolism*, 85(7), pp.2609–2614.

Crandall, D.L., Hausman, G.J. & Kral, J.G., 1997. Review Article A Review of the Microcirculation of Adipose Tissue : Anatomic , Metabolic , and Angiogenic Perspectives. *Microcirculation*, 4, pp.211–232.

Cypess, A.M. et al., 2009. Identification and importance of brown adipose tissue in adult humans. *The New England Journal of Medicine*, 360(15), pp.1509–17. Available

Cypess, A.M. & Kahn, C.R., 2010. The role and importance of brown adipose tissue in energy homeostasis. *Current Opinion in Pediatrics*, 22(4), pp.478–84.

Czaja, M.J., 2010. Autophagy in health and disease. 2. Regulation of lipid metabolism and storage by autophagy: pathophysiological implications. *American Journal of Physiology:Cell Physiology*, 298(5), pp.C973–8.

Darland, D.C. et al., 2011. Vascular endothelial growth factor (VEGF) isoform regulation of early forebrain development. *Developmental Biology*, 358(1), pp.9–22.

Devy, L. et al., 2002. The pro- or antiangiogenic effect of plasminogen activator inhibitor 1 is dose dependent. *FASEB Journal : official publication of the Federation of American Societies for Experimental Biology*, 16(2), pp.147–54.

Dong, H. & Czaja, M.J., 2011. Regulation of lipid droplets by autophagy. *Trends in Endocrinology and Metabolism: TEM*, 22(6), pp.234–40.

Elias, I. et al., 2012. Adipose Tissue Overexpression of Vascular Endothelial Growth Factor Protects Against Diet-Induced Obesity and Insulin Resistance. *Diabetes*, pp.1–13.

Enerbäck, S. et al., 1997. Mice lacking mitochondrial uncoupling protein are cold-sensitive but not obese. *Nature*, 387(6628), pp.90–4.

Fain, J.N. et al., 2004. Comparison of the release of adipokines by adipose tissue, adipose tissue matrix, and adipocytes from visceral and subcutaneous abdominal adipose tissues of obese humans. *Endocrinology*, 145(5), pp.2273–82.

Fain, J.N. & Madan, A.K., 2005. Insulin enhances vascular endothelial growth factor, interleukin-8, and plasminogen activator inhibitor 1 but not interleukin-6 release by human adipocytes. *Metabolism: Clinical and Experimental*, 54(2), pp.220–6.

Farmer, S.R., 2008. Molecular determinants of brown adipocyte formation and function. *Genes & Development*, 22(10), pp.1269–75.

Fernandes-Alnemri, T., Litwack, G. & Alnemri, E.S., 1994. CPP32, a novel human apoptotic protein with homology to Caenorhabditis elegans cell death protein Ced-3 and mammalian

interleukin-1 beta-converting enzyme. *The Journal of Biological Chemistry*, 269(49), pp.30761–4.

Ferrara, N et al., 1996. Heterozygous embryonic lethality induced by targeted inactivation of the VEGF gene. *Nature*, 380(6573), pp.439–42.

Ferrara, N & Henzel, W.J., 1989. Pituitary follicular cells secrete a novel heparin-binding growth factor specific for vascular endothelial cells. *Biochemical and Biophysical Research Communications*, 161(2), pp.851–8.

Ferrara, Napoleone, Gerber, H.-P. & LeCouter, J., 2003. The biology of VEGF and its receptors. *Nature medicine*, 9(6), pp.669–76.

Folkman, J et al., 1971. Isolation of a tumor factor responsible for angiogenesis. *The Journal of Experimental Medicine*, 133(2), pp.275–88.

Folkman, J, 1971. Tumor angiogenesis: therapeutic implications. *The New England Journal of Medicine*, 285(21), pp.1182–6.

Folkman, J, Hahnfeldt, P & Hlatky, L, 2000. Cancer: looking outside the genome. *Nature reviews. Molecular Cell Biology*, 1(1), pp.76–9.

Ford, K.M. et al., 2011. Expression and role of VEGF in the adult retinal pigment epithelium. *Investigative Ophthalmology & Visual Science*, 52(13), pp.9478–87.

Fredriksson, J M et al., 2000. Norepinephrine induces vascular endothelial growth factor gene expression in brown adipocytes through a beta -adrenoreceptor/cAMP/protein kinase A pathway involving Src but independently of Erk1/2. *The Journal of Biological Chemistry*, 275(18), pp.13802–11.

Fredriksson, J Magnus, Nikami, Hideki & Nedergaard, Jan, 2005. Cold-induced expression of the VEGF gene in brown adipose tissue is independent of thermogenic oxygen consumption. *FEBS Letters*, 579(25), pp.5680–4.

Fukumura, D. et al., 2003. Paracrine regulation of angiogenesis and adipocyte differentiation during in vivo adipogenesis. *Circulation Research*, 93(9), pp.e88–97.

García de la Torre, N. et al., 2008. Effects of weight loss after bariatric surgery for morbid obesity on vascular endothelial growth factor-A, adipocytokines, and insulin. *The Journal of Clinical Endocrinology and Metabolism*, 93(11), pp.4276–81.

Gealekman, O. et al., 2011. Depot-specific differences and insufficient subcutaneous adipose tissue angiogenesis in human obesity. *Circulation*, 123(2), pp.186–94.

Gealekman, O. et al., 2012. Effect of rosiglitazone on capillary density and angiogenesis in adipose tissue of normoglycaemic humans in a randomised controlled trial. *Diabetologia*.

Gealekman, Olga et al., 2008. Enhanced angiogenesis in obesity and in response to PPARgamma activators through adipocyte VEGF and ANGPTL4 production. *American Journal of Physiology: Endocrinology and Metabolism*, 295(5), pp.E1056–64.

Gersh, I. & Still, M.A., 1945. Blood vessels in fat tissue. Relation to problems of gas exchange. *The Journal of Experimental Medicine*, 81(2), pp.219–232.

Gesta, S. et al., 2006. Evidence for a role of developmental genes in the origin of obesity and body fat distribution. *Proceedings of the National Academy of Sciences of the United States of America*, 103(17), pp.6676–81.

Gesta, S., Tseng, Y.-H. & Kahn, C.R., 2007. Developmental origin of fat: tracking obesity to its source. *Cell*, 131(2), pp.242–56.

Ghorbani, M., Claus, T.H. & Himms-Hagen, J., 1997. Hypertrophy of brown adipocytes in brown and white adipose tissues and reversal of diet-induced obesity in rats treated with a beta3-adrenoceptor agonist. *Biochemical Pharmacology*, 54(1), pp.121–31.

Goldsmith, H.S. et al., 1984. Lipid angiogenic factor from omentum. *JAMA: The Journal of the American Medical Association*, 252(15), pp.2034–2036.

Goossens, G.H., 2008. The role of adipose tissue dysfunction in the pathogenesis of obesity-related insulin resistance. *Physiology & Behavior*, 94(2), pp.206–18.

Green, H. & Kehinde, O., 1975. An established preadipose cell line and its differentiation in culture. II. Factors affecting the adipose conversion. *Cell*, 5(1), pp.19–27.

Guan, F. et al., 2006. Autocrine VEGF-A system in podocytes regulates podocin and its interaction with CD2AP. *American Journal of Physiology: Renal Physiology*, 291(2), pp.F422–8.

Guerra, C. et al., 1998. Emergence of brown adipocytes in white fat in mice is under genetic control. Effects on body weight and adiposity. *The Journal of Clinical Investigation*, 102(2), pp.412–20.

Gómez-Ambrosi, J. et al., 2010. Involvement of serum vascular endothelial growth factor family members in the development of obesity in mice and humans. *The Journal of Nutritional Biochemistry*, 21(8), pp.774–80.

Hagberg, C.E. et al., 2010. Vascular endothelial growth factor B controls endothelial fatty acid uptake. *Nature*, 464(7290), pp.917–21.

Halberg, N., Khan, T., Trujillo, M.E., Wernstedt-Asterholm, I., Attie, A.D., Sherwani, S., Wang, Z.V., Landskroner-Eiger, S., Dineen, S., Magalang, U.J., Brekken, R. a, et al., 2009. Hypoxia-inducible factor 1alpha induces fibrosis and insulin resistance in white adipose tissue. *Molecular and Cellular Biology*, 29(16), pp.4467–83.

Hausman, G.J. & Richardson, R.L., 2004. Adipose tissue angiogenesis. *Journal of Animal Science*, 82(3), pp.925–934.

Hausman, G.J. & Thomas, G.B., 1986. Structural and histochemical aspects of perirenal adipose tissue in fetal pigs: relationships between stromal-vascular characteristics and fat cell concentration and enzyme activity. *Journal of Morphology*, 190(3), pp.271–283.

Hirning, U. et al., 1989. In developing brown adipose tissue c-myc protooncogene expression is restricted to early differentiation stages. *Cell differentiation and Development*, 27(3), pp.243–8.

Hull, D., 1976. The function of brown adipose tissue in the newborn. *Biochemical Society Transactions*, 4(2), pp.226–8.

Ichimura, Y. et al., 2000. A ubiquitin-like system mediates protein lipidation. *Nature*, 408(6811), pp.488–92.

Inoue, M. et al., 2001. Oxidized LDL regulates vascular endothelial growth factor expression in human macrophages and endothelial cells through activation of peroxisome proliferator-activated receptor-gamma. *Arteriosclerosis, Thrombosis, and Vascular Biology*, 21(4), pp.560–6.

Jozkowicz, A. et al., 2000. Ligands of peroxisome proliferator-activated receptor-gamma increase the generation of vascular endothelial growth factor in vascular smooth muscle cells and in macrophages. *Acta Biochimica Polonica*, 47(4), pp.1147–57.

Kabeya, Y et al., 2000. LC3, a mammalian homologue of yeast Apg8p, is localized in autophagosome membranes after processing. *The EMBO Journal*, 19(21), pp.5720–8.

Kabeya, Yukiko et al., 2004. LC3, GABARAP and GATE16 localize to autophagosomal membrane depending on form-II formation. *Journal of Cell Science*, 117(Pt 13), pp.2805–12.

Kajimura, S., Seale, P. & Spiegelman, Bruce M, 2010. Transcriptional control of brown fat development. *Cell Metabolism*, 11(4), pp.257–62.

Kamba, T. et al., 2006. VEGF-dependent plasticity of fenestrated capillaries in the normal adult microvasculature. *American Journal of Physiology: Heart and Circulatory Physiology*, 290(2), pp.H560–76.

Kolonin, M.G. et al., 2004. Reversal of obesity by targeted ablation of adipose tissue. *Nature Medicine*, 10(6), pp.625–32.

Korac, a et al., 2008. The role of nitric oxide in remodeling of capillary network in rat interscapular brown adipose tissue after long-term cold acclimation. *Histology and Histopathology*, 23(4), pp.441–50.

Kuhn, A. et al., 2002. Expression of endomucin, a novel endothelial sialomucin, in normal and diseased human skin. *The Journal of Investigative Dermatology*, 119(6), pp.1388–93.

Kundu, M. & Thompson, C.B., 2005. Macroautophagy versus mitochondrial autophagy: a question of fate? *Cell Death and Differentiation*, 12 Suppl 2, pp.1484–9.

Kuo, C J et al., 2001. Comparative evaluation of the antitumor activity of antiangiogenic proteins delivered by gene transfer. *Proceedings of the National Academy of Sciences of the United States of America*, 98(8), pp.4605–10.

Lau, D.C. et al., 1990. Influence of paracrine factors on preadipocyte replication and differentiation. *International Journal of Obesity*, 14 Suppl 3, pp.193–201.

Lau, D.C. et al., 1996. Paracrine interactions in adipose tissue development and growth. *International Journal of Obesity and Related Metabolic Disorders,* 20 Suppl 3, pp.S16–25.

Li, Pan et al., 2012. VEGF evokes reactive astroglia to convert into neuronal cells by affecting the biological function of MeCP2 in adult rat brain after cerebral ischemia. *Neurochemistry International*.

Lin, S.-C. & Li, Peng, 2004. CIDE-A, a novel link between brown adipose tissue and obesity. *Trends in Molecular Medicine*, 10(9), pp.434–9.

Liu, Y. et al., 2012. Intracellular VEGF regulates the balance between osteoblast and adipocyte differentiation. *Journal of Clinical Investigation*, pp.1–13.

Lowell, B. et al., 1993. Development of obesity in transgenic mice after genetic ablation of brown adipose tissue. *Nature*, 366(6457), pp.740–2.

Lu, X. et al., 2012. Resistance to Obesity by Repression of VEGF Gene Expression through Induction of Brown-Like Adipocyte Differentiation. *Endocrinology*, 153(July), pp.1–10.

Maharaj, A.S.R. et al., 2008. VEGF and TGF-beta are required for the maintenance of the choroid plexus and ependyma. *The Journal of Experimental Medicine*, 205(2), pp.491–501.

Mayer, H. et al., 2005. Vascular endothelial growth factor (VEGF-A) expression in human mesenchymal stem cells: autocrine and paracrine role on osteoblastic and endothelial differentiation. *Journal of Cellular Biochemistry*, 95(4), pp.827–39.

McAllister, F.F., Leighninger, D. & Beck, C.S., 1951. Revascularization of the heart by vein graft from aorta to coronary sinus. *Annals of Surgery*, 133(2), pp.153–65.

Milosevic, M. & Ukropina, M., 2008. *EMC 2008 14th European Microscopy Congress* 1–5 September 2008, Aachen, Germany A. Aretz, B. Hermanns-Sachweh, & J. Mayer, eds. , 3, pp.113–114.

Miquerol, L. et al., 1999. Multiple developmental roles of VEGF suggested by a LacZ-tagged allele. *Developmental Biology*, 212(2), pp.307–22.

Miquerol, L., Langille, B.L. & Nagy, A., 2000. Embryonic development is disrupted by modest increases in vascular endothelial growth factor gene expression. *Development (Cambridge, England)*, 127(18), pp.3941–6.

Miranda, S. et al., 2010. Beneficial effects of PTP1B deficiency on brown adipocyte differentiation and protection against apoptosis induced by pro- and anti-inflammatory stimuli. *Cellular Signalling*, 22(4), pp.645–59.

Miyazawa-Hoshimoto, S. et al., 2005. Roles of degree of fat deposition and its localization on VEGF expression in adipocytes. *American Journal of Physiology. Endocrinology and Metabolism*, 288(6), pp.E1128–36.

Morita, T., Shinohara, N. & Tokue, A., 1994. Antitumour effect of a synthetic analogue of fumagillin on murine renal carcinoma. *British Journal of Urology*, 74(4), pp.416–21.

Napolitano, L., 1963. The differentiation of white adipose cells. An electron microscope study. *The Journal of Cell Biology*, 18, pp.663–79.

Nedergaard, Jan, Bengtsson, T. & Cannon, B., 2007. Unexpected evidence for active brown adipose tissue in adult humans. *American Journal of Physiology. Endocrinology and Metabolism*, 293(2), pp.E444–52.

Ng, Y.S. et al., 2001. Differential expression of VEGF isoforms in mouse during development and in the adult. *Developmental Dynamics*, 220(2), pp.112–21.

Nicholson, D.W. et al., 1995. Identification and inhibition of the ICE/CED-3 protease necessary for mammalian apoptosis. *Nature*, 376(6535), pp.37–43.

Nisoli, Enzo et al., 1997. Tumor necrosis factor-a induces apoptosis in rat brown adipocytes. *Cell*, pp.771–778.

Orava, J. et al., 2011. Different metabolic responses of human brown adipose tissue to activation by cold and insulin. *Cell Metabolism*, 14(2), pp.272–9.

Ouellet, V. et al., 2012. Brown adipose tissue oxidative metabolism contributes to energy expenditure during acute cold exposure in humans. *Journal of Clinical Investigation*, 122(2).

O'Reilly, M.S. et al., 1994. Angiostatin: a novel angiogenesis inhibitor that mediates the suppression of metastases by a Lewis lung carcinoma. *Cell*, 79(2), pp.315–28.

O'Reilly, M.S. et al., 1997. Endostatin: an endogenous inhibitor of angiogenesis and tumor growth. *Cell*, 88(2), pp.277–85.

Panigrahy, D. et al., 2002. PPARγ ligands inhibit primary tumor growth and metastasis by inhibiting angiogenesis. *Journal of Clinical Investigation*, 110(7), pp.923–932.

Pasarica, M. et al., 2009. Reduced Adipose Tissue Oxygenation in Human Obesity. *Diabetes*, 58(3), pp.718–725.

Patel-Hett, S. & D'Amore, Patricia a, 2011. Signal transduction in vasculogenesis and developmental angiogenesis. *The International Journal of Developmental Biology*, 55(4-5), pp.353–63.

dela Paz, N.G. & D'Amore, Patricia A, 2009. Arterial versus venous endothelial cells. *Cell and Tissue Research*, 335(1), pp.5–16.

Peeters, L.L.H. et al., 2005. PPAR gamma represses VEGF expression in human endometrial cells: implications for uterine angiogenesis. *Angiogenesis*, 8(4), pp.373–9.

Petrovic, M.G. et al., 2008. Local and genetic determinants of vascular endothelial growth factor expression in advanced proliferative diabetic retinopathy. *Molecular Vision*, 14, pp.1382–7.

Pino, E. et al., 2012. Roles for peroxisome proliferator-activated receptor γ (PPARγ) and PPARγ coactivators 1α and 1β in regulating response of white and brown adipocytes to hypoxia. *The Journal of Biological Chemistry*, 287(22), pp.18351–8.

Puigserver, P. et al., 1998. A cold-inducible coactivator of nuclear receptors linked to adaptive thermogenesis. *Cell*, 92(6), pp.829–39.

Puigserver, P., 2003. Peroxisome Proliferator-Activated Receptor-gamma Coactivator 1alpha (PGC-1alpha): Transcriptional Coactivator and Metabolic Regulator. *Endocrine Reviews*, 24(1), pp.78–90.

Rosen, E.D. & Spiegelman, Bruce M, 2006. Adipocytes as regulators of energy balance and glucose homeostasis. *Nature*, 444(7121), pp.847–53.

Rothwell, N.J. & Stock, M.J., 1979. A role for brown adipose tissue in diet-induced thermogenesis. *Nature*, 281(5726), pp.31–5.

Rothwell, N.J. & Stock, M.J., 1983. Luxuskonsumption, diet-induced thermogenesis and brown fat: the case in favour. *Clinical Science (London, England : 1979)*, 64(1), pp.19–23.

Rupnick, M. a et al., 2002. Adipose tissue mass can be regulated through the vasculature. *Proceedings of the National Academy of Sciences of the United States of America*, 99(16), pp.10730–5.

Saint-Geniez, M. et al., 2008. Endogenous VEGF is required for visual function: evidence for a survival role on müller cells and photoreceptors. *PloS One*, 3(11), p.e3554.

Saint-Geniez, M., Kurihara, T. & D'Amore, Patricia a, 2009. Role of cell and matrix-bound VEGF isoforms in lens development. *Investigative Ophthalmology & Visual Science*, 50(1), pp.311–21.

Saint-geniez, M. et al., 2009. An essential role for RPE-derived soluble VEGF in the maintenance of the choriocapillaris. *Retina*, 106(44).

Sakurai, H. et al., 2008. Innate immune response induced by gene delivery vectors. *International Journal of Pharmaceutics*, 354(1-2), pp.9–15.

Seale, P. et al., 2008. PRDM16 controls a brown fat/skeletal muscle switch. *Nature*, 454(7207), pp.961–7.

Seale, P. & Lazar, M. a, 2009. Brown fat in humans: turning up the heat on obesity. *Diabetes*, 58(7), pp.1482–4.

Senger, D.R. et al., 1983. Tumor Cells Secrete a Vascular Permeability Factor that Promotes Accumulation of Ascites Fluid. *Science*, 219(4587), pp.983–985.

Shalaby, F. et al., 1995. Failure of blood-island formation and vasculogenesis in Flk-1-deficient mice. *Nature*, 376(6535), pp.62–6.

Silverman, K.J., Folkman, J & Barger, A.C., 1988. Angiogenic Activity of Adipose Tissue. *Biochemical and Biophysical Research Communications*, 153(1), pp.347–352.

Singh, R. et al., 2009. Autophagy regulates adipose mass and differentiation in mice. *Journal of Clinical Investigation*, 119(11), pp.3329–3339.

Skala, J. & Hahn, P., 1974. Changes In Interscapular Perinatal Adipose Tissue Of The Rat During Development Effect And Early Postnatal Temperature And After Cold Acclimation Of Hormones. *International Journal of Biochemistry*, 5, pp.95 – 106.

Smith, R.E., 1964. Thermoregulatory and adaptive behavior of brown adipose tissue. *Science*, 146, pp.1686–9.

Smith, R.E. & Horwitz, B.A., 1969. Brown fat and thermogenesis. *Physiological Reviews*, 49(2), pp.330–425.

Spalding, K.L. et al., 2008. Dynamics of fat cell turnover in humans. *Nature*, 453(7196), pp.783–7.

Stalmans, I. et al., 2002. Arteriolar and venular patterning in retinas of mice selectively expressing VEGF isoforms. *Journal of Clinical Investigation*, 109(3), pp.327–336.

Sun, K. et al., 2012. Dichotomous effects of VEGF-A on adipose tissue dysfunction. *Proceedings of the National Academy of Sciences of the United States of America*, 109(15), pp.5874–5879.

Sun, K., Kusminski, C.M. & Scherer, P.E., 2011. Adipose tissue remodeling and obesity. *Journal of Clinical Investigation*, 121(6), pp.2094 – 2101.

Tam, J. et al., 2009. Blockade of VEGFR2 and not VEGFR1 can limit diet-induced fat tissue expansion: role of local versus bone marrow-derived endothelial cells. *PloS One*, 4(3), p.e4974.

Tanida, Isei, Ueno, Takashi & Kominami, Eiki, 2004. Human light chain 3/MAP1LC3B is cleaved at its carboxyl-terminal Met121 to expose Gly120 for lipidation and targeting to autophagosomal membranes. *The Journal of Biological Chemistry*, 279(46), pp.47704–10.

Timmons, J.A. et al., 2007. Myogenic gene expression signature establishes that brown and white adipocytes originate from distinct cell lineages. *Proceedings of the National Academy of Sciences of the United States of America*, 104(11), pp.4401–6.

Tiraby, C. et al., 2003. Acquirement of brown fat cell features by human white adipocytes. *The Journal of Biological Chemistry*, 278(35), pp.33370–6.

Tonello, C et al., 1999. Role of sympathetic activity in controlling the expression of vascular endothelial growth factor in brown fat cells of lean and genetically obese rats. *FEBS Letters*, 442(2-3), pp.167–72.

Tran, Khanh-Van et al., 2012. The vascular endothelium of the adipose tissue gives rise to both white and brown fat cells. *Cell Metabolism*, 15(2), pp.222–9.

Trayhurn, P., 2005. Endocrine and signalling role of adipose tissue: new perspectives on fat. *Acta Physiologica Scandinavica*, 184(4), pp.285–93.

Vidal, H., 2001. Gene expression in visceral and subcutaneous adipose tissues. *Annals of Medicine*, 33(8), pp.547–55.

Vineberg, A.M. et al., 1965. Myocardial revascularization by omental graft without pedicle: experimental background and report on 25 cases followed 6 to 16 months. *The Journal of Thoracic and Cardiovascular Surgery*, 49, pp.103–29.

Vohl, M.-C. et al., 2004. A survey of genes differentially expressed in subcutaneous and visceral adipose tissue in men. *Obesity Research*, 12(8), pp.1217–22.

Wacker, A. & Gerhardt, H., 2011. Endothelial development taking shape. *Current Opinion in Cell Biology*, 23(6), pp.676–85.

Walshe, T.E., Dole, V.S., et al., 2009. Inhibition of VEGF or TGF-{beta} signaling activates endothelium and increases leukocyte rolling. *Arteriosclerosis, Thrombosis, and Vascular Biology*, 29(8), pp.1185–92.

Walshe, T.E., Saint-Geniez, M., et al., 2009. TGF-beta is required for vascular barrier function, endothelial survival and homeostasis of the adult microvasculature. *PloS One*, 4(4), p.e5149.

Wang, J., Lou, P. & Henkin, J., 2000. Selective inhibition of endothelial cell proliferation by fumagillin is not due to differential expression of methionine aminopeptidases. *Journal of Cellular Biochemistry*, 77(3), pp.465–73.

Wu, J. et al., 2006. Molecular cloning and characterization of rat LC3A and LC3B--two novel markers of autophagosome. *Biochemical and Biophysical Research Communications*, 339(1), pp.437–42.

Xue, Y., Petrovic, N., Cao, Renhai, Larsson, O., Lim, S., Chen, S., Feldmann, H.M., Liang, Z., Zhu, Z.Z., et al., 2009. Hypoxia-independent angiogenesis in adipose tissues during cold acclimation. *Cell Metabolism*, 9(1), pp.99–109.

Yatagai, T. et al., 2003. Hypoadiponectinemia is associated with visceral fat accumulation and insulin resistance in Japanese men with type 2 diabetes mellitus. *Metabolism: Clinical and Experimental*, 52(10), pp.1274–8.

Ye, J. et al., 2007. Hypoxia is a potential risk factor for chronic inflammation and adiponectin reduction in adipose tissue of ob/ob and dietary obese mice. *American Journal of Physiology. Endocrinology and Metabolism*, 293(4), pp.E1118–28.

Zelzer, E. et al., 2002. Skeletal defects in VEGF(120/120) mice reveal multiple roles for VEGF in skeletogenesis. *Development (Cambridge, England)*, 129(8), pp.1893–904.

Zhang, Q X et al., 1997. Vascular endothelial growth factor is the major angiogenic factor in omentum: mechanism of the omentum-mediated angiogenesis. *The Journal of Surgical Research*, 67(2), pp.147–154.

Zhou, Z. et al., 2003. Cidea-deficient mice have lean phenotype and are resistant to obesity. *Nature Genetics*, 35(1), pp.49–56.